DEVELOPMENT OF SCIENCE-BASED PERMITTING GUIDANCE FOR GEOLOGICAL SEQUESTRATION OF CO_2 IN DEEP SALINE AQUIFERS BASED ON MODELING AND RISK ASSESSMENT

FINAL SCIENTIFIC REPORT

Reporting Period Start Date: October 1, 2004

Reporting Period End Date: June 30, 2006

Jean-Philippe Nicot[1], Principal Investigator, and Prasad Saripalli[2]

With

Renaud Bouroullec[1]

Hugo Castellanos[1]

Susan Hovorka[1]

Srivatsan Lakshminarasimhan[1]

Jeffrey Paine[1]

Yiling Yang[2]

Date Report Issued: September 2006

DOE Agreement No. DE-FC25-04NT42210

Contractor Name and Address:

[1]Bureau of Economic Geology
John A. and Katherine G. Jackson School of Geosciences
The University of Texas at Austin
Box X, University Station, Austin, TX 78713-8924

[2]Pacific Northwest National Laboratories
790 6th Street
Richland, WA 99354

DISCLAIMER

ABSTRACT

Underground carbon storage may become one of the solutions to address global warming. However, to have an impact, carbon storage must be done at a much larger scale than current CO_2 injection operations for enhanced oil recovery. It must also include injection into saline aquifers. An important characteristic of CO_2 is its strong buoyancy—storage must be guaranteed to be sufficiently permanent to satisfy the very reason that CO_2 is injected. This long-term aspect (hundreds to thousands of years) is not currently captured in legislation, even if the U.S. has a relatively well-developed regulatory framework to handle carbon storage, especially in the operational short term. This report proposes a hierarchical approach to permitting in which the State/Federal Government is responsible for developing regional assessments, ranking potential sites ("General Permit") and lessening the applicant's burden if the general area of the chosen site has been ranked more favorably. The general permit would involve determining in the regional sense structural (closed structures), stratigraphic (heterogeneity), and petrophysical (flow parameters such as residual saturation) controls on the long-term fate of geologically sequestered CO_2. The state-sponsored regional studies and the subsequent local study performed by the applicant will address the long-term risk of the particular site. It is felt that a performance-based approach rather than a prescriptive approach is the most appropriate framework in which to address public concerns. However, operational issues for each well (equivalent to the current underground injection control -UIC- program) could follow regulations currently in place.

Area ranking will include an understanding of trapping modes. Capillary (due to residual saturation) and structural (due to local geological configuration) trappings are two of the four mechanisms (the other two are solubility and mineral trappings), which are the most relevant to the time scale of interest. The most likely pathways for leakage, if any, are wells and faults. We favor a defense-in-depth approach, in which storage permanence does not rely upon a primary seal only but assumes that any leak can be contained by geologic processes before impacting mineral resources, fresh ground water, or ground surface. We examined the Texas Gulf Coast as an example of an attractive target for carbon storage. Stacked sand-shale layers provide large potential storage volumes and defense-in-depth leakage protection. In the Texas Gulf Coast, the best way to achieve this goal is to establish the primary injection level below the total depth of most wells (>2,400 m–8,000 ft). In addition, most faults, particularly growth faults,

present at the primary injection level do not reach the surface. A potential methodology, which includes an integrated approach comprising the whole chain of potential events from leakage from the primary site to atmospheric impacts, is also presented. It could be followed by the State/Federal Government, as well as by the operators.

TABLE OF CONTENTS

EXECUTIVE SUMMARY

The primary objective of the study was to develop a document providing guidance for carbon storage permitting. This topic is still in a state of flux. The scope of work consisted of

- reviewing and evaluating permitting procedures in related fields, including deep-well injection, gas storage, nuclear waste disposal;
- performing numerical modeling of long-term CO_2 leakage after a data-gathering phase,
- assessing risks of sudden and diffuse releases, and
- providing recommendations for developing a permitting protocol by incorporating insights gained from procedural review and from modeling and risk assessment performed in the study.

Review of current relevant permitting procedures led to the conclusion that none is directly applicable to carbon storage. Despite the presence of buoyancy and short-term operational aspects (underground injection control [UIC] Class I nonhazardous wells, natural gas storage) or the long-term aspect (nuclear waste), procedures addressing the combined issues of long-term storage of large amounts of a reactive buoyant fluid are missing. The oil and gas industry alone routinely injects such large volumes (UIC Class II wells). In all cases, postclosure monitoring is minimal when it is required—a common factor in all types of underground storage: siting must be done so that no long-term monitoring is required. For CO_2 injection, current UIC prohibition of any leakage from the injection horizon is not realistic or even desirable. CO_2 is generally not toxic and some leakage, in the statistical sense, can be tolerated. However, no consensus exists on the amount of leakage that would be permissible and still address the concern of high atmospheric CO_2 concentrations.

Work focused on the State of Texas because of its large capacity for storage and its abundance of CO_2 sources. In particular, the Texas Gulf Coast (TGC) is an attractive target because stacked sand-shale layers provide large potential volumes and defense-in-depth leakage protection. Major leakage pathways have been identified in Texas: boreholes (particularly older abandoned wells), faults, and seal heterogeneities. Well conduits represent the most direct conduit to fresh ground water and the ground surface. A study of a well dataset in the context of evolving state and federal regulations led to the following age groups relative to the quality of well plugging/abandonment: post-1983, 1983–1967, 1967–1935, and pre-1935. However, the assurance of a good plugging job does not guarantee the integrity of the well relative to CO_2. Current studies suggest that CO_2 could degrade enough of a cement plug to create an escape pathway. Even wells abandoned at current standards cannot be guaranteed to be leak-free in the long term. It is not even certain that their long-term probability of leakage is smaller than that of wells drilled in the late 19th century, although short-term (decades) leakage probability is likely less. On the other hand, favorable local factors (e.g., borehole closure due to clay action) could mitigate leakage. In addition, a comprehensive statistical analysis of the >130,000 wells in the TGC clearly shows that a deepening trend in the past century, which continues today but with a clustering in the 1,500- to 3,000-m (5,000- – 10,000-ft) depth range. This analysis suggests that CO_2 should be injected as deep as economically feasible.

Carbon storage modes are generally described according to their trapping mechanisms (capillary, solubility, structural, and mineral). Mineral (immobilization through reaction with rock matrix) and solubility trappings are the ultimate fate of injected CO_2 and could be locally important. The current work, however, focuses on capillary and structural trappings. Capillary trapping results from the hysteresis inherent in multiphase flow processes that leave a trail of

immobile free-phase supercritical CO_2. Estimation of the impact and capacity of capillary trapping requires a fine-tuned knowledge of both flow at the microscopic scale and formation heterogeneity. Capillary trapping does not require an obstacle to flow in order to be efficient; the moving CO_2 plume will leave behind a trail at residual saturation, attenuating it until it is exhausted ("open traps"). This property makes capillary trapping also an efficient process for limiting and absorbing leakage from the primary injection level ("defense in depth") and reinforcing the concept of deeper injection. On the other hand, structural trapping involves domal-like structures, in which CO_2 can accumulate ("closed traps" analogous to oil and gas traps). This work analyzed the topography of a regional TGC formation and a likely candidate for injection in Texas (Oligocene Frio Formation). Faults could also create a direct connection to the atmosphere. However, most TGC faults present at the primary injection level do not reach the surface. Other leakage pathways, such as a closed trap overflowing through spill points, or seal failure, can be accommodated by the capillary trapping mechanism, which again provides a defense-in-depth mechanism. The effectiveness of this mechanism depends on the level of heterogeneity of the formations that must be thoroughly studied.

Any permitting of saline aquifer carbon storage must address the primary reason for implementing it: reduction of CO_2 atmospheric concentrations, which translates into large injection volume that must be "mostly" contained for long periods of time. However, current procedures break down for large volumes. Although current legislation addresses operational issues, no regulatory framework addresses long-term aspects of carbon storage. A solution is to shift the permitting from a rule-based process to fulfilling some well-defined, performance-based criteria. Performance-based permitting puts the burden of proof onto the applicant raising the anxiety level of the State agency because of the inherent uncertainty associated with it. It follows that permitting should be done at the regional level ("risk assessment") rather than at the well level, and the burden to show that the site is safe should be on the operator rather than a box-checking exercise by the regulator. This arrangement allows flexibility and innovation in the design of the injection operations. Because total reliance is placed on the geology to contain CO_2 for thousands of years, it is critical that the geology, including well-understood and accurately represented stratigraphy and structure, be a central part of any permitting process. It follows that some form of performance assessment through risk analysis is needed. Similarly, different aspects of monitoring (assessment of total injection volume, detect leakage, etc.), whose technology seems to develop and progress at a quick pace, cannot be assumed to last long after site closure. We have proposed a hierarchical approach in which the State/Federal Government is responsible for developing regional assessments ranking potential sites ("General Permit") and lessening the applicant's burden if the general area of the chosen site has been ranked more favorably. The general permit would involve determining in the regional sense (1) structural controls, (2) stratigraphic controls, and (3) petrophysical controls on the long-term fate of geologically sequestered CO_2. The state-sponsored regional studies and the subsequent local study performed by the applicant would address the long-term risk of the particular site. Operational issues for each well (equivalent to the current UIC program) will follow regulations currently in place. A recurrent observation during this work was the lack of easily accessible data. Geologic-themed databases could provide a lot of information but would also require a lot of effort to collect it. Information on operations and engineered systems ("wells") is harder to gather and is mostly anecdotal. In this context, we developed semianalytical and numerical tools (STOMP-CO2) that could be used in the permitting process.

INTRODUCTION

Generalities

Geological sequestration of CO_2 (also called *carbon storage*) has been recognized as an important way to mitigate the increase in atmospheric CO_2 (Bruant et al., 2002; Gale, 2004; IPCC, 2005, Chapter 5) and has been touted as a way to address global warming (NRC, 2006). Injection of CO_2 has the additional benefit of aiding in oil recovery (Enhanced Oil Recovery, EOR), if it is injected into oil reservoirs if some physico-chemical conditions are met (Holtz et al., 2001). CO_2 Enhanced Gas Recovery (EGR), a novel concept, may also grow from a few current experimental projects to a more widespread technology. CO_2 could also enhance coalbed methane recovery (ECBMR) because carbon dioxide sorbs more strongly to coal than methane does. All this has led to the concept of stacked storage. First, CO_2 is used to economically recover more hydrocarbons and jump-start the second step. This second step involves injection of larger volumes of CO_2 in neighboring saline aquifers using pipelines and other needed infrastructure built during the first step. The current work mainly addresses this step of injection in saline aquifers.

Carbon storage will strongly take hold in the industry only if it can be demonstrated that the hazards involved are known and that their potential negative consequences can be mitigated. The primary objective of this study is to develop a document to guide permitting of geological sequestration of CO_2 by reviewing permitting procedures in other programs, results of related research programs, and results of modeling and risk assessment. Permitting is critical to stakeholders (industry, regulators, environmental groups, the public at large) because restrictive permitting could markedly limit the use of geologic sequestration, although overly lax regulation could result in widespread public objection to the technique or negative consequences. Legislation and regulations for EOR and ECBMR are already in place that address the important operational issues of the injection phase. This study focuses on long-term (hundreds to thousands of years) postclosure migration of CO_2 in the subsurface, less so on the fate of CO_2 remaining in the formation(s). IPCC defines plant life time as *medium term*, whereas *short term* involves operational decisions and *long term* suggests a duration of from 100 years to a few centuries (IPCC, 2005, p.1–23). Millennia are qualified as *very long term*. This work emphasizes Texas, which contains two important hydrocarbon provinces on the world scene (the Permian Basin and the Gulf Coast), with excursions in other geographic areas when

appropriate (Ohio–West Virginia). Both large volumes of CO_2 are currently being released, and high-quality data are available from pilot injections in these areas. The emphasis on Texas is appropriate because about 40% of the electric power in Texas is generated by coal-fired power plants, often located above formations that are good candidates for CO_2 sequestration (**Figure 1**). The study is, however, limited to the Texas Gulf Coast for two reasons, the first of which is the abundance of saline aquifer candidates (Hovorka et al., 2000) as well as the abundance of sources (Hendriks et al., 2002). Administrative limits defining the Texas Gulf Coast for this work are shown in **Figure 2**, which do not discount the possibility that additional CO_2 could come from out of state. A second reason for locating the study along the Texas Gulf Coast is that many reservoirs are susceptible to CO_2 flooding (Holtz et al., 2001). Historically, for a variety of reasons (e.g., CO_2 availability via pipelines developed primarily to access the Permian Basin, Texas), most CO_2 floods in the state have taken place in West Texas and far fewer in the Gulf Coast. The Texas lignite belt is also located in the Gulf Coast area but further inland (e.g., Kaiser et al., 1980). The concept of stacked storage makes it likely that CO_2 captured from the coal-fired power plants will be initially transported by pipeline toward the coast, where it is most likely to be used, although it could be injected in deep unminable coal seams in a later stage (e.g., Hernandez et al., 2006). Another tangential reason is that the Texas Gulf Coast has a very low level of seismic activity (Frankel et al., 2002; Hovorka et al., 2003) and is not a credible candidate for any type of volcanic activity in the near future. We will also develop the contention that a depth of ~3,000 m (10,000 ft) is ideal for CO_2 storage because (1) most well bores do not reach that depth, (2) it maximizes storage (Holtz, 2006), and (3) it increases natural defenses against leakage.

A typical 500-MW coal-fired plant releases approximately 2.9 Mt CO_2/yr (0.8 Mt C/yr). Because capture consumes energy, a 500-MW plant would have to send 3.4 Mt CO_2/yr (0.9 Mt C/yr) to storage if 85% of the CO_2 present in the flue gas is captured (IPCC, 2005, p.1–15). At the Sleipner site, Norway, 1 Mt CO_2 is injected annually. The injected amount is higher at Weyburn, Canada (~1.5 Mt), and Salah, Algeria (~1.2 Mt), and even higher in EOR operations, such as at Rangely, Colorado, and in the Permian Basin, Texas. Most projects will inject a CO_2 flux within the 1 to 10 Mt/yr range, equivalent to 850 to 8,500 gpm or 1.2 to 12 MGD or 29,000 to 290,000 bbl/day, assuming a CO_2 downhole density of 0.6 t/m^3. Such flow rates will most likely require multiple injection wells but could require only one well (with the caveat that a second one may

be mandated by rule to receive the CO_2 flux when the first one is down). A related study investigating the capacity of the Frio Formation to accept fluids in the Southern Gulf Coast (Nicot et al., 2005, p.160) found, using actual Class II well specifics, actual formation parameters, and current rule requirements, that the median injection flow rate is ~280 gpm, with the 95th percentile being in thousands of gpm.

The terms *sequestration* and *storage* are used interchangeably in this report. Strictly speaking, sequestration carries a concept of permanence, whereas storage does not. If sequestration implies that the CO_2 will stay underground forever, storage can be understood in at least two ways: either CO_2 will be retrieved for industrial or other use at a later time or it will progressively leak. Another term with possibly multiple meanings is *leakage*, which can be understood as any migration from the primary formation in which CO_2 was injected. Or it can be more restrictively defined as migration beyond the deep subsurface into the fresh-water zone and then into the biosphere. Terminology is an important part of public acceptance, and agencies should carefully think about naming their program and the nomenclature that they use. This report also uses the term *abandoned wells* in a broad sense: all nonactive wells either plugged according to regulations or orphan, but not in temporary standby, are included.

Technical Aspects

Below a depth of ~800 m in average pressure and temperature conditions, CO_2 is supercritical, with a density in the 600 to 800 kg/m^3 range and a viscosity at least one order of magnitude lower than that of water. The large resulting mobility contrast between water and CO_2 has a deep impact on the system-flow dynamics resulting in the following four main categories for CO_2 underground storage modes in saline aquifers:

- residual or capillary trapping owing to multiphase flow processes (e.g., Akaku et al., 2006; Akervoll et al., 2006; Ide et al., 2006);
- solubility trapping through the dissolution of CO_2 into the aqueous phase;
- structural trapping, when fluid is trapped in the fashion of hydrocarbon accumulation, and hydrodynamic trapping (e.g., Bachu and Adams, 2003), when the residence time and flow rate of both water and supercritical fluid are so low that CO_2 is essentially trapped; and
- mineral trapping due to the reaction of CO_2 with host rocks (e.g., Gunter et al., 2000; Xu et al., 2003; Xu et al., 2006).

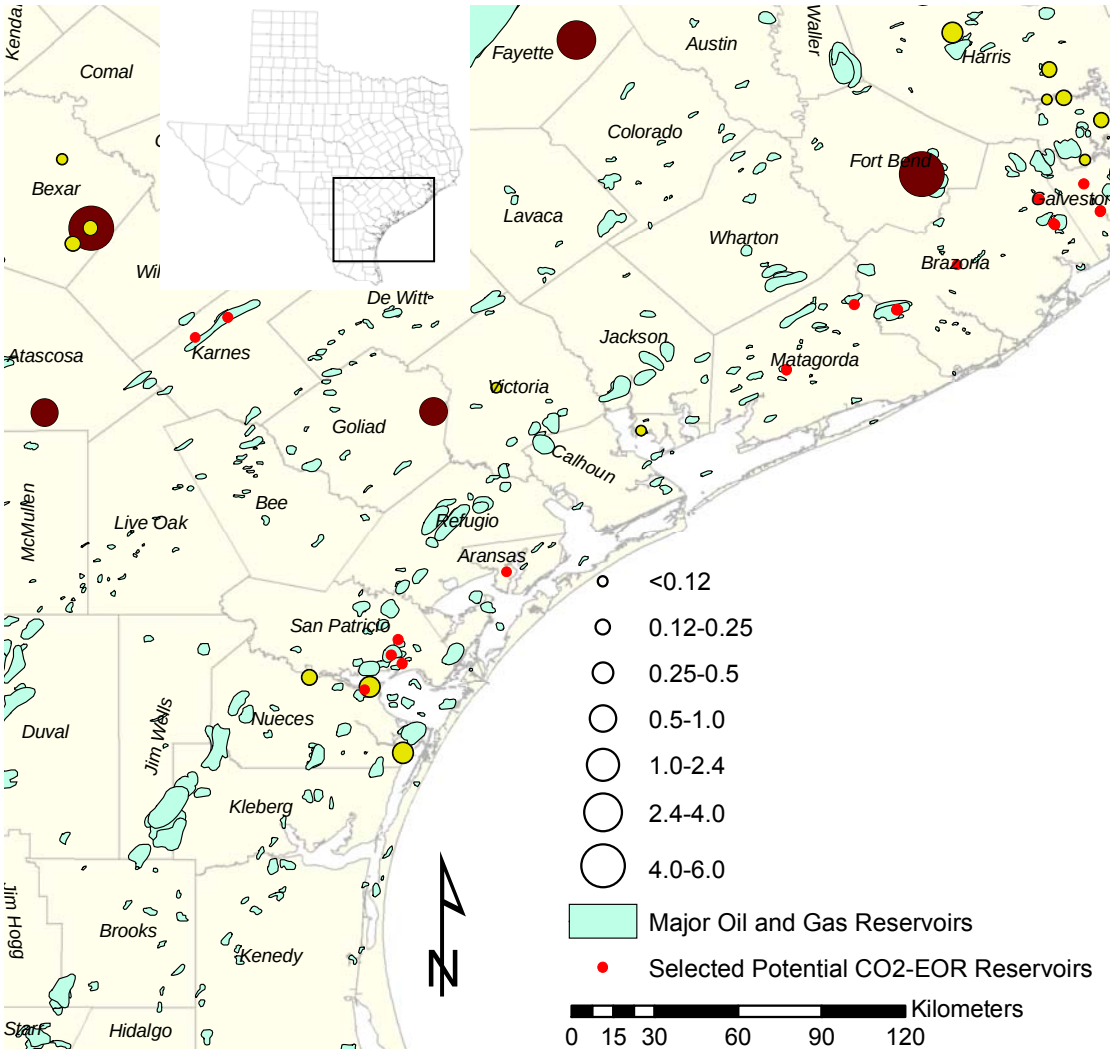

Source: Power plants: DOE/EIA (2002 and 2003); Oil and gas reservoirs: Galloway et al. (1983) and Kosters et al. (1989); EOR reservoirs: Holtz et al. (2005) and Nuñez-López and Holtz (2006); units are Mt C/yr.

Figure 1. Location of coal-fired power plants (brown circles), natural-gas-fired power plants (yellow circles) and some potential candidates for CO_2-EOR. Major oil and gas reservoirs are also shown for reference.

One can also add sorption trapping, important for coal seams and black shales, as well as cavern trapping in salt domes. Several studies have suggested that mineral trapping, although representing the ultimate fate of CO_2 in the subsurface, is a slow process (e.g., Noh, 2003), except maybe in basalts, and that short- to medium-term (tens to hundreds of years) trapping mechanisms are capillary (e.g., Kumar, 2004) and structural trapping. The Frio experiment, where 1,600 tons of CO_2 was injected into a saline formation at a depth of ~1,500 m (~5,000 ft) in the Texas Gulf Coast (e.g., Hovorka et al., 2005; Kharaka, et al., 2006) has

confirmed the validity of the process. In general, solubility trapping seems also to be a minor component of the total storage, although induced water density changes may alter flow dynamics. The convection put forward by some researchers (e.g., Ferer et al., 2002; Ennis-King and Paterson, 2003) seems to be effective only in a higher permeability medium. However, dissolution could be enhanced through engineering solutions (e.g., Leonenko et al., 2006; Georgescu et al. 2006). One of the goals of this report is to investigate the ways through which structural and capillary trapping mechanisms can fail and the resulting implications for permitting.

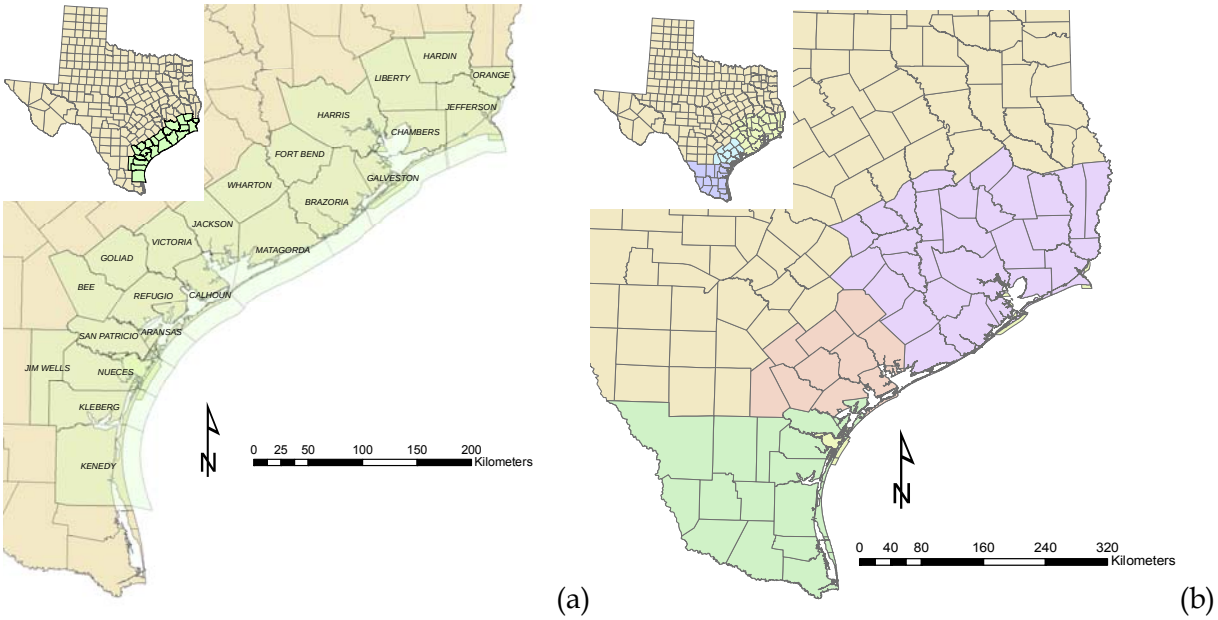

Figure 2. Map showing (a) the 23 Gulf Coast counties and (b) the three RRC districts (2, 3, and 4) used in the statistics work

The capillary trapping mechanism does not perform well if the CO_2 path is cut short intrinsically by fingering or by external features, such as a well or a conductive fault. Similarly, structural trapping is ineffective if seals are poor and/or some of the CO_2 can leak at natural spill points. Of all the mechanisms, only structural trapping is typical of hydrocarbon accumulations and it only requires a seal. It can be argued that solubility trapping does require a seal too because water flows. However, it is much less critical than for structural trapping because CO_2-enriched water tends to sink owing to density differences.

A good understanding of CO_2 leakage entails a good knowledge of the local geology, and the general geology of the Gulf Coast is simple, albeit complicated in the details (e.g., Ambrose et al., 2006; Appendix A). It consists of thick Tertiary and Quaternary wedges (totaling

several kilometers) of alternating sandy and clayey layers resulting from the deposition by rivers of their sediments in deltas and farther out in the ocean in multiple, offlapping cycles that record deltaic and shoreface progradation (**Figure 3**). The process, resulting in fluvial, deltaic, barrier bar/strandplain, and slope/basin depositional systems, such as those of the modern Mississippi River and smaller coastal rivers, is still active today. Growth faults, resulting from sediment loading on unstable substrates, periodically develop. Intermittent movement along these growth faults has accommodated accumulation of enormous masses of sediments. Growth faults are mostly syndepositional faults (still active in the Houston area on sediments of wedge "6" of **Figure 3**) but could be reactivated at a later time. In the northern section of the Texas Gulf Coast, salt domes have been moving upward from the kilometer-thick Louann salt layer. This movement has resulted in a contrast in oil traps and, consequently, in carbon storage potential targets, where, in the Houston area, upturned sediments abutting diapirs act as a trap, whereas farther south, in the Corpus Christi area, oil reservoirs are made by more common structural and stratigraphic traps.

What are the Objectives of this Work?

Development of permitting guidelines for geologic sequestration of CO_2 is a primary goal of this project. Development of reliable guidelines is critical to ensuring the selection of safe, suitable sites that are monitored effectively and provide long-term subsurface storage of CO_2. To accomplish this objective, we will perform the following tasks: (1) review and evaluate permitting procedures in related fields (deep-well injection, natural gas storage, nuclear waste disposal), (2) determine what data are needed to perform a risk assessment and collect them if possible, (3) develop a risk assessment approach, and (4) provide recommendations drawn from risk assessments performed in this work but also gathered from the literature, as well as drawn from our general work experience dealing with subsurface processes.

Slow, long-term leakage is an inescapable part of any large injection program. Slow leakage is, however, acceptable because stabilization of the atmospheric concentration at a reasonable level for a long enough period is the goal of carbon storage. In any case, most accumulations of natural fluids leak. Oil and gas reservoirs provide a good tool for assessing leakage despite a few differences to be detailed later. These reservoirs are construed as perfect containers because they were able to trap hydrocarbons through geologic times (although numerous wells could have destroyed their initial integrity). Some hydrocarbon accumulations

have been trapped for hundreds of millions of years. However, more recent reservoirs may represent only some dynamic steady state between leakage and charge from a feeding downdip source. In addition, it is also known anecdotally that most hydrocarbons generated in the deep subsurface were not trapped but were released to the surface through geologic times. The real question then is "what fraction of the generated amount has leaked to the surface?"

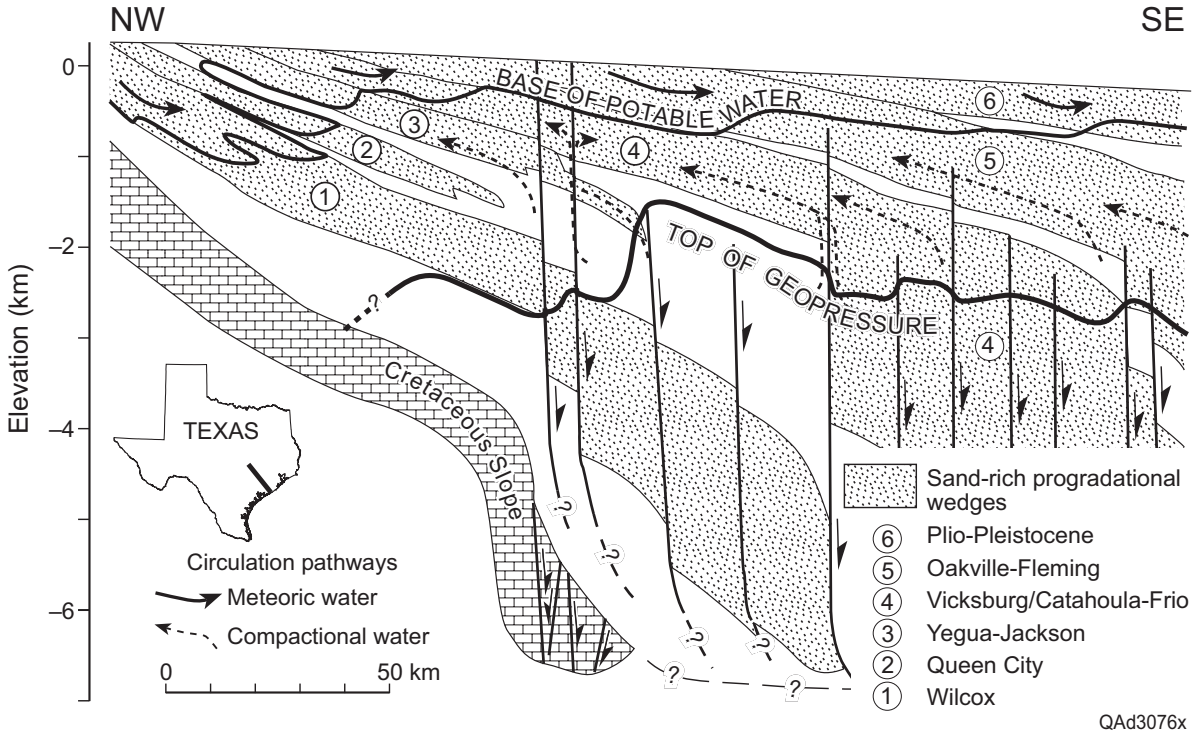

Source: Adapted from Galloway (1982) and Galloway et al. (1982)

Note: Wedges of interest for carbon storage are #4 (Vicksburg/Frio) overlain by a regional seal (Anahuac Shale, white wedge between #4 and #5) and #5 (Oakville/Fleming) overlain by another regional seal (*Amphistegina B* Shale, white wedge between #5 and #6), complementing the low permeability of the upper half of the wedge (Burkeville confining system). The last major progradation wedge of Plio-Pleistocene age (#6) is still active and too shallow to be of prime interest for CO_2 storage.

Figure 3. Southern Gulf Coast major sand-rich progradational packages and growth-fault zones beneath the Texas Coastal Plain.

A succinct description of leakage consequences can be put into a matrix with three entries: timeframe (short/long term), footprint (local/global), and rate (catastrophic/diffuse) (**Table 1**). Consequences are related to the health and safety (H&S) of facility staff and neighbors, local environment (tree kill and other biological effects on animals, decrease in agricultural yield, heat island effect, seismicity), alteration of minerals and energy (oil, gas, geothermal, etc.), and water (brine displacement, contaminant mobilization) resources and

global environment (global warming). Catastrophic risks do not include operational risks, such as a well blowout, but, rather, natural sudden releases. For example, Birkholzer et al. (2006) and Pruess and Garcia (2002) suggested that CO_2 loss through fault zones could lead to substantial fluxes from the reservoir through self-enhancing processes, possibly periodically (fault-valving).

Comprehensive list of hazards have already been compiled in several publications (e.g., Saripalli et al., 2002a; Wilson, 2002). Short-term catastrophic risks and asphyxiation risks are likely to retain the public's attention. The 1986 Lake Nyos catastrophe (e.g., Zhang, 1996) could generate public anxiety vis-à-vis CO_2 storage, despite the lack of similarity between possible storage sites and the Lake Nyos area (in particular, local topographic features preventing the plume from dispersing). The Lake Nyos catastrophic event suddenly released 0.1 to 0.3 Mt CO_2 (Zhang, 1996). A similar event in Texas lakes and reservoirs is unlikely to happen mainly because CO_2 would not accumulate at the bottom of a lake, thanks to the annual turnovers due to seasonal temperature changes. Leakage from natural CO_2 accumulation at Mammoth Mountain released 0.2 Mt CO_2 in 1996 (Farrar et al., 1999), which caused trees to die within an area of approximately 0.4 km^2 (100 acres). More likely local hazards include impacts on the ground water (heavy metal mobilization, brine displacement, and other flow-regime changes because of CO_2 interaction with underground rocks and fluids) and at the surface (CO_2 concentration, radon and other gas stripping, microseism and fault reactivation, soil heave, impact of water well mechanical integrity, etc.). Some external economical risks are also present: uncontrolled oil mobilization and natural gas contamination. Global risks (storage performance) obviously result from an increase in atmospheric CO_2 through a release flux of the stored volume that would be larger than the global injection rate and that would negate its effectiveness.

Table 1. Simplified table of hazards.

	Short-Term (preclosure injection period)		**Long-Term (postclosure)**	
	Catastrophic	**Diffuse**	**Catastrophic**	**Diffuse**
Local	√ H&S	√ H&S, L. Env.	√ H&S, L. Env.	√ H&S, L. Env.
Global	N/A	Can be fixed	N/A	√ Global Env.

Report Content

As described in the initial work plan ("proposal"), the objective of this study was to develop science-based permitting procedures for CO_2 sequestration based on

- review of existing permitting procedures (Task 1),
- simulation of flow and transport of CO_2 in a generic reservoir and evaluation of CO_2 migration pathways (diffuse vs. focused) and potential leakage (Task 2),
- valuation of risk on the basis of probability distributions of input parameters (e.g., permeability, densities of faults, abandoned) and related consequences,
- ranking of parameters analyzed in the risk assessment to allow site characterization and monitoring in order to focus on critical parameters for CO_2 sequestration (Task 3), and
- recommendation for permitting guidance (Task 4).

Overall, this report follows this initial description. Not including this introduction, the work is divided into five sections. In Section I, we summarize pertinent aspects of current permitting procedures of carbon storage analogs, corresponding to Task 1 of the grant. Section II contains general material addressing parts of Task 2. Section III and the beginning of Section IV develop Task 3 issues, after describing potential injection horizons in the Gulf Coast in order to explain the nature of the geological components relevant to leakage (formations, seals, faults). Section III presents some aspects of risks linked to wells, faults, and the nature of the overlying layers. Quantification of related hazards (Task 2) is presented in Section IV. Using all information presented in the other sections, Section V, as called for in Task 4, puts forward permitting guidelines, as well as relevant aspects of monitoring and allied issues. Appendix A contains specific notes about the geology of Texas and the Gulf Coast. Targeted information on oil leakage and fault analysis is provided in Appendices B and C, respectively. Appendices D and E develop numerical aspects of the scaling analysis used in the report. The semianalytical and numerical models used in Section IV are presented in Appendices F and G. Appendix H lists papers, abstracts, and presentations stemming from this work.

EXPERIMENTAL METHODS

No experimental methods or equipments were used in this study.

RESULTS AND DISCUSSIONS

I. Compilation of Permitting Requirements

The Compilation of Permitting Requirements section addresses Task 1 of the agreement. Central to all industrial projects is the permitting process, particularly its cost and what it involves in terms of time investment. The first step in developing guidance for permitting CO_2 sequestration sites is to evaluate all applicable permitting approaches, such as those previously developed for deep-well injection, gas-storage systems, and radioactive waste disposal. Many of the substances being considered in these permit processes are hazardous and/or radioactive, whereas CO_2 is generally regarded as nontoxic and not hazardous. CO_2 is generally not considered as a waste (Coddington, 2006, oral communication; Van Voorhees, 2006, oral communication), but there are legislative efforts in that direction; a Supreme Court decision is expected in 2007 on whether to label CO_2 a pollutant (Massachusetts et al. vs. EPA et al., case 05-1120). Nevertheless, the general approach used may be adapted for CO_2 sequestration sites. On the other hand, CO_2 is routinely injected into the subsurface for EOR, although the permitting process for this type of injection focuses on resource protection and short-term environmental protection, and it does not assess the effectiveness of the subsurface geology in isolating CO_2. In general there is no provision or limited provisions for postclosure monitoring. Any CO_2 storage project needs to address these issues, but in addition it must guarantee that CO_2 will be reasonably sequestered in the long term in order to be effective in obtaining reduction in atmospheric concentrations. This latter requirement could translate into additional constraints in the permitting process or additional assurances required to make the CO_2 credits fungible.

There are two broadly defined legislative philosophies: goal oriented and design oriented. Examples for the former include one-of-a-kind nuclear waste disposal facilities, where it is required that the dose at some locations be below legislated levels, which is true for both high-level and low-level facilities. Facility design and other means to reach the goal are left to the operator/applicant under general rules set by the responsible agency. On the other hand, design-oriented legislations spell out construction specifications (e.g., area of review of fixed radius, thickness of cement plug). This last type of legislation is well suited to standardized features built in numerous occurrences each year (e.g., oil and/or gas production well, underground injection control UIC Class II injection wells). An equivalent description of the

approaches would be "process based" and "regulation driven". The two philosophies are not mutually exclusive, as demonstrated by current UIC Class I legislation. It requires no leakage of the injected fluid outside of the injection formation, but it also requires an operator to follow strict design specifications. In general, the larger the project or/and the longer the timeframe, the more latitude is given to the project designer/operator. This policy structure directly parallels the end members of the many ways that carbon storage permitting could be approached: from the reservoir scale and single-well injection operation, to the basin scale, with hundreds of injection wells injecting over a few decades to a few centuries.

The following compilation, pertaining to permitting requirements in the U.S., does not pretend to be comprehensive in all aspects of permitting but focuses on three selected aspects of permitting: is it process-based or regulation-driven, what is the level of subsurface characterization needed, and how is postclosure monitoring approached?

I.1 Injection Wells

Injection wells, whatever the material injected, have to abide by UIC rules. The UIC program was established in 1980 at the Federal level, with EPA following the Safe Drinking Water Act (1974) and the Resource Conservation and Recovery Act (1976). Its implementation is in general delegated to the states. The UIC program defines five classes of wells (e.g., EPA, 2002): Class I, which is used to inject hazardous, industrial and municipal wastes; Class II , which is used to inject fluids related to oil and gas production; and Class III , which is used to inject fluids for mineral extraction. Class V includes all other types of wells and Class IV has been banned. A large body of information can be found on EPA and Ground Water Protection Council (GWPC) websites. The UIC program focuses on protection of ground-water resources. It essentially states that the quality of the ground water should not be degraded by injection operations. All permits of Classes I through III follow the same basic process: geologic characterization to define "underground source of drinking water" (USDW), demonstration of integrity of seal and well penetrations in area of review, and calculation of injectivity of receiving zone from which maximum surface injection pressure will be defined. Permits are issued for a given period, at given maximum pressure, at a given maximum flow rate, and in a given interval of a given formation. In addition, for Class I wells, nature of the injected hazardous fluids is also defined within strict compositional range(s). The UIC program emphasizes pressure impacts of injection, with a secondary emphasis on transport (Class III

wells, "no migration" petition for Class I wells). Class I to III fluids do not have the density or viscosity contrast brought forward by CO_2, except possibly municipal wastes. Possible detrimental impacts on aquifers of carbon storage include acidification of the aquifer if it has no buffering capacity and displacement of saline formation fluids into potable water supplies. In the only case of CO_2 injection in a saline aquifer for disposal purposes—at the Frio experiment site in Texas—a Class V research or experimental permit was agreed on because of the limited amount injected, that is, ~1,600 tons of CO_2 (Hovorka et al., 2003). It was not possible to apply for a Class II well because injection was not related to hydrocarbon production, despite the use of an abandoned oil well retrofitted as a monitoring well.

Florida municipal waste wells are probably the closest operations to CO_2 injection because of the buoyancy of the waste and the large volumes involved. Failure to appropriately characterize the primary seal is the main reason for current and past contamination problems (McNeill, 2000). Zinni (1995) hypothesized that Class I wells in Louisiana could also jeopardize USDW water quality through leaking faults, but he was refuted by Warner (1997).

Area of Review and Emphasis on Pressure

Pressure-effect emphasis in the regulations led to the concept of area of review (AOR). It has been traditionally defined by a fixed radius with a strong regulatory requirement that the injectate stays within the injection layer, although a calculated zone of endangering influence (ZEI) is another option. The fixed AOR radius was chosen to include the footprint of the cone of influence around the well where the fluid is pressured by the injection and covers the area where corrective actions may have to be taken to protect USDW. The UIC 40 CFR defines AOR in §146.03 as "*the area surrounding an injection well described according to the criteria set forth in §146.06 or in the case of an area permit, the project area plus a circumscribing area the width of which is either ¼ of a mile or a number calculated according to the criteria set forth in §146.06.*" Within the AOR, before starting any injection, an operator must identify all wells penetrating the injection zone or the confining zone (§146.64) and assess their status for possible corrective action. The legislation, however, does not carry an absolute requirement of locating known abandoned wells whose exact location has been lost. The overarching purpose of the AOR is protection of drinking water resources due to pressure buildup in the injection zone. Drinking water resources, also called USDW, are defined in §146.03 as a formation with water quality below 10,000 mg/L total dissolved solids. In addition, water wells and land and mineral ownership

within the AOR should be documented. The AOR applies mainly to Classes I through III and focuses on the pressure aspect of the injection. Within an AOR, the operator must make every effort to characterize and to plug, if needed, all well penetrations into the injection formation within a given radius (at least 2 miles as required by federal law and 2.5 miles in Texas for Class I and 0.25 mile for Class II). In the case of an area permit, as is often the case for Class III wells, the AOR includes the area being permitted, with a buffer zone whose width is numerically equal to the "radius." An unsuccessful but reasonable and honest effort may be deemed to be sufficient by the regulating agency to award the permit (especially for Class II wells).

Section UIC 40 CFR §146.06 states that the AOR should be determined for each well or field through either a zone of endangering influence (ZEI) or a fixed radius, which cannot be smaller than ¼ mile. The radius of the ZEI is calculated as the lateral distance in which the pressures in the injection zone may cause migration of the injection and/or formation fluid into a USDW. Some EPA offices are questioning the adequacy of a fixed radius for traditional injection wells (Frazier et al., 2004), which can certainly be justified in the case of CO_2 injection. A fixed radius of influence seems impractical and would in most cases be larger than the 2.5 miles required by UIC Class I rules. The typical elongated shape of a trap (see **Figure 12**) does not fit well into a circular area of review.

In most cases, Class I hazardous waste wells must meet the additional "no-migration" petition, in which the operator shows, through numerical modeling, that the waste will stay confined to the injection zone for at least 10,000 years. The requirements of the geological review emphasize the characterization of faults and fractures, both laterally in the injection formation and above in the injection zone. Current requirements from the Railroad Commission of Texas (RRC) for Class II wells (RRC, 2006) include making best efforts to identify all wells in a ¼-mile radius of the proposed injection well and providing evidence that all abandoned wells intersecting the injection formation have been plugged. In some circumstances, this radius can be increased to ½ mile (shallow disposal wells in the Barnett Shale area of North-Central Texas). Class III wells are used for (1) solution mining or in situ leaching for production of sulfur and salts and (2) metals (uranium, gold, copper), respectively. A relevant aspect of Class III permits is that they often involve multiple wells permitted at the same time in an area permit. Because the mineral deposit targeted may be above the lowermost USDW (the aquifer is then "exempt"),

Class III permit also involve several monitoring systems during operations. Monitoring is done at the edges of the injected domain in the injection formation, as well as in the aquifers above and below the injection horizon (for example, 30TAC §331.82).

Acid gas (mixture of H_2S and other gases with a dominant fraction of CO_2) permitting is probably the current closest analog to CO_2 injection because it is injected for disposal. A total of ~44 sites in Canada and ~20 in the U.S. capture, transport, and inject acid gas (Bliss, 2005). In the U.S., those wells are Class II wells, with some additional restrictions because of the hazardous nature of H_2S, and are covered by current legislation.

Monitoring Requirements

Monitoring is often required only on the injection well during its operational life and shortly thereafter. There are several monitoring procedures in place related to the injection well, including the mechanical integrity test (MIT), internal and external to the well bore. However, there is generally no requirement for ambient monitoring of the injection formation. Similarly, there is no requirement to monitor aquifers, including USDW aquifers, above the injection formation. The concern might be not to create additional leakage pathways, as has happened in several instances in Florida (McNeill, 2000). Postclosure monitoring, if any, generally involves pressure measurements until the impact of the cone of influence subsides below the base of the lowermost USDW. In the case the most similar to carbon storage, Florida requires monitoring wells below, in and above the injection formation as well as within the USDW. There, leaking fluids have been detected in several USDW (McNeill, 2000).

During the operational phase, monitoring of the injection well is always required, particularly pressure on the annulus. Monitoring of water quality in the lowermost USDW and in the first aquifer overlying the injection zone can also be required (Rule §331.63g, TAC, 2006) for Class I wells. This monitoring must take place "*until pressure in the injection zone decays to the point that the well's cone of influence no longer intersects the base of the lowermost USDW or freshwater aquifer*" (Rule §331.68b, TAC, 2006, for Class I). Monitoring of the USDW is rarely undertaken in Texas for Class I and is not required for Class II wells (Platt, 1998). Monitoring wells, especially if located upgradient in the injection horizon, may turn out to be an additional leakage pathway. As noted by Benson et al. (2002, p. 91) for Class I wells, nonmandatory monitoring only exposes an operator to litigation, and many may be reluctant to implement it.

I.2 Natural Gas Storage

Many natural gas storage projects use depleted oil and gas reservoirs, salt or granitic caverns, or saline formations. Although permit requirements for natural gas storage may apply to some extent to CO_2 sequestration, the time periods for such storage are much shorter (<1–3 yr) than the times required for CO_2 sequestration. The RRC of Texas presents monthly statistics on natural gas storage in the State (http://www.rrc.state.tx.us/divisions/gs/rap/gsrap.html). It reports that, in December 2005, there were a total of 21 natural gas storage facilities in depleted oil and gas reservoirs and 14 natural gas storage salt caverns. Chapters §3.96 and §3.97 of the Texas Administrative Code address gas storage in reservoirs and salt caverns, respectively. Permitting of these structures is focused on operating pressures. It is Class II wells that have to follow the requirements of Area of Review, and monitoring of injection wells is more stringent than that of other Class II wells. Depleted oil and gas reservoirs, aquifers, and salt caverns are all used to store natural gas. They operate on cycles of production/injection on an annual or shorter basis. Overall, rules are those of UIC Class II injection wells. An interesting aspect in Texas is the requirement of leak detectors installed on wells located less than 100 yards from buildings and other places where people can gather (RRC, 16TAC, §3.96(i) and §3.97(h)(4)). This is an analog mostly relevant to the operational period. There is no postclosure monitoring requirement related to leakage because the reservoir/aquifer/cavern is generally blown down before closure and is left pressure depleted, with no driving force for leakage.

I.3 Nuclear Waste Disposal

Although CO_2 is currently not classified as a waste, its disposal, like that of nuclear waste, includes the necessity of long-term confinement. Solid and nuclear waste disposal falls under RCRA and NWPA and is regulated by EPA and NRC, respectively. Both low-level and high-level nuclear waste disposal sites are process driven, with a focus on risk assessment, numerical modeling, and site characterization. Use of risk-informed, performance-based analysis is written into the regulations (NRC policy statement 60CFR 42622 "Use of Probabilistic Risk Assessment Methods in Nuclear Activities").

An approach that has worked well for nuclear waste disposal is the feature, event, and processes (FEPs) approach, which consists of building, initially through brainstorming, a list as comprehensive as possible of potential issues that can affect the site or the region. Subsequent work consists of sorting and grouping these in categories and subcategories. The next step

assigns some kind of probability to each FEP, as well as the possible consequence for the system. In general, permitting of nuclear facilities focuses on the individual performance of the usually unique features that make the site desirable. There are three main aspects to the studies: (1) compilation of FEPs, along with their probability and consequences; only those FEPs having a probability of less than one in 10,000 over 10,000 years are considered in the next step; and (2) performance assessment (PA) modeling. The great difficulty of PA is that predictions are projected far into the future. PA studies require field measurements and laboratory experiments to calibrate the model. The literature is extensive about the (in)validity of such a jump (Oreskes et al., 1994; Ewing et al., 1999; Konikow and Ewing, 1999; Bredehoeft, 2005). In general, permitting of nuclear waste disposal sites also calls for a limited monitoring period—hence the importance of the third element, quantification of uncertainty that can be due to a lack of knowledge or to an inherent variability.

The Waste Isolation Pilot Plant (WIPP) in Carlsbad, New Mexico, which opened in 1999, is scheduled to operate for a few decades. Current plans for the WIPP facility call for a postclosure monitoring for "*as long as practicable, and/or until the DOE can demonstrate to the EPA that there is no significant concern to be addressed by further monitoring*" (DOE, 2005, Section 5). Line 40 CFR §191.14(b) states that "*Disposal systems shall be monitored after disposal to detect substantial and detrimental deviations from expected performance. This monitoring shall be done with techniques that do not jeopardize the isolation of the wastes and shall be conducted until there are no significant concerns to be addressed by further monitoring*." Postclosure monitoring includes surveillance of the overlying aquifer for a duration on the order of 1 century. It is unclear whether this period is enough for problems to appear in the monitoring system. The facility is designed to contain the waste for at least 10,000 years. This was also the initial regulatory time frame envisioned for the proposed Yucca Mountain facility in Nevada, although it is likely to be significantly increased to include a higher risk period however far in the future. A recent decision by the U.S. Court of Appeals for the District of Columbia (Nuclear Energy Institute, Inc., v. EPA, case 01-1258, July 2004) compels the EPA to look further into the future than 10,000 years. Monitoring is obviously not an option for such long time frames, and the facility must be designed to withstand such time. The WIPP site in New Mexico has included a confirmation period of postclosure monitoring until performance can be reasonably proven to behave as expected (Benson et al., 2002, p.133), and it could be as long as 1 century.

I.4 Conclusions

Table 2 contains a summary of salient points. No current permitting procedure addresses, in the same regulation, three of the major characteristics of CO_2 sequestration: large volumes, buoyancy of the fluid, and long-term capture for centuries or millennia. Buoyancy is addressed in natural gas storage, CO_2 EOR (UIC Class II wells), and nonhazardous Class I wells (municipal waste) regulation, and securing the stored material in the long run is approached in Class I hazardous and nonhazardous waste and low-level and high-level nuclear waste disposal. Large injection volumes (essentially water, sometimes contaminated) is practiced by the oil and gas industry (see Section II). Developing procedures for use during the injection phase is within the realm of current legislation and does not represent a departure for current usage. On the other hand, long-term storage is typically demonstrated by performance assessment using more or less conservative assumptions. A simple performance assessment, combined with prescriptive rules, is used for injection of hazardous Class I wells, whereas very sophisticated, expensive, and time-consuming performance assessments are used in the case of nuclear waste (for both high- and low-level material).

Conduits for leakage to USDW can be natural (faults) or human made (wells). In the case of traditional water injection, hazardous or not, injection pressure is the driving force behind leakage, and mainly faults and wells are of concern. In the case of injection of a buoyant fluid such as CO_2, gravity forces continue acting, even after dissipation of the pressure pulse. No permitting process currently enforces long-term monitoring. On the contrary, the focus is on engineered and natural barriers to contain the waste/product. The reliance on engineered features may be problematic for long-term storage because of the lack of a long track record (hundreds of years, at best, in most cases). It follows that predictions with the help of numerical modeling are a crucial part of the permitting process. It is thus imperative to ensure that all important processes are included and modeled (they might be different from site to site). The scientific community is still in that investigating phase.

The EPA's current view seems to favor an absolute prohibition of fluid movement into any USDW for Class I and II wells, although the SDWA itself does not impose such a prohibition (Michel Paque, GWPC, CO2SC Symposium, Berkeley, CA, March 20–22, 2006, Conference). This interpretation was reiterated by new permitting requirements of municipal wells (Class I nonhazardous), where fluid movement could be recorded in a USDW without

necessarily endangering it. It is, however, sensible to think that the EPA might remain flexible as draft carbon storage regulation evolves.

Table 2. Compilation of permitting requirements

Permit	Process	Monitoring	Comments
UIC Class I (hazardous wastes)	Mostly regulatory driven with a "No-migration petition."	Operation and postclosure monitoring: limited to injection well pressure. No monitoring wells.	
UIC Class I (industrial and municipal wastes) Permit	Regulatory driven. Injected fluid must be confined to the injection zone.	Operation and postclosure monitoring: limited to injection well pressure. However, nonhazardous Class I well permits in Florida require USDW monitoring because of the buoyancy of municipal wastes, but enforcement is lax (Benson et al., 2002, p.100). No monitoring wells.	Performance established by predictive modeling.
UIC Class II (oil/gas injection well, including EOR)	Regulatory driven.	No postclosure monitoring.	
UIC Class III (mineral extraction, solution mining)	Regulatory driven.	Extensive operational monitoring. No postclosure monitoring	
UIC Class V		No monitoring	
Low-level nuclear waste	Fully process-driven approach in combination with risk assessment.	Monitoring until confirmation that the site is working properly.	Performance established by predictive modeling.
High-level nuclear waste	Fully process-driven approach in combination with risk assessment.	?	Performance established by predictive modeling.
Natural gas storage in aquifers or depleted oil and gas reservoirs	Fully regulatory driven.	Monitoring of the injection well(s) during operational life of facility. Rarely ambient monitoring wells. No postclosure monitoring.	Abandonment is done at low pressure.
Natural gas storage in salt caverns	Fully regulatory driven.	Monitoring of the injection well(s) during operational life of facility. No postclosure monitoring.	
Acid gas injection (U.S.)	Regulatory driven.	No postclosure monitoring.	

II. Carbon Storage in the Texas Gulf Coast

II.1 Oil and Gas Reservoirs

To analyze impact of leakage globally, one must first understand potential location of storage sites and allowable leakage rates. A high storage site density will be more prone to leakage because of the likely saturation of the potential buffers. It is thus relevant to take a detour on methods for estimating regional capacity. Carbon storage poses new challenges related mainly to CO_2 buoyancy and to the huge injection volumes needed to make a significant impact. The contiguous U.S. emits more than 2.9 Gt CO_2/yr from relatively large stationary sources (Dooley et al., 2006, p. 28), a sizable fraction of which comes from Texas. Municipal waste waters are injected at a rate on the order of 0.5 Gt/year, mainly in Florida (Wilson and Keith, 2003; EPA, 2002, p.7). Volumewise this is equivalent to 0.3 to 0.4 Gt CO_2/year. Class I hazardous waste volumes are much smaller. In 2002, a total volume of 5,370 million barrels (MMbbl) of mainly water was injected through Class II injection wells in Texas (RRC Website). This is equivalent to 0.850 Mt water per year (**Figure 5**), whose volume is similar to 500 to 650 Mt of supercritical CO_2. RRC reports for previous years show similar numbers. It should be noted that most of that volume is also produced and that the net balance for the subsurface fluid volume is ~0. Operators in the Permian Basin (**Figure 4**) inject ~30 Mt/yr CO_2, maybe half of it recycled. It is thought that the SACROC unit, making up about 40% of the injected volume, has accumulated more than 55 Mt CO_2 since injection started in the early 1970s. It follows that more than 100 Mt CO_2 is most likely already sequestered in the Permian Basin. The higher injected volumes in the Permian Basin are a reflection of the operational technique (waterfloods) and geologic reality (little natural water drive). The natural water drive existing in many Gulf Coast reservoirs also suggests that operators should not expect pressure-depleted reservoirs because water would have invaded the space previously occupied by the produced hydrocarbons. Acid-gas injection was also small by those standards in 2001 (Heinrich et al., 2003).

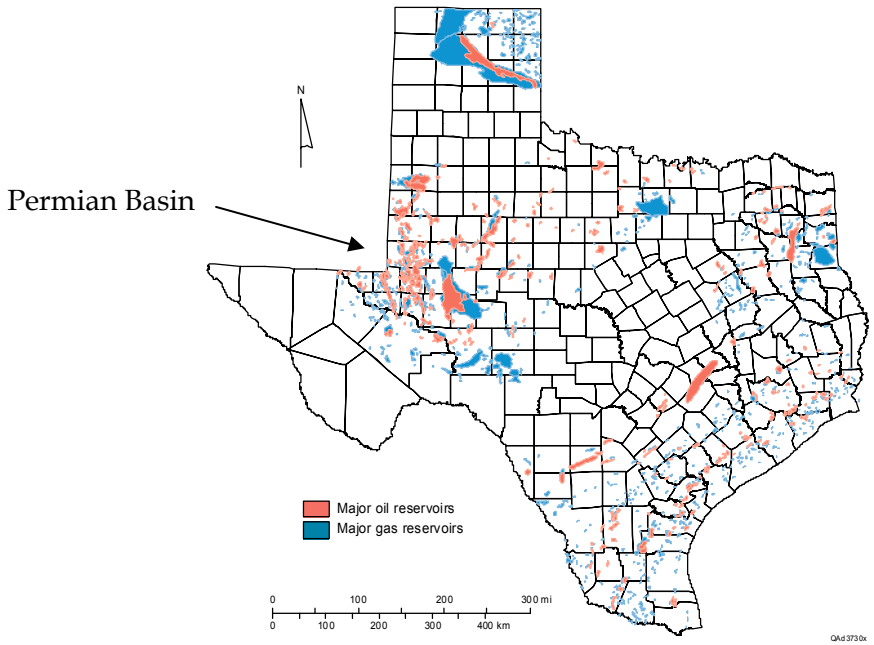

Source: Bureau of Economic Geology (BEG)
Figure 4. Map of major oil and gas fields in Texas

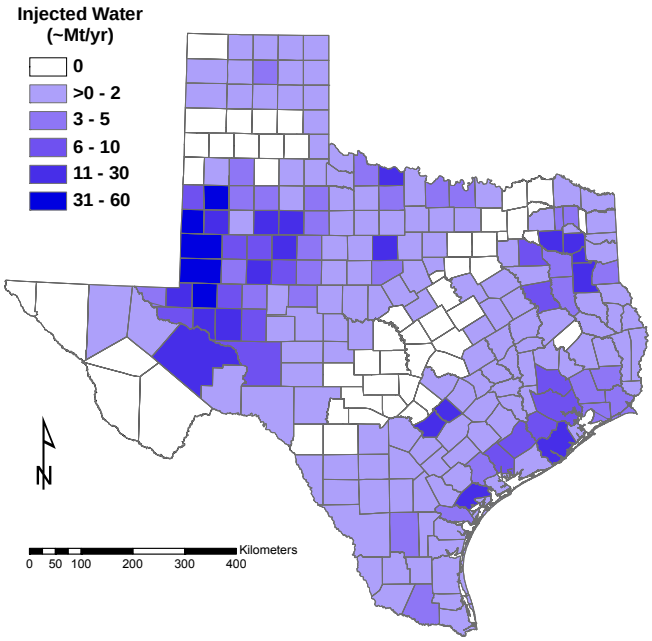

Source: RRC Website
Figure 5. Annual injected water volume per county related to oil and gas production (year 2002)

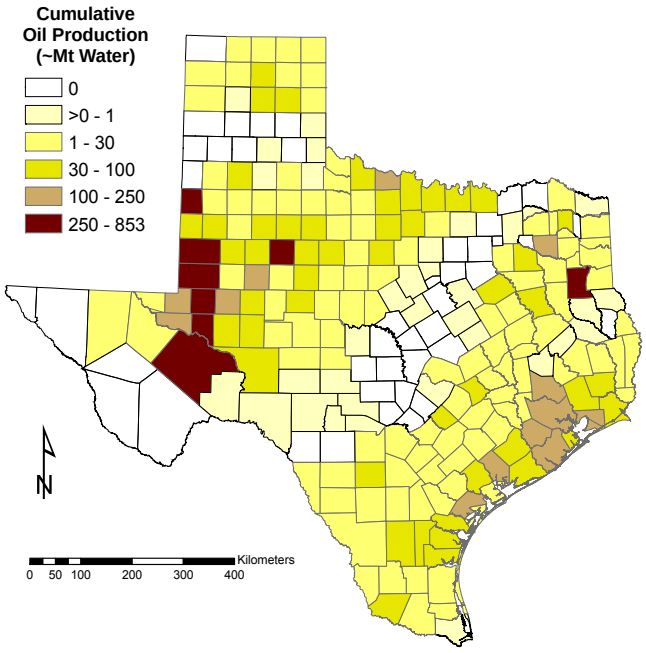

Source: RRC Website

Note: Production provided in barrels has been converted to m^3 and then equivalent million tons of water for easy comparison with CO_2 injection volumes. Volume changes from reservoir to stock tank has been neglected

Figure 6. Cumulative oil production per county

From the end of the 19th century, cumulative oil production is on the order of ~18 billion barrels (Bbbl) for RRC districts 2 through 4 (**Figure 2**) (total of 60 Bbbl in Texas). Including offshore fields, the U.S. has produced ~190 Bbbl as of 2006 (EIA Website). Given a median American Petroleum Institute (API) density of 34 in districts 2, 3, and 4—that is, a density of ~0.855—this volume can be converted to ~3 Gt of water (a total of 10 Gt in Texas; **Figure 6**). This translates into an absolute upper limit of 1.5 to 2.5 Gt of CO_2 (6 to 8 Gt in Texas) that could be injected in already discovered oil fields. Additional capacity from gas fields could be as high as 10 times this amount (Holtz, personal communication, 2006; Bergman et al., 1997). The actual capacity is likely to be much lower than that absolute upper limit of ~660 Gt, as suggested by the 98 Gt CO_2 (~140 Gt water) cited by IPCC (2005, p. 5–32) for the whole U.S.

Storage estimates in saline aquifers vary widely (1,000–56,000 Gt CO_2, IPCC, 2005, p. 5–34 & ff). The scientific community has not agreed yet on the total capacity in oil and gas fields or saline aquifers, at a world, regional, or local scale.

II.2 Storage Locations and Volumes

Previous work has already shown that the Texas Gulf Coast has a high potential for sequestering large volumes of CO_2 in saline aquifers (Hovorka et al., 2000). This section builds on the work previously done by Hovorka et al. (2004a), Doughty et al. (2004), Hovorka et al. (2004b), and Pruess et al. (2001), who relied mainly on CO_2 saturation in the pore space to access capacity. Other methods for devising capacity have also been put forward. Some studies focus on the CO_2 that can dissolve in water and assume that most of the basin will be filled with CO_2-rich brine (e.g., Bachu and Adams, 2003; Brennan and Burruss, 2003). We assume that dissolution in a large volume of the basin is a long-term process and that structural and capillary trapping are more representative of capacity. Using the former method, Dooley et al. (2006, p.17) estimated at 3,630 and 12 Gt CO_2 the U.S. capacity of saline aquifers and depleted oil and gas reservoirs, respectively.

Hovorka et al. (2004a) defined a (specific) capacity C as the volume fraction of a formation or some domain of a formation able to contain CO_2 as $C=C_iC_gC_h\phi$, where ϕ is the porosity. Parameter C_i is the intrinsic capacity function of the CO_2 saturation—in general $C_i \cong \widetilde{S}_g$, where $\widetilde{S}_g$ is some central value of the gas saturation. The geometric capacity C_g accounts for nonidealized behaviors, such as dipping formations and partially penetrating injection wells. Hovorka et al. (2004a) also defined a heterogeneity factor C_h that accounts for bypass resulting from geological variability; this factor is related to sweep efficiency. The capacity is understood as the capacity of the injection horizon (Hovorka et al., 2004a). We extend the definition to include all volumes contacted by the CO_2, and we define the total capacity CV as the sum of the formation of individual subdomains k of volume V_k, where intrinsic and geometric capacities can be assumed constant:

$$CV = \sum_k C_{ik} C_{gk} \phi_k V_k \cong \sum_k \widetilde{S}_{gk} C_{gk} \phi_k V_k$$

In this report, the target-rich Gulf Coast has been subdivided into multiple subdomains that can be grouped into three categories of increasing interest for CO_2 injection, using geological criteria (see Section III.1): (1) salt domes and the surrounding formations, whose dip will lead any injected fluid to the dome; (2) updip sections of the subdomains that may or may not be the current locus of oil and/or gas reservoirs; these sections are typically well-rich; and

(3) downdip sections of those subdomains. The geological characteristics of these subdomains have been analyzed statistically, as described later.

II.3 Acceptable Surface Leakage Rates

Acceptable surface leakage rates are related to the to-be-agreed-upon atmospheric CO_2 stabilization level (i.e., in the range of 450 to 650 ppm) and its implementation in time and space, as well as emission reduction from the primary sources. Fugitive leaks from other operational features such as pipelines and processing units should also be taken into account. Surface leakage is not necessarily equal to the leakage from the injection zones because, as will be described later, several mechanisms can capture the leaking CO_2 on its way to the surface. Gale (2004) suggested that the leakage rate should be <0.1% of the injected volume per year. IPCC (2005) stated that the fraction retained in storage is "very likely" (that is, a probability between 90 and 99%, according to IPCC definitions) to exceed 99% over 100 years (that is, leakage rate <0.01%) per year and is "likely" (probability between 66 and 90%) to exceed 99% over 1,000 years (leakage rate <0.001% per year). In a thorough analysis, Hepple and Benson (2005) put forward similar numbers and suggested that an annual surface leakage rate <0.01% would ensure effectiveness of carbon storage for all IPCC forecast scenarios (IPCC, 2000) but that an annual surface leakage rate of 0.1% would still be acceptable. Global injection operations will not last forever; the injection time frame could be ~ 1 century (e.g., Caldeira et al., 2004), the time to transition to a mostly carbon-free energy source. Others have proposed longer time frames—1,000 to 10,000 years (e.g., Brennan and Burruss, 2003).

A few groups have tentatively computed leakage from specific sites. At Weyburn, Monitor Scientific (2005, GWPC Portland conference; Strutt et al., 2002) estimated that the cumulative leakage rate in 5,000 years through the ~1,000 wells contacted by the EOR would be 0.03 Mt (0.14% of the 20 Mt CO_2 in place). Oldenburg and Unger (2003) presented simulations of CO_2 surface fluxes assuming leakage rates at the base of the unsaturated zone. Oldenburg et al. (2002) noted that a large storage site of 200 Mt of CO_2 *uniformly* leaking 1% of the initial stored amount per year would produce a flux smaller than natural fluxes due to plant metabolism, whereas leakage focused on a fault could be much higher. NGCAS Forties oil field, in the North Sea, was also studied extensively, and leakage was estimated to be negligible. IPCC (2005, Chapter 5) referenced studies suggesting that leakage is small: ignoring abandoned wells, the Forties oil field in the North Sea will experience no more than a 0.2% loss of stored CO_2 from the

injection formation after 1,000 years, whereas modeling of Sleipner field, also in the North Sea, suggested that no CO_2 will reach the seafloor before 100,000 years. As a matter of comparison, natural fluxes have also been estimated. Mörner and Etiope (2002) presented natural CO_2 fluxes from a variety of environments, in particular, active tectonic areas. The value spread is large but mostly within 0.01 to 1 Mt CO_2/yr (their Tables 1b and 2a), with corresponding fluxes in the 0.1 to 10 Mt CO_2/yr/km^2 range. In the course of the CO_2 EOR flood at Rangely, Colorado (Klusman, 2003a), 23 Mt of CO_2 was stored between 1986 and 2003. Leakage at the surface minus the biological signal has been calculated to be less than 0.0038 Mt/yr over 78 km^2 (~0.13 g/m^2/d) and more likely ~0.00017 Mt/yr (determined by using isotopes). The biological signal is estimated at 3.8 g/m^2/d (summer) and 0.23-0.33 g/m^2/d (winter). Natural fluxes typically vary from ~4 to thousands of g/m^2/d, but most likely in the 10 to 100 g/m^2/d range. Natural background soil fluxes at CO_2 EOR, Weyburn, Canada, were reported at 12.7 g/m^2/d (2002) and 68.8 g/m^2/day (2001) (Strutt et al., 2002); there is so far no evidence of diffuse gas leakage.

III. Leakage Pathways

A risk assessment study starts off with a compilation of the hazards associated with a process (Step 1: identify hazards). It then calculates its likelihood (Step 2: determine probability distribution of hazard) and researches its consequences and magnitude of the consequences (Step 3: consequence evaluation). Important Step 4 consists of the uncertainty analysis (Rechard, 1999). If, in layman's terms, risk of a particular event often equates with the consequences of that event, a more scientific approach defines risk as a function of both probability and consequences. An approach typically taken in risk analysis of industrial and/or engineered systems (e.g., power plant, industrial site, space shuttle) consists of building a fault tree, which is a mapping of a succession of events and determining the ultimate probability of the consequences of the primary event. However, natural systems hold extreme uncertainty relative to their human-made counterparts, and the approach is not necessarily feasible in the field of CO_2 subsurface storage.

In this section we assume that the operational risks have been fully addressed—that is, that the injection horizon has been carefully chosen to maximize the sweeping area, that the number of wells and their locations have been well engineered to avoid seal overpressure and potential subsequent fracturing, and that the subsurface has been sufficiently characterized and sited away from large faults (at least those located updip). We focus more on determining hazards and their probability rather than on estimating their consequences.

An important body of work is available on specific aspects of CO_2 storage risk (well leakage, health and safety aspects at the surface near a storage site, etc.). This is an active field of research with several workshops organized and proceedings and reports published every year. Several international groups have been developing guidelines and analyses related to risk. The International Energy Agency Greenhouse Gas (IEA GHG) R&D program, funded by multiple countries and private sector sponsors, developed the most comprehensive risk study to date in analyzing the Weyburn project in detail (Wilson and Monea, 2004). The European Union-funded SACS project and the CO_2 Capture Project (CCP), whose goal was to monitor the Sleipner project, focused more on monitoring than on the risk aspects. Another North Sea reservoir (the Forties) underwent a qualitative risk analysis (e.g., Ketzer et al., 2005). Other sites (in Salah, Algeria, and Snöhvit, Norway) may undergo risk analysis. However, all sites studied in some detail are oil reservoirs under CO_2 flood, and there has been, so far, no detailed risk

analysis of saline aquifers. Most national organizations or programs have also shown a strong interest in risk assessment: GEODISC in Australia (Bowden and Rigg, 2004), TNO in The Netherlands, and SINTEF in Norway.

The CO_2 storage community is also very active in building and developing tools to model risks and their consequences using off-the-shelf software—for example, Goldsim (e.g., Pawar et al., 2006, at Los Alamos National Laboratory), Crystal Ball® (Walton et al., 2004)—or dedicated software—for example, CQUESTRA (Walton et al., 2004, LeNeveu et al., 2006). Software models are also being developed specifically to handle carbon storage at Idaho National Laboratory and PNNL.

The FEP approach used for high-level radioactive waste disposal may be extremely useful in developing a comprehensive list of potential issues that need to be considered in permitting geologic sequestration of CO_2. However, the user of FEP approach should be careful in not being lost in cataloging numerous very improbable events. At least two organizations have developed FEP databases: the Dutch TNO-NITG, supported by the CO_2 Capture Project, and Quintessa, a private sector company, supported by the Weyburn Project. Other projects have also been through a more informal process.

CO_2 can leak as supercritical fluid (buoyant and less dense than surrounding fluids) and then as gas in the saturated zone, but also in the unsaturated zone and in the atmosphere (denser than surrounding fluid, mostly air). It can also leak as CO_2-saturated brine that will outgas near the surface, where the confining pressure is lower. It is generally recognized that there are two main avenues for sudden, possibly high-rate, and catastrophic leakage: wells and faults (e.g., IPCC, 2005). They can also be effective at releasing CO_2 at a low rate. A third pathway, spill point from closed traps, is considered less risk-prone because it includes built-in safeguards. For example, the longer the path to the surface/shallow subsurface, the more capillary trapping will take place. Hence, the focus of this section is to describe and quantify wells, faults, and spill points in the Gulf Coast area as a template for possible studies elsewhere.

III.1 Conceptual Model for the Creation of Subdomains

An overview of the geology of the Gulf Coast is given in Appendix A. The main points pertinent to this section's discussion are: (1) there are thick layers of alternating "sand" and "shale," with a fraction of the latter and the total formation thickness increasing gulfward; (2) the layers are compartmentalized by both growth faults, with strike approximately parallel

to the shore, and whose dip flattens gulfward and radial faults form slowly raising salt domes; and (3) fault movement and other processes have created rollover anticlines and other structural traps for buoyant fluid (e.g., **Figure 7** and **Figure 8**). The charging process can be conceptualized as described in **Figure 9**, and it can be applied to CO_2 migration (as will be described in **Figure 12** below).

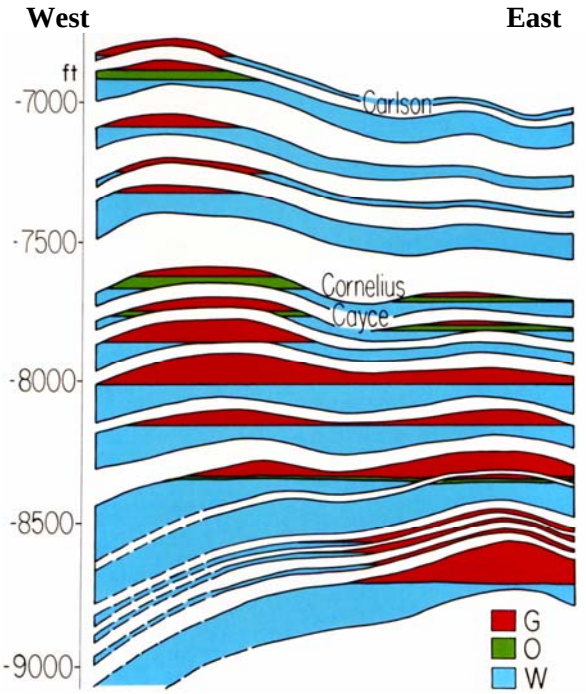

Source: Tyler and Ambrose (1985)

Note: This is a very large gas play with some large oil reservoirs (Carlson, Cornelius, Cayce). It represents a common type of trap in the Gulf Coast.

Figure 7. West-east strike-oriented cross section of the double-crested rollover anticline that forms Markham North-Bay City North field in Matagorda County, Texas

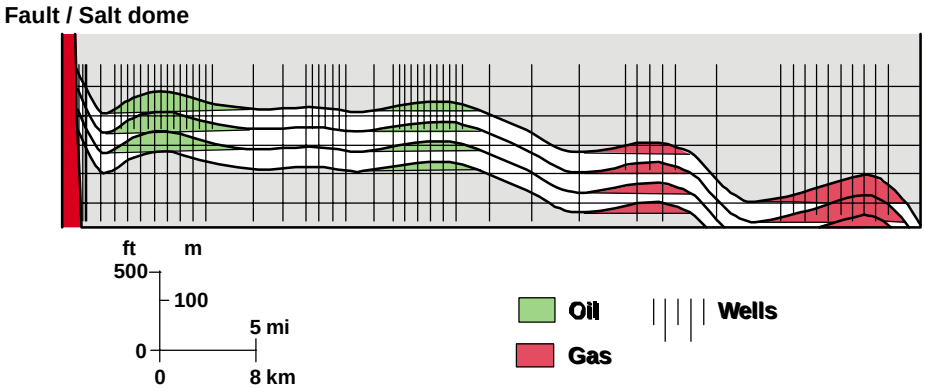

Note: Well density is higher in traps. Natural gas often accumulates downdip because it is generated last and displaces oil previously present in the trap

Figure 8. Cartoon of hydrocarbon accumulation in the Texas Gulf Coast

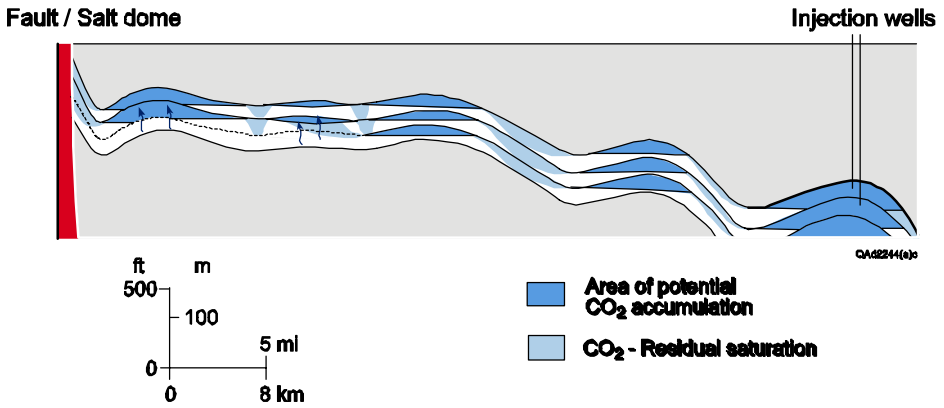

Note: Both closed traps, where water is at residual saturation, and open traps, where CO_2 is at residual saturation, are shown.

Figure 9. CO_2 travelpath and trapping mechanisms

This buoyant migration leads to the description of two types of traps: closed traps, where water is at residual saturation and CO_2 occupies the remainder of the pore space, and open traps, where CO_2 is at residual saturation and where water can flow freely.

Closed Traps

Despite a general gentle dip toward the Gulf of Mexico, local geometry of the layers does include numerous structural traps (e.g., Galloway et al., 1983; Kosters et al., 1989), owing to the activity of growth faults and radial faults around salt domes and to the deformation near diapirs. Hydrocarbon traps represent good analogs for closed CO_2 traps. They occur in areas where these sediments have been tilted or deformed within anticlinal structures bounded by growth faults. Deformation of strata above the kilometer-thick Jurassic Louann salt layer has resulted in a contrast in types of structural traps. In the northern section of the Texas Gulf Coast, salt movement has been focused around piercement diapirs, resulting in numerous and complex traps associated with locally steeply dipping strata. Farther south, regionally aligned reservoirs in the Corpus Christi area are more commonly created by structural and stratigraphic traps along the downthrow of growth faults. This contrast in trap style is visible on a map of oil and gas well surface locations (Galloway et al., 1983; Tyler et al., 1984, p.31; Kosters et al., 1989), which are clustered around salt domes in the Houston area and more spread out elsewhere (**Figure 10**).

Open Traps

Within the range of buoyancy of most hydrocarbons (more than oil, less than gas), CO_2 will also follow similar pathways and accumulate in similar traps, as described in the previous

section. However, if the injected volume is larger than the capacity of the first encountered trap, CO_2 will continue to flow upward until it reaches another trap, leaving behind a trail at residual saturation (**Figure 9**). It follows that closed traps are charged with CO_2, with water at residual saturation, whereas open traps consist of the trail of the CO_2 plume at residual saturation. Relying on capillary trapping will work well if the two other avenues for leakage, wells and faults, can be shown to impact the behavior of the storage site only minimally. Capacity of an open trap depends on the heterogeneity of the injection formation and on that of the overlying layers (**Figure 11**). Potential subsurface storage sites in sedimentary basins fall into a large range of geological heterogeneity, and the Gulf Coast is rather heterogeneous by those standards.

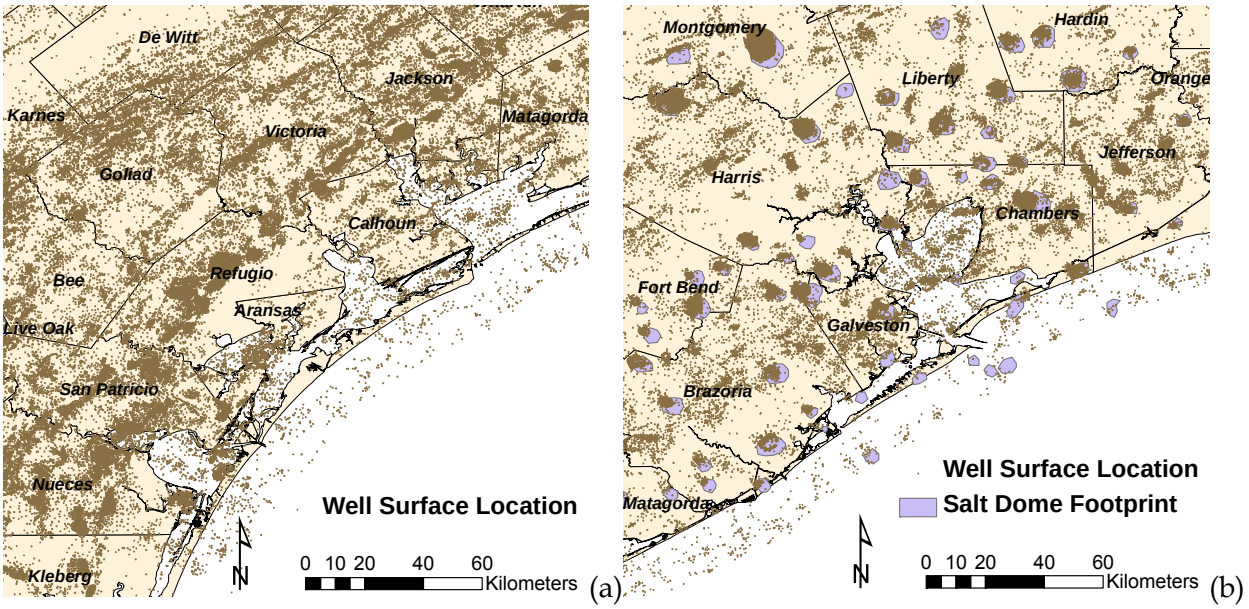

Source: RRC digital map data

Note: Note the contrast in style between the Houston area, where a significant fraction of wells and hydrocarbon traps are related to salt domes, and the Corpus Christi-Victoria area, where salt domes are deeper or nonexistent. More than 100,000 well locations are displayed.

Figure 10. Surface well location in the (a) Corpus Christi-Victoria and (b) Houston areas

Application to Selected Area of the Gulf Coast

In order to estimate capacity from open and closed traps, we collected and interpreted data from Geomap (http://www.geomap.com) structural maps for the upper Gulf Coast. As an example, we used the top of the Frio Formation. Multiple similar maps can be produced for the main formations of the Gulf Coast, with variations from the example presented both because of faults tapering off with depth and toward the surface and because of the increased impact of salt domes with depth. We divided the top Frio structure into "drainage basins"

under conditions of buoyant flow. We digitized the outlines of these drainage basins and the area of structural closure on the structural trap within the drainage basin. We also measured the throw on faults that compartmentalize the region. Areas with likely higher-than-background risk of leakage, including oil fields characterized by closely spaced wells, and highly complex zones around salt domes were also digitized. From this database, we could create a probabilistic model for the geologic features that CO_2 would encounter when it is released from a well in any location. The database can also be used in a deterministic sense to assess capacity of the subsurface from a given location. **Figure 11** shows CO_2 being released at a well, traveling across a drainage basin to accumulate in a structural trap, exceeding the storage capacity of that trap, and spilling into the next basin, where the process is repeated. Capacity can be calculated by summing the trapping mechanisms along this flow path, which include CO_2 trapped by capillary processes as residual saturation, dissolved CO_2, and CO_2 trapped in structural traps.

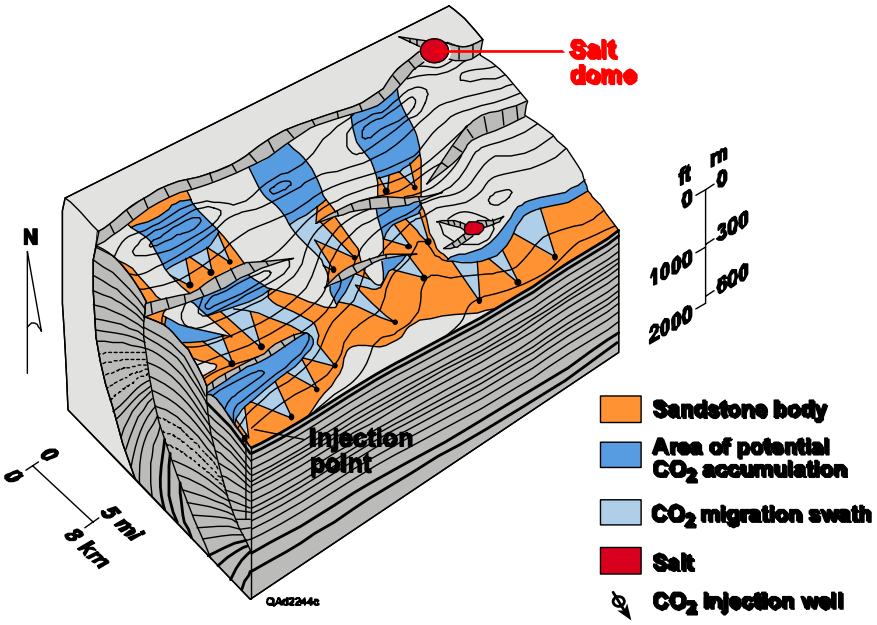

Note: Sand bodies are typically fluvial channels or deltaic accumulations. CO_2 migrating upward fills up closed traps and leaves a trail at residual saturation between them. Closed traps are often well expressed next to a growth fault (visible on the vertical panel of the block diagram).

Figure 11. Example of CO_2 migration in a typical Gulf Coast setting

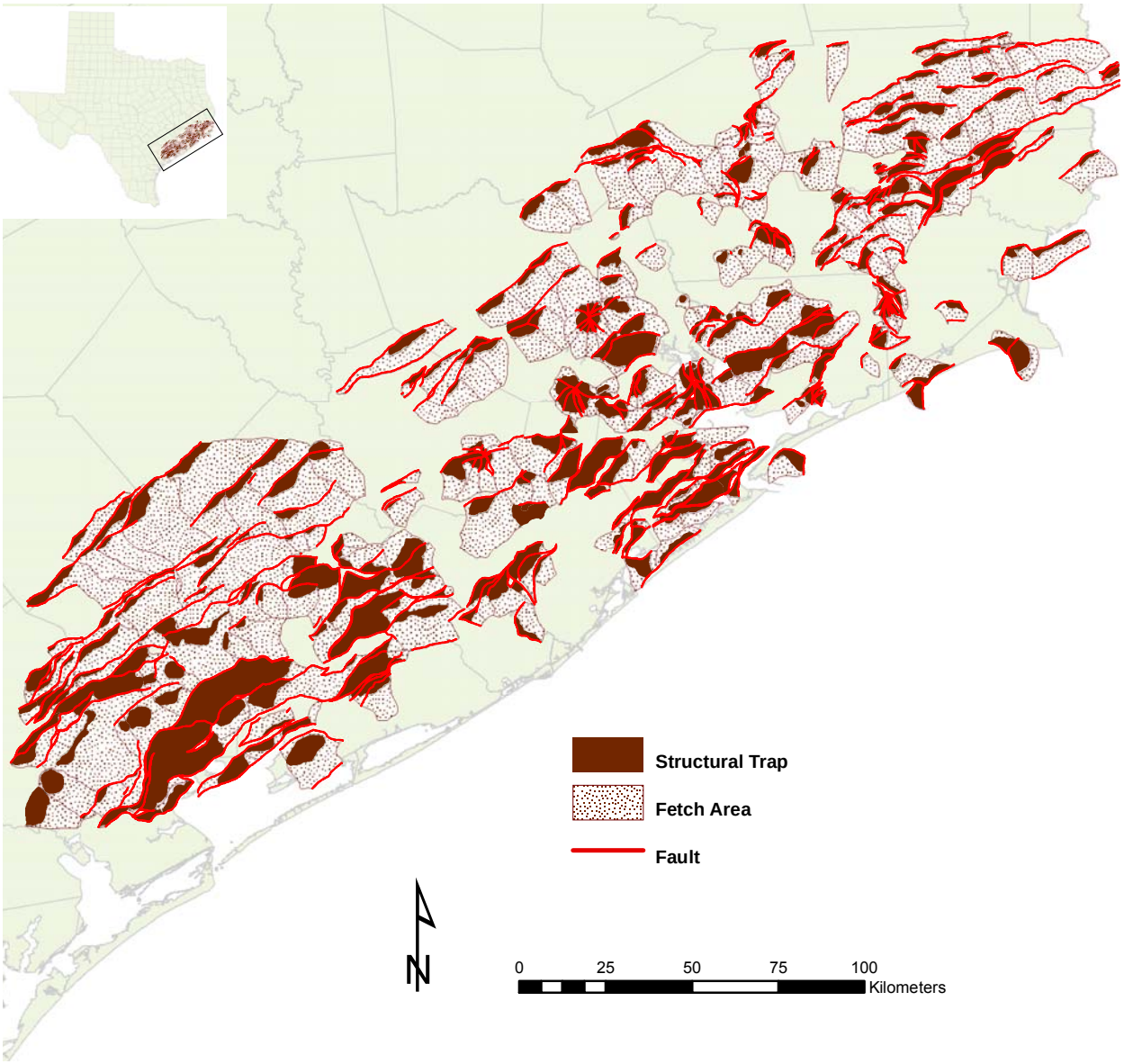

Note: Closed structural traps abut growth faults, whereas each open trap ("fetch area") is located downdip of the associated closed trap (more than one fetch area can lead to a single closed trap). Areas left in background color eventually lead to a salt diapir and are not primary targets for CO_2 injection.

Figure 12. CO_2 trapping on top of the Frio or equivalently beneath the base of the regional seal (Anahuac Shale)

Actual mapping of the structural traps on top of the Frio Formation (**Figure 12**) clearly shows the impact of growth faults on the location of the traps. A total of slightly more than 400 coupled fetch/closure areas are represented over an area of ~40,000 km² (~16,500 mi²). A statistical analysis of the data will be done in a later section, but about half of the study area is left in the background color because any injected buoyant fluid particle will ultimately reach a

salt dome (salt domes are structurally complex and not likely the first choice for large injection operations). The presence of deep salt domes generates a bulge in the top of the Frio Formation, as evidenced by some radial features visible on the map. Approximately 15% of the area (~6,000 km^2) corresponds to structural traps, whereas about 35% (~14,000 km^2) corresponds to the downdip fetch areas leading to the traps.

III.2 Well Leakage

This work does not focus on future injection wells whose construction characteristics will be tailored to CO_2 storage. Their safeguards are assumed sufficient to make their potential leakage small when compared with that of older wells. Again, the concern with well leakage is not so much with CO_2 injection wells or future wells that can be outfitted to resist CO_2 attacks, than it is with the abundance of older wells in parts of the world, including Texas. This section attempts to describe well leakage as it applies to the Texas Gulf Coast. Leakage through well-punctured seals has been a concern since the onset of enhanced oil recovery. A worldwide well density map (**Figure 13**) suggests that the problem is most acute in the Western Gulf Coast (mainly Texas), the Permian Basin (again, mainly Texas), and the Alberta Basin, where the well density is higher than 2.3 wells/km^2. There are also other smaller areas of concern in the U.S. The very fact that the Texas Gulf Coast is an oil-rich province makes it attractive for CO_2 sequestration (abundance of seals and traps). However, it also brings the inconvenience, from an integrity standpoint, of multiple perforations. It is true that these formations contained oil and gas for millions of years with negligible leaks (see Appendix A for more details), but they had not yet been punctured by millions of direct conduits between the subsurface and the ground surface. The well density on the Texas Gulf Coast is ~4 wells/km^2, but it is not uniform (**Figure 10**) and it is obviously concentrated in areas with traps and hydrocarbons. Salt domes have a particularly high well density, sometimes reaching a few hundreds of wells per square kilometer. Compare this figure with the reported average value of 4 wells/km^2 in Gasda et al. (2004) for the Alberta Basin. Spatial well density is related to hydrocarbon accumulation volume but also to formation permeability and to number of stacked productive formations. A typical lease size of 40 acres (0.162 km^2) will have one production well for a particular reservoir, but the piece of land could host more wells, all tapping different reservoirs.

Three main variables relate to well leakage: well density (how many wells per unit area?), well depth (how deep is the well and in which formations are the completion intervals?),

and well age (an older well is more likely to experience leaks because environmental rules have become progressively stricter in the 20th century). Inadvertent intrusion when a well is drilled in the formation tens to hundreds of years after CO_2 emplacement is not considered. The assumption that a CO_2 injection well will be built or retrofitted to very strong and durable standards and will not be a leakage source even in the long term is reasonable but possibly wrong. Smith (1993, p.5) reported that more than 3 million wells have been drilled in the U.S. for oil and gas exploration and production, one-third of them in Texas. He also stated that there are more than 14 million active water wells and most likely many more abandoned ones. An interesting issue that we will not be able to solve in this report is whether recent wells are truly more CO_2-leakage resistant than older wells in the long run.

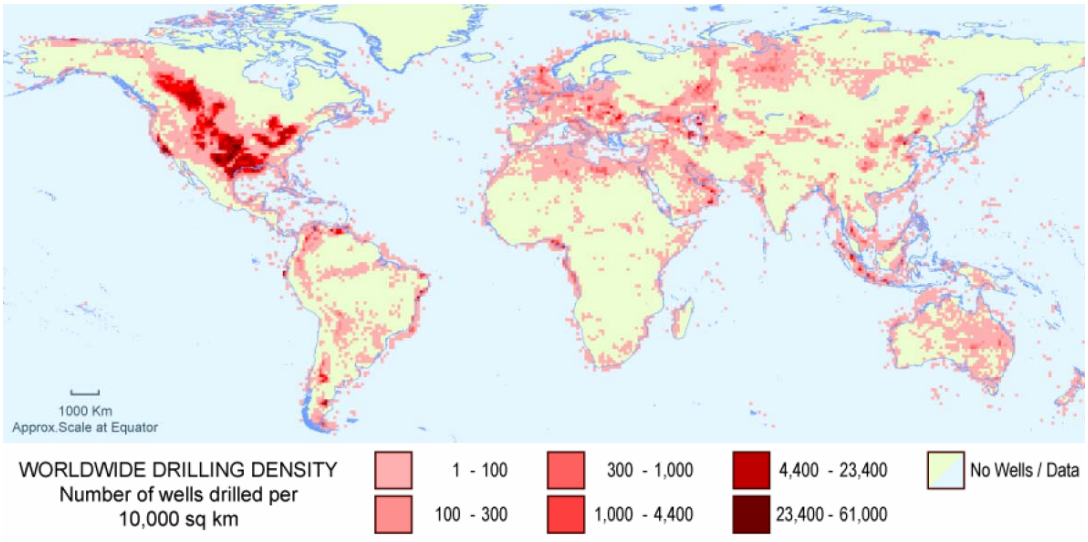

Source: IPCC (2005, Figure 5.27)
Figure 13. Worldwide well density map

III.2.1 Introduction

Texas has a long history of hydrocarbon production. The first successful oil well drilling occurred in the East Texas Basin at Oil Springs near Nacogdoches in 1866. The first major discovery followed in 1894 with the Corsicana field, still in the East Texas Basin. A few years later, hundreds of wells in the area produced most of the state's production (~0.07MMbbl/yr). The discovery of Spindletop field in the upper Gulf Coast Basin, at the edge of Beaumont, near the Louisiana state line, launched the modern age of hydrocarbon production in Texas (18 MMbbl/yr in 1902). Many other fields were discovered in the upper Gulf Coast Basin in that same decade, mainly on salt dome structures, which was the focus of exploration at that time in the wake of the Spindletop salt dome discovery. Smaller discoveries were also made in South

Texas in the lower Gulf Coast Basin. Then oil production extended to the Fort Worth Basin around Wichita Falls, north of Dallas. In the twenties more fields were discovered in those same basins, as well as in the Texas Panhandle and West Texas. In the thirties, a map of the oil and gas producing areas would have looked similar to that of today. Events following the discovery of the supergiant East Texas field in the East Texas Basin led to an awakening by the State of a need for State-enforced rules to regulate the oil and gas industry. Consequently, it was not before the early thirties that the RRC was truly able to implement rules concerning well density and, a matter of concern in this study, well abandonment. By then, hundreds of thousands of wells had already been drilled and abandoned. In 1936, there were, in Texas, a total of ~70,000 wells producing mainly oil (419 MMbbl/yr). As of the end of 2003, there were ~150,000 and 70,000 wells producing mainly 357 MMbbl/yr of oil and 5.67 Tcf of gas, respectively (RRC Website). In addition, there were ~30,000 injection wells, 35,000 service wells and ~110,000 administratively inactive wells. Count plots, such as **Figure 14**, helps explain the well population through time. Gas production is not too sensitive to world events because of its mainly regional markets, as demonstrated by the lack of deviation from a slow growth trend. On the other hand, oil production responds strongly to world events: a slight slump in growth at the end of WWII (A), and then a steady growth in the fifties and sixties (B), interrupted in 1971 by the decision of the RRC to lift production limits that led to a decrease in oil prices (C). A strong recovery (D), owing to higher prices at the time of the oil embargo of 1973 and the Iraq-Iran war (1980–1988), and a sharp drop (E) due to a later collapse of oil prices in 1986 are eventually followed by the slow production decrease, with minor peaks, of mature basins (F).

III.2.2 Historical Look at Well Technology and Regulations

Risk of leakage through abandoned wells is a function of the rules, both toward drilling and abandonment, enforced at the time of plugging (if any); of the care expressed by the operator during the plugging operation; and of the materials used in the plugging operation. Plugs serve two purposes: (1) to isolate and prevent fresh water or other resources to drain and (2) to prevent cross-contamination. Because leakage is most likely to occur through wells drilled and abandoned early in the production history of a basin, a look at the history of plugging and its techniques is warranted. Wells consist of a succession of casings having different diameters that are introduced in a borehole. The most common configuration includes a surface casing, running from the surface to some depth, in general below the base of the USDW, and a

production casing running from the shoe of the surface casing to the formation of interest. The surface casing's main role is to protect fresh water from contamination of fluids. Typically, a surface casing is not required for shallower wells, at least in Texas, if the production casing is cemented from the shoe to the ground surface. Historically, the trend of these rules had been toward a greater protection of the hydrocarbon resource, but also of the shallow aquifers, potential sources of drinking water. Warner (1996, p.11) noted that until the 1970s, the surface casing was meant to protect water resources with a total dissolved solids (TDS) (<3,000 mg/L) lower than the current limit (10,000 mg/L).

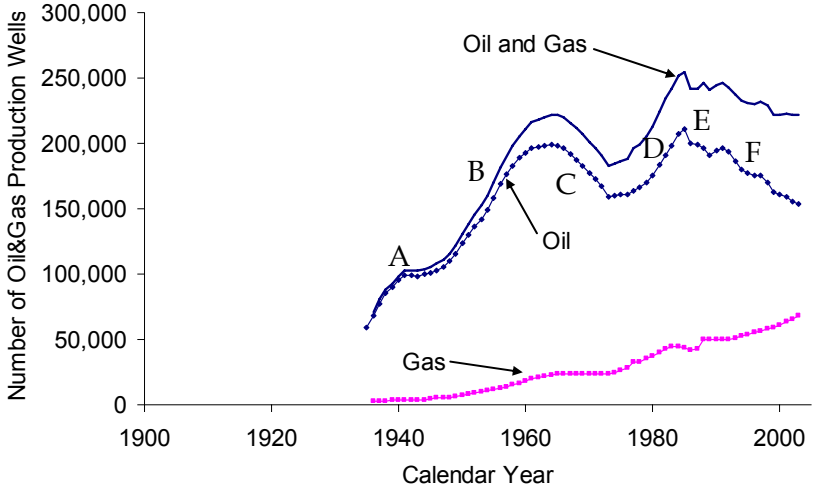

Source: RRC Website
Note: Service wells (including injection wells) and dry holes not included; explanation for letters in text
Figure 14. Oil and gas production well count in Texas through time

As described below, examination of the rules leads to the grouping of wells into four time categories according to their abandonment year: post-1983, 1983–1967, 1967–1935, and pre-1935. Relative to the protection of fresh water, watershed years are 1934, 1967, and 1983. These categories are justified by the following events. In 1934, the RRC promulgated specific plugging instructions, and did so again in 1967. Another important period not captured in the category breakdown is the then-recent widespread use of improved cement additives in 1953, following standardization by the API. Improvement of the quality of material used in well construction and abandonment led to an overall improvement of well abandonment. However, enforcement was still an issue. Another incremental quality improvement in well abandonment occurred in 1983 because of increased scrutiny by the State. However, as Ide et al. (2006) suggested, many

wells could have been left unplugged in 1986 after many companies became bankrupt (peak E in **Figure 14**), overwhelming agency enforcement staff. Targeted studies on hundreds of West Texas (Warner et al., 1997) and Gulf Coast (Warner et al., 1996) wells also suggest that natural breaks relative to the quality of plugging were 1967 and 1983. Johnston and Knape (1986) stated than there is a high probability that wells abandoned after 1967 are properly plugged.

There is plenty of anecdotal evidence that well abandonment was not executed in the spirit of the regulations until recently. Out of 19 penetrations in the area of review of the new well drilled for limited CO_2 injection at the Frio site, only three had been plugged with cement below the lowermost USDW. Most of these wells had been drilled in the 1950s and plugged in the 1970s (Hovorka et al., 2004b, p. 125).

III.2.2.1 Well Construction and Abandonment Rules

In the 19th and early 20th centuries, the Texas state legislature passed a few laws aimed at conserving oil and gas and at protecting producing formations (**Table 3**). In 1919, Senate Bill 350 set down general plugging rules. They were little observed or enforced (RRC Website). Regulation did not start to take hold before the 1930s, after the discovery of the super-giant East Texas oil field and subsequent events. Before that time, little thought was given to well abandonment, and wooden plugs, if any, were common (Smith, 1993, p. 8). The year 1934 saw the first specific plugging rules, which required the producing formation to be plugged with recirculated cement. One of the methods used was the balance method, which involved injecting cement slurry through the inside of a pipe until cement level outside and inside the pipe were the same. The pipe was then removed. In the two-plug method, two plugs that isolated the cement slurry were run. The two-plug method is superior to the balanced method, which is in turn superior to the bailer method. A previously widespread method, which led to many problems, was to bail cement slurry behind the pipe. Other formations, such as water-bearing formations, could be plugged with mud-laden fluids. In 1957, protection of fresh water was made a requirement. However, records, if any, are often missing, and it cannot be assumed that abandonment was done properly. Pervasive problems created by previous poor abandonment techniques led to the creation by the RRC of "Well Plugging Funds" in 1965. As of 2005, the program had plugged over 20,000 wells. The years 1966–1967 represent a second milestone in the history of protection of the drinking water resource because of improved regulations on surface casing. The RRC (2000, p.2) stated that an average of $4,500/well was

needed to plug wells (from 1984 through 1999, the RRC had plugged 15,169 wells at a cost of ~$66 million (RRC, 2000, p.5) and was doing it at a rate of more than 1,000 wells/yr (1,218 in 2004), including 50 to 150 priority I (actively leaking) wells per year. It is funded by revenue collected from the oil and gas industry. As of 2000, there were, across Texas, more than 25,000 delinquent shut-in wells (that is, not active but not abandoned). As of end of 2005, the RRC estimates that there were 15,000 orphaned wells (that is, with no owner to turn to in case of problems) in Texas.

Prior to the 1930s, cable tool drilling with no need for drilling fluid was mainly used. Crude rotary drilling rigs appeared in the 1930s. Considerable progress was then made in the 1940s because of the war effort, and most post-1940 wells have been drilled using this technology, allowing greater depths to be reached. Initially water mixed with cuttings made up the drilling fluid and early on, bentonite and barite were added to improve mud stability and increase mud weight (Johnston and Knape, 1986). The industry then transitioned to the complex and sophisticated drilling muds used nowadays.

Table 3. Milestones for well construction and abandonment in Texas

Date		Well Construction/Abandonment
1866		*First producing Texas well drilled at Melrose, Nacogdoches County*
1891		*RRC founded to oversee railroads*
1899		*Legislature enacted H.B. No.167, "An Act to Provide for the Inspection of Refined Oils Which Are the Product of Petroleum, and Which May Be Used for Illuminating Purposes Within This State, and to Regulate the Sale and Use Thereof, and to Provide Penalties for the Violation of Same."*
1899	S	H.B. 542 $100 fine for failure to plug wells according to statutes, but RRC had no enforcement authority
1901		*First salt dome discovery, and first great gusher brought in at Spindletop, Jefferson County*
1905	S	Legislature amended Act of March 29, 1899, declaring an emergency pertaining to regulations of the drilling, operation, and abandonment of oil, gas, and water wells.
1917		*Legislature declared pipelines to be common carriers and gave RRC jurisdiction over same. This was the first act to designate the RRC as the agency to administer the laws relating to oil and gas.*
1919	S	RRC adopted first Statewide Rule regulating the oil and gas industry. RRC Oil and Gas Division created S.B. 350 about plugging rules. "All dry or abandoned wells must be plugged by confining all oil, gas or water to the strata in which they occur by the use of mud-laden fluid" and a $5,000 fine for failure to do so
1934	S	Specific plugging instructions issued (cement was required to be circulated through tubing or drill pipe across producing formations; nonproducing formations could be plugged with mud-laden fluid if no high-pressure sands were encountered).
1940s		*Transition from cable-tool frilling rig to rotary drilling rigs*
1951		*Legislature authorized the RRC to plug improperly capped oil wells that were flowing salt water into the Frio River, McMullen County*
1955	S	RRC adopted Statewide Rule 55, regarding fresh-water pollution abatement, including

Date		Well Construction/Abandonment
		for wildcat operations
1957	S	Protection of fresh-water sands (early version of "surface casing" requirement) was made a requirement
1950s		*Records often missing; cannot assume abandonment was done properly*
1965	S	Legislature enacted the Well Plugging Statute, placing a duty on the operator, nonoperator, and landowner to plug abandoned oil and gas wells or dry holes and a duty on the Commission to determine whether wells were properly plugged; and the act also gave to the State a cause of action if the Commission plugged the wells and also authorized the Commission to accept money to properly plug wells (general fund).
1966-1967	S	RRC Special Order No. 20-56,535 contained many of the current well plugging requirements (Statewide Rule 14 "Plugging"). - Cement emplaced with the circulation method - 10-ft cement plug on top of the well - 100-ft cement plug placed above uppermost perforated horizon - If production casing was removed (or not installed), 100-ft cement plug centered on the surface casing shoe should be installed; same on fresh-water formations located below the surface casing but initially protected by the production casing
1974	F	Safe Drinking Water Act
1976	S	Statewide rules 13 "Casing, Cementing, Drilling, and Completion Requirements" and 14 "Plugging" were initially promulgated; multiple amendments followed.
1980	S	RRC amended section pertaining to plugging wells. Plugging operations on each dry or inactive well must be commenced within a period of 90 days after drilling or production operations have ceased and must be pursued with diligence until completed.
1980	F	UIC Regulations promulgated (Federal)
1981	S	H.B. 1379 gave RRC comprehensive authority to regulate underground injection activities
1983	S	Amendments were made to Statewide Rule 13 "Casing, Cementing, Drilling, and Completion Requirements," detailing technical requirements for the casing and cementing of oil, gas, and other wells subject to the RRC jurisdiction. Rules were made more specific: Only approved cementers can perform cementing operations
1983		*Well Plugging Fund supported by fees on new wells and penalties instead of general fund*
1985		*House Bil1 2431 required filing with the RRC a copy of each electric log made after September 1, 1985, in conjunction with the drilling of a well.*
1988	S	Statewide Rule 14 "Plugging" was amended to make permanent the provision that dry or inactive wells have up to 1 year before plugging must begin.
1991		*Well Plugging Fund replaced by Oil Field Cleanup Fund (OFCU Fund) (State)*
1993		*RRC approved a well-plugging priority system that included additional environmental, wildlife, and human health factors.*

Italics: event related to oil and gas production history
S = State; F = Federal legislation
Source: RRC (2000), Warner (2001), and RRC Web pages
(http://www.rrc.state.tx.us/history/history/hist.html)

III.2.2.2 Material Quality

Three types of material—cement, mud, and steel—need to be examined in the light of their resistance to corrosion, both under "natural" conditions and in the presence of CO_2. Prior to 1928, the cementing industry manufactured only one type of material for well cementing (Montgomery and Smith, 1959, p. 13; Smith, 1976, p. 3). In 1940, there were two types of

Portland cement (Smith, 1976, p. 2) and three additives. That same year, bulk cementing was introduced. Before, only sacks were used. Since then, API has devised several classes of cement for different well conditions (pressure, temperature, and chemical conditions, in particular, resistance to sulfate attack). Starting in the late 1940s, the number of additives available on the market progressively grew. The API published for the first time in 1953 national standards on cements for use in wells (Smith, 1976, p.7). Operators were then able to tackle more difficult cementing jobs and ensure a better cement placement. Still, the rules in place were not fully followed and/or enforced. Nowadays, multiple additives are available for custom jobs. Cement can shrink (most common) or expand during curing, depending on the additives (typically sulfate based). Shrinkage is a function of the availability of water and can be between 0.5 and 5% (Baumgarte et al., 1999).

Regulations called for mud-filled sections between cement plugs, and rotary-drilled dry holes without proper plugging records can be assumed to have been left mud filled because there is no economic incentive to recover the mud (Johnston and Knape, 1986). Attention to mud is most relevant to older dry holes. Water-based muds could include clay minerals, lime, gypsum and other additives in variable proportions. Gel strength of water-based mud increases indefinitely with time at a fast rate first, and then more and more slowly, but the gel becomes denser with time (filtration loss into adjacent formation) or it will break down into pockets of filtercake and fluid (Johnston and Knape, 1986, p. 97) and could lose its barrier effect. Bentonite muds do not solidify and stay in a liquid state, whereas lime and gypsum muds could solidify (Johnston and Knape, 1986, p.90). Currently, water-based drilling muds are used from the surface to depths of ~1,500 m (~5,000 ft), after which depth, oil-based drilling fluids are used. After drilling, the well bore is filled with a completion fluid, generally a brine.

Although sometimes protected from ambient liquids by scale, the degradation rate of casing, typically made of carbon steel, is high in wet environments containing CO_2. Metals tend to degrade faster in acidic conditions. Corrosion could also be slowed because of the buffer effect of limestone, carbonate clasts, and calcite. IPCC (2005, Chapter 4) suggested 0.7 mm/yr from experiments on coupons. In any case, the installed well materials have been chosen and designed to withstand production and related processes only for the life expectancy of a field—that is, optimistically, for 50 years. Although they can last longer, as supported by anecdotal evidence from the Frio experiment where a well from the 1950s was in good shape when

reentered, how the materials will behave in a CO_2-rich environment is still an open and debated question.

III.2.2.3 Quality Assurance during Well Operations

The current common prevalence of cement bond logs and tools shows that adequate cement interface with the formation on one side and the tubing on the other side is still a problem. It is particularly a problem when a well is readied for production, and it also occurs during plugging and abandonment, especially in slanted wells. Often the problem does not lie in the quality of the material used but in the quality of the plugging/abandonment performance. Smith (1976, p. 3) mentioned that a 1928 study on Gulf Coast cores that suggests that those deep wells of the time (>610 m [>2,000 ft]) show a high failure rate, often due to mud contamination. Heathman et al. (1994) noted that problems prevalent in the 1930s were still common in the 1990s. Primary causes of failure identified in their study include poor mud removal (most common), unstable cement slurries, insufficient slurry volume, and poor job execution.

Mud contamination is the most common failure mode. The two-plug method, which limits mud contamination, was patented by Halliburton in 1922 (Smith, 1976, p. 4). Use of centralizers, which help distributing the cement more uniformly in wells with tubing, was not introduced until 1930 (Smith, 1976, p. 4). Precise quantity of cement needed for a thorough job was not accessible before the invention and widespread use of a caliper survey instrument in the 1940s. In the past, plug location was not checked but assumed to be where located, as planned. Now, tagging of the plug, where a drill pipe or some other device is inserted to check the location of the plug, is mandatory and a third person must observe the plugging operations. In addition, since 1997, only preapproved plugging operators have been allowed to perform plugging operations. All this suggests that the quality of the plugs is getting better because their emplacement date is closer to the present, although the question of the resistance of the material to corrosion in CO_2-rich environments is still open.

III.2.3 Well Leakage Pathways

Potential well leakage pathways have been described in many publications (e.g., Gasda et al., 2004; IPCC, 2005). Interface between cement and casing and between cement and tubing is of particular concern for CO_2 leakage when the well is not simply left open. In a recent study, Bachu and Watson (2006) determined from regulatory mandatory reports that ~4.6% of wells in Alberta, Canada, show some kind of vent flow or, less commonly, gas migration, apparently

most often from the shallow subsurface (90% of cases <210 m [<700 ft]). There are also less obvious properties that can create well leakage pathways, in particular, the relative stiffness of cement, casing if any, and formations and their evolution through time. These different well-bore elements could settle or react differently to pressure changes (fluid withdrawal or injection, subsidence, etc.).

In addition to "regular" pathways present in typical subsurface environmental conditions, carbon storage introduces a significant corrosion enhancer. In batch experiments, Portland cement degrades rapidly in the presence of CO_2; corrosion attacks on well materials is slower but still of concern. There have been several analytical solutions to leakage through wells applicable to CO_2 storage (e.g., Avci, 1994; Striz and Wiggins, 1998; Nordbotten et al., 2004; Nordbotten et al., 2005). However, attempts to use those solutions and models have been hampered by a severe lack of actual field data.

Cement Degradation

Cement degradation in wells has been a concern for a long time (e.g., South and Daemen, 1986). The main degradation processes in the subsurface are sulfate attack and carbonation. Several groups at leading institutes (e.g., in the U.S., Los Alamos National Laboratory, Princeton University) are actively investigating the issue of cement degradation in the presence of CO_2 (or carbonation) in the subsurface. Experiments tend to suggest that Portland cement can be easily degraded, but field observations, especially in the Permian Basin, do not support this conclusion so far. Laboratory experiments are designed to enhance contact between the CO_2-rich solution and cement, contact that may not be as pronounced in the subsurface. Attacks on cement are often located at interface either with tubing or formation. An explanation may be that experiments are designed to favor CO_2 contact with the cement, whereas, in actual wells, CO_2 has to diffuse into fresh cement. As for any other water-rock interactions, overall rate is impacted, not only by the intrinsic rate, but also by the relative surface area and availability of reactants.

Cement is a mixture of mainly portlandite ($Ca(OH)_2$) (20–25 wt.%) and multiple phases of hydrated calcium alumino-silicates in a gel of calcium silica hydrate (60–70 wt.%). Carbonation of cement is thermodynamically favored through the conversion of portlandite into calcite in the more acidic conditions produced by the presence of CO_2 ($Ca(OH)_2 + CO_2 = Ca\,CO_3 + H_2O$) and the alteration of the calcium-silica hydrate into calcite and an amorphous

silica gel (C-S-H + CO_2 = $CaCO_3$ + SiO_2am). In good-quality cement, carbonation has a beneficial effect of decreasing porosity and permeability and increasing mechanical strength. Molar volume of portlandite and calcite is 33.056 and 36.934 cm^3/mol, respectively (Wolery and Daveler, 1992). Increase in volume could also have the downside of favoring cracking. Treatment by supercritical CO_2 has been suggested to improve cement quality for waste disposal (Rubin et al., 1997; Hartmann et al., 1999; Purnell et al., 2001). However, carbonation increases shrinkage upon drying (prompting crack development possibly filled with calcium carbonate) and lowers the alkalinity of interstitial water (Kosmatka and Panarese 1994, p. 72). Carbonation also has the effect of decreasing pH, which leads, in porous, low-quality cement, to an increase in corrosion of metals, such as tubing. After initial carbonation stages, if CO_2 is still available, dissolution and leaching of calcite can occur (bicarbonation) ($CaCO_3$ + H_2CO_3 (aq) = $Ca(HCO_3)_2$ (aq)). An increase in porosity/permeability may then result. Some have suggested that cement permeability, not accounting for possible cracks, may increase by 3 orders of magnitude, from 0.001 md initially to 1 md after 100 to 1,000 years (Zhou et al., 2004). The poor-quality cement put in place before the API standardization and advances of the 1950s is likely porous and will be very susceptible to carbonation. Cement degradation increases with decreasing pH and increasing temperature. Cement in a carbonate environment is more protected than in a sandstone environment because carbonate minerals buffer pH. It would seem that the solution would be neutralized as the cement reacts; however, some have suggested (Celia, oral communication, 2005) that the process is self sustained because of well coning. There are many ways to improve future cement formulations to resist CO_2 attacks, e.g., calcium phosphate cements or resins. However, it is not clear whether they will be used instead of Portland-based cements.

Sulfate attack is another common cement degradation mode. Specific cement formulations, low in aluminum (ASTM Type II and V, API Type C), are designed to withstand this type of attack, but they did not exist for most of the first part of the 20th century. Sulfate attacks lead to (1) byproduct formation, with a volume larger than that of initial constituents, and (2) potentially, to cracking. Sulfate concentration in most of the Frio Formation, an ideal target for carbon storage, is low except in a few instances in South Texas (Morton and Land, 1987; Kreitler et al., 1988, Tables 3 to 5; Land and Macpherson, 1992), but it is not true for all Gulf Coast formations. The low sulfate concentrations most likely result from a reducing

environment in the slightly acidic (pH = 5–6, Kreitler et al., 1988, p. 181), organic-rich waters. Organic acids contribute up to half of the total alkalinity (Kreitler et al., 1988, p. 141)—a consequence of the numerous hydrocarbon sources. Frio brines are generally noncorrosive, as anecdotally shown by the good condition of the casing of the monitoring well of the Frio experiment drilled in 1951 (Hovorka et al., 2003, p. 97).

III.2.4 Well Data Collection

Currently no agency or private information vendor has a comprehensive list of oil and gas wells ever drilled in Texas. At the inception of API numbering and following a regulatory impetus, data collection has improved considerably since the 1970s. RRC has an extensive set of data, not all of them in electronic format, and additional information can often been found in county courthouses when a specific location is being studied. RRC regularly updates several databases, some of which are the basis for the work presented below. Arguably the most complete set of well locations can be found in the GIS maps available for a fee at RRC ("Digital Map Data"). These provide location coordinates, location reliability, well type (among ~100 types: oil/gas injection/production, dry wells, service wells, geothermal wells, etc.). An additional database, the "API Well Database," is associated with the Digital Map Data and includes an API number when available (about half of the wells), as well as completion and plugging dates. Location information for older wells (~400,000 wells) comes from digitization of older maps. However, other types of information are often lacking. The "Digital Map Data" present information on ~1,100,000 well locations across Texas. On the other hand, the "Well Bore Database" is a most complete database, with historical well-bore information. It provides completion, plugging, formation, and other information related to the well-bore history of all wells with an assigned API number. Dummy API numbers have been assigned to old wells drilled prior to implementation of the API numbering technique (1977). The API number is a unique number allowing cross-referencing of databases. The "Well Bore Database" contains a total of ~860,000 wells with location information. Although in an ideal world the two sets of data would be perfectly consistent, in reality, many wells in the "Well Bore Database" have only approximate locations, whereas many wells precisely located on GIS maps lack historical information. They, however, provide global information on more than 800,000 wells. The total number of oil and gas wells is probably at least twice this number. It follows that the currently operating wells represent only a small fraction of the total number of wells in Texas and that

most of the wells are operationally abandoned. Technically, the expression "abandoned wells" refers to those wells abandoned and plugged according to the regulations in place at abandonment time. In this report, we make no distinction between abandoned wells sensu stricto and orphan wells, whose owners have disappeared without properly abandoning the well. A "Field Database" is also available. It contains information about the ~75,000 oil and gas fields (administratively defined) in Texas, including year of discovery, average depth and cumulative production, as well as the current number of wells in operation.

We contacted RRC and purchased, or otherwise obtained, the "Field Database," the GIS maps and the "Well Bore Database." The latter is in Oracle format and required lengthy processing to be in a format exploitable for this work. Merging and queries from other databases were also required to obtain better latitude/longitude information. Private vendors can provide well location coverage, but they focus more on more recent production data (e.g., drillinginfo.com, Datastar, IHS, Laser, etc.). RRC also owns a database with more than 1,000,000 well locations in a GIS format. However, about half of these do not have an API number that would allow us to link them with the "Well Bore Database," which contains the information needed for this work. Out of the ~800,000 wells listed in this database and covering the 254 Texas counties (~135,000 with location coordinates in the 23 Gulf Coast counties), we selected the 79,281 contained in the 23 Gulf Coast counties. We were able to find accurate locations for 39,065 of these wells; **Figure 15** shows an example. In the past 20 years, an additional 10,000±2,500 wells (oil and gas production and dry holes) have been added annually to the Texas well count (RRC Website).

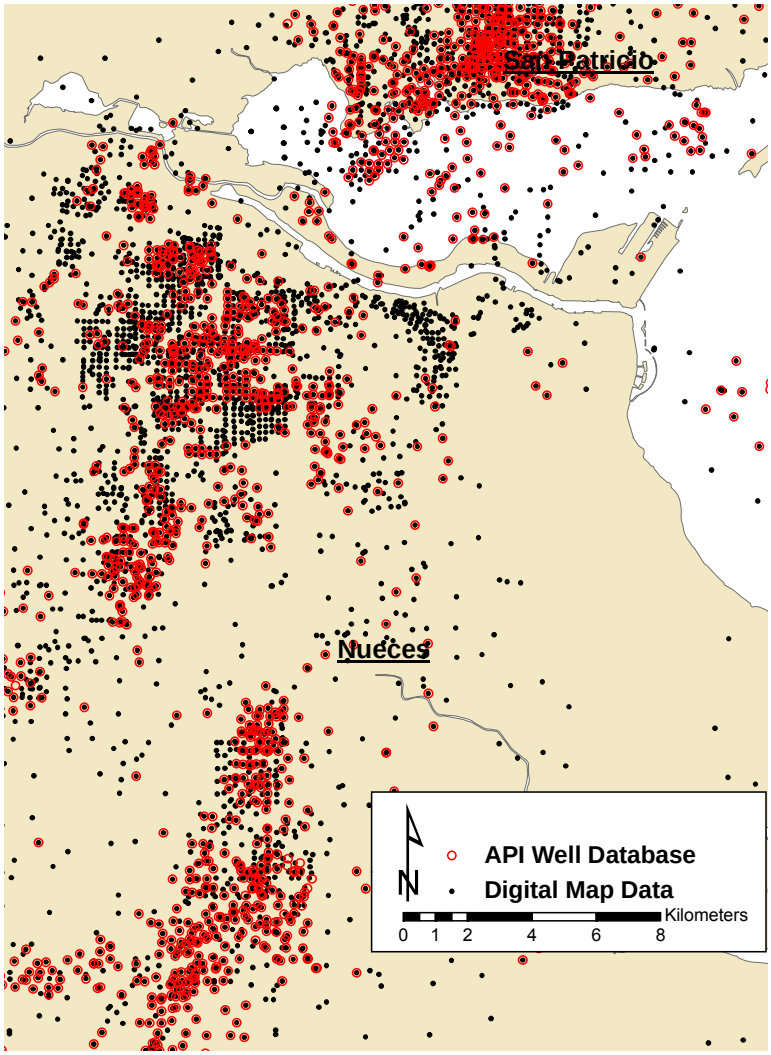

Source: RRC databases

Note: There are a total of ~1,500 wells with depth information out of a total of ~3,900 wells represented in the selected area.

Figure 15. Map of the Corpus Christi area (Nueces and San Patricio counties) showing contrast between database with location only (digital data map) and database with location and well depth information (API well database)

The Texas Water Development Board (TWDB) and Texas Commission on Environmental Quality (TCEQ) keep track of water wells, most of them shallower than most hydrocarbon-production-related wells. A registered water well driller is required by law to send in a report to the State for every well that is drilled. This requirement began in 1965, and it is estimated that approximately 500,000 water wells have been drilled in Texas since then (TWDB Website, 2005). The TWDB database contains information about ~130,000 of those wells, 14,665 of which are located in the selected 23 Gulf Coast counties, and within this area at least

9,000 were completed before 1965. Other types of wells also exist: waste disposal (>100 class I wells), geothermal, and solution mining. These are numerically insignificant, and their construction follows more stringent UIC rules.

III.2.5 Well Distribution Statistics

Examination of oil/gas field average depth as a function of year of discovery (**Figure 16**) clearly shows that operators went (or were able to go) deeper and deeper to access the hydrocarbon resource but that a significant fraction of the fields at any given time is in the 1,500 to 3,000-m range (5,000–10,000-ft). In other words, the slope for the trend of the deepest producing fields through time is much steeper than that of the average field. The time/depth density is consistent with the observations made about **Figure 14**, with the additional information about completion depth also shown by **Figure 17**. The two major peaks and the dip of the 1970s are all present. The density plot also illustrates that approximately 10% of the fields are deeper than 3,000 m (10,000 ft) (0.3% deeper than 4,570 m [15,000 ft]), 30% are shallower than 1,500 m (5,000 ft) (7% shallower than 2,500 ft), and 60% are included in the 1,500 to 3,000 m (5,000 to 10,000 ft) interval.

Total well depth plotted against completion and abandonment years displays a pattern similar to that of the fields (**Figure 18**). The database has only 78 wells completed before 1934 and grossly underestimates the number of older wells. Before the 1930s only the out of the ordinary wells made their way to RRC central records (deep for their time, good producers, etc.). An alternative explanation is that the database contains mostly pre-1934 wells that had been recompleted and plugged at a later date, when regulations and record enforcement were stricter. The vicinity of the City of Corsicana, Navarro County, location of the first Texas fields to produce oil and gas in important quantities, had 47 wells in 1897, and an additional 342 were drilled in 1898 (Handbook of Texas Online). Spindletop oilfields, on a salt dome on the Texas-Louisiana border, had hundreds of wells in the early 1900's. RRC does not have complete records for wells drilled before the 1930's. The low abandonment well density (**Figure 18**b) before 1974 (year of the Safe Drinking Water Act) is a sampling artifact because of lack of records. Anzzolin and Graham (1984) suggested that there are a total of ~1,650,000 such wells across the U.S. (**Figure 19**). There is also a discrepancy between the number of wells recorded as completed (that is, just after drilling) and abandoned. It most likely represents a bias in which operators are inclined to report drilling information more than they are inclined to be diligent

about reporting plugging or even doing the plugging. Another partial explanation could be the lag between completion and abandonment, as well as recompletion or deepening of older wells. However, this explanation is unlikely to hold for wells completed before 1950.

A plot of the average total completion depth at 1,830 to 2130 m (6,000–7,000 ft) (**Figure 20**) illustrates that it has not changed significantly since the 1940s, reflecting the simple fact that most fields are located in the 1,500 to 3,000 m (5,000–10,000 ft) interval. Observations by Johnston and Knape (1986) can be added as a complement to the conclusions drawn from these density plots. They undertook a comprehensive study of the impact of abandoned wells on ground-water resources. They interviewed specialists and concluded that wells drilled and abandoned prior to 1930 are probably not much deeper than 915 to 1,220 m (3,000 to 4,000 ft), with a maximum of 1,830 m (6,000 ft) (p. 5, 78, 80). In addition, wells drilled during the 1920s apparently range from 150 to 305 m (500–1,000 ft) deep, with a maximum of 760 m (2,500 ft). Cumulative distribution function (CDF) curves for selected time intervals (**Figure 21**, **Figure 22**, and **Figure 23**) depict and quantify that observation. **Figure 23**, where all CDFs are superimposed, illustrates that the general shape of the distribution stays the same, with some shifting and difference at both ends. The differences at the end of the distribution are confirmed by a closed distribution exercise (**Table 4**). All well depth distributions are well fitted by gamma distributions, as indicated by passable goodness of fit values for Chi-Square and Kolmogorov-Smirnov tests. Other distributions with slightly better fit values were also sometimes suggested (logistic, Student-t), but gamma distribution was retained for all categories for consistency. In general, distribution peaks are not well captured, and terrible values for the Anderson-Darling test, which put more weight on distribution tails, are obvious. This observation suggests that the underlying actual distribution is more complex and that the distribution should be captured in a Monte Carlo analysis by the data themselves rather than a relatively poor fit.

As expected, water well total depth is much smaller than that of oil and gas wells (**Figure 24**). Although the sample is smaller than the total number of water wells, it is thought to be representative of the whole population or to slightly biased toward deeper wells because many early 20th-century shallow domestic wells are not in the TWDB database. It follows that most wells are in the shallowest section of usable quality water and clearly above the minimal injection depth for CO_2 storage.

To get a better picture of the uneven well distribution through space, a spatial analysis and well count was performed in ArcGIS 9.1 using the "point distance" tool. We did it after creating a 1-km-square grid and leaving the appropriate buffer so as not to bias the results with areas having no data. Results are presented in histograms (**Figure 25** and **Figure 26**) showing the number of wells existing within a given radius of any arbitrary point located within the 23 counties considered (shown in **Figure 2**). **Figure 25**a shows not only that more than 70% of the Gulf Coast area has four or fewer wells within a 1-km radius, but also that approximately 1% has more than 40 wells within that same radius. The left-hand-side column of **Figure 26** illustrates that the likelihood of having no wells within a 1-km radius increases with depth. The top row of **Figure 26** should match **Figure 25** but does not because **Figure 25** uses all well data, whereas **Figure 26** uses only those wells with depth information. As expected and demonstrated by other plots, the number of wells within a given distance of a given point increases with distance, possibly to very high values, which is likely related to the presence of salt domes. Salt dome areas typically experience the highest surface well density.

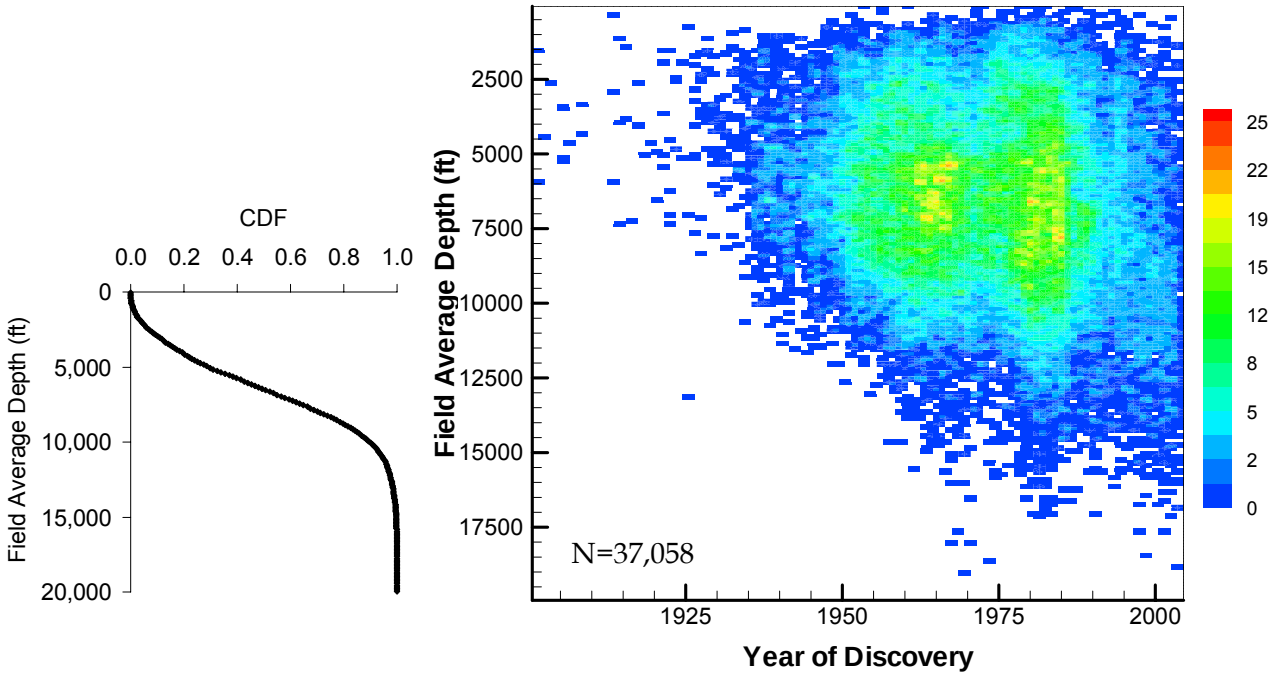

Source: RRC field database
Note: Bins are 1 year/100 ft (1ft = 0.3048 m)
Figure 16. Time/depth density of oil and gas fields in RRC districts 2, 3, and 4

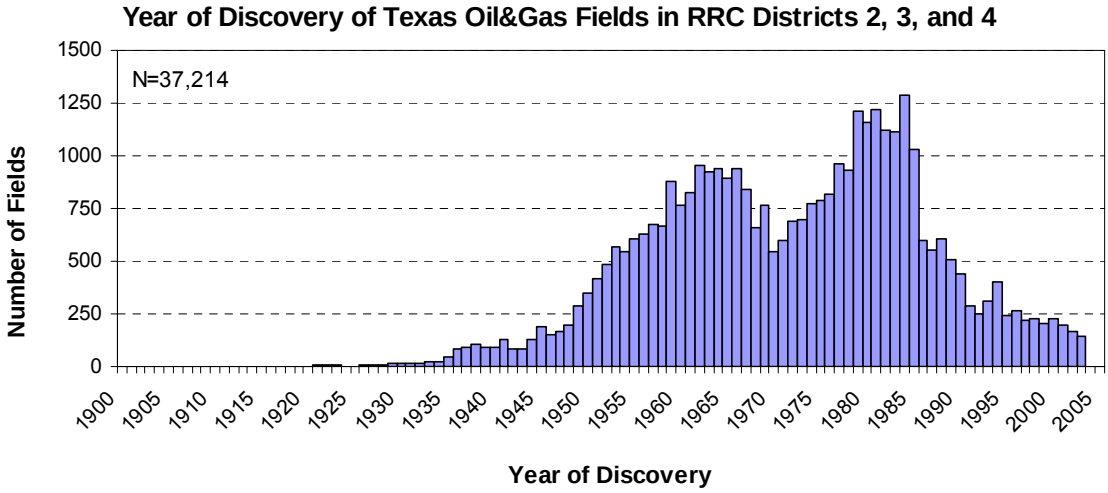

Source: RRC field database
Note: median year is 1973
Figure 17. Distribution of the year of discovery of oil versus number of fields in RRC districts 2, 3, and 4

(a)

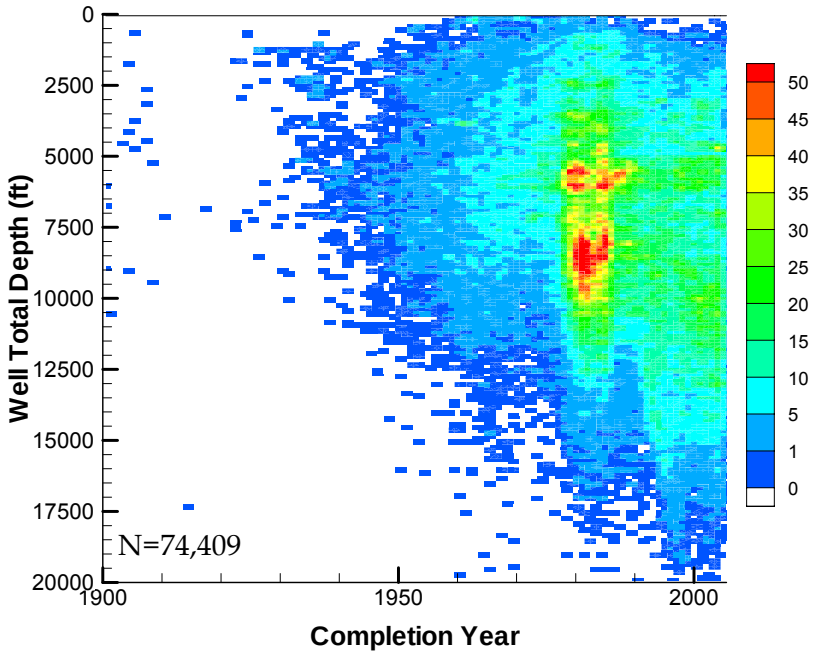

(b)

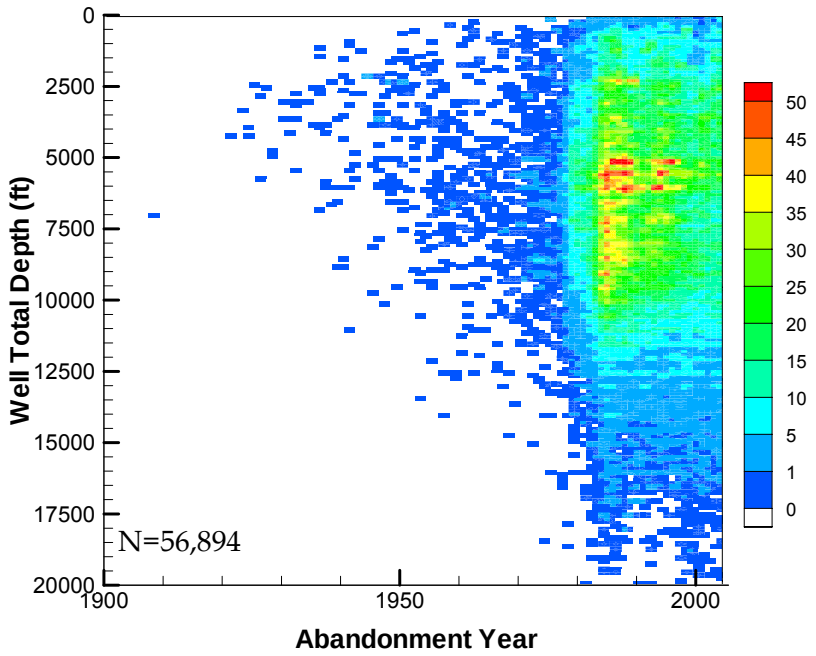

Source: RRC API Well Database

Note: Bins are 1 year/100 ft (1 ft = 0.3048 m)

Figure 18. Time/depth density of oil and gas wells with available data in RRC districts 2, 3, and 4; (a) completion year and (b) abandonment year

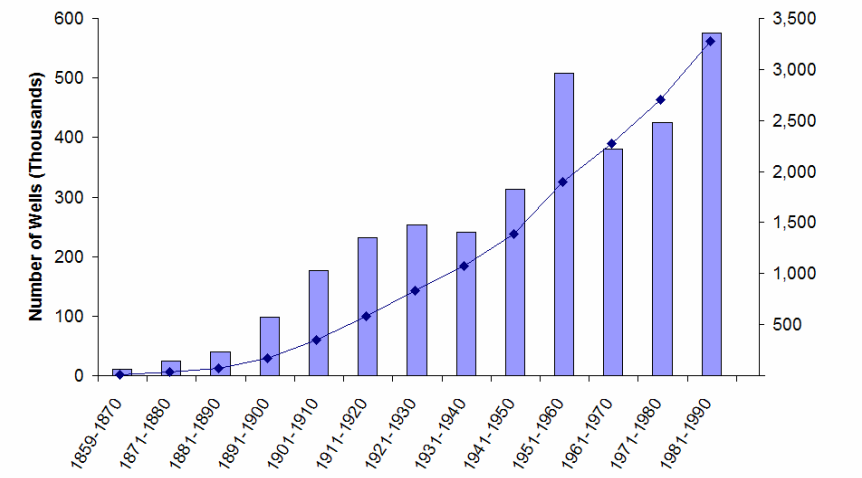

Source: Anzzolin and Graham (1984); World Oil (1992)
Figure 19. Tentative abandoned well count in the U.S. (1859-1974), including dry holes

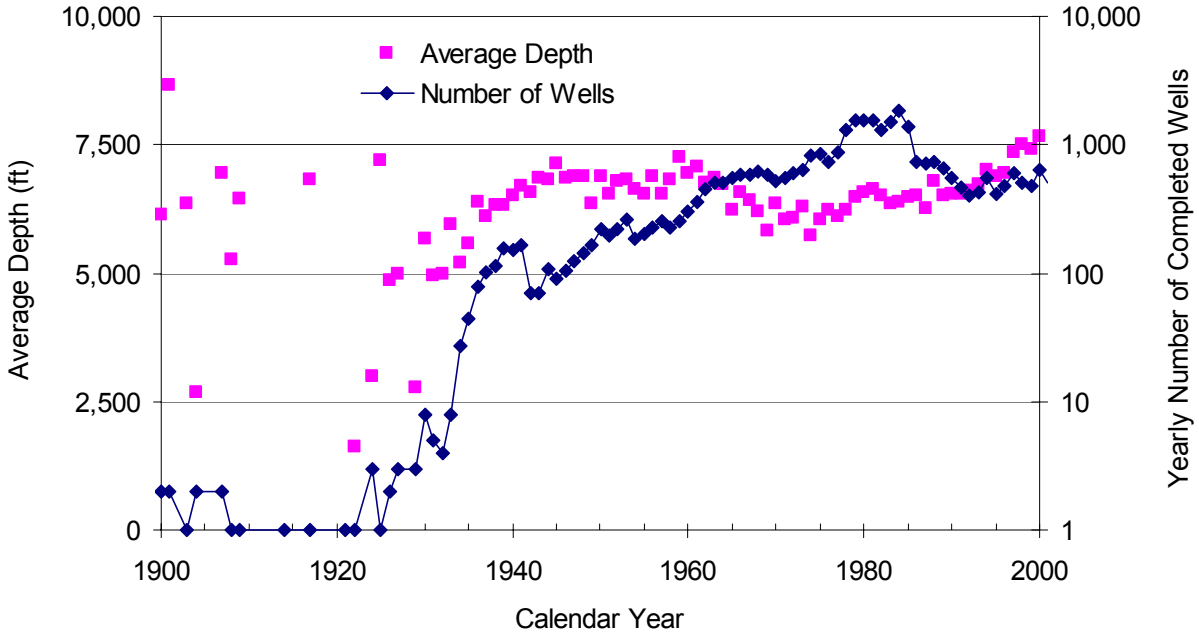

Source: RRC Well Bore Database
Figure 20. Average completion depth as a function of time, and the number of wells used in the computation (RRC districts 2, 3, and 4)

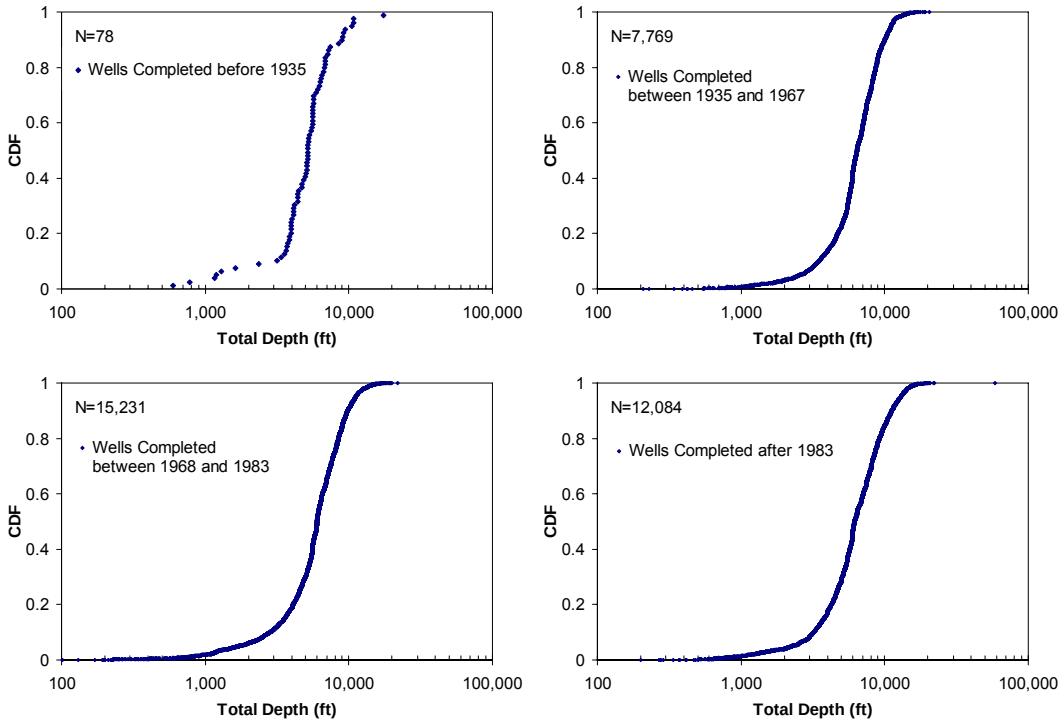

Source: RRC Well Bore Database

Figure 21. Depth distribution of wells completed in selected time intervals

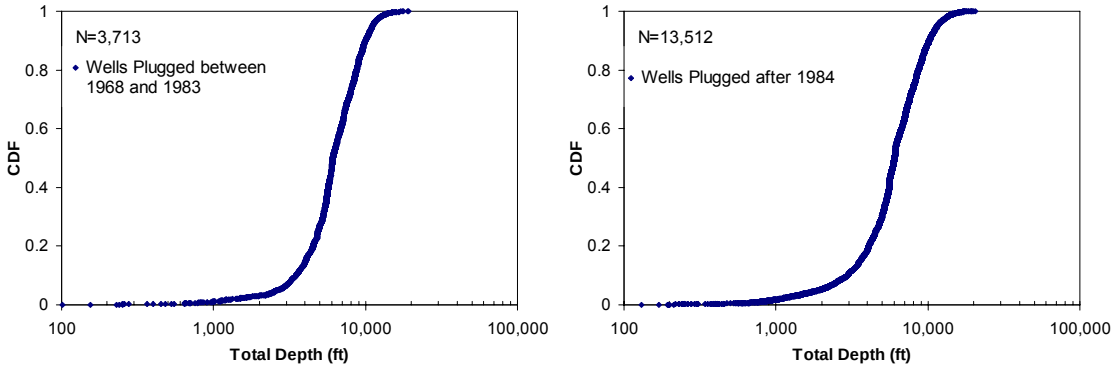

Source: RRC Well Bore Database

Figure 22. Depth distribution of wells abandoned in the selected time intervals

(a) (b)

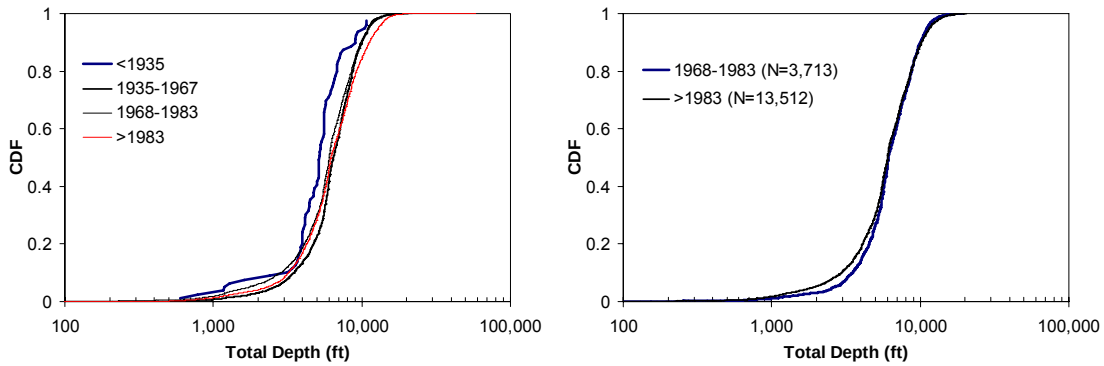

Source: RRC Well Bore Database

Figure 23. Depth distribution of and (a) completed and (b) abandoned wells

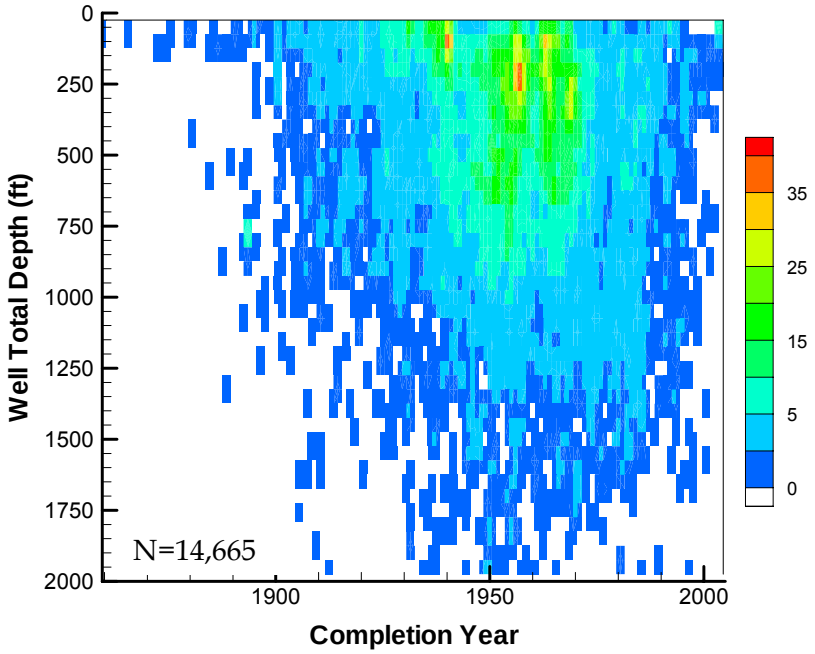

Source: TWD Website

Note: Bins are 1 year/50 ft (1 ft = 0.3048 m); Y-axis has been arbitrarily stopped at 2,000 ft.

Figure 24. Time/depth density of water-supply wells in the Gulf Coast area (RRC districts 2, 3, and 4)

(a)

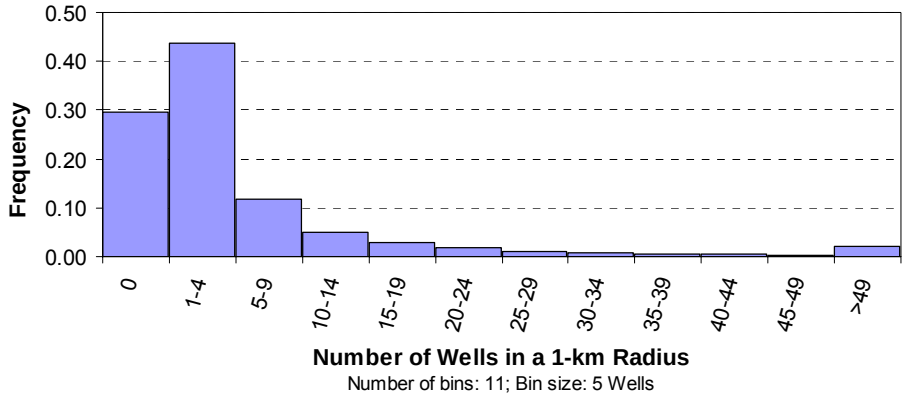

(b)

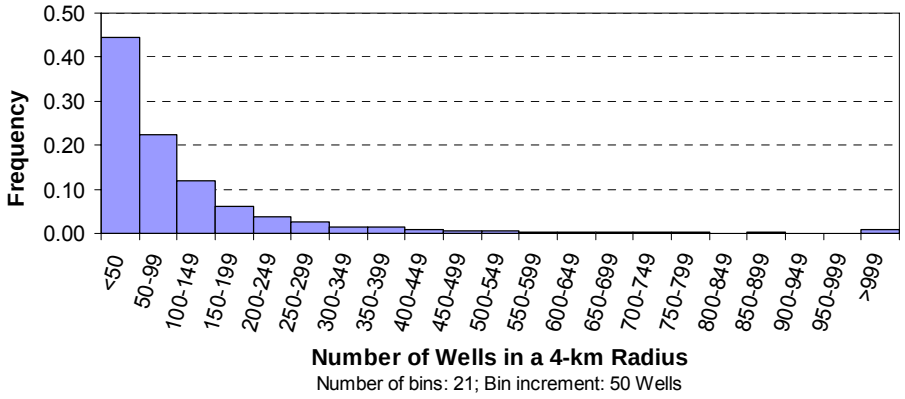

(c)

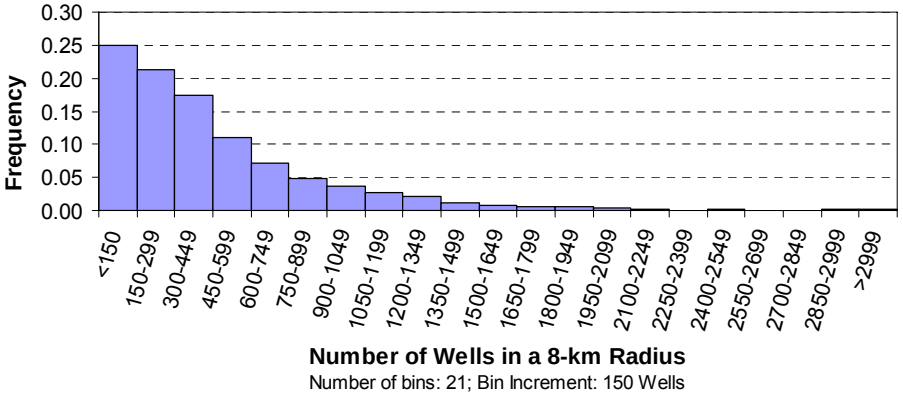

Source: RRC digital map data

Figure 25. Distribution of wells at a given distance from an arbitrary point located in one of the counties of interest: (a) 1 km, (b) 4 km, and (c) 8 km.

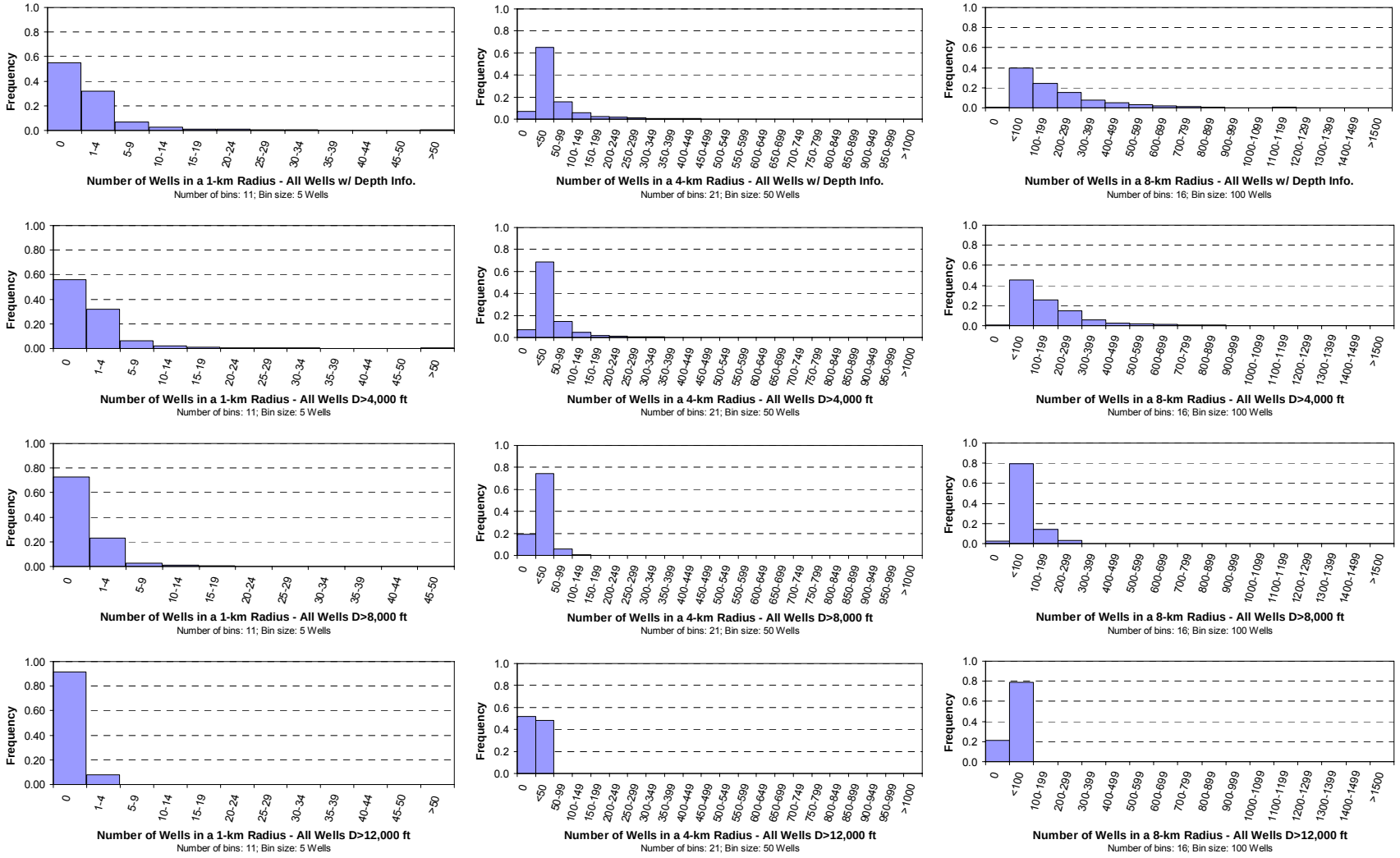

Source: RRC API well database

Figure 26. Histogram matrix showing number of wells in a given radius (1, 4, or 8 km—horizontal direction) below a given depth (all, >4,000 ft, >8,000 ft, and >12,000 ft—vertical direction) at an arbitrary point within the 23 counties (4,000 ft =1,220 m; 8,000 ft = 2,440 m; 12,000 ft = 3,660 m)

Table 4. Goodness of fit statistics for well depth distribution

Parameter	Data Mode	Data Mean	Data Standard Deviation	Distrib.Law Preferred / (Best Fit)	Distrib. Mean	Distrib. Standard Deviation	Goodness-of-fit Tests A-D	C-S χ^2 / d^o	K-S
Well depth (ft) Wells plugged between 1968 and 1983—3,713 points	6,000	6,553	2,605	Gamma	6,553	2,597	6.7	395	0.05
Well depth (ft) Wells plugged after 1983—13,512 points	5,200	6,393	2,875	Gamma	6,393	2,868	22.1	1207	0.04
Well depth (ft) Wells completed between 1937 and 1967—7,769 points	6,000	6,681	2,541	Gamma	6,681	2,537	13.7	658	0.05
Well depth (ft) Wells completed between 1968 and 1983—15,231 points	6,000	6,287	2,767	Gamma	6,182	2,798	33.0	1671	0.05
Well depth (ft) Wells completed after 1984—12,084 points	8,000	6,817	3,195	Gamma	6,817	3,165	16.7	1046	0.04
Well depth (ft) All completed wells—35,162 points	6,000	6,554	2,885	Gamma	6,554	2,868	62.9	4097	0.04

Note: Goodness-of-fit tests: A-D = Anderson-Darling; C-S = Chi-Square; K-S = Kolmogorov-Smirnov
1 ft = 0.3048 m
Explanations: AD<1.5, C-S>, and K-S<0.03 indicates a good fit; fitting computations done with Crystal Ball

III.3 Faults

For a fault to be a leakage pathway, at least three factors must be met (Warner, 1997): (1) CO_2 must reach the fault, (2) CO_2 phase must have sufficient pressure, and (3) fault must be transmissive, especially in the vertical direction. Faults are typically described either as a leakage pathway or as a sealing feature. In actuality, most probably act as both at different locations of the fault plane and at different points in time. Faults may allow flow in only one or two of the possible three directions (across the fault and transversally or vertically along the fault plane) or a combination of these (Harding and Tuminas, 1988; Knott, 1993; Ligtenberg, 2004). There is a huge body of literature about fault seals in the petroleum literature, fault being one of the main hydrocarbon trapping features. Faults are envisioned mostly as features sealing most of the time but that would let fluids through by pulses. Regional tectonic stresses are currently low and extensional in the Gulf Coast area, and most of the faulting is related to sedimentation. Three main types of faults are represented in the Gulf Coast area: syndepositional growth faulting (listric normal and their possibly associated antithetic members), radial faults associated with shale or salt piercement structures, and, less commonly, regional postdepositional faults. Growth faults form contemporaneously with sedimentation, with a fault throw increasing with depth. They stay active until the sediment load has been better stabilized and until the next unconsolidated sediment package adjusts itself by creating its own set of growth faults. These faults remain active in areas where sedimentation is still active (e.g., Houston area). Salt domes produce radial fault patterns, whose throw can be important but quickly attenuated away from the dome. As seen previously (**Figure 7**), folding and its associated traps is allied with faulting and diapirs. More information about faulting is given in Appendix A.

III.3.1 Fault Geometry

In the Gulf Coast, growth faults are organized in systems with major faults that extend along strike 20 to 50 km (**Figure 12** and **Figure 27**). Growth faults are often arcuate in plan view, denoting their origin as mass wasting accommodation. To illustrate that faults are generally restricted to one depth section of the subsurface, five areas with available 3D-seismic information were examined through a detailed mapping of fault pattern and density at different depths (**Table 5**).

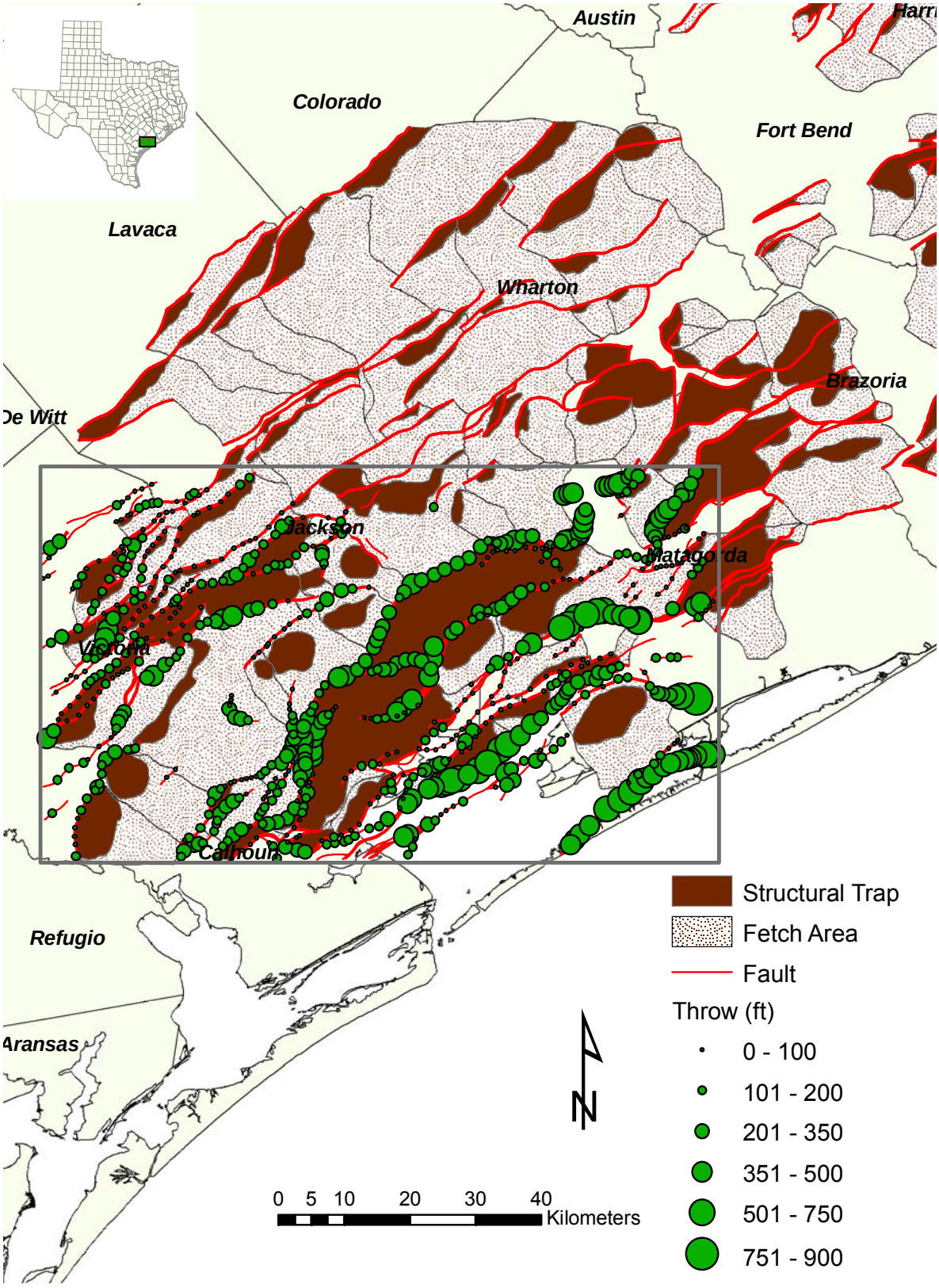

Figure 27. Distribution of (growth) fault throw within a ~100 × 60 km rectangle

Table 5. 3D-seismic survey location

Name	Location	Area (km^2 / mi^2)
GC1	Gulf Coast	195 / 75
GC2	Gulf Coast	440 / 170
Stratton	West of Corpus Christi	20 / 7.7
Liberty	Salt dome—Houston area	44 / 17
Gillock	Salt dome—Houston area	23 / 9

Note: exact location of sites GC1 and GC2 not provided because of proprietary information

For each of the five 3-D seismic surveys, six structure maps were constructed to represent the density of faults at different depths (±460 m **[±**1,500 ft] vertical sampling), to verify fault lateral distribution versus depth, and to test the possibility of vertical connectivity through fault relays. A series of seismic-reflection profiles were used to map the structure and fault distribution at six different levels approximately 500 ms apart. The shallowest horizon was interpreted near 500 ms (460 m [1,500 ft]), and the deepest at near 3,000 ms (3,660 m [12,000 ft]). Time-depth relations were used through velocity measurements at wells drilled in these areas. Horizon picking was done every 10 × 10 lines and traces for every surface in each survey. Interpreted horizons were then carried out, preparing for calculating continuity (coherency) maps. The end result was s fully interpreted horizon/layer, and the coherency gaps are faults represented by polygons. Seismic data were used in identifying principal fault plane geometry. Faults were correlated using an integrated loop method that requires that seismic indications of structural elements must correlate to intersecting and nearby parallel lines. Fault correlations were also based on fault plane shapes and stratal geometries found at both upthrown and downthrown sides of the faults. Coherency seismic attributes, which measure trace-to-trace similarity of the seismic waveform, were also used for mapping faults. Variable seismic windows 40 to 100 ms were designed to measure the incoherency in seismic markers in order to generate the best image of the principal faults. The small correlation windows were used at the shallow intervals where the quality of seismic data is better. The larger correlation windows were performed at the deeper level, where a low signal-to-noise ratio was encountered. **Figure 28** shows a coherence map through the Stratton seismic volume and highlights individual fault expression. Picking errors can bias the result of the coherence extraction; therefore, vertical sections through the seismic volumes were used to QC the results.

Faults for the GC1, GC2, and Stratton field sites impact mainly the Frio Formation and are traditional growth faults, whereas faults impacting the Liberty and Gillock sites are related to salt diapir growth. Vertical sections across Stratton field (e.g., Hardage et al., 1994) (**Figure 28**

and **Figure 29**) in the Frio Formation provide an example of growth faults not impacting overlying layers. Shorter, along-strike, second-order faults, numbered "Fx," (**Figure 30**) are also visible. Those second-order faults whose dimension statistics for Stratton field will be derived later are important for studying the compartmentalization of an area. Sites GC1 and GC2, also located in the Gulf Coast area, (**Figure 31**) show a similar picture, with clear attenuation of growth faults toward the surface. **Figure 31**c clearly shows the radial pattern of some smaller faults due to the localized upward motion of shales which are the result of primary growth fault movement. Faults associated with salt domes also show horizons where faulting is concentrated (**Figure 32** and **Figure 33**). It would be, however, imprudent to apply such conclusions to all diapirs.

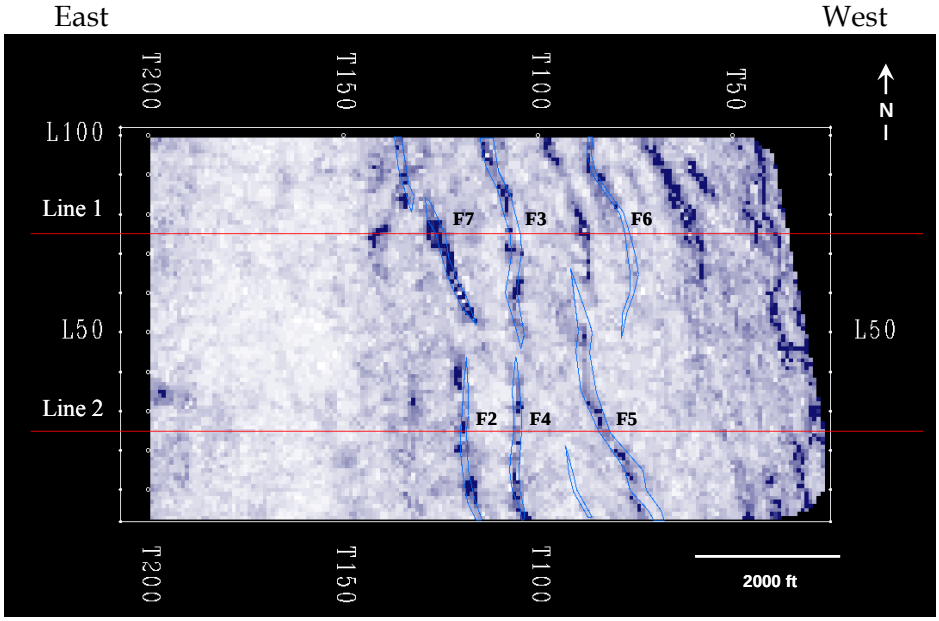

Figure 28. Coherency map in Stratton 3-D measured at a deep layer (±7,000 ft = ±2,130 m) showing the faults affecting the area. White areas coincide with continuous seismic marker (layer) with no faults. Blue areas represent incoherent event or cracks. Faults are represented by polygons with light-blue outlines. Lines 1 and 2 are shown in the next figure.

We used a simple quantitative method to calculate the variation of fault density with depth. Once horizons and faults were mapped and correlated in each seismic volume, we measured fault length and distances between faults in matrix form for each horizon and recorded them in Excel files. The measurements were made along regular selections of vertical sections in each seismic volume. The selection of vertical sections was chosen to capture the best

representation of faults in each seismic volume, taking into account the coverage area of seismic data.

East West East West

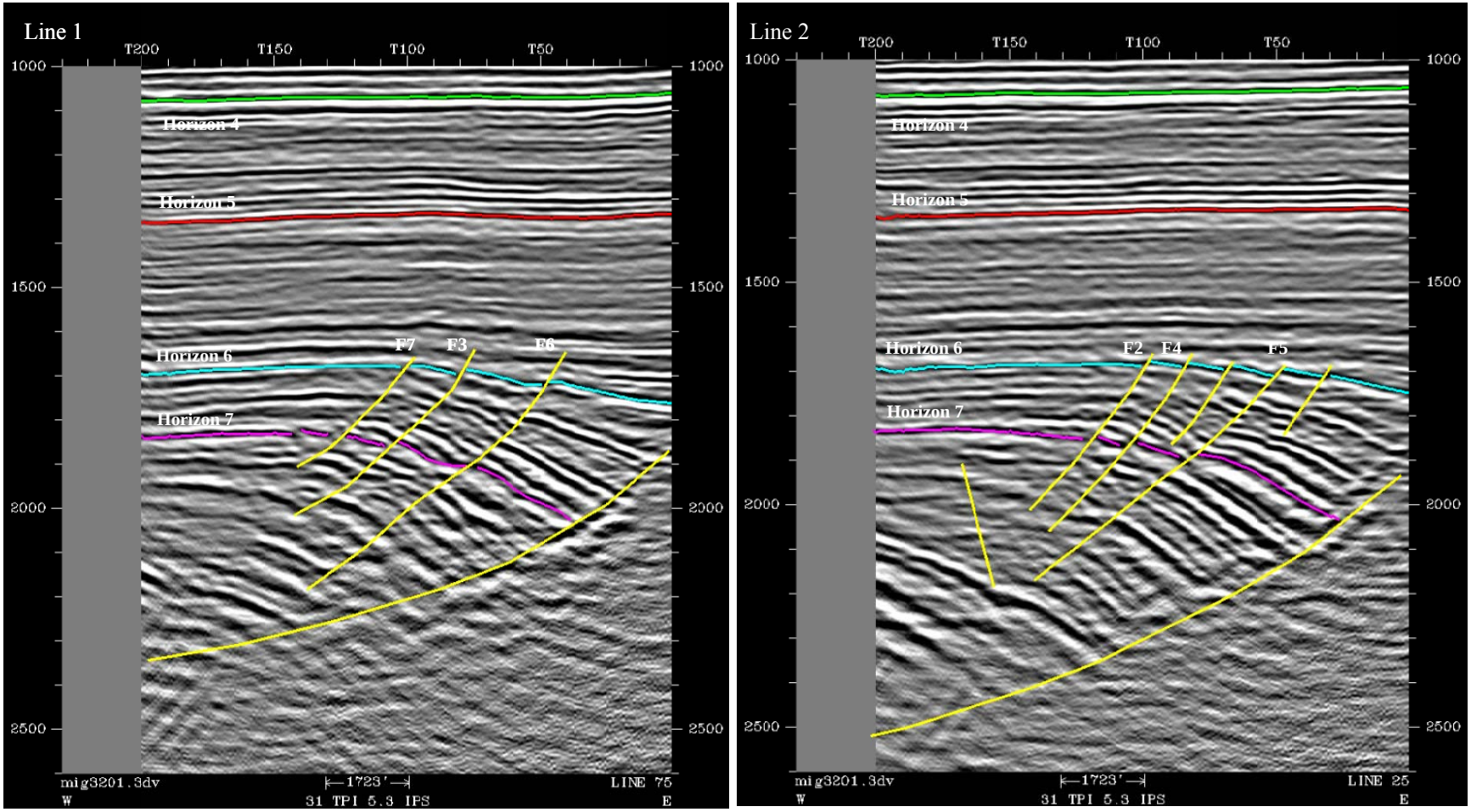

Note: Vertical scale in milliseconds. See **Figure 33** for representative depth equivalence. Fault identification numbers are consistent with previous figure.

Figure 29. Lines 1 and 2 are examples of vertical sections chosen to best represent faults in the Stratton area.

(a)

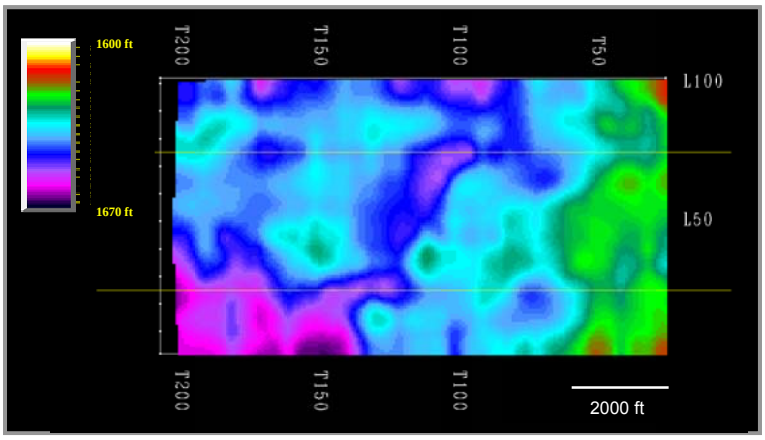

(b)

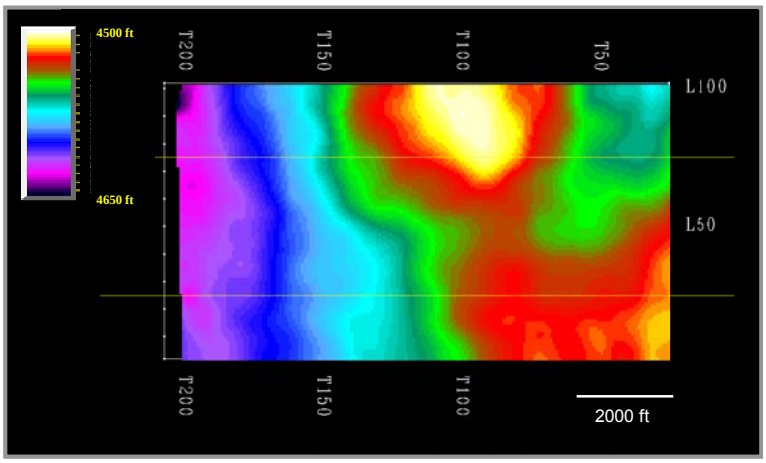

(c)

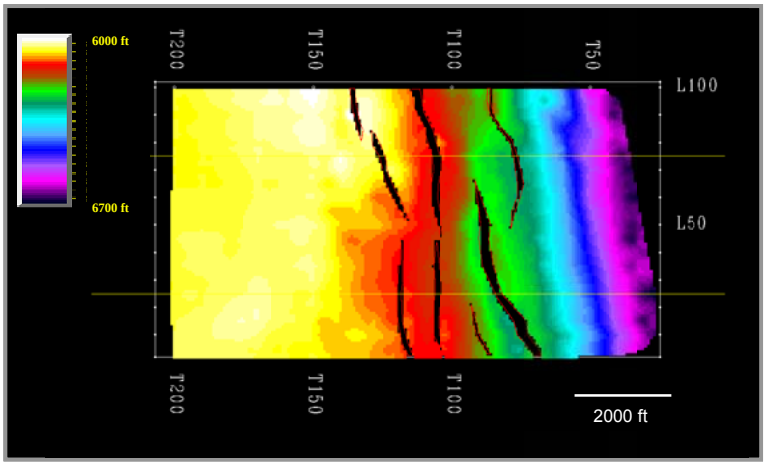

Note: Brighter colors denote structure highs, and darker colors indicate depressions or structure lows. Faults are represented by polygons. Depths of ~2,000, 6,000, and 7,000 ft show no fault, faults with smaller throws, and faults with larger throws, respectively.

Figure 30. Structure maps in Stratton area constructed at three depth levels: (a) shallow, (b) moderate, and (c) deep. The maps depict the population of the fault density varying with depth.

(a)

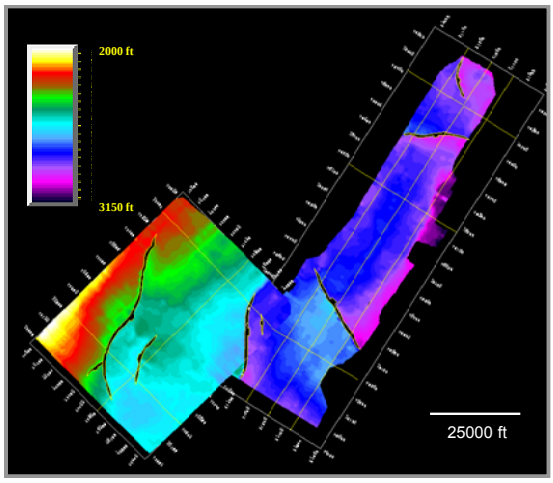

(b)

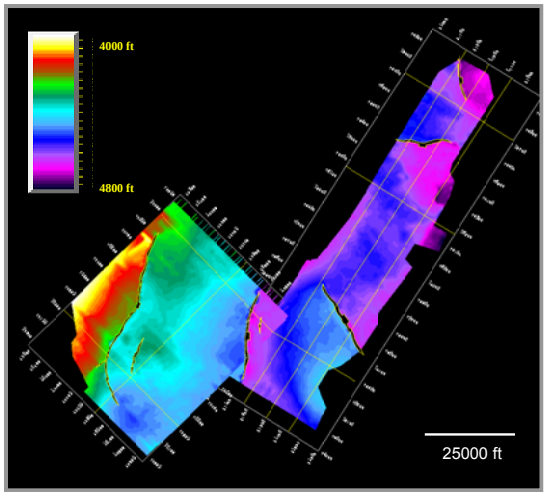

(c)

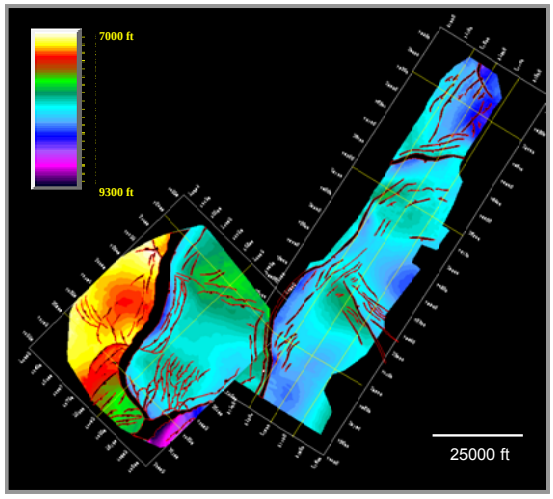

Note: Brighter colors denote structure highs, and darker colors indicate depressions or structure lows. Faults are represented by polygons.

Figure 31. Structure maps in GC1 and GC2 areas constructed at three depth levels: (a) shallow, (b) moderate, and (c) deep (±10,000 ft = ±3,050 m). The maps depict the population of the fault density varying with depth.

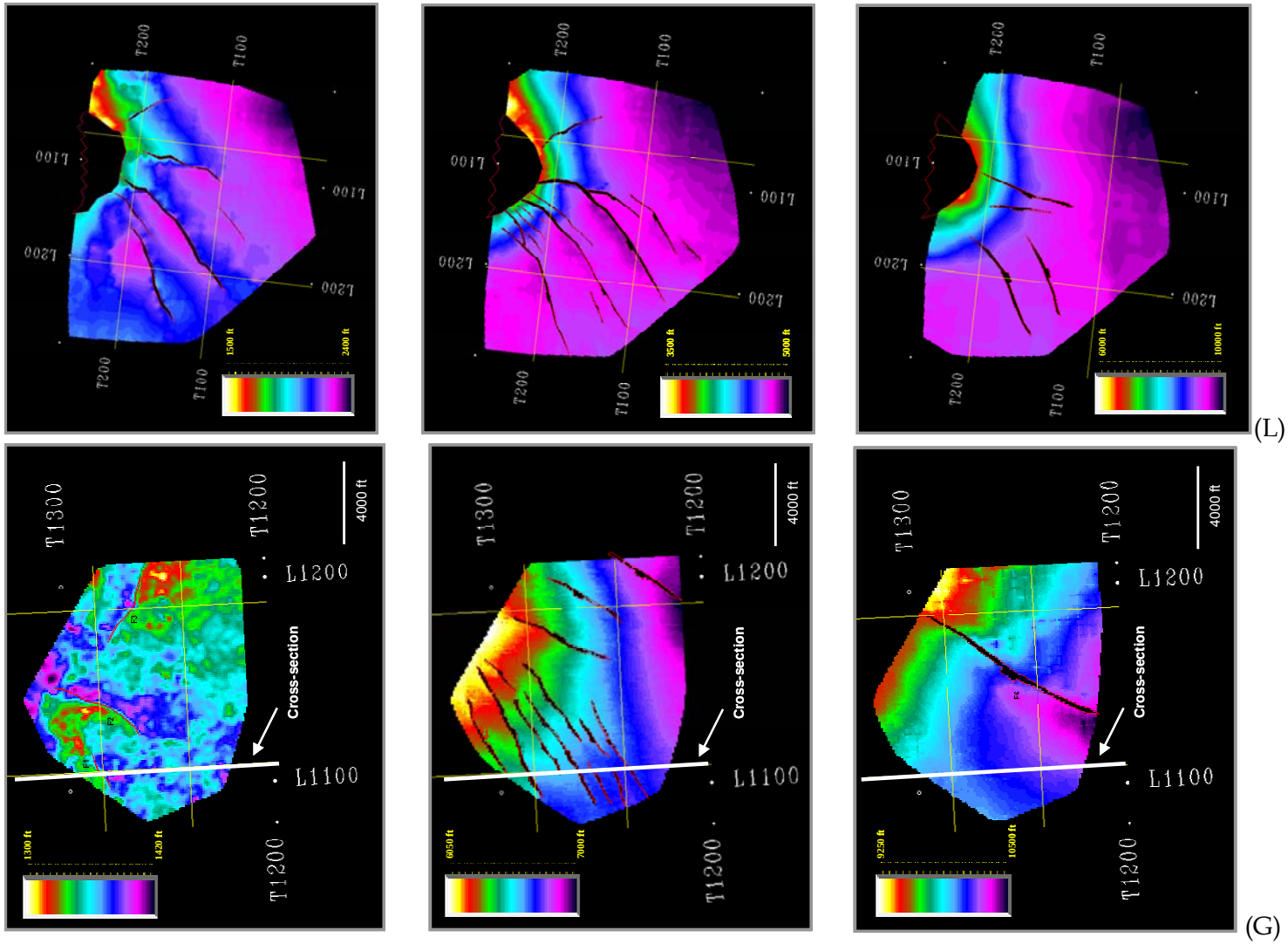

Figure 32. Structure maps in Liberty (L) and Gillock (G) areas constructed at three depth levels: (a) shallow, (b) moderate, and (c) deep (±10,000 ft = ±3,050 m). The maps depict the population of the fault density varying with depth. Brighter colors denote structure highs, and darker colors indicate depressions or structure lows. Faults are represented by polygons.

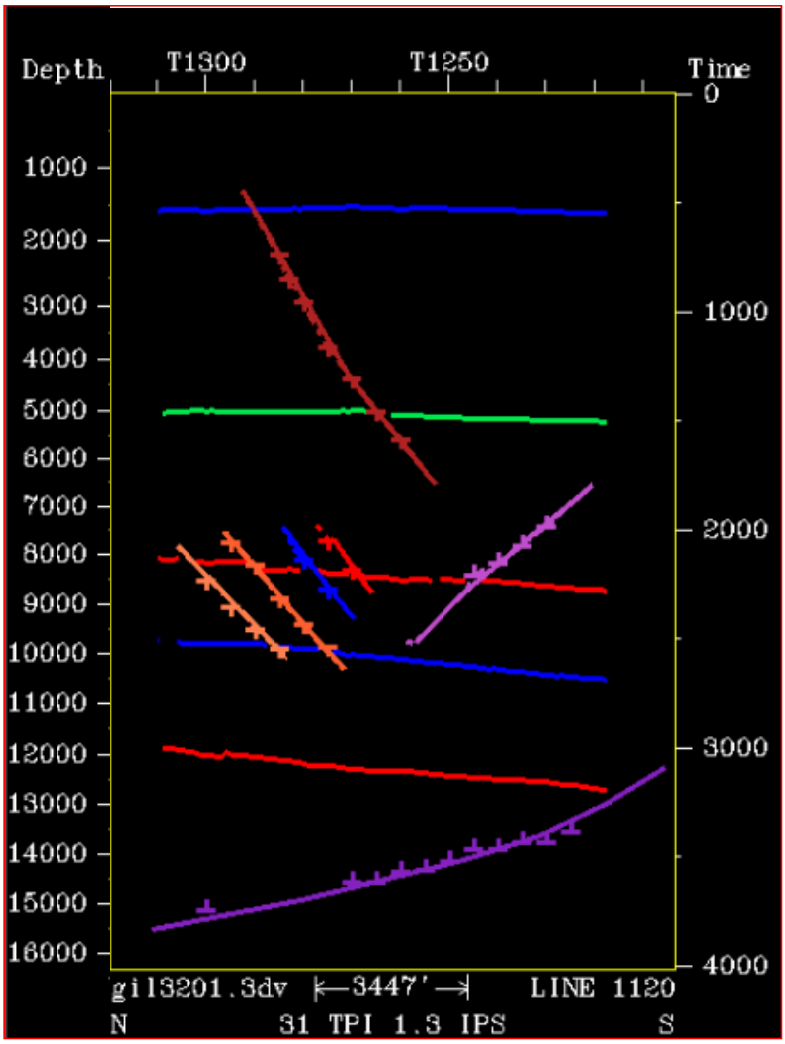

Note: See **Figure 32** (G) for location of the cross section. Stratigraphic horizons are denoted by approximately horizontal lines, whereas faults are more inclined and show data picks.

Figure 33. Gillock cross section showing denser faults at the interval between 8,000 and 9,000 ft (2,440 and 2,740 m) compared with the faults affecting the deeper levels.

III.3.1.1 Fault Spacing and Fault Length

Knowledge of fault and fracture/joint density and aperture can help in quantifying CO_2 leakage. It has been noted that field observations at some scales can be extrapolated to other scales because fault parameters generally follow a power law (Bonnet et al., 2001): $N = bX^{-c}$, where b and c are empirical constants and N is the cumulative number of faults whose measure of interest (length, spacing, displacement, aperture, etc.) is larger than X. Power law distributions plot as a line on log-log charts. Alternatively, fault/fracture length and spacing have often been described as having a lognormal distribution because they are biased toward small lengths. Some authors (e.g., Bonnet et al., 2001) favor a power law distribution because of

the likely incomplete sampling on the small length side. This is true not only in the field, but also in seismic surveys whose resolution is such that faults with small offsets are not visible from reflection data. This study, however, focuses on larger faults, more likely to have a larger vertical extent.

Along-strike length of all second-order faults was recorded for Stratton field, as well as for sites GC1 and GC2. A total of 7 and ~70 faults have been measured, respectively, with the help of imaginary scanlines (**Figure 28** and **Figure 34**). Length distributions are presented as a CDF (**Figure 35**) and with the power law assumption (**Figure 36**). The cumulative coefficient *c* of the power law describing the relationship number of faults larger than a given length to that given length is *c*=1.25 (**Figure 36**) over an area of 635 km^2. This number was obtained with a number of samples (~100) at the limit of the validity of the method (Bonnet et al., 2001) but on a length range covering 2 orders of magnitude. This value of the coefficient is consistent with Table 2 of Bonnet et al. (2001) and falls within the average of seismic studies (a=c+1~2.25) (Figure 12 of Bonnet et al., 2001). CDFs of the fault spacing (**Figure 37**) and its percentiles (**Table 6**) suggest that in the GC1 and CG2 sites (covering 635 km^2) fault density increases with depth, albeit irregularly.

Table 6. Fault spacing percentiles

Horizon (ms)	Equivalent Depth (ft)	# of points	5th Perc. (km)	25th Perc. (km)	50th Perc. (km)	75th Perc. (km)	95th Perc. (km)
3,000	12,000	63	0.24	0.59	0.98	2.19	6.69
2,400	9,500	137	0.23	0.45	0.68	1.13	5.66
1,800	6,500	9	N/A	1.72	5.31	13.7	N/A
1,300	4,500	6	N/A	N/A	3.14	N/A	N/A
900	3,000	11	N/A	N/A	N/A	N/A	N/A
500	1,500	2	N/A	N/A	N/A	N/A	N/A

1 ft = 0.3048 m

III.3.1.2 Fault Displacement

Fault displacements, as measured from the map of the top of the Frio Formation (**Figure 27**), show a lognormal distribution of mean and standard deviation of 63 and 55 m (207 and 180 ft), respectively (**Figure 38**). As expected, it also shows, on average, an increase of maximum fault displacement with fault length (**Figure 39**). The relationship between fault displacement and length has been extensively studied (Bonnet et al., 2001, p.365). Power law distribution for both length *L* and maximum displacement *D* translates into the following relationship: $D \propto L^n$, where *n* is an exponent. Yielding et al. (1996, Table 1) found that *n* ranges from 1 to ~2.

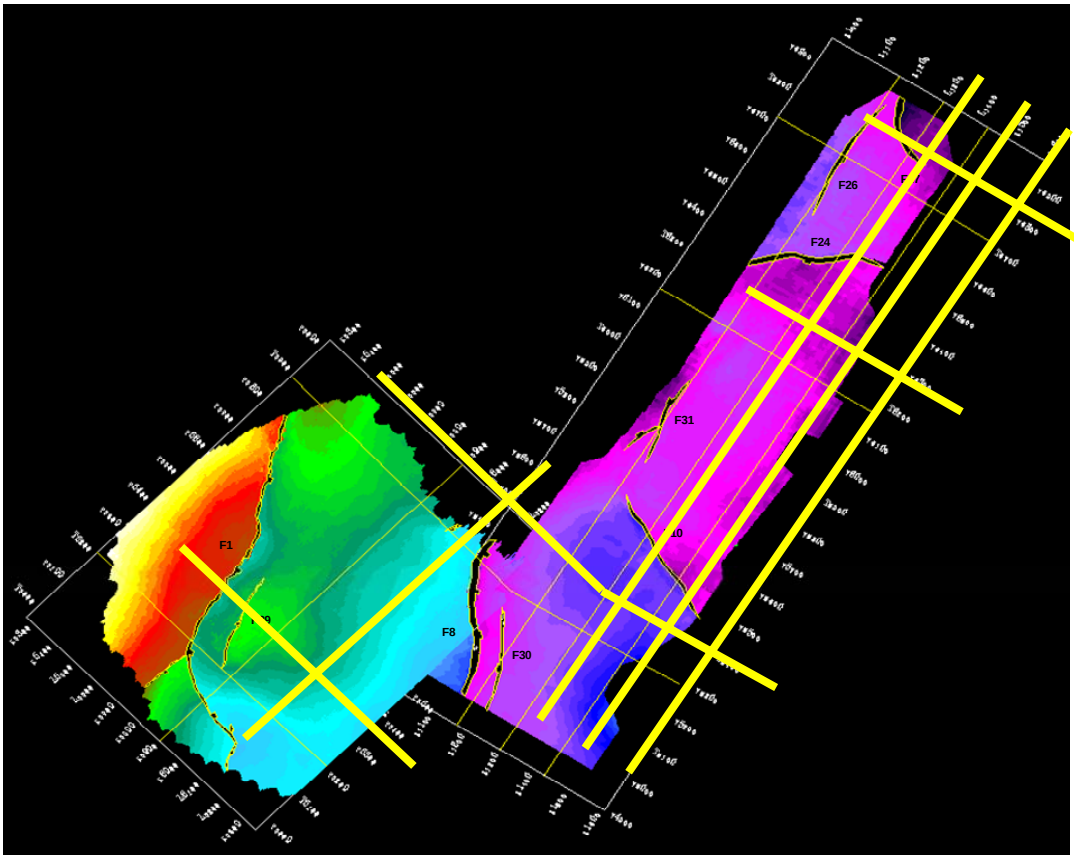

Source: Horizon 4—1,800 ms for sites GC1 and GC2
Note: all faults have been given numbers, as seen for some of them in the graphic
Figure 34. Fault scanlines for sites GC1 and GC2

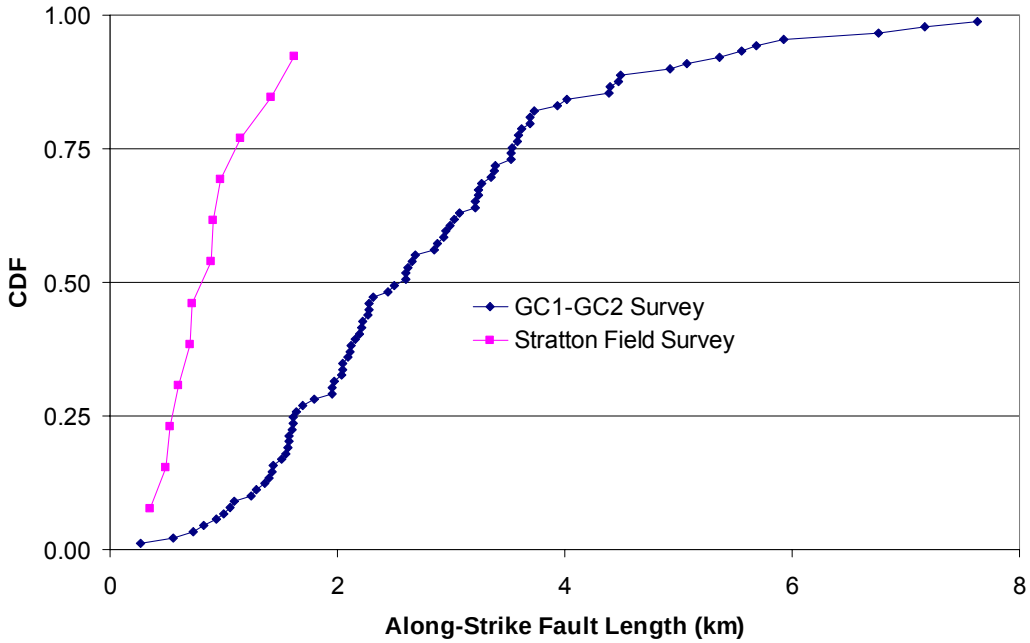

Source: GC1 and GC2 sites (**Figure 31**) and Stratton field data (**Figure 29**)
Figure 35. CDFs of fault length (GC1 and GC2 sites and Stratton field)

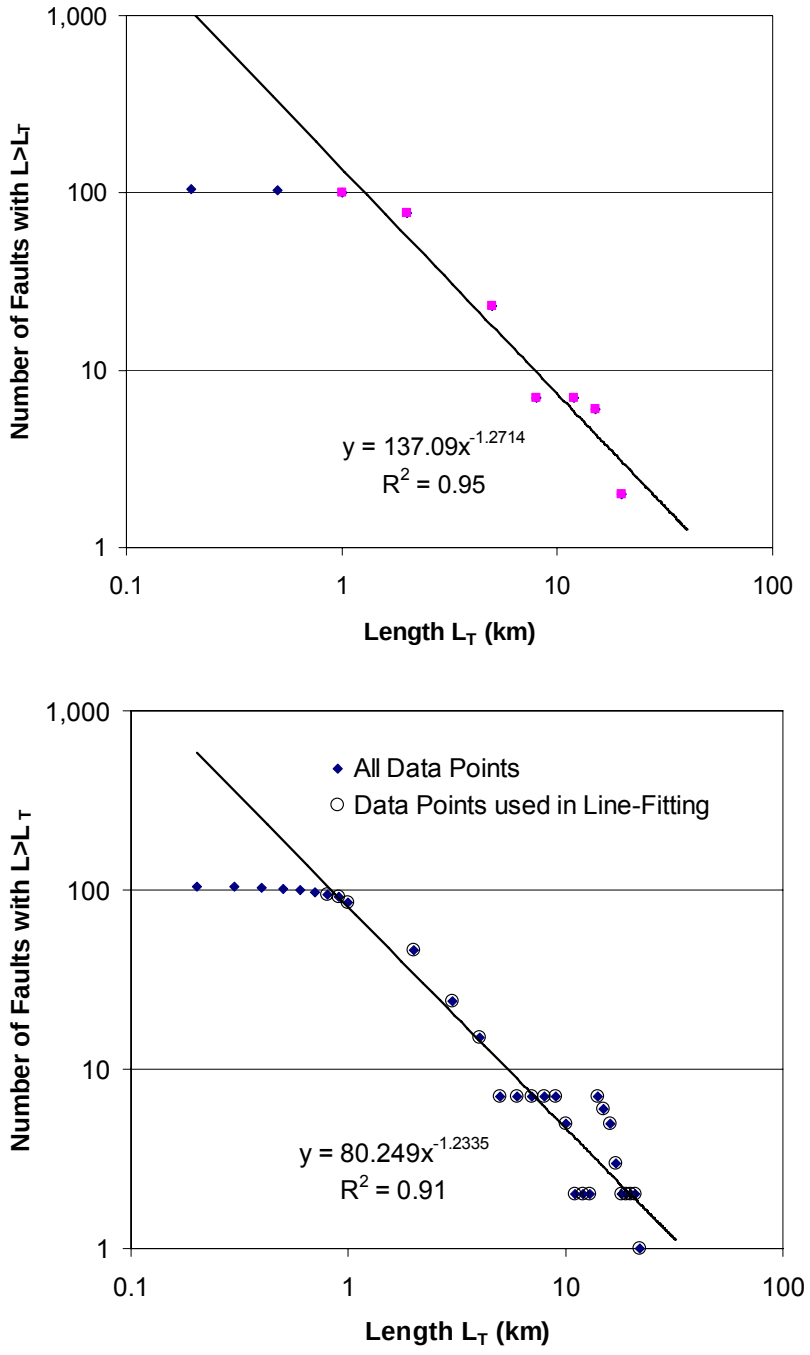

Source: GC1 and GC2 sites (**Figure 31**)

Note: Regional first-order growth fault has been added relative to **Figure 35**. Coefficient of the power law was computed with samples of fault length >1 km. Shorter fault lengths have not been sampled comprehensively.

Figure 36. Power law distribution of fault length (GC1 and GC2 sites)

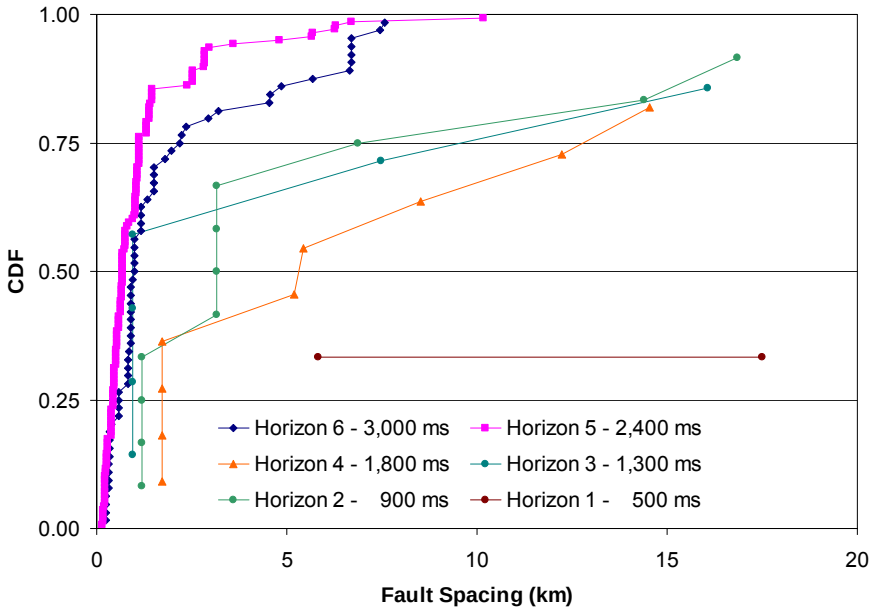

Source: GC1 and GC2 sites (**Figure 31**)
Note: The shallowest horizon (horizon 1) has only two data points and has been included to confirm the trend discussed in the text
Figure 37. Distribution of spacing between second-order faults

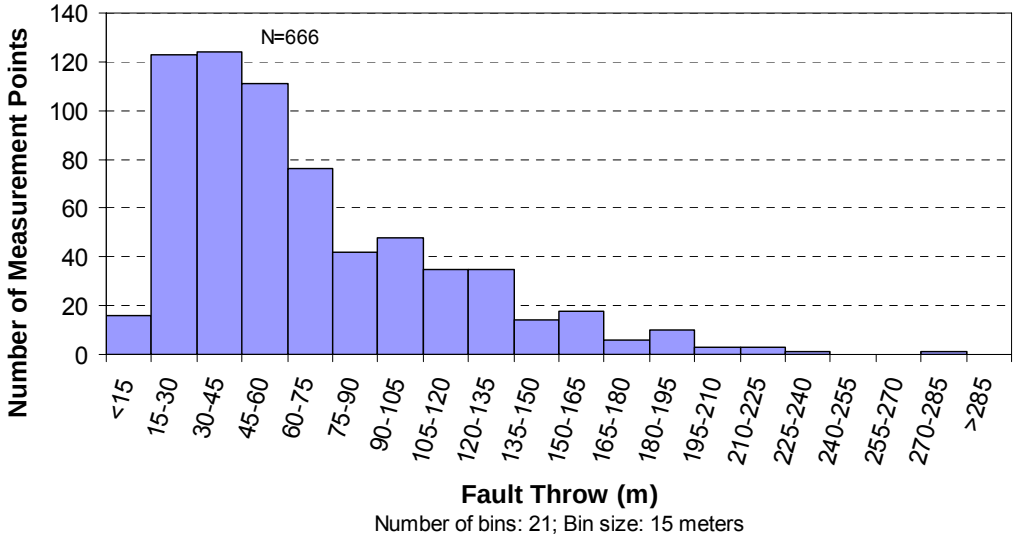

Note: Throw measurements from map are accurate within 16 m (±8 m) [50 ft (±25 ft)]
Figure 38. Fault throw distribution at the top of the Frio

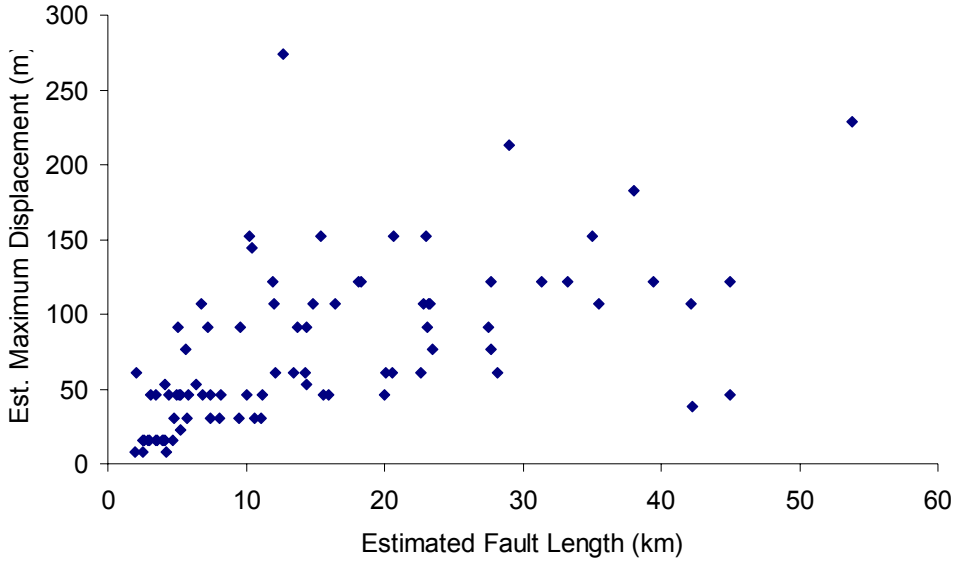

Figure 39. Cross-plot of estimated fault length and displacement

III.3.1.3 Trap Size within Fault Compartment

The distribution of trap and fetch areas, as described in **Figure 12** and Section III.1, follows an approximate lognormal distribution (**Figure 40** and **Table 8**), illustrating their generally small size (median at 8.0, 14.4, 21.9 km^2 for the trap, fetch, and combined areas, respectively). A similar work on their height (**Figure 41** and **Table 8**) leads also to approximate lognormal distribution with median of 45 and 275 m for the trap and fetch areas, respectively. These numbers are consistent with our knowledge of the Gulf Coast, where a long, shallow-dipping run-up leads to a domal structure. These results are consistent with the work done by Morton et al. (1983, Table 5), who looked only at fault compartments (that is, the sum of trap and related fetch subdomains) in the Frio of South and Central Texas. Although average size of the compartments in their study (**Table 7**) are somewhat smaller (16th percentile 1.5 and 3.6, median 5.7 and 11.2, 84th percentile 17.6 and 32.9, and average 11.9 and 19.2, respectively), the agreement is much better when Central Texas data are considered. In both cases, as in their additional dataset on the Wilcox Formation, the distribution is skewed toward the small compartment, suggesting a lognormal distribution.

Table 7. Statistics of the fault compartment

	16th Perc	**50th Perc.**	**Average**	**84th Perc.**
Morton et al. (1983) (mi^2)	1.5	5.7	11.9	17.6
Closure + fetch This study (mi^2)	3.6	11.2	19.2	32.9

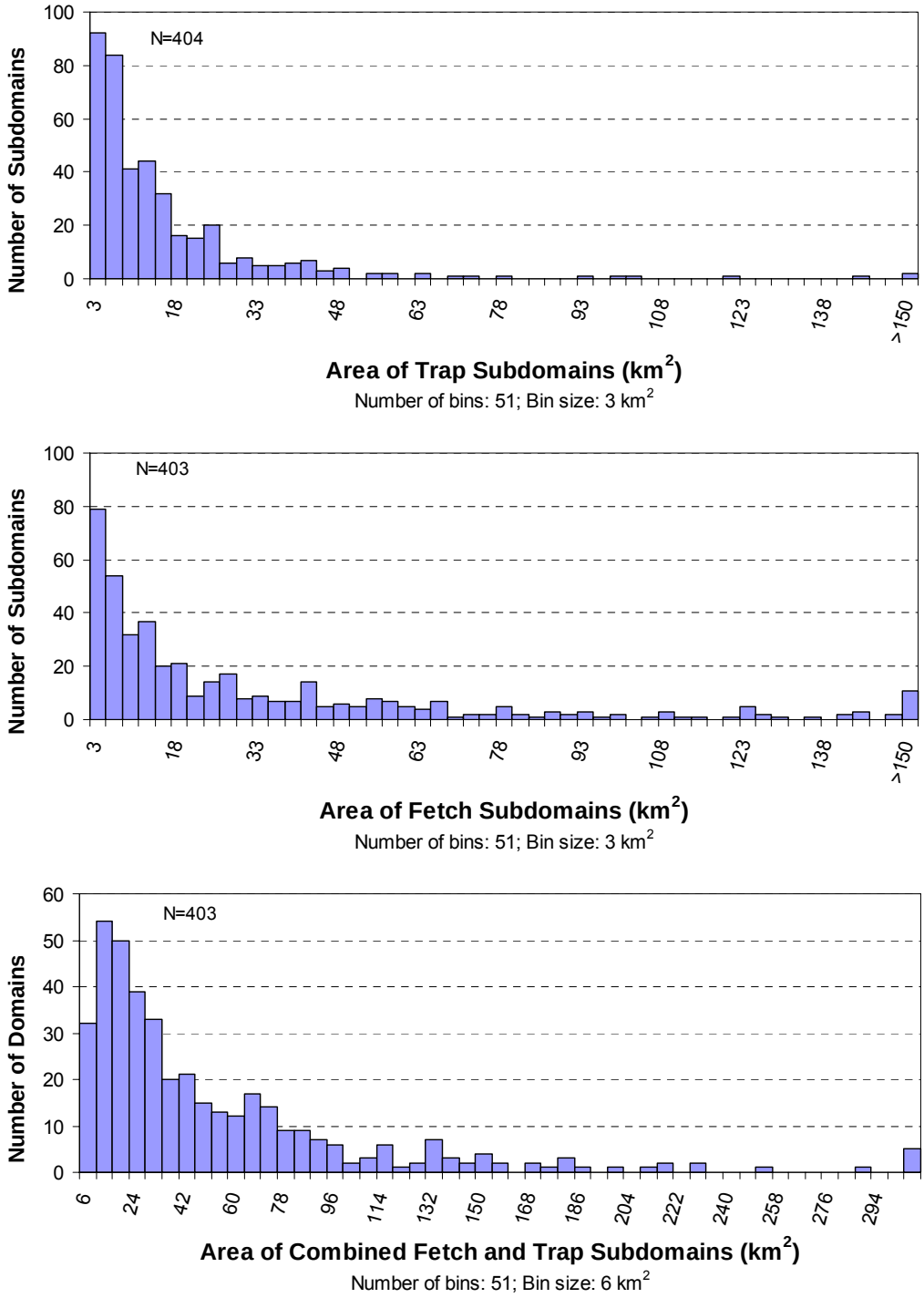

Note: Last bin includes all samples with values larger than the bin before last (>60 or >120 km²). Occurrence of closure areas with two fetch areas and closure areas with no fetch areas explains the slight discrepancy in the number of fetch and closure areas.

Figure 40. Statistical distribution of trap and fetch subdomain area

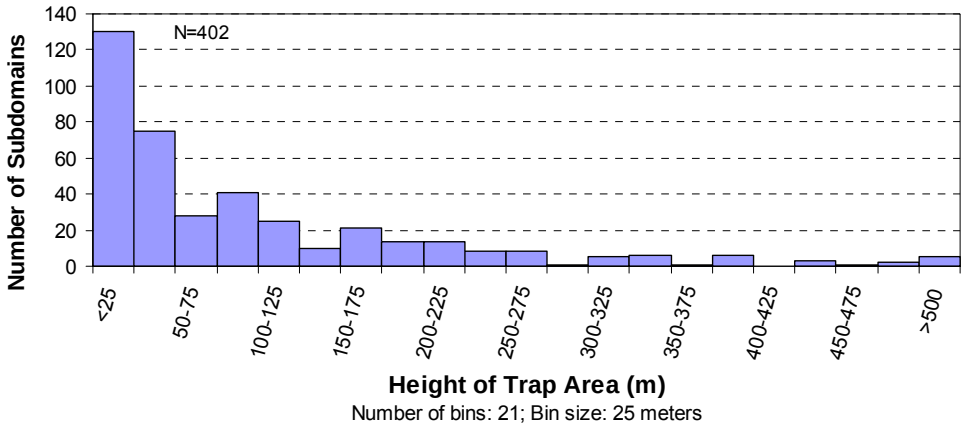

Figure 41. Distribution of height of trap areas

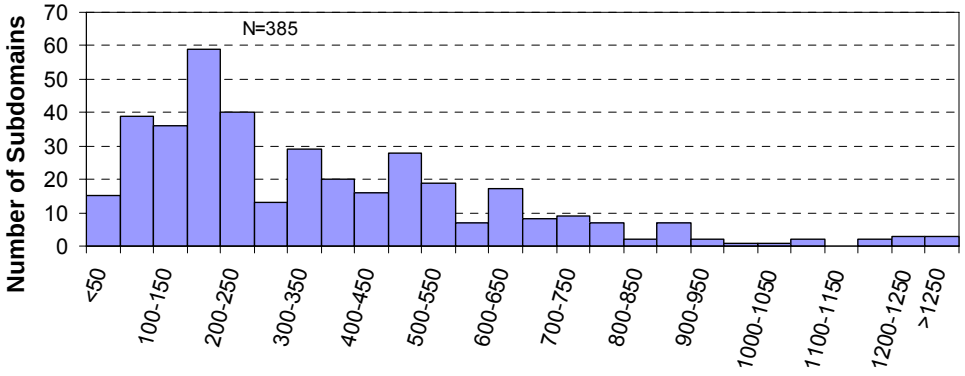

(a)

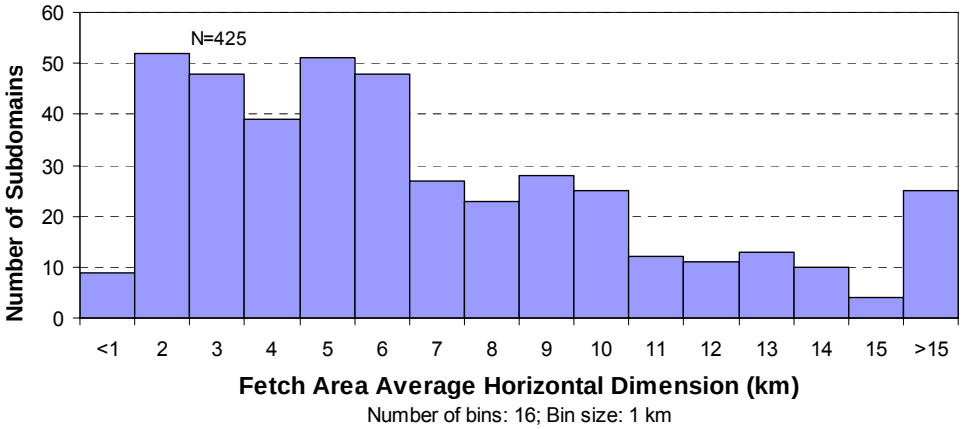

(b)

Note: average dimension computed in ArcGIS, with perimeter P and area A of the fetch area as the geometric mean of the solution of the following quadratic equation:

$x^2 - (P/2)x + A = 0$ assuming fetch areas are shaped as rectangular quadrangles.

Figure 42. Distribution of (a) vertical height and (b)average horizontal dimension of fetch area

A computation of trap capacity (**Figure 43**) can be performed by assuming that CO_2 density is 700 kg/m^3, that sand porosity is 30%, that sand fraction is 30%, that the area is cone shaped (1/3 of the product of the area by height), and that gas saturation is 70%. Trap height was also measured from contour maps. **Figure 43** suggests that most traps will not hold more than 10 Mt CO_2, an amount smaller than the lifetime output of a typical power plant (5 Mt/year for 30 years).

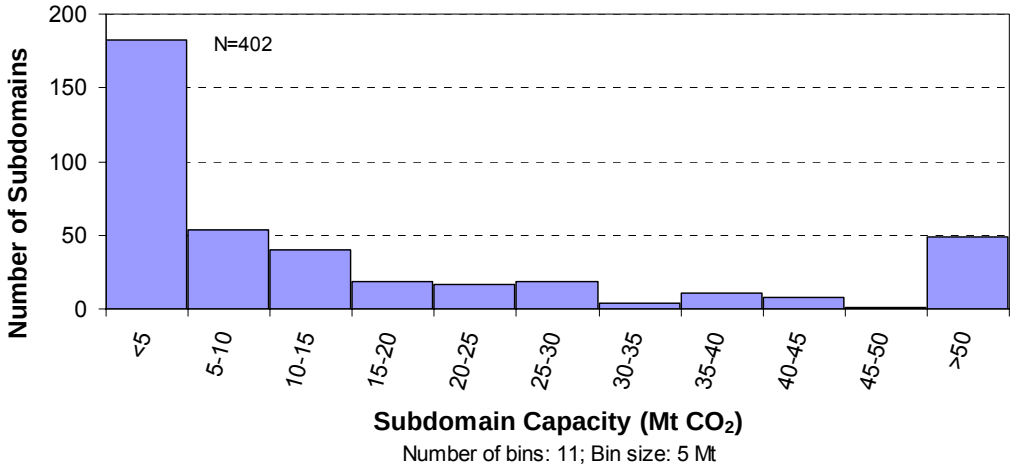

(a)

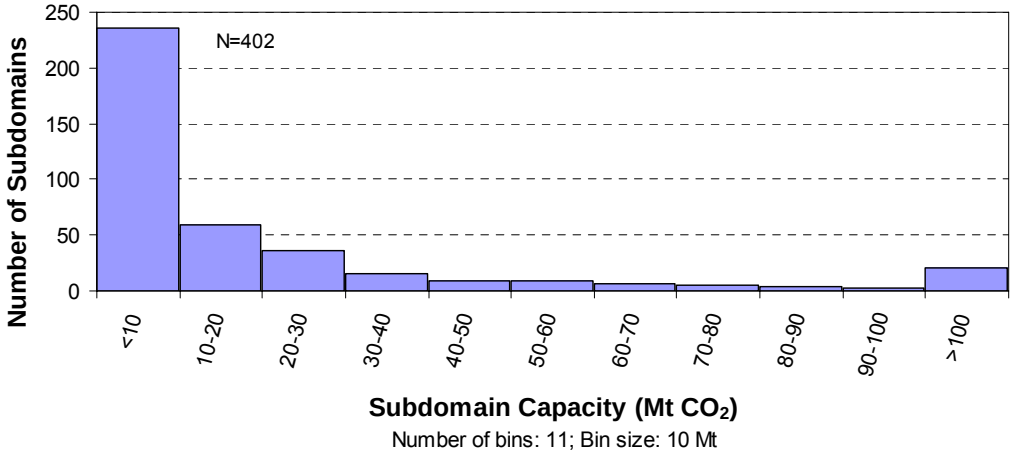

(b)

Figure 43. Distribution of trap subdomain capacity with a bin size of (a) 5 Mt and(b)10 Mt

Table 8. Goodness-of-fit statistics for structural features

Parameter	Data Mean	Data Standard Deviation	Distrib. Law Preferred / (Best Fit)	Distrib. Mean	Distrib. Standard Deviation	Goodness-of-Fit Tests A-D	C-S χ^2 / d^o	K-S
Trap area (km^2)	14.72	26.33	Lognormal	14.73	25.55	0.32	9.86 /	0.03
Fetch area (km^2)	32.56	48.17	Lognormal	40.52	121.65	1.75	31.38 /	0.05
			(Weibull)	Location=0.06,Scale=9.75 Shape=0.69		1.00	33.80	0.04
Combined area (km^2)	49.73	59.26	Lognormal	51.86	77.93	0.35	12.24 /	0.04
Height of trap area (m)	98.62	115.83	Lognormal	100.93	156.74	6.43	421.78	0.14
			(Weibull)	Location=4.45,Scale=84.44 Shape=0.82		5.49	411.73	0.13
			Most likely multimodal					
Height of fetch area (m)	348.86	276.87	Lognormal	364.51	374.67	2.24	125.08	0.08
			(Weibull)	Location=12.19,Scale=359.6 Shape=1.22		1.22	61.60	0.06
			(Gamma)	Location=12.78,Scale=221.1 Shape=1.52		0.98	76.77	0.06
Trap capacity (Mt)	32.29	123.45	Product of 2 Lognormal = Lognormal	37.31	249.00	1.08	25.16	0.05
Original oil in place, RRC districts 2,3, and 4 (10^6 m^3)	4.24	14.44	Lognormal	2.9	5.8	22.46	339.23	0.11
Fetch area horizontal dimension (km)	6.54	5.09	Lognormal	6.70	6.10	1.15	30.43	0.05
			(Gamma)	Location=0.56,Scale=4.13 Shape=1.45		0.31	24.70	0.03
			(Weibull)	Location=0.58,Scale=6.31 Shape=1.18		0.92	27.46	0.04

Note: Goodness-of-fit tests: A-D = Anderson-Darling; C-S = Chi-Square; K-S = Kolmogorov-Smirnov
Explanations: AD<1.5, C-S>, and K-S<0.03 indicates a good fit; fitting computations done with Crystal Ball

III.3.2 Fluids and Faults

Faults can localize fluid circulation or act as seals. The nature and configuration of the material present within the fault planes are the main parameters affecting the hydraulic properties of the fault. Fault quiescence or activity also greatly affects the fluid history within the fault plane. The geometry of the fault is another parameter that affects fault gouge nature and distribution along the fault plane and indirectly impacts fluid circulation. Four scales of investigation concerning the relationship between fault geometry and fluid circulation can be highlighted: (1) basin scale, in which fluid migration and accumulation along faults are related to large-scale geological parameters such as basin fill, tectonic events, and burial and thermal histories. Subsurface studies (Welte et al, 1997; Colling et al., 2001) or modeling studies are used for investigation at that scale; (2) fault system or reservoir scale, in which fluid migration and accumulation along faults are related to local fault system geometry; at that scale, fault connectivity and distribution are the main geometrical characteristics affecting fluid distribution and possible migration; (3) fault zone scale, in which fluid migration and accumulation along faults are related to small-scale characteristics such as gouge nature, distribution, and geometry within the fault zone; and (4) grain scale, in which fluid migration and accumulation along faults are related to microscopic parameters. The main parameters include fault zone material, grain-size distribution, and porosity configuration.

III.3.2.1 Fluid Circulation

Fluid circulation can be very rapid when associated with earthquakes or certain human activities. Some studies show fluid leakage related to earthquakes (Schwartz and Coppersmith, 1984; Sibson, 1989). This phenomenon, called *fault-valving*, (Sibson, 1990) is defined by a succession of fluid flux—fluid accumulation periods leading to overpressure. Interseismic periods show the presence of an impermeable fault zone (e.g., clay-rich gouge in the fault core), which becomes permeable owing to fluid injection in the fault zone. Therefore, a fault growth event can allow overpressured zones, originally intercepted by impermeable faults, to abruptly release fluids upward through the fault plane that just became permeable. Other studies indicate that human activity such as hydrocarbon production or dam construction (Kisslinger, 1976; Maury, 1997) can allow reactivation of faults. These studies show fluid pressure variations that trigger faulting with seismicity of magnitude 4 to 6 (Maury, 1997). In petroleum fields, such phenomena are observed during reservoir depletion and are often recorded during fluid injection (e.g., Snipe Lake, magnitude 5.1; Gasli, Ouzbekistan, magnitude 7, Maury, 1997). Many

other observations show that fluid circulation is mostly slow: oil migration within faults, oil seeps at fault tips, water leakage through faults, water table and spring behavior changes associated with earthquakes along the active fault zone, and mineralization within the fault zone.

Fluids can have physical (fluid pressure) and/or chemical (e.g., dissolution) effects on faulting. Variation in fluid pressure may influence permeability and deformational mechanics (Fisher and Zwart, 1996). Overpressure increases permeability and decreases fault effective stress, allowing the fault to move more easily. Such variation of fluid pressure can trigger fault growth periods without any change in regional tectonic stress. On the other hand, a decrease of fluid pressure (e.g., fluid leakage) can "freeze" fault activity. The presence of impermeable intervals (e.g., shales) within a permeable stratigraphic series (e.g., sands) can allow local fluid pressure to increase by differential compaction, which can trigger rupture (faulting) (Mandl, 1988). The dissolution and precipitation of solids due to fluid interaction are common processes within fault zones. These processes are more efficient when fluids and solids are in chemical imbalance (Feucht and Logan 1990) and when fluid circulation sustains this imbalance (De Boers, 1977; Gratier et Guiguet, 1986; Parry et al., 1988). The right chemical balance can trigger sealing of the fault plane. These effects can also vary spatially when different rock types are connected to a single fault plane, which can allow dissolution, transport of fluid, or mineralization. Microstructural evidence of porosity reduction indicates that dissolution-precipitation processes are important for fault weakening in hydrothermal conditions (Streit and Cox, 2000). Natural faults may therefore be weaker than predicted by dry frictional experiments if pore fluids migrating through active faults activate dissolution-precipitation processes.

III.3.2.2 Fault Hydraulics and Sealing Processes

Faults seal by several processes: (1) diffusive mass transfer, (2) crystallization, (3) plastic deformation, (4) cataclasis, and (5) clay smearing. Studies on pressure-solution processes in relation to diagenesis (Durney, 1972; Angevine and Turcotte, 1983; Fuchtbauer, 1983) indicate that diffusive mass transfer occurs at depths greater that 1,000 to 1,500 m. Nevertheless, pressure solution processes become more predominant owing to (1) grain-size reduction (Weyl, 1959; De Boers, 1977), (2) temperature increase (De Boers, 1977), and (3) clay presence (De Boers, 1977). Crystal growth can increase sealing of tension cracks and faults by reducing pore

configuration. These processes reduce porosity and permeability (Knipe, 1992). The rearrangement of crystals by elastic deformation within the fault zone can affect the spatial permeability configuration and potentially increase fault sealing. Grain size and pore size are reduced by cataclasis (matrix porosity) (Pittman, 1981; Aydin and Johnson, 1983; Antonellini et al., 1994). Nevertheless, increase of fracture density (fracture porosity) by cataclasis can have the opposite effect and can increase permeability (Crawford, 1998).

Pores can be plugged or filled by clay material (sometimes bitumen), which reduces porosity of the fault core. Clay occurrence in fault zones has been documented by many authors (Niger Delta: Weber et al., 1978; Gulf Coast: Smith 1980; North Sea: Knott, 1993). The presence of clay within the fault core can be explained by several processes that are regrouped under the term of smearing (Lindsay et al., 1993):

- Clay intrusion by diapiric processes (Bruce, 1973; Lyndsay et al., 1993)
- Segmentation with remaining contact of shaly intervals by fault array within a composite fault zone (Smith, 1980; Downey, 1984)
- Cementation due to clay minerals transported by fluids within the fault zone (Wu, 1978)
- Clay shearing (Weber et al., 1978) related to incorporation of clay within the fault core followed by ductile shearing during fault movement
- Abrasion that relates to cataclasis of fault core material down to a clay grain-size material (Lindsay et al., 1993)

Fault zone hydraulic properties have been evaluated using analog and natural examples. These studies allow quantifying of porosity and permeability in deformed zones. Measurements have been obtained on (1) sheared porous sandstone (Antonellini et al., 1994), (2) deformed clay samples (Al Taaba and Wood, 1987), and (3) fault gouge (Faulkner and Rutter, 1998; Gibson, 1998;). Analog models (Crawford, 1998; Zhang et al., 1999) and outcrop studies (Engelder, 1974; Chester and Logan., 1986; Rutter et al., 1986; Antonellini et al., 1994; Faulkner and Rutter, 1998; Gibson, 1998) demonstrate the variability of processes within the fault zone. Different studies describe physical or physico-chemical mechanics within the fault zone, such as grain-size reduction (Aydin and Johnson, 1983) and dissolution and mineral growth (Pittman, 1981; Knipe, 1992). These phenomena often reduce fault permeability and allow faults to act as barriers for fluid circulation. These studies do not account for the longitudinal drains often

observed (Sibson, 1987; Gratier et al., 1993). Results of these studies show a reduction of permeability in the deformed material (fault core) (Gibson, 1998) and the presence of an anisotropic permeability configuration that follows the clay mineral orientation (Faulkner and Rutter, 1998) and that is proportional to the deformation applied (Vasseur et al., 1995; Zhang et al., 1998).

III.3.3 Fault Leakage

III.3.3.1 Leakage in Space

Faults limit cross-fault flow for two reasons—juxtaposition of permeable strata against less permeable layer and clay smearing along fault planes (Yielding et al., 1997). Juxtaposition considers the nature of the contact between sediments on both sides of a fault plane (Downey, 1984; Knipe, 1992; Jones and Knipe, 1996). The juxtaposition is efficient as a barrier if low-permeability intervals on the upthrown side of a fault plane are in contact with high-porosity intervals on the downthrown side of the fault plane (e.g., shale interval present on upthrown side of a fault down to the downthrown side spill point within a sandstone interval). Other authors (Smith, 1966; Watts, 1987) introduced the concept of a membrane for a fault working partly as a barrier and where there are juxtaposed sedimentary series across the considered fault plane. Processes involved in the membrane concept take into account capillary and fluid pressure within the rock. Such an approach allows investigation of a more dynamic fluid/fault relationship, with faults acting either as barriers or conduits in relation to a wide range of parameters. It has been observed that fluid circulation along fault planes is concentrated in the outer damage zone, where small connected fractures are observed. In contrast, the fault core shows a decrease of cross leak (transversal permeability) due to cataclasis, clay smearing, and other processes that reduce local fluid movement. These results indicate that fluid circulation can occur upward along transversally sealed fault planes. Numerous observations indicate that faults play a major role in the migration pathways of rock fluids. Studies of hydrocarbon seeps are important sources of information about leaking systems (Peckmann et al., 1999; Campbell et al., 2002). Several giant oil and tar accumulations were discovered from their leakage to the surface, e.g. Athabasca (Canada), Maracaibo province (Venezuela), Akanskoye (Volga-Urals), Surakhanskoye (Azerbaijan), Masjid-i-Suleman (Zagros, Iran), and Tampico province (Mexico).

III.3.3.2 Leakage in Time

Most faults have complex episodic behavior that is related to fault geometry, décollement zone characteristics (in the case of salt or shale-related growth faults),

loading/burial history, and fluid/pore pressure characteristics. Most of these parameters are interconnected (e.g., burial affects compaction and fluid movements), and the kinematic study of faults is often a difficult task.

For Morrow et al. (1981) and Morris et al. (1996), continuous or discontinuous fault behavior is related to the shear strength of the fault plane. This parameter is related to mechanical properties of the faulted rock and to the preexisting fault plane's geometrical properties (e.g., a highly rugose fault plane allows higher fault stress; Miller, 1996). Some permeability studies on faulted rock masses (Barton et al., 1995) present strong evidence that faults that are critically stressed in the current stress field (i.e., capable of slipping) are permeable, whereas those that are not critically stressed are not permeable.

Wiprut and Zoback (2000) proposed that as gas accumulates in a permeable reservoir bounded by a sealing fault, pore pressure at the fault/reservoir interface increases because the pore-pressure gradient in the gas is considerably less than the hydrostatic gradient owing to the lower density of the gas. As the height of the gas column increases, at some point pore pressure will be sufficient to induce fault slip (reactivation), providing a mechanism to increase fault permeability and allow leakage from the reservoir. These authors studied a normal fault in the northern North Sea that followed the Sibson (1990) fault-valve model (or pressure-regulated valve), in which sealed faults allow pressures to accumulate and rise to a certain value before fault slippage occurs and fluids leak upward along the fault.

Cartwright et al. (1996) and Bouroullec (2001) showed that normal syndepositional faults have mechanical thresholds that, if exceeded, allow fault activation. Faults accumulate stress by friction and pore pressure rise during small fault growth activity that leads to a sealing of the fault (period of fault inactivity), followed by a more intense fault growth period, during which fluids are released and pore pressure drops. Bouroullec (2001) documented this phenomena using throw versus depth analysis on 81 normal faults located in the Gulf Coast, Texas. Each fault shows a different mechanical threshold at which slippage occurs. This threshold is reached after a period of fault inactivity that allows pore pressure to increase and reach a critical value. The fault-slip rates measured for these faults are higher after an inactive period. This result is interpreted as an increase of fluid amount within the fault planes that allows decreasing of fault friction (lubrication).

Hooper (1991) presented a long list of evidence that a growth fault can seal or actively transmit fluids. Galloway (1982) showed in a South Texas uranium province that currently sealing or minimally leaking growth faults were conduits in the past, as demonstrated by mineralogical evidence. Reducing fluids were released periodically, allowing the precipitation of uranium, traveling with meteoric waters. Similarly, generally higher water salinity of the uranium province has also been attributed to periodic deep discharges into the shallow aquifers. Current temperature distribution data also suggest that the same Wilcox fault trend is at least periodically leaking (Bodner and Sharp, 1988). In this case, as in most other cases, the length of leaking vs. sealing periods remains an unresolved problem.

III.3.4 Fault Parameters

The ultimate effect of faulting is compartmentalization of the subsurface. Fault properties will control the open/closed nature of the compartments that will, in turn, control injection pressure, maximum capacity for CO_2 storage, and leakage potential. Relevant parameters for fault/fractures include orientation, length, density, and flow properties. Many studies have been performed on the compartmentalization of oil and gas reservoirs by faults and the impact of fault tightness on flow properties. Sealing properties of faults can be described as membrane or static sealing, which results from capillary forces and is relevant to multiphase flow, or as hydraulic-resistance or dynamic sealing, in which low permeability of the medium impedes flow (valid in both single- and multiphase flow) (Watts, 1987).

By studying the juxtaposition of lithology across fault planes in cross section (one dimensional, Knipe, 1992) or over the entire fault plane (two dimensional, Yielding et al., 1997), it is possible to characterize the distribution of permeability in relation to the host rocks series. Shale gouge ratio (SGR) has been used as a parameter for estimating fault seal (Yielding et al., 1997). SGR takes into account the proportion of clay in the gouge in relation to the quantity of clay in the sediments on both sides of the fault plane and in relation to the fault throw. Some have questioned its accuracy and have suggested that it underestimates fault sealing strength (Eichhubl et al., 2005). It is defined by:

$$SGR = \frac{\sum V_{sh} B}{D} \text{ with } \sum B = D$$

where V_{sh} is clay fraction over thickness B, and D is fault throw. Clay fraction is not defined as the percentage of clay mineral in a small sample but as the fraction of clay beds of sufficient

thickness to be recognized on geophysical logs. Total thickness $\sum B$ must be equal to the throw and be measured in the fault section of interest. It follows that *SGR* must be in the 0 to 100% range. In most cases, some average measure of V_{sh} is equated with *SGR*. Calibration is required to determine the leaking threshold in a particular site. It follows that this approximation is more valid for faults with larger throws, where the average shale content of the formation will approach V_{sh} and *SGR*. James et al (2004), Yielding et al. (1997), and Yielding (2002, p. 2), following Watts (1987), postulated that the probability that clay smear is continuous is close to 1 for V_{sh}>40% or SGR>20%, that is, that any fault section with a SGR higher than 20% is membrane sealing. Higher SGR values do not translate into better sealing performance. Several other measures have been developed, including the Clay Smear Potential (CSP), which takes into account the potential for a clay-rich interval to be incorporated within the fault zone (clay shearing).

Some have correlated this easy-to-compute SGR parameter with more complicated parameters. For example, Bretan et al. (2003) calculated the following expression for capillary entry pressure P_c (in bar) of the fault gouge:

$$P_c = 10^{\left(\frac{SGR}{27} - C\right)}$$

where *C* is a constant equal to 0.3 for depths less than 3 km (~9,850 ft), 0.25 for depths between 3 km and 3.5 km (~11,500 ft), and 0 for depths larger than 3.5 km. This expression assumes an oil density of 0.6 t/m^3 and a correction factor should be applied before its use in carbon storage computations. Another important parameter is permeability. Once the membrane seal is breached, the next defense against leakage is slowness of flow across the seal (hydraulic seal). Hydraulic seals may be insufficient to retain hydrocarbons for geologic periods, but they could perform satisfactorily for CO_2 storage, especially because of the compounding effects of relative permeability, expected to be small at low, nonwetting fluid saturation. Manzocchi et al. (1999) suggested a simple curve-fitting relationship to estimate the seal permeability *k* (in mD):

$$\log k = -4SGR - \tfrac{1}{4} \log D\,(1 - SGR)^5$$

where *D* is the displacement (throw) in meters or, more simply, $\log k = -5SGR$. However, Sperrevik et al. (2002) showed that those expressions do not capture actual measurements well.

III.3.5 Application to Gulf Coast

We estimated a reasonable trap volume distribution in a previous section using topographic attributes. Another way to estimate trap size is to use the volume of fluids trapped in them. Cumulative oil production from individual reservoirs is easily obtained from the RRC database (**Figure 44**). More than 80% of the individual reservoirs have a capacity of less than 5 million m^3 (roughly equivalent to 3.5 Mt CO_2). A comparison of **Figure 44**c and **Figure 43**b shows that there is an order-of-magnitude discrepancy between the computed size of traps and the measured size of reservoirs (original oil in place—OOIP), as illustrated by **Figure 45** and **Figure 46**. The discrepancy can be explained by an erroneous parameter estimation of trap size, by an inadequate extrapolation of the distribution at the top of the Frio to the whole Tertiary and Cretaceous sections, or by an incomplete filling of the trap containing the reservoir. However, it is more likely that reservoir size is not controlled by spill-point limited hydrocarbon trapping but by failure of membrane sealing across either the seal caprock or the fault, or maybe both. Another possibility is the presence of subtle spill points noticeable only through large-scale detailed mapping. It should be noted that, in contrast to oil and gas accumulations where across-fault leakage may cause the loss of the hydrocarbon resource, across-fault CO_2 leakage will be attenuated through capillary trapping in the formation across the fault. In addition, upward along-fault leakage of hydrocarbons may generate useful exploration clues, whereas the same process for CO_2 storage must be avoided.

In order to understand the odds of leakage occurring on these reservoir-bounding faults, five Frio wells from across the study area (**Table 9**) were logged and sand/shale thickness was extracted. It is imprudent to make generalizations from only five wells, but **Figure 47** suggests that it may take a throw of 200 m, in some cases, for the shale fraction (equated here to the SGR) to reach the value of 40%, determined previously as the threshold at which a fault is in all likelihood sealing. As can also be seen on the plot, 50 or 100 m of throw is sufficient to reach 40% in many cases. The fault throw distribution (**Figure 38**) shows that a significant fraction (~40%) of the measured throws is less than 50 m. This observation could explain why the oil reservoirs do not realize maximum trap capacity. Zieglar (1992) also suggested that most oil reservoirs are not filled to the spill point.

However, it is important to note that a smaller trap capacity at a longer time period (millions of years) does not necessarily mean that the trap cannot hold CO_2 at full capacity for a

much shorter timeframe but is still sufficient to accomplish the goals of carbon storage (a few thousand years).

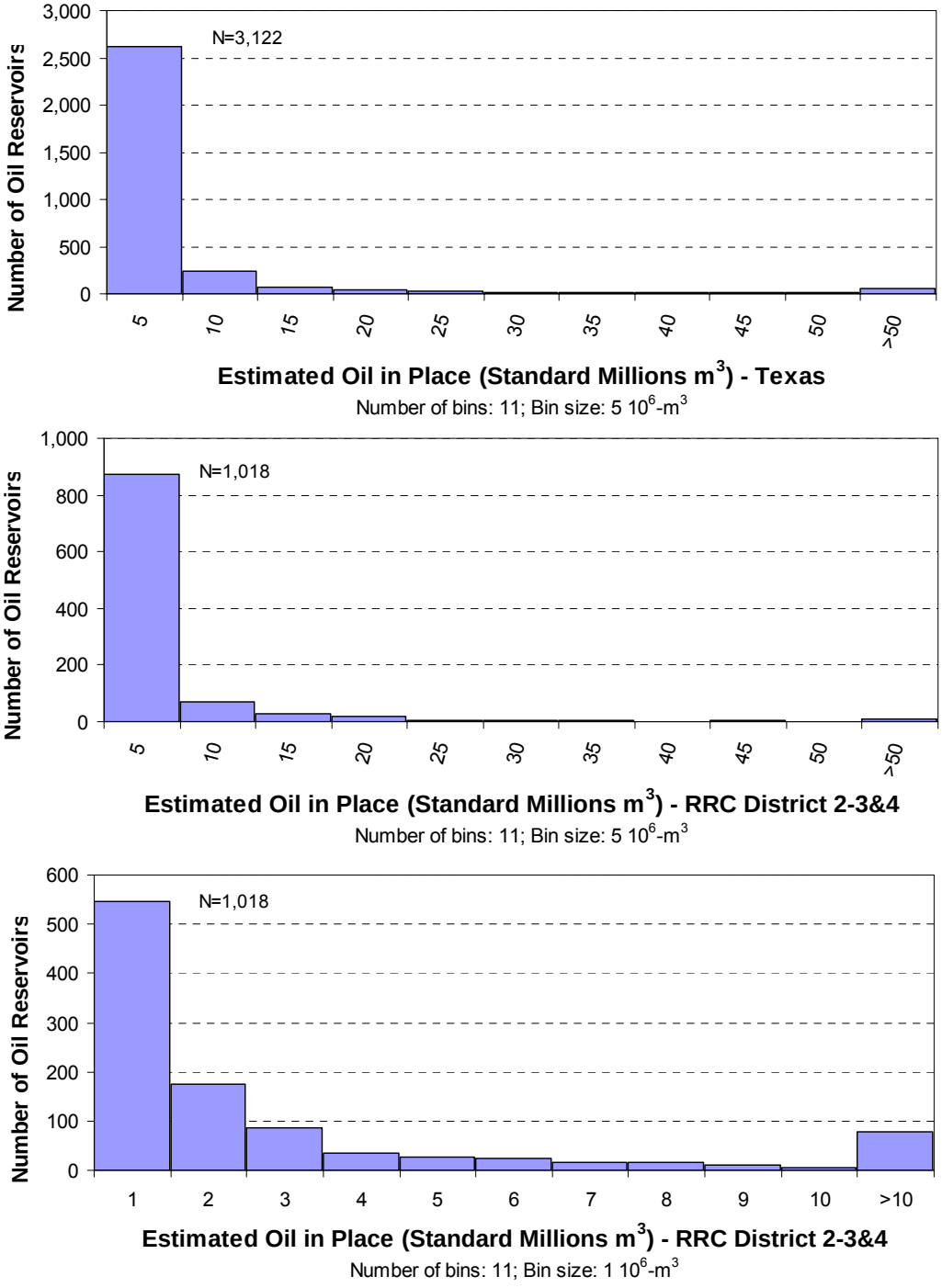

Figure 44. Oil in place as a proxy for reservoir pore volume: (a) in Texas; (b) in RRC districts 2, 3, and 4; and (c) still in districts 2, 3 and 4, but with a focus on the smaller reservoirs.

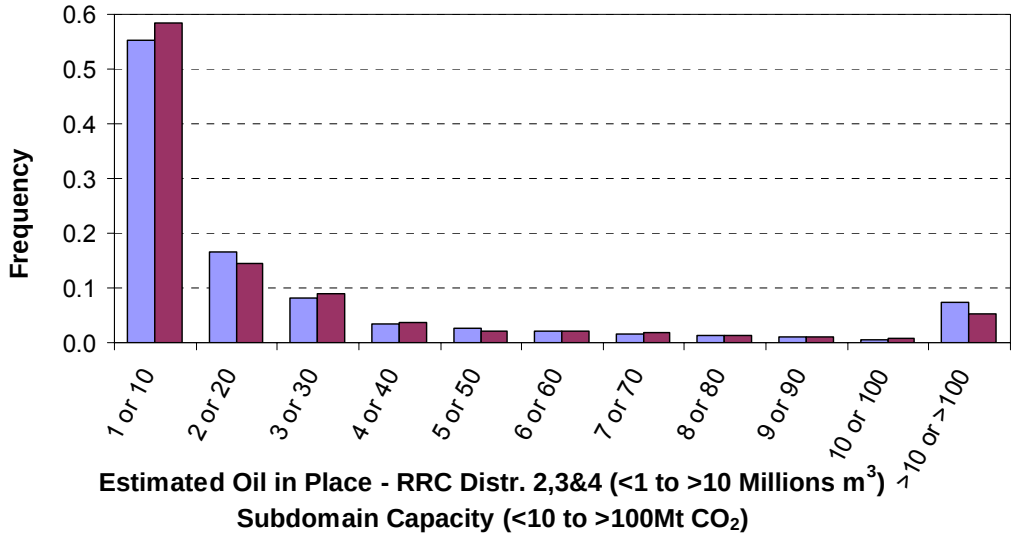

Note: "1 or 10" applies to oil in place ("1") and subdomain or trap capacity ("10") and shows the one order of magnitude discrepancy

Figure 45. Comparison of normalized distributions of OOIP and estimated trap size

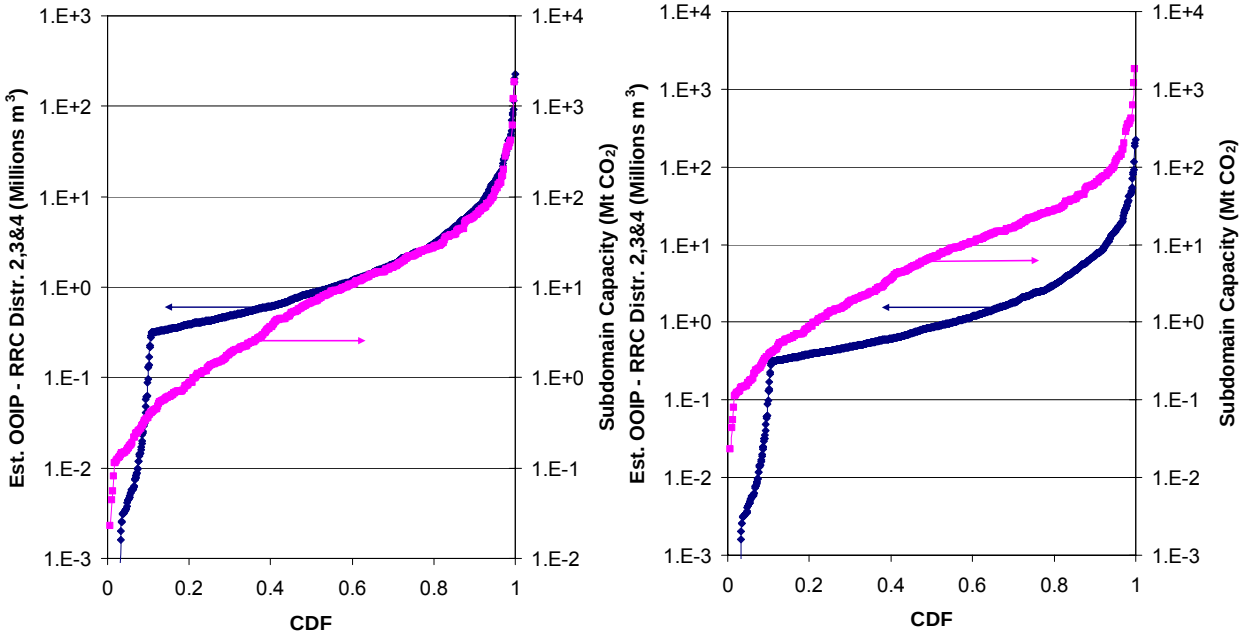

Figure 46. CDFs of OOIP and estimated trap size

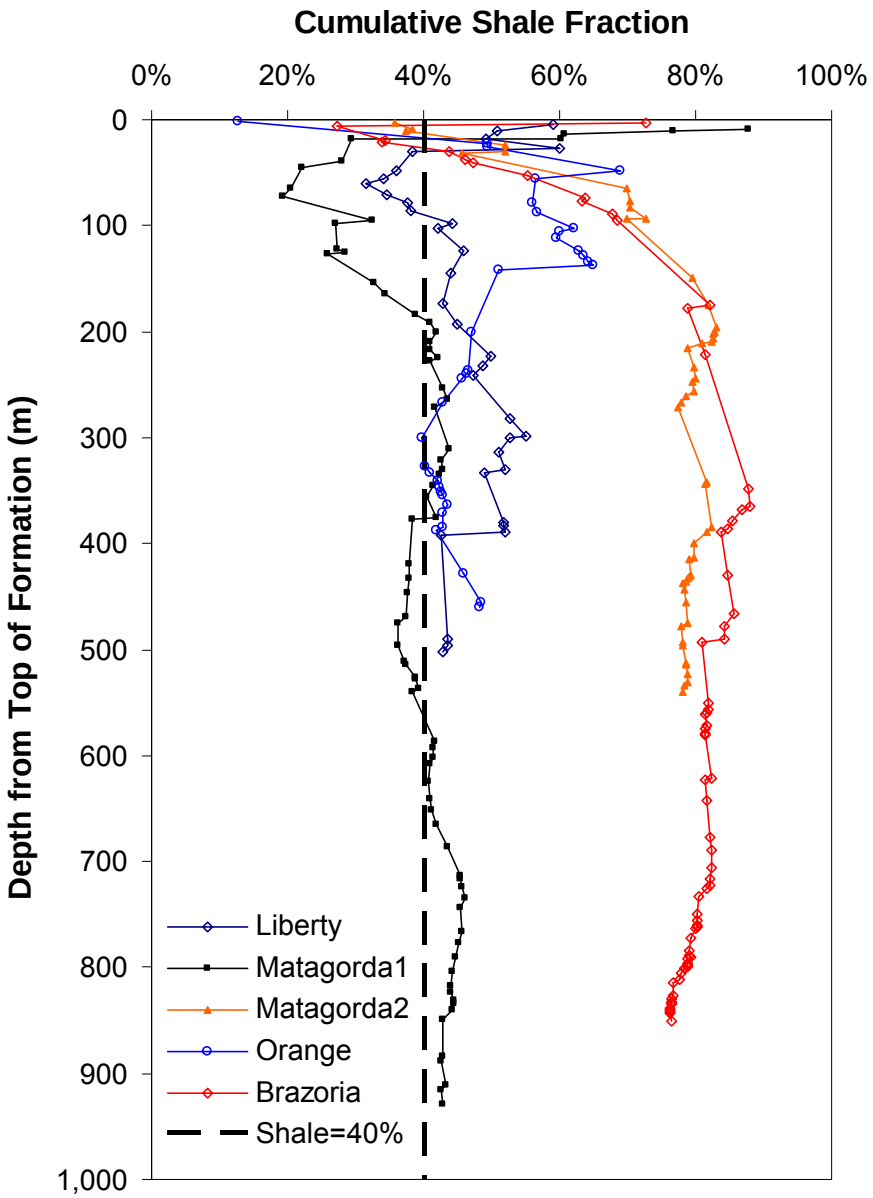

Figure 47. Shale fraction in selected wells

Table 9. Parameters of selected wells

Well Information	County	Completion Date	Depth to top of Frio (m)	Frio Thickness (m)
Floyd L. Karsten Sun Gulf Humble tract 2 Well #4 South Dayton	Liberty	2/19/1953	1390	530
Mid-Century Oil and Gas Co. Florence Howard A-1 Wildcat	Matagorda	2/23/1963	2485	935
Monsanto Chemical Co. Doman #1 Wildcat	Matagorda	8/29/1960	2332	547
Gulf Coast Leasehold, Inc. Lutcher Moore 1, Wildcat	Orange	7/9/1953	2153	770
Phillips Petroleum Company Houston M #2, Chocolate Bayou	Brazoria	6/2/1956	2768	853

III.4 Heterogeneity and Depositional System Architecture

Capillary trapping does not require a seal to be effective. It depends on (1) the volume of the saline formation contacted by the CO_2 plume, (2) the heterogeneity of the formation, and (3) its rock petrophysics and capillary properties. The importance of formation heterogeneity has been noted multiple times, for example in Hovorka et al. (2004a), Doughty and Pruess (2005), and Ambrose et al. (2006). Petroleum engineers have been concerned by the impact on oil recovery of heterogeneity and barriers to flow and particularly by shale stringers (e.g., Mattax and Dalton, 1990, p. 37). Current industrial CO_2 injection for disposal (Sleipner in the North Sea and In Salah in Algeria) uses horizontal wells, which may have been chosen for engineering reasons, but they also maximize sweep efficiency. Sleipner field data show that lower-permeability stringers have a large impact on the spreading of the CO_2 plume and increase aquifer contacted volume. The 300+-meter-thick marine Utsira sands of Miocene age at the Sleipner site consist of a lowstand turbidite fan complex of stacked sands, with small, thin shales (Chadwick et al., 2004). It follows that the basin fill has been interpreted as a relatively homogeneous graben fill of fine sand, with very thin but laterally extensive intercalations of a shaly nature, and overlain by several massive shales. The baffling effect of shaly stringers retards possible leakage but perhaps, more importantly, they increase the path to possible leakage point(s), increasing the capillary trapping effect and decreasing the likelihood of leakage. It follows that optimal permeability and heterogeneity exist. The high permeability of a clean sand will favor injectivity but also shortcut most of the formation if too homogeneous. This fact has also been recognized in the oil industry, which has introduced the use of polymer flooding to limit preferential flow. On the other hand, the Gulf Coast area displays a high level of heterogeneity (**Figure 11**), conditions being particularly favorable for containing leakage from the main storage area, and it is promising as an overall attenuation process. However, an excessive heterogeneity will translate into numerous hard-to-reach insulated sand pockets. The question of the migration mode, between the end-members of a widely diffuse spreading and of a localized fingering/channeling, remains open, although all indicators point to a limited role for fingering (e.g., Kumar et al., 2004; Bryant et al., 2006).

III.4.1 Geometry

Numerous studies have focused on an understanding of formation geology and depositional systems because they control formation heterogeneity and subsequent flow. When studying clastic sedimentary deposits, geologists often draw sand-percent maps whose contour

line trends direct sedimentologic interpretation. For example, fingers stemming from an axis suggest a deltaic environment, and elongated contour lines parallel to an ancient shoreline suggest a barrier or strandplain type of environment. Understanding and mapping of depositional systems are important because of their influence on sediment grain size and sand/shale body dimensions. There have been many studies of aquifer heterogeneity and of its importance on flow and transport (e.g., Galloway and Hobday, 1996; Koltermann and Gorelick, 1996; Eaton, 2006). There have been many approaches to reproducing the fundamental heterogeneity of the subsurface in models (Fogg et al., 1983; Fogg, 1986, 1989; Koltermann and Gorelick, 1996). Petroleum literature is also awash with reservoir monographs detailing the importance of an accurate knowledge of heterogeneity. The industry as a whole has moved from simple geostatistical models that, in general, do not take into account underlying geology, except maybe by attributing some anisotropy, to full-fledged geocellular models (software packages such as RMS, Gocad, or Petrel) that integrate borehole information with current knowledge of depositional systems (e.g., McKenna and Smith, 2004). Another, more economical, approach is to use transition probability statistics (Carle and Fogg, 1996; Elfeki and Dekking, 2001; Hovorka et al., 2003, p. 12; Doughty and Pruess, 2005). Geophysical logs are extensively used to obtain such information. For instance, channels appear as blocky, high-resistivity zones with no significant shale break. High-resistivity zones of several thin sands separated by muds can be interpreted as transitional facies from channel to interchannel areas.

Geology is extremely relevant to leakage potential. Gulf Coast depositional systems result from the interplay of sea-level variations, sediment supply, tectonics, and other factors. See Appendix A for relevant geological facts. In simple terms, a long depositional history results in alternating layers of sandy and shaly sediments. The Gulf Coast sediment package may contain as much as 70% clay, mudstone, and similar rocks, which increase gulfward. This observation is consistent with the estimation that 60% of all sedimentary rocks are mudrocks (Potter et al., 1980) and >75% for clastic-filled basins (Jones and Wang, 1981). The sediments are brought by rivers to the coast and farther out where they accumulate, according to the energy level of the depositional system and to their grain size. If we examine the nature of the accumulation at one point in time, the depositional systems will be fluvial (sand/silt) and interfluvial (silt/shale and minor sand), deltaic and associated systems along the coast, and then farther away from the coast, mainly mud. Vertically, at a first rough approximation, because the

accumulation is prograding, we would encounter first, at depth, oceanic muds, then deltaic and associated systems, and finally terrestrial (fluvial and associated) systems. The picture is then complicated by sea-level variations, in which during high sea level, mud facies can directly cover fluvial depositional systems (e.g., Anahuac Shale) by the action of growth faults. A variety of scales related to the size of geologic features can be considered in developing flow properties: basin (100's of kilometers), depositional systems (10's of kilometers), local channels (kilometers), etc. Depositional environments, however, are the scale of interest in this study. For all practical purposes in this work and more generally for a regional approach, sediments can be divided into two types: sand and shale (e.g., Sminchak et al., 1996; Andrade et al., 2000; King et al., 2002).

Some previous studies have looked into Gulf Coast sediment heterogeneity. The Fogg et al. (1983, p. 18) numerical modeling of formations with similar architecture sheds some light on the topic. They suggested, through numerical modeling, that sand bodies within formations with less than 20 percent sand are not connected. This observation was made on the fluvial sands of the Wilcox Group. They also concluded the regional K_v/K_h ratio to be on the order of 10^{-4} (Fogg et al., 1983, p. 35), much smaller than the currently accepted ratio of 0.5 to 0.1 for sandstone aquifers. Similarly, ground water numerical models of the Carrizo-Wilcox, Queen City, and Sparta Formations have concluded that regional vertical conductivity is orders of magnitude smaller than regional horizontal permeability (Dutton et al., 2003; Kelley et al., 2004). This suggests that multiple mud and silt layers have a large impact on the flow system.

III.4.2 Dimensions and Connectedness

There is an extremely rich literature on depositional systems in the Texas Gulf Coast because of the abundance of oil and gas targets. Continuity of the fast pathway is the most important control on flow, in particular sand-body interconnectedness (Fogg, 1986; Koltermann and Gorelick, 1996). A study, reported by Galloway and Hobday (1996, p. 349), set the threshold for connectivity at 40% sand content. Sand bodies can arrange themselves geometrically in a variety of ways with little overlap or consequent overlap (i.e., a new sand body is eroding or remobilizing part of an older one). Weber and van Geuns (1990) and Mijnssen (1991) differentiated three categories: layer cake, with extensive sand sheets; jigsaw puzzle, with connected sand bodies of different flow properties and possible low-permeability baffles at the transition, and labyrinth, where sand body continuity is more tortuous if it exists. They also

suggested minimum well spacing that would allow satisfactory characterization of the reservoir: 305 to 366 m (1,000–1,200 ft), 183 to 244 m (600–800 ft), and 61 to 91 m (200–300 ft), respectively. In addition, unique features such as incised valley fills (e.g., Yoakum Channel of middle Wilcox age in the Gulf Coast) perturb the local stratigraphic composition and could be fast pathways to the surface and should be carefully mapped.

Two studies are of direct interest to this report. Fogg (1989) did a stochastic analysis of aquifer interconnectedness of the Wilcox Group along the Gulf Coast. He described Wilcox thick, blocky sand lying primarily along the meanderbelts of mixed- to suspended-load fluvial systems with a conductivity of 1 to 10 m/d (~1–10 D); conductivity of interchannel sediments is one order of magnitude less. Sands are generally less than 30 m (100 ft) thick (p. 11); paleochannels are ~300 m (1,000) ft wide (p. 31), consistent with mixed-load fluvial, as suggested by the range of the width/depth ratio of 10:40 usually reported for mixed-load rivers (1,000/<100 yields >10). Actual lateral extent of accumulation in the meanderbelt is wider because it consists of several channels combined (Fogg, 1989, p. 32). Galloway et al. (1982) did a regional statistical analysis of the Frio Formation. Collecting data from hundreds (~860) of geophysical logs, they extracted statistics on sandstone and shale-bed thickness and interbedding. Five types of depositional systems were examined: fluvial, delta, barrier, strandplain, and shelf. Both sandstone and shale-bed thickness was determined to be lognormal (**Table 10** for statistics). Fogg (1989, p. 27ff) also found that sand thickness follows a lognormal distribution by studying a section of an earlier sedimentary wedge, the Wilcox Group, which had been deposited in mainly a fluvial environment (p. 13).

Continuity of sandstones was also assessed by Morton et al. (1983). Continuity and geometry vary considerably, depending on the depositional system. Fluvial sands are more likely to be continuous in the dip direction, whereas delta-front sands are continuous in all directions. Strandplain and barrier sands are more likely to be continuous in the strike direction. Maps of modern Gulf Coast deposits show simple examples (e.g., Fisher et al., 1972). Application of current flow properties (porosity, permeability) to ancient sandstones cannot be made because compaction has not taken place yet. Similarly, relative volumes between sandstones and shales are likely to be altered by the burying of the sediments. Spatial relationships, however, will stay approximately the same.

Table 10. Frio sand body statistics

	Number of Samples	Bed Thickness at -1 σ (ft)	Median Bed Thickness (ft)	Bed Thickness at +1 σ (ft)	Average Bed Thickness (ft)	σ(ln(Thickness -ft))
SANDSTONE						
Strandplain	1,335	8	17	35	29	0.74
Fluvial	2,311	10	18	33	28	0.60
*Fluvial***	*540*	*12*	*23*	*44*	*27*	*0.63*
Delta	2,253	14	25	42	36	0.55
Barrier	1,263	19	37	72	55	0.67
Shelf	396	7	18	47	33	0.95
SHALE						
Strandplain	1,414	46	84	150	118	0.59
Fluvial	2,351	32	56	96	77	0.55
Delta	2,261	26	47	87	66	0.60
Barrier	1,267	17	37	78	59	0.76
Shelf	358	70	150	320	300	0.76

Source: Galloway et al. (1982), Table 1, except ** from Fogg (1989)

III.4.3 Petrophysics

Understanding CO_2 leakage requires knowledge of porosity, permeability (including relative permeability), and capillary properties (particularly entry pressure). Another important characteristic is residual saturation of both water and CO_2. Several modeling studies have examined and ranked parameters impacting leakage. TOUGH2 simulations in preparation for the Frio experiment (Hovorka et al., 2003; Hovorka et al., 2004a) targeted water and CO_2 residual saturations. Bossie-Codreanu and Le Gallo (2004) found that the most important parameters are horizontal to vertical permeability ratio, seal permeability, and residual saturation. Permeability ratio varies from sample to regional scale. The previous section addressed regional scale.

III.4.3.1 Porosity and Permeability

Numerous publications have described porosity and its changes as a function of depth in Tertiary Gulf Coast sediments (e.g., Loucks et al., 1984). In general, porosity and permeability decrease with depth because of compaction and cementation but can rebound through dissolution of grains and cement (Loucks et al., 1977). Average sandstone porosity varies from 30% or higher close to the surface, to 10% at depths of 6,100 m (20,000 ft), with large variations at any depth, depending on the depositional system. Permeability (k in mD) is also positively

correlated to both porosity (ϕ with ϕ<1) and depth, although there is again a large range at any depth (e.g., average trend from Figure 9 in Loucks et al., 1984, is $\log k_h = 15.4\phi - 2$). Hovorka et al. (2003, p. 106) presented a relationship developed for a delta-front sandstone ($\log k_h = 6 + 7.86 \log \phi$). Several empirical formulae for the ratio of vertical to horizontal permeability have also been developed (e.g., in Hovorka et al., 2003, p. 106, and Holtz, 2003, $k_v/k_h = 22.68\phi - 5.36$, but were bounded between 0.1 and 1). Holtz and McRae (1995) studied porosity, permeability, and other parameters of the Frio Formation in the southern Gulf Coast Basin analysis area. They used a data set largely overlapping that was used in this study. They concluded that permeability and porosity are strongly correlated with depositional facies. They also developed statistical distribution functions for permeability and porosity.

III.4.3.2 Capillary Properties

Knowledge of permeability and porosity allows for a general understanding of the behavior of CO_2 in the subsurface. Knowledge of capillary properties, however, is key to an accurate quantitative modeling of its behavior, particularly when accessing capillary trapping mechanism (e.g., Akervoll et al., 2006). However, if BEG and the oil and gas industry in general have plenty of data on porosity and permeability, capillary pressure is harder to gather in the generally older fields of the Gulf Coast. The onshore Gulf Coast is a mature exploration and production area with a general lack of good capillary data (offshore would be different). Extrapolations can nevertheless be done. Capillary pressure is more a function of depth than of the age of the formation, which has been observed in reservoirs north of the San Marcos Arch (between Corpus Christi and Houston) to Louisiana on one side and in those reservoirs south of the San Marcos Arch on the other side (many more rock fragments and feldspars make the diagenesis different, and reservoirs are in general tighter south of the San Marcos Arch).

In nature, residual saturations occur because of hysteresis, that is, the present saturation state is a function of previous saturation history. Thus, capillary trapping modeling requires hysteresis to be modeled, which is generally characterized by two bounding curves describing drainage and imbibition behavior. For example, a drainage curve depicts the behavior of the system when nonwetting fluid saturation increases, e.g., (wetting) water draining from a laboratory column while (nonwetting) air saturation increases or injected (nonwetting) CO_2 pushes away (wetting) resident brine. Similarly, imbibition occurs at the tail of the injected slug, when (wetting) resident brine repossesses the volume vacated by the moving (nonwetting) CO_2,

process —in essence it is similar to a slug of (wetting) water (for example, precipitation event) displacing (nonwetting) air. At the same fluid pressure, drainage and imbibition saturations are different due to the variability of pore space width. During the drainage and imbibition process, some of the wetting and nonwetting fluids, respectively, gets disconnected from their flowing phase and cannot be removed. The nonremovable saturation is called residual saturation, which is more a function of pore size to throat size ratio rather than just pore size. High ratios trap more nonwetting fluid at residual saturation However, no single number describes residual saturation. It is a function of the maximum saturation that was reached by that phase during partial drainage or imbibition. If in the laboratory, full drainage and imbibition are open to experimentation; in nature, the system is often in some intermediate state. Saturation hysteresis also impacts permeability, which undergoes similar path-dependent behavior (e.g., Juanes et al., 2005).

Maximum gas (or nonwetting) residual saturation (S_{grm}) results from the imbibition of a rock that was initially fully drained of its water (wetting fluid), that is, which is at water residual or irreducible saturation (S_{wirr}). Many empirical correlations between porosity, permeability, entry pressure, nonwetting and water residual saturations have been developed locally: as seen above, porosity and permeability are positively correlated; porosity on the one side and residual saturation and entry pressure on the other side are negatively correlated. In general S_{grm} increases as porosity decreases, suggesting that there is an optimal porosity, in which the amount of fluid trapped at residual saturation is highest (Holtz, 2005, p. 34). There is also competition between decreasing porosity and decreasing trapped CO_2 and increasing CO_2 density with depth under local conditions. In the Gulf Coast, the optimum is broad (from 2,740 to 3,960 m [9,000 to 13,000 ft]).

Empirical residual gas saturation S_{gr} as a function of porosity was given by Holtz (2006), who used published data $S_{gr} = -0.3108\ln(\phi) - 0.127$ (**Figure 48**). Frio Formation data are consistent with the expression. The average CO_2 residual saturation in the 20 to 40% porosity range is then 15 to 25% (Holtz, 2002). Another empirical expression is given in Holtz (2002), $S_{gr} = 0.54473 - 0.9696\phi$. The two empirical expressions differ by less than 10% for porosity values higher than 0.16. Using the Holtz (2005) expression, amount of gas trapped ϕ_{gr} is given by $\phi_{gr} = -\phi\left(0.3108\ln(\phi) + 0.127\right)$. This function has a maximum of ϕ_{gr}=0.075 at ϕ=0.24.

Irreducible water saturation is given by Holtz (2002), $S_{wirr} = 5.6709\text{x}\left(\text{Log}\left(k\right)/\phi\right)^{-1.6349}$ where $k = 7\times10^{7}\phi^{9.606}$.

Average irreducible water content in the 20 to 40% range of porosity is approximately 0.03, irreducible water saturation decreasing from S_{wirr}=0.33 at ϕ=0.2 to S_{wirr}=0.13 at ϕ=0.4. These values translates into a CO_2 saturation >70% in structural traps. An important conclusion of capillary properties gathered from Frio material is that low water residual saturation and high gas residual saturation compare with that of the more classical model. IPCC (2005, p. 5–13) noted that residual CO_2 saturation typically averages smaller values, from 30 to 60%. Doughty and Pruess (2005) showed the importance of this observation for the modeling of the Frio experiment. Saturation has also been estimated as a function of other parameters: saturation decreases approximately as the logarithm of the distance to the well during injection. Saripalli and McGrail (2002) provided the following relationship: , $S_g = \text{-}0.148\ln(r) + 1.5634$ which reasonably matches the Buckley-Leverett solution after 27 years of injection in a simple system. Land (1968) proposed that residual saturation S_{gt} is a function of the initial saturation $S_g$of the nonwetting phase and is given by:

$$S_{gt} = \frac{S_{gi}}{1 + CS_{gi}} \text{ with } C = \frac{1}{S_{gt,\max}} - \frac{1}{S_{g,\max}}$$

where C is the Land trapping parameter computed from maximum gas saturation $S_{g,max}$ and maximum trapped saturation $S_{gt,max}$ associated with the bounding imbibition curve.

Averages can be computed from the large body of data accumulated during hydrocarbon production in Texas. This statement is especially true for permeability and less for capillary properties (**Table 11**). Because **Table 11** was developed with data from oil fields, corrections are needed before it can be applied to CO_2 as a nonwetting fluid. In addition, recovery efficiency is a function of rock and reservoir properties (permeability, heterogeneity) and drive mechanism (water, gas cap expansion, solution gas, and gravity drainage drives), but it can be qualitatively used to compare trapped volumes estimated by other means.

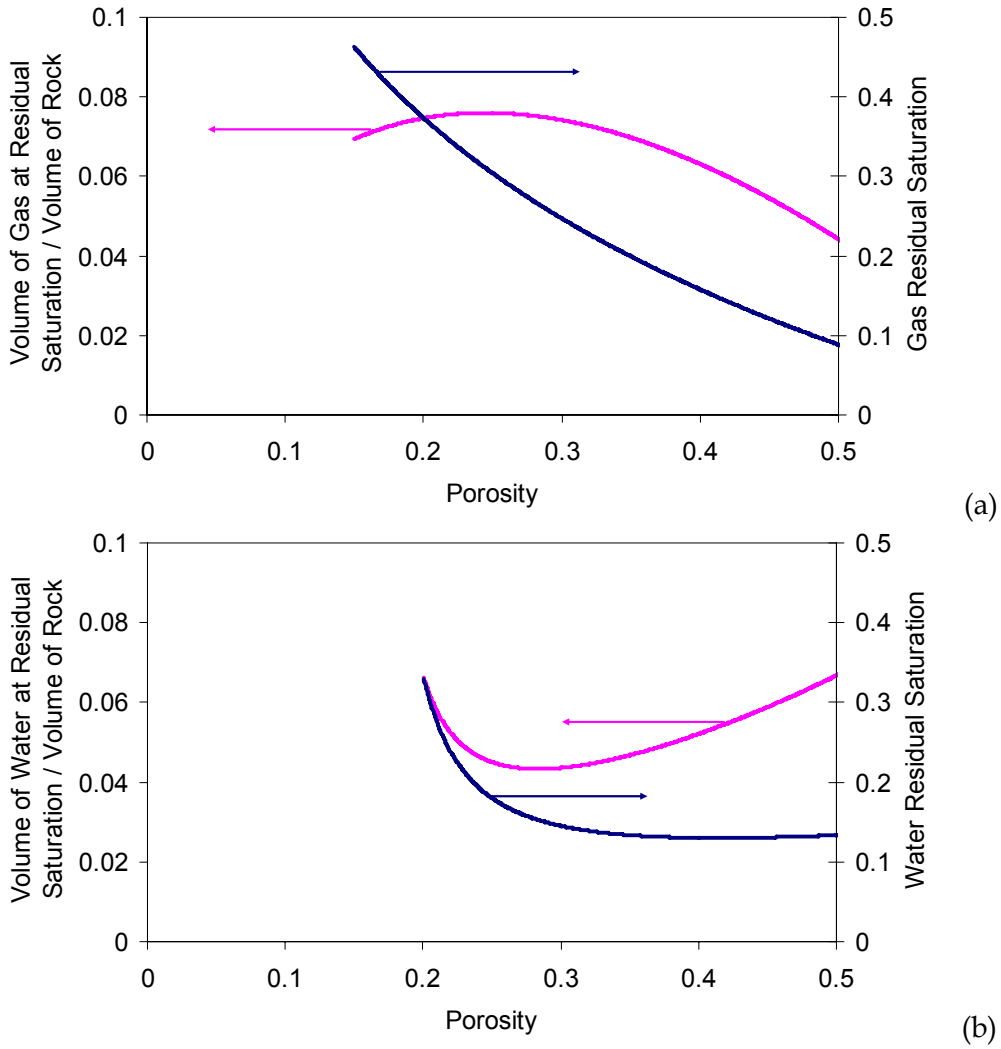

Figure 48. Frio-specific (a) maximum gas and (b)water residual saturation

III.4.4 Application to the Gulf Coast

In this section, we tentatively examine open traps and quantify capillary trapping. Results are based on Gulf Coast data presented in Section III.3.1 and on the scaling analysis detailed in Appendices D and E. Scaling analysis captures semiquantitatively the formation volume contacted by a plume as a function of geometric and flow parameters. The analysis can be applied to spreading from either a leakage point or an injection well. These two cases differ mainly in their flow rates. An important parameter is the aspect ratio a of the advancing plume (plume length/plume width(s)). We assume a case with a dip θ_x of a few degrees only in the x direction. This case can be thought of as an injection well in the downdip section of a fetch area. CO_2 will travel to the structural trap by leaving behind a trail at residual saturation whose total mass is being estimated next.

Table 11. Average flow parameters of oil reservoirs in the Gulf Coast

Play	(Range), % OOIP-weighted Average recovery efficiency [1]	% OOIP-weighted residual oil saturation (%) [2]	% OOIP-weighted water saturation[2]	Permeability geometric average[3] (mD)
Fluvial	(24-49) 36			
Fluvial/deltaic	(24-69) 40	33.9	27.4	423
Deltaic	21-80) 68	17.4	25.5	231
Barrier/strandplain	(38-69) 50	25.2	27.6	435

Source: [1]: Tyler et al. (1984, Table 2); [2]: Tyler et al. (1984, Table 4)—average of plays 1, 2, 3, 5 for deltaic; 6, 8, 10 for barrier/strandplain; 9, 11 for fluvial/deltaic; [3]: Holtz et al. (2001, Table 1)—average of rows 22, 24, 30 for deltaic; 26, 28, 29 for barrier/strandplain; row 27 for fluvial/deltaic

Note: individual data are weighted by OOIP because oil-rich areas are more likely to also contain favorable traps.

Combining Equations 42 to 45 of Appendix D with results of **Table 22** (Appendix E) yields, with the assumption that the dip is small (but nonzero):

$$a_{xz} = \frac{z_0}{x_0} \approx \frac{0.3230}{0.4037} K_r^z \cot\theta_x \approx 0.8 K_r^z / \theta_x$$

$$a_{yz} = \frac{z_0}{y_0} \approx \frac{0.3230}{1.0039} N_G \cos\theta_x \approx 0.32 N_G$$

where K_r^z is the vertical to horizontal permeability ratio (Equation 10a of Appendix D) and N_G is the gravity number (Equation 11 of Appendix D but with the caveats of Appendix E). Assuming dips in both horizontal direction and horizontal permeability isotropy, Equations 53 and 54 of Appendix D become:

$$a_{xz} = \frac{z_0}{x_0} \approx 0.7 K_r^z / \theta_x \text{ and } a_{yz} = \frac{z_0}{y_0} \approx 0.7 K_r^z / \theta_y$$

Permeability ratios are relatively well known at the core level (Holtz, 2003) and represent an upper bound to the permeability ratio (vertical/horizontal) at the reservoir scale because

fractures are not commonly described in Texas Gulf Coast reservoirs. Assuming a dip of 4° and a permeability ratio of 0.2,

$$a_{xz} = a_{yz} = \frac{z_0}{x_0 \text{ or } y_0} \approx 2 .$$

Residual saturation in the Gulf Coast formations as a function of the porosity is also known (Holtz, 2005). It should be noted that the scaling analysis was done assuming no capillary forces, but it turns out that the contacted volume is similar with or without capillary forces included in the model, as discussed in Appendix E. If one assumes that residual saturation decreases exponentially from the central axis of the leakage zone of radius *R*, average saturation in the contacted area is:

$$\int_0^R S_r(r) r dr \Big/ \pi R^2 .$$

Application of this formula translates into an average residual saturation of 10% if maximum residual saturation is 20%. Assuming a contacted volume of cylindrical shape with an aspect ratio one order of magnitude smaller (to match a more reasonable permeability ratio for a large formation volume) and a porosity of 30%, 1 Mt of CO_2 can be stored in a plume height of 280 m (920 ft).

III.5 Seals

It is worth noting that oil and gas reservoirs are often referred as to "with a perfect seal," notwithstanding that most reservoirs do leak, especially gas. In addition, the multiple perforations introduced by wells breach the seal and could hinder the permanence of storage. The possible presence of unique geological features, perhaps compromising seal integrity, must be noted (incised valleys; chimneys; other seal discontinuity, for example, erosional in nature; permeability window; faults). This section is focused on the microscopic properties that make a seal effective. We already treated leaking fault/fracture (e.g., Corcoran and Doré, 2002; Jimenez and Chalaturnyk, 2002).

Seals are characterized by their capillary and permeability properties, as well as by their ability to resist rupture under increased pressure. Seals can lose their barrier action through two main mechanisms: capillary leakage and hydraulic fracturing. The consensus is that diffusion through the seal is not an issue (e.g., Gale, 2004; Ketzer et al., 2005). Some researchers have also put forward the possibility of chemical attack of the CO_2 on the seal material. Hydraulic

fracturing results from overinjection/overpressure when formation pressure is high enough to overcome tensile strength and confining stress of the formation and occurs mainly at the bottom of the seal. Some have noted that it can be repeatedly healed (numerical modeling by Rutqvist and Tsang, 2002). Capillary leakage can be easily examined through core experiments after correction as needed for wettability and brine/CO_2-rich phase interfacial tension.

$$z_{\max} = \frac{P_c}{\Delta\rho\, Gr} \text{ with } P_c = \frac{2\sigma\cos\theta}{r}$$

where r is the minimum pore radius joining connected pores (estimated with mercury injection porosimetry), z_{max} is the maximum column height, Gr is the hydraulic gradient, and θ is the contact angle of the nonwetting fluid against rock and water. Capillary pressure is a function of the pore size but also of the interfacial tension between water and gas (at reservoir conditions water—supercritical CO_2 ~20 mN/m; water—methane gas ~50-60 mN/m) and of the wettability. Zieglar (1992) presented statistics for the hydrocarbon columns in California and Rocky Mountain areas. Seals (mainly shales) can withstand hundreds to thousands of feet of hydrocarbon column. Column height computed or observed for oil and natural gas can be converted to that of supercritical CO_2. Interfacial tension of the CO_2/water and CH_4/water systems generally decreases with increasing pressure, temperature with values for the latter system being typically higher. The effectiveness of a seal is related directly to some measure of the pore size ("r"). Silt-rich shales will have a lower resistance to membrane failure because the pores are larger on average. Knowledge of depositional system and sequence stratigraphy will help the researcher in locating and understanding the extent of those seals.

Combining buoyancy and capillary forces shows that the column height for seal failure through capillary leakage is a function of the ratio of interfacial tension (IFT) and density difference $\sigma/\Delta\rho$, all other parameters being the same (e.g., Watts, 1987). The larger the ratio, the higher the column the seal can sustain. In general, CO_2 requires better seals because of the combination of buoyancy and IFT forces. Seal thickness has no role in initiating capillary leakage and is not relevant until flow has started—in which case, the low permeability of most seals combined with a large thickness will act as an additional barrier. This remark is more relevant to CO_2 storage, whose timeframe is much smaller than oil and gas migration (thousands vs. millions of years). In that case, seal thickness can have a significant impact of CO_2 leakage retardation.

III.6 Leakage Analogs

Several reports and papers (e.g., Benson et al., 2002) have focused on the lessons learned through industrial (UIC Class I and Class II wells, natural gas storage in either (1) aquifers and oil and gas reservoirs or (2) salt caverns) but little on the lessons that can be learned from hydrocarbon primary and secondary migrations.

III.6.1 Industrial Analogs

Industrial analogs make the case that short-term carbon storage is generally safe: natural gas storage, EOR projects (West Texas fields, Weyburn), Class I liquid waste deep well injection, and injection of acid gas (especially Alberta Basin in Canada), as well as ongoing sequestration projects (e.g., Sleipner in the North Sea). Other studies have described natural analogs. Several geologic objects have been proposed as natural analogs to CO_2 storage, such as large natural CO_2 accumulation (e.g., Bravo Dome, McElmo Dome, Sheep Mountain), although it is not simple to infer engineered site leakage rates from natural leakage rates because the latter occur at random and in formations that may not be chosen for carbon storage (e.g., Mammoth Mountain, California). Natural gas analogs are not necessarily direct, good analogs because of differences in capillary properties. Hydrocarbon accumulations are another natural analog that may shed light on leakage. Hydrocarbon seals have been often described as "perfect" because they have held buoyant accumulations for millions of years. However, the seals are now punctured by wells, and study of natural leakage rates in the Gulf Coast from oil and gas deposits may tell us otherwise.

No leakage has been observed in major carbon storage operations (**Table 12**), but it must be noted that the time frame is very short. At SACROC, in the Permian Basin, anecdotal evidence suggests that, if leakage is present, it is small. Only about one-third of the injected CO_2 is recovered. The remainder is assumed sequestered. Productive formations above and below do not show the impact of CO_2. However, a small leak would not be noticed especially in a sparsely populated area.

III.6.2 Natural Analogs

Numerous publications have already addressed leakage from natural CO_2 accumulations. However, little has been published in the carbon storage literature on leakage from oil and gas reservoirs or more generally in the migration from source rock to traps and from (leaky) traps to the surface. It is generally recognized that all hydrocarbon basins have some expression at the surface, although not necessarily directly above the accumulations

(Abrams, 2005). Appendix B provides an overview of the current understanding of hydrocarbon leakage in sedimentary basins. Not surprisingly, migration pathways have been described in a way similar to those of potential CO_2 storage sites: along strata driven by buoyancy and hydrodynamic forces, along faults and fractures owing to the sometimes higher conductivity, and across seals overcoming capillary forces (Abrams, 2005).

Table 12. List of selected operations/areas where leakage can be assessed

Project	Injection (Mt CO_2/yr)[1]	Purpose	Information on Leakage
West Texas Area	~30	EOR	Anecdotal evidence of leakage, not widespread
Sleipner, North Sea	1 (23 cumulative expected)	Disposal in saline aquifer	No leakage reported
Weyburn, Canada	1-2 (21 cumulative expected)	EOR	No leakage reported
Rangely, CO	1 (~22 stored)	EOR	Possible leakage reported at less than 0.01% of volume stored[2]
In Salah, Algeria			
Alberta Basin, Canada	0.45 composite across all sites (~2–3 total to end of 2003)	Disposal of acid gas in saline aquifers	No leakage reported
Frio Brine Project, TX	1.6×10^{-3} Total	Pilot in saline aquifer	No leakage reported
West Pear Queen, NM			

Note: [1]Data from IPCC, 2005, Chapter 5; [2]Klusman, 2003a and b

Oil seeps can be a good analog because they tell us how universal leakage is and give us some idea of the rates (Cathles, 2004). An important point to keep in mind is that oil and gas reservoirs have been emplaced and have leaked through geologic times (millions to tens to hundreds of millions of years) but the time scale envisioned for carbon storage is orders of magnitude smaller (thousand of years). It follows that processes important for hydrocarbon leakage may not be relevant for carbon storage. Migration of geologic fluids such as oil and gas presents an interesting analog to CO_2 storage. CO_2 is less buoyant than natural gas but more than oil, and many sedimentary basins favorable for storage are also rich in hydrocarbons (Gulf Coast, Alberta Basin). Both primary, when oil matures and leaves the source rock, and secondary, when oil collects into traps, migrations are of interest. During secondary migration, hydrocarbons flow continuously, thanks to buoyancy and hydrodynamic forces overcoming capillary forces. Several questions relevant to CO_2 storage can be addressed: why is there no trail of residual saturation (because it is dissolved into water, eaten by bugs, etc.)? How long did it take for the hydrocarbon to collect into traps? (Residual saturation is a function of initial

saturation). Secondary migration can be vertical but also lateral for tens to hundreds of miles in structurally simple basins (Galloway and Hobday, 1996, p. 398).

Reservoirs of some oil provinces are hundreds of millions years old (e.g., Permian Basin of West Texas) and oil and/or gas has been trapped for as long. However, reservoirs do leak, as illustrated by tar pits in California and other well-known oil seeps. It has been estimated that only 5% of the oil and gas generated from source rocks is trapped (McDowell, 1975). McDowell, (1975) estimated that the produced oil is a few percent of oil generated in most basins, maybe up to 10 percent in few basins. Moshier and Waples (1985) reached similar conclusions. This leakage has been used by oil companies as an exploration tool, and numerous papers are devoted to the topic. Understanding of this leakage is relevant to the problem at hand because, in the Gulf Coast, CO_2 will be stored in similar environments and leaks might follow the same paths. There are significant gas leaks in the offshore Gulf of Mexico (Cathles, 2004), thought to be mainly through faults (Whelan et al., 2005), although gas chimneys, where the seal has been broken, have also been described. By hydrocarbon-rich basin standards, Frio Formation is not rich in organic matter (<0.5%), but there is a tremendous amount of it that turned out to be diluted by the massive sediment influx of Frio times. This suggests that the hydrocarbon expulsion of low-quality source rocks has been quite effective (Galloway et al., 1982, p. 38). There is, however, a large range in the proportion of hydrocarbon trapped during secondary migration. Oil migration is often attributed to fault/fracture pathways, either preexisting or created by the overpressure existing in most mature basins. It could also simply move updip. By studying two cores in the Frio Formation of Brazoria County at a depth of 3 to 5 km, Capuano (1993) suggested that significant flow can occur through microfractured shales. This suggestion would help explain deep-subsurface geochemical processes (Milliken and Land, 1994).

IV. Quantification of Risks

Risks of an event have been defined as the product (or some convolution) of the probability of the event (hazard) and some measure of its adverse consequences, be they financial, environmental, or otherwise. Quantifying risk helps decision-makers or, as in the present case, regulators. Using the product operator to define risk breaks down for very low probability or very high consequences. Using the product as a measure of risk may lead to some undesirable consequences. It could put a high-probability event on the same footing as a low-

consequence "cost" and a low-probability event on the same footing as a high "cost" (Rechard, 1999). An arguably low-probability-with-high-consequences event would be a catastrophic pneumatic eruption event or massive seal fracturation. The first step in consequence evaluation is to use some average (or expected) input or, perhaps, a best estimate or upper bound. However, this configuration rarely yields the average (or expected) consequence because the processes involved are complex. Only in the general case of a linear function is the expected consequence obtained from the treatment of the expected input. This observation underlines the necessity of doing a full-fledged uncertainty analysis, possibly a Monte-Carlo analysis, as a second step and of avoiding being too conservative (that is, choosing input so that the output consequence might be "worse" than it should be). Introducing too much conservatism could unnecessarily overestimate risks and possibly undermine public confidence (Rechard, 1999). One of the difficulties of risk assessment is adequate understanding of statistical dependence and how parameters are correlated—in particular, possible balancing effects (when one parameter leads to a failure, a negatively correlated one mitigates the negative outcomes in most cases) or common-mode failures (e.g., Ang and Tang, 1990), when two positively correlated parameters would lead to failure. Porosity and permeability, for example. Although one of these two parameters cannot be derived from the other by just knowing its value, they are clearly correlated within one rock type (sandstones with higher porosity are also likely to have higher permeability). In other examples, fault zones are associated with formations with higher dip angles or well density negatively correlated with formation permeability but positively correlated with number of productive formations. Engineered systems lend themselves more easily to probability analyses than do natural systems. Natural systems are more complex, generating hidden correlations through feedbacks not obvious to determine and, in general, larger uncertainties. Carbon storage includes a mix of natural and engineered systems.

Probability comes into play because of the inherent uncertainty of the data. Uncertainty is classically divided into two broad categories (e.g., Paté-Cornell, 1996). One arises from heterogeneity and variability (also called "stochastic uncertainty" or randomness) and is subject to observation. An example of it is permeability, which, provided enough samples, can be described accurately enough. Another example is the failure rate of injection wells or the yearly amount of rain at a given location. The other form derives from lack of information and

ignorance ("epistemic uncertainty"), such as the likelihood of a seismic event of high magnitude in the Gulf Coast. Most experts will recognize that the probability is low but would be hard-pressed to provide a number. No data can substantiate a value other than the next. Epistemic error can lead to dangerous systematic errors, whereas random errors may cancel each other out somewhat. A typical way to handle this issue is to call a panel of experts and to process their answers. Bayesian theory can link these two categories by improving on a mere educated guess as information grows. Another way to deal with the difference between the two kinds of uncertainty is to realize, for example, that permeability is variable with a probability distribution. However, the distribution parameters are not well known and are thus themselves uncertain (second type of uncertainty). Another example of uncertain data of the second kind is chemical properties, such as properties of the CO_2-brine system with impurities: they don't vary through time or space but can be uncertain. Spatial or time variability of natural parameters cannot be changed, but uncertainty can.

Risk-assessment probabilistic approaches require accurate probability distribution. Otherwise conservative upper bounds should be used or sensitivity analyses to determine the impact of gathering new data. The purpose of the hazard and consequence assessment is to quantify the risk associated with different parameters by estimating the probability of a particular outcome on the basis of bounding estimates or probability distributions of different input parameters times the consequence of that output. Several probability distributions can be used to describe the range of values of a parameter (e.g., Mishra, 2002). The uniform (or log-uniform) distribution is bounded, and any value between the bounds has the same probability. It is often chosen when little is known about a parameter. The triangular distribution, also bounded, is used when the researcher has some sense of what the mode of distribution should be but it is still very subjective. Other distributions—bounded (e.g., beta), semibounded (e.g., lognormal, Weibull) or unbounded (e.g., normal), continuous (all of the above), or discrete (e.g., binomial, Poisson)—are used when more is known about the parameter distribution. Overall, choice of distribution does not matter much, given that the coefficient of variation is not too large (<30%) (Mishra, 2002) and that the interest is not in extreme values. The 95th confidence interval is very sensitive to uncertainty distribution. Often parameters of these more sophisticated distributions are themselves uncertain, and the common usage is to have them follow a uniform or triangular distribution. For example, assume that porosity follows a normal

distribution. The mean can be defined as itself following a triangular distribution with a mode of, say, 0.25 and minimum and maximum of, say, 0.20 and 0.27, and the standard deviation following a uniform distribution in the 0.03 to 0.06 range. There is, however, no theoretical development to suggest that this is the most appropriate route for dealing with uncertainty.

Numerical quantification of risk can be arranged in three categories: historical, nearly historical, and new (Wilson and Crouch, 2001, Chapter 2). Historical risks occur at a frequency high enough to develop statistics and infer probability distributions for accurate predictions if records are available (e.g., hurricane frequency in the Gulf of Mexico), perhaps including time or spatial trends if appropriate. If there is not enough historical data to develop accurate statistics, an upper bound can often be formulated (e.g., deaths from nuclear accidents in the U.S.). New risks include events that have not been observed yet, either because they are rare or because they are truly new. Probability can be inferred through expert elicitation, professional judgment, and the like (the so-called "Delphi" studies).

A variety of codes are used to simulate CO_2 flow and transport in the subsurface, either from academic organizations—including TOUGH2 developed by LBNL and STOMP-CO2 developed by PNNL—or commercial entities, variations of ECLIPSE (developed by Schlumberger) or GEM (developed by Computer Modeling Group). Some of the available codes have been compared (e.g., Pruess et al., 2004). In any case, any model should follow a validation process that would include showing that the technical basis for the model is adequate for its intended use and demonstrating that the model is sufficiently accurate for its intended use. This validation applies, in particular, to the treatment of multiphase flow, where an accurate approach to hysteresis is necessary to model the trapping mechanism that is most efficient in the short term (capillary trapping). Class I no-migration petitions have historically been done with relatively simple single-phase flow and transport codes (e.g., SWIFT, Reeves and Cranwell, 1981, and subsequent versions). However, any modeling of a CO_2 injection must include a multiple-phase flow simulator, with a good module describing the CO_2 equation of state as a function of temperature, pressure, and other components. The level of sophistication for representing subsurface geology in petroleum reservoir simulators far exceeds that generally used in environmental studies, although methods are starting to cross over, particularly to the benefit of environmental studies.

IV.1 Probability Estimation

IV.1.1 Wells

Abandoned wells can leak because the abandonment procedure has not been followed carefully, because actions, although rightly performed, did not lead to expected results, or because procedures are not geared toward long-term protection. However, in general, comprehensive data sets documenting well leakage across industries using wells are lacking, as has been recognized in several recent, specialized conferences regrouping experts on this matter (2005 IEA GHG Well Bore Integrity Workshop in Houston, TX; 2005 EPA Workshop On Modeling and Reservoir Simulation for Geologic Carbon Storage in Houston, TX; 2006 IEA GHG Well Bore Integrity Workshop in Princeton, NJ). According to discussions with professionals, little information is available in the public domain related to well failure, which is likely due to a lack of data availability or data not being systematically compiled rather than commercial interest protection. However, there is plenty of anecdotal evidence, some of which is described below, suggesting that leakage does happen. On the other hand, one cannot assume that all wells will leak.

IV.1.1.1 Literature Survey

Accessible numbers on well leakage cover a large range, obscuring the conclusions that can be drawn from observations. From 1996 through 2003, there have been 7 documented instances of contamination of underground sources of ground water from an inventory of 50,000 permitted, mostly Class II, UIC wells (Richard Ginn, UIC Director at RRC, 2004, oral communication). Class I well performance is periodically examined. Class I represents a very small subset of all wells, but they are closely monitored and could suggest a lower bound for the occurrence of problems. A General Accounting Office report (GAO, 1987) recorded approximately 10 documented contaminations out of ~100 hazardous waste Class I injection wells. All reported failings were related to injection well construction or operation. Another report, produced at the same time by the UIC, mentions one case of USDW contamination that could be attributed to unplugged wells. Apparently no hazardous Class I well leak has occurred since 1988 (Benson et al., 2002, p.76), when more stringent regulations were adopted. Florida has the bulk of the nonhazardous waste Class I wells (>100). Texas hosts a sizable number (~50), but they are constructed to hazardous waste Class I standards. Not coincidently, only Florida reports cases of USDW contamination (e.g., McNeill, 2000) by nonhazardous Class I wells with relaxed standards relative to hazardous Class I wells. In Florida, 3 wells have had confirmed

USDW contamination out of 93 nonhazardous Class I wells (Beard, 2003). It should be noted, however, that, in most cases, there is no monitoring outside of the injection well itself.

South and Daemen (1986, p. 24) cited a 1974 PNNL report, stating that the probability of failure of seals in a typical oil well was 1×10^{-4} per year. Borehole sealing was a worry for the Nuclear Regulatory Commission at the time that it was investigating nuclear waste storage at multiple potential sites. Several studies, including that of South and Daemen (1986), were undertaken at the time to understand the risk of well leakage, especially in using data from the oil and gas industry which, then and now, operated the bulk of the deep wells. Another reference cited in the same report and dating from 1971 mentioned that this probability is higher than 1×10^{-5} per year. South and Daemen (1986) also mentioned that most leaks occur along the well annulus. These numbers are interesting because they may include those older wells of concern and may also integrate practical knowledge that has been lost since then. Rish (2003) estimated that there is less than 1×10^{-5} probability that a hazardous waste Class I well would leak during the life of the facility. Clark (1999), cited in Benson (2002, p. 90), found through a detailed probabilistic analysis that probability of failure of any well component was lower than 2×10^{-6}.

Paine et al. (1999), when investigating, shallow ground water and surface water salinization problems in West Texas in Runnels County, concluded that a significant fraction of them came from leaking wells. A shallow formation (Coleman Junction Formation of Wolfcampian age at the base of the Permian Epoch in the Permian Basin) located ~250 m (~800 ft) bgs is artesian, which could be considered mimicking a pressure increase due to CO_2 injection. Most of the wells are from 20–30's through the 60's. A total of 39 geophysical anomalies fit the profile of a leaking well and at least 718 wells are in the area. A rough approximation yields that 39 out of 718 known wells are leaking/have leaked in the past (~5%). The values are conservative because other wells may be leaking below the surface and were not caught by the shallow geophysical survey. With the assumption that well failure is uniformly distributed through time over a period of years, we can conclude that the yearly failure rate would be $\sim1\times10^{-3}$. It should be noted that the formation water of the Coleman Junction Formation is considered corrosive.

Warner et al. (2001) presented results of a study in which they selected 66 fields across 9 Gulf Coast counties. Out of 3,249 pre-1967 abandoned wells known to exist, only 2,562 had

location information; that is, at least 21% of wells are known to exist, but their location is unknown. The whole pre-1967 set were then randomly sampled, and ~10% of the wells in each field were chosen for further study (that is, a total of 359 pre-1967 wells). None of them had plugging information in the electronic database, as was also observed in this work. A manual search in the RRC files provided information on 82% of those wells. There was no plugging information on 18% of the pre-1967 wells. On the other hand, study of post-66 abandoned wells shows that plugging information exists for almost all of them.

Nichol and Kariyawasam (2000) attributed a mean time to failure to different well components using shut-in wells in the offshore Gulf of Mexico, although they were mainly concerned with a direct oil leak from the formation to the well head. Leaks through plug were given a mean time to failure (MTTF) of ~ 23,000 years (2×10^8 hours) for non-sour reservoirs (that is, with little H_2S and related compounds) and half of that for sour reservoirs. Woodyard (1982) gave an MTTF of 144 years for production and surface casing.

IV.1.1.2 Mitigating Factors

A fair risk assessment will take into account not only adverse conditions, but also positive elements that might retard a leak. They include heaving shales, sink zones, mud gels, and others such as caving sands and the self-sealing of cement cracks. However, the mere presence of a natural barrier does not guarantee its effectiveness.

IV.1.1.2.1 Heaving Shales and Sink Zones

Shale sloughing (caving in) or squeezing (expanding), although a hazard and inconvenience when drilling boreholes, has possible positive effects after abandonment (after all, bentonite is in common use for sealing boreholes). It is common for *uncased* boreholes in the Gulf Coast area to undergo immediate borehole closure (Johnston and Knape, 1986, p. 13, 84, 92, 97; Warner et al., 1997; Philip Papadeas and Dan Collins, Sandia Inc, personal communication, 2005), especially in Miocene and Pliocene formations (Warner et al., 1997, p. 7). Warner et al. (1997, p. 8) gave a list of formations with shales containing montmorillonite and/or bentonite and that were prone to such processes: the Pliocene Willis Formation, Miocene Goliad Formation, Miocene Lagarto Formation, Miocene Oakville Formation, Oligocene Anahuac Formation, and Oligocene Vicksburg Formation). All but the last overlie the Frio Formation. Cased wells will be susceptible to the same processes after corrosion of the casing and tubing. Lithologies such as unconsolidated shale, consolidated bentonitic shale, salt, and anhydrite are prone to this phenomenon. Warner et al. (1997, p. 15) also specified that this phenomenon

occurred in a depth interval from a few hundred feet below ground surface to about 1,200 m (4,000 ft). Other areas of the state with an even higher well density, such as West Texas, do not generally show such problems because the material is older and consolidated (although Triassic red beds are also sometimes sloughing prone). Clark et al. (2003) described a test well at a depth of ~900 m (~3,000 ft), where the closure was effectively observed.

Sink or thief zones are underpressured or normally pressured formations that can capture and divert flowing fluids before they reach the BUQW) (Warner et al., 1997, p. 16). In the Texas Gulf Coast, sand layers with higher permeability than the defective well bore are abundant and will play that role.

IV.1.1.2.2 Drilling Mud

Dry holes are quickly abandoned, leaving drilling mud inside the borehole because there is no economic incentive to recover it. Mud gel strength typically increases with time and temperature and until the gel structure is broken, the mud will stay unbroken and unaffected. Displacement pressure P_D needed to overcome the gel resistance is given by $P_D = a \times GS \times h / D$ where a is a unit conversion factor, GS is the gel strength, h is the height of the mud column, and D is the hole diameter (Johnston and Knape, 1984, p. 10). In working operating conditions, mud gel strength is less than 1 lb/100 ft², but once settled, it can increase to values as high as 100 lb/100 ft². Hovorka at al. (2003) used a value of 20 lb/100 ft² in the Frio experiment application. Johnston and Knape (1984) suggested that a minimum value of 25 lb/100 ft² be used for abandoned wells, although it is not clear what the mud quality of the earlier wells was. This value corresponds for ~1,500 m (5,000 ft) mud column in a 15-inch hole to an extra pressure of 765 kPa (111 psi) (in addition to the column weight) needed to move the column. This value is not very large but may be enough to limit the impact of pressure on the outer edges of the radius of influence in the case of brine displacement due to the pressure increase but probably not enough to impede CO_2 leakage.

IV.1.2 Faults and Heterogeneity

Few papers have investigated fault leakage risk in a probabilistic sense. Jones and Hillis (2003) proposed a model in which the probability of having a substantial hydrocarbon column p_H can be expressed by

$$p_H = \{1 - (1 - a)(1 - b)\}(1 - c)$$

where *a*, *b*, and *c* are the probabilities of membrane and hydraulic sealing, juxtaposition sealing, and the fault being reactivated after charge, respectively. This formulation assumes that all three characteristics are independent, which might not be the case. They also put forward a measure of uncertainty through what they called a *data web*. Each axis of the web corresponds to a type of data, and a degree of uncertainty is associated with it. Data types include fault throw, sedimentary architecture, stratigraphic clay content, and fault zone architecture (how many slip planes are present?). The overall uncertainty is the average of these individual contributions. Heterogeneity description is important for understanding flow but also to estimate capillary trapping: will the CO_2 move in a large front or through fingers. Once fingers are present, the fluid will keep flowing through the path, where the relative permeability is the highest, (that is, fingers) and have limited contact with the rest of the formation. A simple, very rough calculation shows that residual trapping of the leaking flux can potentially capture a significant amount of the leaking CO_2. Assuming a porosity of 25% and a residual saturation of 20%, an average sweeping footprint radius of 750 m, an injection depth of 3,000 m, a favorable formation fraction volume of 0.25, and a supercritical CO_2 density of 650 kg/m^3, the volume of CO_2 that can be trapped before reaching a depth of 1,000 m is ~30 Mt CO_2.

IV.2 Hazard Consequences

This section focuses on a risk assessment methodology that extends from leakage from the reservoir to impacts in aquifers, soils, atmosphere, rivers, and lakes proposed by Saripalli et al. (2002). It is applied to the Mountaineer site in West Virginia. The impacts of CO_2 leakage on human and ecosystem health are gauged by estimating fluxes and concentrations of CO_2 in the aquifer, soil, atmosphere, and surface-water bodies from leakage rates from the reservoir seal using semianalytical models (Saripalli and McGrail, 2002; Saripalli et al., 2002). A major human and ecological risk is a sudden, acute release of stored CO_2 through wells due to well-cap failure and through fracture and fault zones, which could cause a ground-hugging CO_2 cloud to settle in the vicinity of the injection field. Although unlikely (Holloway, 1997), such an event could be the most hazardous scenario (Cox et al., 1996). In contrast, diffuse leaking CO_2, although not immediately hazardous, has been shown to adversely impact vegetation (Farrar et al., 1995). The effect of diffuse, long-term CO_2 leaking and partitioning into the atmosphere, soil, and ground water and surface-water bodies is likely to be an adverse perturbation of the carbon

balance rather than a toxic effect. It would also be viewed as a compromise of the primary objective of CO_2 storage, which is a reduction of atmospheric carbon.

IV.2.1 Description of an Integrated Assessment Model

In this task, we demonstrate the use of a multiphase, multicomponent flow and transport simulator (STOMP-CO2), described in Appendix G, as well as simpler, semianalytical modeling approaches (Saripalli and McGrail, 2002), described in Appendix F, to provide key inputs (fate and reactive transport model results) needed for risk and consequence assessment and policy and permitting recommendations. To feasibly site and operate a geological CO_2 sequestration project, it is essential to have a clear understanding of the hazards, risks, and consequences associated with each phase of its life cycle, including siting/licensing, capital construction, operation, closure, and long-term integrity monitoring. At a local or regional scale, impacts of a geological sequestration project on soil, water and air quality, mineral resources, agriculture, ecosystems and biota, geological impacts, archaeological impacts, economical impacts, and community perceptions (of equity, safety, and economic and environmental consequences) are important to such assessment. The risk and consequence assessment methodology presented here uses a typical deep-well injection field as the central source of hazard and leakage of CO_2 to the various environmental media as the primary risk driving event. It can serve as a basis for permitting for projects involving the geological sequestration of CO_2, by using ranges of permissible risks and consequences to each of the risk receptors at the different scales described earlier.

A hazard is a situation or event that could occur during the project life cycle, which has the potential for injuring humans and animals, causing damage to the property, or environment, or an economic loss. Risk is a combination of the probability or frequency of occurrence of a hazard and the magnitude of the consequences. Because hazard is the source of risk, risk assessment typically involves the identification of hazards, their probability or frequency, and a measure of their consequence. The potential hazards associated with geological injection and sequestration of CO_2 are listed in **Table 13**. A relevant example is the case of natural gas storage, in which a total of 22 potential root causes for such releases were identified and ranked in terms of relative risk by a panel of experts (Bennion et al., 1995; Harrison and Ellis, 1995). The greatest single identified risk was wellhead failure, resulting from a vehicular collision; however, risks over the lifetime of CO_2 sequestration reservoir could be

considerably different. The present risk and consequence assessment is based on the assumption that leakage of sequestered CO_2 is the primary source of risk. Hazards not related to the leakage of CO_2, such as accidents during construction for example, are not included in this assessment. Realization of any of the hazards listed in **Table 13** is either caused by or will lead to the leakage of the sequestered CO_2, or both, which is defined as the undesirable migration of CO_2 from the reservoir to potential-risk receptor media, including air, ground-water, surface waters, soil, and buildings. Concentration of CO_2 in various media is commonly used in environmental and toxicological literature as a measure of environmental impacts. Shown in **Table 14** are ranges of CO_2 concentrations in different environmental media, under normal environmental conditions.

Over a period of 25 years, of 432 underground storage facilities in place, only 5 incidents were reported to be U.S. Department of Transportation (DOT) reportable incidents, with damages of more than $50,000, none of which was serious (Harrison and Ellis, 1995). We assumed 1 serious incident in 25 years over 500 sequestration facilities, which yields a P_H = 0.00002. Similarly, five moderately serious leakage incidents over the same domain yield a P_H of 0.0001. We assume that 1% of the caprock area spread over an area of review of 50-km radius is fractured and another 1% is highly permeable. A more accurate assessment of frequencies will be site-specific, given the characterization data. Once the frequency of occurrence of a hazard event is calculated, risk (R) can be calculated using $R = P_H C_H$. Risk is defined with reference to a receptor (**Table 13**), presented as a relative measure (R × 100,000) for each environmental medium, due to each hazard. Such calculations are useful in identifying high-risk hazards and investigating them in greater detail. For the example case, it can be seen that a fractured caprock poses the most risk to all environmental media, although its severity of consequence is much less than a well blowout or seismic hazard, which are far less likely.

Fate and transport models can serve as an effective basis for developing permitting tools for a given site, in an integrated manner. We have used a reservoir-scale numerical model and extended it further, to develop an integrated assessment framework that can address the risk and consequence assessment, monitoring networks design, and permitting guidance needs. The modeling approach is 'integrated' in two senses: (1) modeling of the entire geosystem, which includes the host formation, overburden including the vadose zone, the shallow subsurface and the surface (air, soil and water) environments, which are the ultimate risk receptors, and (2) use

of the same underlying modeling framework to assess the fate and transport of injected CO_2 and tracers, risk and consequence assessment, and sensor-based monitoring network design. The method was used to simulate sequestration of CO_2 in moderate quantities at a hypothetical injection site.

Table 13. Consequence value for hazards

Media*	Consequences		
	Severe [1]	**Moderate [0.5]**	**Low [0.1]**
Air (280 ppm)	Lethal, habitat loss (>10%)	Injuries (> 5%)	Discomfort (> 1%)
Bldgs (280 ppm)	Injury, evacuation (> 5%)	Irritation, discomfort (> 2%)	Noticeable, no harm (> 1%)
Ground water (10^{-4} M or 0.2%)	Acidity, well corrosion, irrigation loss (> 6%)	Mild acidity and corrosion (> 2%)	Elevated, low acidity without significant impacts (> 0.2%)
Surface water (10^{-5} M; 0.022%)	Acidity, CO_2 explosion, fish kills (> 2%)	Higher acidity, mild toxicity Effect on irrigation (> 1%)	Elevated, low acidity with no significant impacts (> 0.022%)
Soils (1-2%)	Low pH, tree kills, animal deaths (> 8%)	Moderate acidity, tree/ crop/soil cover loss (> 3%)	Mild suppression in pH with no significant impacts (> 2%)
Biota (10^{-5} M)	O_2 depletion, lethal (>4%)	Injury of life functions (> 2%)	Mild toxicity (> 0.5%)

Note: (x) is concentrations of CO_2; [x] is magnitude of consequence
Note: *Normal concentration shown for each medium within ( )

CO_2 pollution in ground water causes loss of wells, pumps, and pipes owing to corrosion and failure of pumps owing to gas lift. Acidic irrigation waters may be harmful to crops. High CO_2 levels may impair respiration in fish (Ross et al., 2000). On the basis of similar reports, it is reasonable to specify a CO_2 concentration range of 1 to 6.3% in water to be progressively stress inducing to biota. Elevation of CO_2 concentrations in the soil gas owing to leakage from below is likely to lower soil pH and adversely impact the chemistry of nutrients, redox-sensitive elements (Fe, Mn, As, and Se), and trace metals (Cu, Zn, and Pb), as well as plant growth (Farrar et al., 1995). Reduction of soil pH by even one unit can lower crop yield. Trees in a 30-hectare zone at Mammoth Mountain (soil CO_2 concentration >30%) were found to be dead irrespective of the age or species. In summary, elevation of soil CO_2 concentrations above 5% has deleterious effects on plant health and yield, severe effects in the 5 to 30% range, and lethal above 30%. Consequence tables have been prepared for various media, which can be

linked to a computer model, to assess risk via consequence. Leakage and distribution modeling presented earlier can be used to estimate the ranges of CO_2 concentrations within the medium and fluxes at the media interfaces, to locate appropriate consequence values.

Table 14. Frequencies of (P_H) of hazards, consequence, and risk

Hazard event	P_H	Consequence [Risk = P_H × Consequence × 100,000]					
		Air	Bldg.	GW	SW	Soil	Biota
1.							
1A.	0.00002	1 [2]	1 [2]	0.5 [1]	0.5 [1]	1 [2]	1 [2]
1B.	0.0001	0.5 [5]	0.5 [5]	0.2 [2]	0.2 [2]	0.5 [5]	0.5 [5]
1C.	0.001	0.1 [10]	0.1 [10]	0.05 [5]	0.05 [5]	0.1 [10]	0.05 [5]
2.							
2A.	0.01	0.3 [300]	0.3 [300]	0.3 [300]	0.3 [300]	0.3 [300]	0.2 [200]
2B.	0.01	0.1 [100]	0.1 [100]	0.2 [200]	0.1 [100]	0.1 [100]	0.05 [50]
2C.	0.0001	0.8 [8]	0.8 [8]	0.8 [8]	0.8 [8]	0.8 [8]	0.8 [8]

Note: GW = ground water; SW = surface water
1. **Well-head failure** (1A. major wellhead failure, 1B. moderate, sustained leak, 1C. minor leaks of joints); 2. **Caprock failure** (2A. Fractured caprock, 2B. High permeability zones, 2C. Seismic induced failure)

As detailed in Appendix F, the "Integrated Fate and Transport Modeling, Risk and Consequence Assessment" methodology presented consists of an assessment of (1) normal ranges of CO_2 concentrations in the environmental media of interest, (2) consequences of exceeding these normal CO_2 concentrations, (3) possible perturbations in CO_2 concentrations in each of the environmental media owing to the occurrence of any of the hazards considered, and (4) risks, using the data from tasks 2 through 3 above as a basis, in concert with the probability or frequency of occurrence of a given hazard.

IV.2.2 Application to the Mountaineer Site

IV.2.2.1 Site Description

Mountaineer field drilling and seismic characterization data available to-date (Gupta et al., 2005) were used as the primary input for this assessment. The stratigraphic detail and approximate hydraulic properties of the 37 lithology layers representing the site geology in the model are summarized in **Table 15**. The sandstone formation that shows higher porosity and permeability was selected as host formation in the test run. The interval of the Rose Run formation is between 7,726 and 7,842 ft. A detailed model consisting of 39 lithology layers and 122 distinct hydraulic properties, which faithfully represent the Mountaineer field site data from the injection horizons all the way to the surface through the vadose zone, was developed. The van Genuchten model (1980) was used to describe saturation-capillary pressure relations,

and the Burdine (1954) pore-size distribution model was used to calculate gas and aqueous relative permeabilities. The van Genuchten parameters were roughly estimated using hydraulic conductivity and water content on the site.

Simulations were conducted assuming two-dimensional radial symmetry about the injection well by injecting CO_2 in an interval aligned to the vertical boundary of the Rose Run Formation. The simulation grid covered a vertical depth of 7,842 ft (194 grid nodes) and a horizontal radial distance of 26,400 ft (70 grid nodes). Vertical grid spacing varied from 0.5 ft to 10 ft in the Rose Run Formation, and 0.5 ft to 100 ft up to the ground surface. Horizontal grid spacing varied from 1 ft near the injection well to 3,547 ft to the outer boundary. A downward pressure gradient of 0.49 psi/ft was used to initialize the pressure field for the simulation and was also assigned to the outer vertical boundary away from the injection well. Atmospheric pressure was enforced at the top boundary, and zero flux at the bottom boundary is assumed. Temperature is assumed to vary linearly from 15^{o}C at the top to 60^{o}C at the bottom. The injection of CO_2 was calculated using a well model.

Three different simulation cases were run to assess the leakage of CO_2 into the caprock. Case 1 (base case) hydraulic conductivities were obtained from site characterization. Cases 2 and 3 are modified from case 1 to cause increasingly leaky caprock zones. In case 2, three artificial vertical high-permeability zones above the host formation were created away from the injection well at locations 16.8 to 14.5 ft, 195.6 to 226 ft and 537.8 to 620.4 ft. Hydraulic conductivities were increased to 20 times the base case value. In case 3, hydraulic conductivities from the caprock to the ground surface were randomly increased to 10 times the base case value using a random bit generator. A total injection period of 10 years was used for cases 1 through 3. Injection was at constant pressure, assuming a well pressure gradient of 0.7 psi/ft and an injection length of 14 ft from the bottom of the host formation.

Table 15. Site characterization and hydraulic property data used in the integrated model

Layer	Lithology	Depth (ft)	Porosity	Permeability (D)
1	Ground Surface/Alluvium	0-85	0.3	5.0E+00
2	Undiff. Penn Bedrock	85-1156	0.1	2.0E-02
3	Sharon Sandstone	1156-1235	0.125	3.0E-01
4	Maxville Limestone	1235-1260	0.05	1.0E-04
5	Cuyahoga Shale	1260-1724	0.02	1.0E-06
6	Sunberry Shale	1724-1734	0.02	1.0E-06
7	Berea Sandstone	1734-1754	0.13	3.0E-01
8	Chargin Shale	1754-2670	0.02	1.0E-06
9	Lwr Huron Shale	2670-3180	0.02	1.0E-06
10	Java Shale	3180-3279	0.02	1.0E-06

Layer	Lithology	Depth (ft)	Porosity	Permeability (D)
11	Pipe Creek Shale	3279-3295	0.02	1.0E-06
12	Angola Shale	3295-3454	0.02	1.0E-06
13	Rhinestreet Shale	3454-3559	0.02	1.0E-06
14	Hamilton Shale	3559-3578	0.02	1.0E-06
15	Marcellus Shale	3578-3586	0.02	1.0E-06
16	Onondaga Shale	3586-3740	0.02	1.0E-06
17	Oriskany Sandstone	3740-3750	0.03	1.0E-05
18	Helderberg Limestone	3750-3914	0.03	1.0E-05
19	Salina Dolomite	3914-4269	0.03	1.0E-05
20	Newburg Sandstone	4269-4279	0.03	1.0E-05
21	Lockport Dolomite	4279-4572	0.03	1.0E-05
22	Niagaran Hill Shale	4572-4778	0.03	1.0E-05
23	Dayton/Casing Shell Limestone	4778-4785	0.03	1.0E-05
24	Brassfield/Packer Shell Limestone	4785-4871	0.03	1.0E-05
25	Tuscarora/Clinton Sandstone	4871-5011	0.03	1.0E-05
26	Medina Sandstone	5011-5018	0.03	1.0E-04
27	Queenston Shale	5018-5121	0.02	1.0E-06
28	Martinsburg Shale	5121-6141	0.02	1.0E-06
29	Point Pleasant Shale	6141-6295	0.02	2.0E-06
30	Trenton Limestone	6346-6461	0.03	2.0E-06
31	Black River Limestone	6461-6957	0.03	1.0E-06
32	Gull River Limestone	6957-7015	0.03	1.0E-06
33	Lower Chazy Limestone	7015-7073	0.03	2.0E-06
34	Glenwood/Wells Creek Shale	7073-7151	0.03	1.0E-04
35	Unconformity Sandstone	7151-7181	0.03	1.0E-05
36	Beekmantown Dolomite	7181-7726	0.03	2.0E-06
37	Rose Run Sandstone	7726-7842	0.08	1.0E-02

Note: 1 ft = 0.3048 m

IV.2.2.2 Simulation Results

Sandstone zones at the 7,726 to 7,842 ft depth interval are the 'host formation' zone, and the Beekmantown Dolomite layers above this zone, approximately 545 ft thick, is considered the low-permeability caprock. For cases 1 through 3, total CO_2 injected was 37,000 tons. Actual injection rates for the pilot test are not yet determined but could be higher than those simulated here. Assuming the density of supercritical CO_2 to be 600 kg/m^3 results in an injection rate of 6167 m^3/year, over a 10-year injection period. It should be noted that this test injection volume is significantly less than the injection volumes anticipated at field-scale implementation of sequestration projects, which may typically inject several thousand cubic meters of CO_2 per day. It can be seen that supercritical CO_2 extended to around 800 ft in the radial direction and penetrated 20 ft into the caprock after the injection stopped (**Figure 49**). After 80 years of equilibration, penetration depths into the caprock are about 20 ft, 180 ft, and 80 ft for cases 1, 2, and 3, respectively. Case 2 indicates that leakage through a rock containing high-permeability zones, such as abandoned wells and fractures, poses the highest risk.

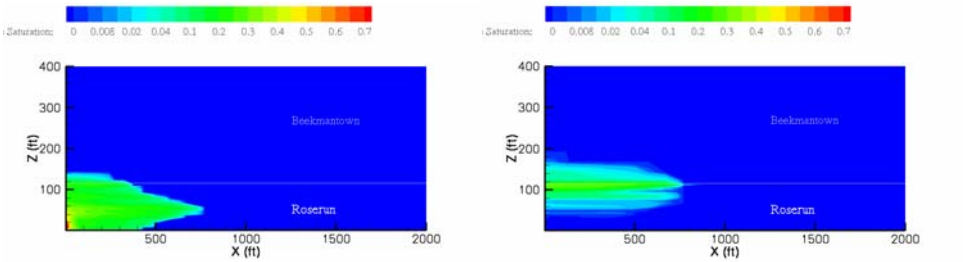

CO_2 saturation at 10 years (left) and 100 years (right) for case 1—base case

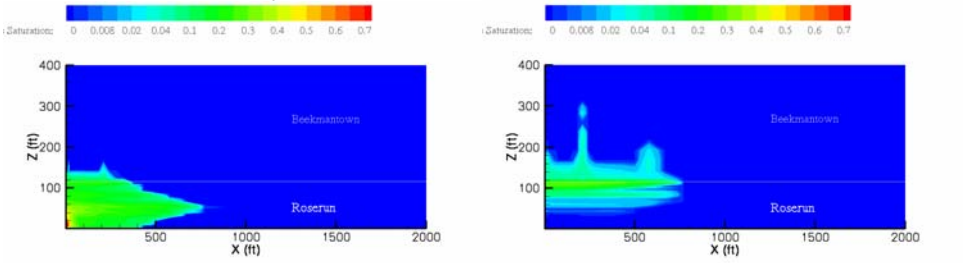

CO_2 saturation at 10 years (left) and 100 years (right) for case 2: artificially leaky permeability pathways (caprock permeability increased 20 times throughout overburden)

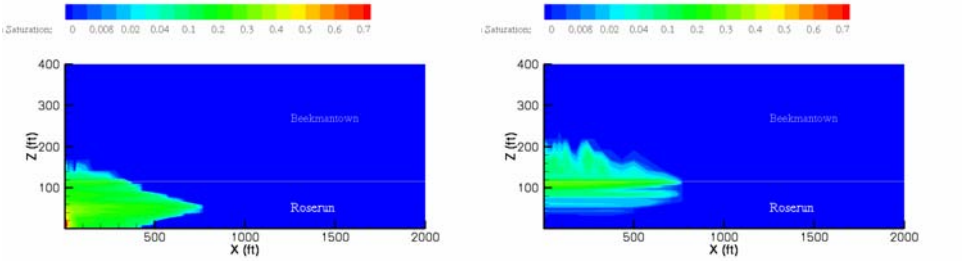

CO_2 saturation at 10 years (left) and 100 years (right) for case 3—artificially high permeability pathways (caprock permeability increased 20 times in random locations

Figure 49. Simulation results: CO_2 saturations

IV.2.2.3 Risk Assessment

Simulation results from the three cases were used to assess elevation in CO_2 concentrations that was likely in each of the risk receptor compartments. Results indicate that change (elevation) in the ambient air or water phase concentrations in each of the risk receptors is not significant, even after 100 years of monitoring. This observation translates into very low risk values, as shown in Table 14 (risk shown within [ ] parenthesis for each receptor). Two important reasons for these low risk values should be noted. First, the Mountaineer site considered comprises a considerably thick overburden zone of low permeability and a caprock region of very low permeability. Artificially increasing the permeability of these layers by a factor of 20 (simulation cases 2 and 3) in random locations caused elevated penetration and leakage of CO_2 into the overburden. However, it was not sufficient to cause elevated ultimate concentrations of CO_2 in the risk receptor regions after 100 years and, hence, additional risks. Another important reason for the low reported risks is that the total injected volume of CO_2 over a 10-year period is significantly lower than the volumes typically injected at operating power plant sites. This is consistent with the Mountaineer pilot project demonstration at a small scale but does not represent a realistic industrial-scale project. Increasing the total volume of CO_2 injected may lead to increased risk values. The present results should be construed only as relevant to the pilot-scale cases shown. The methods presented are useful for larger scale injection projects, which may be simulated in the future under this project.

The integrated numerical fate and transport model presented here demonstrates risk and consequence assessment at field scale, design and implementation of technologies for monitoring and verification, and regulatory evaluation for permitting purposes. Results show that such an integrated modeling effort would be helpful in meeting project objectives during different stages, such as site characterization, engineering, permitting, monitoring, and closure. A reservoir-scale numerical model was extended further to develop an integrated assessment framework that can address risk and consequence assessment, monitoring networks design, and permitting guidance needs. The method was used to simulate sequestration of CO_2 in moderate quantities at a hypothetical injection site. Results indicate that at relatively low injection volumes planned for pilot scale demonstration at this site, risks involved are minor to negligible, owing to a thick, low-permeability caprock and overburden zones. Such integrated modeling approaches, coupled with risk and consequence assessment modeling, are valuable to project implementation, permitting, and monitoring, as well as site closure. More generally,

residual saturation and permeability ratio emerge as the most relevant parameters. As concluded in Saripalli et al. (2002), moderate winds can also apparently disperse most of the CO_2 flux reaching ground surface, which will not be a risk for a living organism.

V. Permitting Guidelines

As numerous technical analyses of carbon storage are going forward in the field, regulatory aspects must also be examined (e.g., Benson et al., 2002; Forbes, 2002; Reiner and Herzog, 2004; Wilson, 2004). There have been efforts by governmental or pseudo-governmental agencies or groups to clear up the permitting field: Intergovernmental Panel on Climate Change (IPCC, 2005), Interstate Oil and Gas Compact Commission (IOGCC) (Bliss, 2005), Groundwater Protection Council in past recent conferences, and the EPA, including joint conferences with GWPC. The recent Request for Proposal (RFP) put forward by the FutureGen initiative has also illustrated the complexity of permitting issues (http://www.futuregenalliance.org/). It is clear that carbon storage cannot go forward without a clear representation of what the permitting process should be. Additional issues, at least as important, will be only touched upon in this report: liability and ownership. Permitting, liability, land and mineral-rights ownerships are interdependent components of a comprehensive package that the Federal Government needs to assemble with strong input from the States as to who would be ultimately responsible for the implementation of carbon storage in their respective states.

The IOGCC composed one of the most specific and practical reports on permitting of geological carbon storage. The IOGCC task force thinks that neither Class I nor Class V wells are the right regulatory framework for CO_2 injection (Bliss, 2005, p. 4 and 52) and suggests that a subclass of Class II wells or a new class with similar features be used instead. IOGCC also strongly suggests letting the states manage the permitting and that a strong involvement from all stakeholders is needed from the start (Bliss, 2005, p. 53). However, IOGCC recommendations focus on well permitting and lack the global long-term considerations that will make a carbon storage program worthwhile and successful. Similarly, EPA is still scanning the permitting field with the options of sponsoring a new subset of Class I, Class II, or Class V, or a new Class VI altogether. In the short term, it is more than likely that EPA will support experimental Class V wells, as was done on the Frio experiment (Hovorka et al., 2003). Class V wells can be deep and are sometimes constructed to Class I standards. The deepest class V well, located in Paradox Valley, CO, injects ~0.25 Mt a year of saline water in the Precambrian Bedrock at a total depth of

~4,850 m (~15,900 ft) and is allowed to operate at pressures higher than fracture pressures (Bundy, 2003). The City of El Paso will inject at a depth of ~1,200 m (~4,000 ft) desalination concentrates with a TDS of ~6,000 mg/L into a 7,000 mg/L Paleozoic aquifer at a rate of ~3 MGD (equivalent to ~4 Mt per year) (Hutchison, oral communication, 2006).

In effect, permitting of a carbon storage site must address two intertwined aspects: permitting of the facility itself (similar to permitting a nuclear waste site or a gas storage cavern), including postclosure monitoring, and permitting of the wells. These two overlapping aspects of permitting reproduce the distinction between short-term (injection wells and operations) and long-term (injectate containment) already discussed in previous sections. The main reason to go forward with carbon storage is public interest and general welfare. The CO_2-EOR framework is already in place and performs well, as evidenced by the Permian Basin experience. More generally, steps for the individual well and operations permitting are likely to be similar to those of one of the current UIC classes. However, permitting of wells, although necessary, is not sufficient. The long-term big picture must be included in the permitting process from the start. The permitting process should focus on the facility, not on the wells, whose permitting will logically derive from the permitting of the facility. On the other hand, companies and private enterprises also take the financial risk of accepting CO_2 for storage. Incentives not to make upfront expenses too high must be present in devising the permitting procedure. In addition, permitting requirements will have a significant impact on the feasibility of a project. This section will not develop a comprehensive list of administrative tasks to accomplish, but rather provide science-based guidance to what the general philosophy of the permitting process should be.

A typical field-scale geologic sequestration operation will require more than one injection well. Such a multiwell and multisite injection pattern is necessary to accommodate the large volumes of injection (several tens of Mt CO_2 injected at a single site). The regional impact of such multiple injection sites should be considered together, during the permitting process for geologic sequestration. A hierarchical modeling and analysis approach to permitting geologic sequestration sites is proposed. Permitting assessment at a regional scale seems to be a prudent way to develop permitting guidelines. This would translate to permitting applications guidance in the following way. Phase I: A state agency responsible for the permitting process of geologic sequestration carries out regional-scale assessments for suitable target regions, on the basis of

sophisticated modeling and extended input data sets. A national agency, such as EPA, could also be involved when UIC oversight responsibility has not been delegated to the state. Phase II: Counties, metropolitan areas and subregional agencies will carry out a subregional scale assessment using inputs and insights from Phase I as well as from Phase III. Phase III: Individual operators apply for permits (as is the case with deep injection wells), on the basis of inputs from Phase I and II, plus relatively simpler modeling of specific injection parameters. Phase III corresponds to the existing permitting processes implemented by state agencies for Class I hazardous waste injection wells. The regional agencies mentioned in Phase II are typically the current permitting authorities for injection wells. Such phasewise, hierarchical permitting process would be helpful in adequately addressing public and stakeholder concerns related to the impact and safety of geological sequestration operations, while fully utilizing existing permitting infrastructure and methodologies.

V.1 Operational Solutions That Could Expedite Permitting

One way to alleviate long-term leakage and create a proper site assessment is to recognize that leakage will happen and that interferences between different injection sites are likely. This will create liability and ownership issues that must be addressed (e.g., Wilson, 2003; de Figueiredo, 2005; de Figueiredo et al., 2005). In case of trespass, courts have generally ruled on the side of the secondary and tertiary recovery operator under the argument that a less valuable substance was replaced by a more valuable substance (Wilson, 2003). It is not clear whether this will hold in the case of CO_2 storage. Although not strictly technical in nature, these issues could impede or delay a wide implementation of carbon capture and storage. The permitting must then be done so that it will alleviate those concerns as much as possible, as described in this subsection.

V.1.1 Field Unitization:

Unitization of mineral rights is often realized when economic incentives are present. It consists of an agreement between owners of multiple contiguous parcels or leases to efficiently produce mineral products, generally oil and gas. It is typically implemented in the second stages of production, when secondary or tertiary recovery is needed. Each owner receives a part of the profit, regardless of where in the unitized field the hydrocarbon is produced. Compulsory unitization can be forced by the competent authority. Van field in East Texas was the first field to be unitized in the 1930s in the Midcontinent area (*Handbook of Texas* online). In

West Texas, Scurry County producers formed the SACROC unit in the 1950s (still under CO_2 flood after more than 30 years). A few other Texas fields have been unitized (e.g., Conroe in 1978, Yates in 1976, Spraberry-Dean in the 1960s) (**Table 16**), although the practice is not widespread in Texas. For example, the supergiant East Texas field (~200 square miles) is not unitized, although there is a common reinjection program, operated by the East Texas Salt Water Disposal Company (~100 injection wells). Size of unitized fields varies between a few square kilometers to a couple of hundred kilometers (**Table 16**). This dimension range is compatible with carbon storage, although it should be noted that unitization is done for a specific formation in which the EOR is taking place and not on the whole volume of the footprint of the unitization domain.

V.1.2 As Deep as Possible

Small, individual leak probability for a given well does not justify taking specific measures before injection on a given ordinary well; however, their shear number increases the leakage probability to unsustainable levels and forces the operator/regulator to undertake a global strategy. There are at least three reasons to favor deep injection. (1) If CO_2 is injected deep, below present and past reservoirs, seals, most likely good in their pristine state, would not be punctured by numerous wells. (2) Many researchers have also used models to show that heterogeneity both at the formation level and at the site level decrease leakage because of the increased capillary and dissolution trappings. (3) In the Gulf Coast, it appears that the optimal depth to inject CO_2 due to rock properties (porosity) and CO_2 density varying in opposite direction is ~3,000 m (~10,000 ft) (Holtz, 2005). An additional reason is the inevitably limited amount of resources available for site characterization. Additional pieces of information are always welcome when studying a site. However, the true goal is not a perfect knowledge of the site but enough confidence in its performance that CO_2 will most likely behave as expected. A deeper injection level may not be as well characterized as a shallower level because of the relative paucity of data owing to the lack of well penetrations. On the other hand, the confidence that the site will not leak into or through UDSW is increased.

Injecting CO_2 offshore to avoid older boreholes could be beneficial. This approach, however, will not provide the confidence given by the capillary trapping mechanism unless the injection is also performed deep below the seafloor. Impacts of leakage to the seafloor would also have to be reckoned with and understood. In addition, it is currently viable only in the

western Gulf of Mexico because of the offshore moratorium ("Outer Continental Shelf Moratorium") elsewhere in the U.S.

V.1.3 Smallest Footprint

Ownership issues can be partly dealt with by devising an injection site with a surface footprint as small as possible. In the Gulf Coast, this would entail favoring stacked storage in multiple formations to limit the footprint and the need for land ownership and mineral rights. Such an injection site will also decrease the footprint of the CO_2 "bubble(s)" for liability and area of review (orphan and abandoned wells, faults).

Table 16. Selected unitized fields, mainly in West Texas

Unit Name	Size[A] (acre/km^2)	Comments	Source[B]
SACROC Unit	~50,000/202	Permian Basin, Scurry County	Hawkins et al. (1996), SPE35359; Langston et al. (1988), SPE17321
Yates field Unit	26,400/107		Gilman et al. (1995), SPE28568; Tank (1997), SPE35244
Goldsmith San Andres Unit (GSAU)	18,240/74	Formed 1952 Permian Basin, Ector County	Jazek et al. (1998) SPE48945
Sharon Ridge Canyon Unit (SRCU)	13,712/55	Permian Basin	Brinkman et al. (1999), SPE56882
Sundown Slaughter Unit (SSU),	8,700/35	Permian Basin, Hockley County	Folger (1996) SPE35410; Folger and Guillot (1996), SPE35189; Guillot (1995), SPE30742
Ford Geraldine Unit (FGU),	~8,500/34	Northern Reeves and northeastern Culberson Counties	Lee and El-Saleh (1990), SPE20227; Pittaway and Rosato (1991), SPE20118
Goldsmith and Ector Unit (Gandu)	8,520/34		Hollar (1996), SPE35237
North Robertson Unit (NRU)	5,633/23	Permian Basin, Gaines County. 144 active producing wells, 109 active injection wells, and 6 water supply wells in 1996	Davies et al. (1996), SPE35183
Mallet Unit (Slaughter field),	4,780/19	Cochran and Hockley Counties	Kuo et al. (1990), SPE20377
South Welch Unit	3,360/14	Formed 1968	Keeling (1984), SPE12664
West Seminole San Andres Unit,	2,782/11	Gaines County, formed 1962	Barrett et al. (1977), SPE6738
Alvord South (Caddo Cong.) Unit	2,291/9	Wise County, formed 1966	Craig (1985), SPE14309
Other unitized fields include **Dollarhide Devonian** Unit (Bellavance, 1996, SPE35190); **North Dollarhide** Unit (Kovarik et al.,1994, SPE27678 and Hill et al., 1994, SPE27676); **Prentice Northeast** Unit (PNEU) in the Permian Basin, Yoakum and Terry Counties (Rogers, 1989, SPE18822); **Means San Andres** Unit in the Permian Basin, Andrews County (Stiles, 1983, SPE11987); **Anton Irish Clearfork** Unit (AICF) (Ilseng et al., 1983, SPE11930); **Fullerton Clearfork** Unit (FCU) in the Permian Basin, Andrews County, with 529 active producers and 432 active injectors in 1994 (Bane et al., 1994, SPE27640); **Seminole San Andres** Unit (SSAU) in the Permian Basin, Gaines County, with 427 producing wells and 161 injection wells in 1988 (Millard, 1988, SPE17290); and **Hawkins Field** Unit in the East Texas Basin.			

Notes: [A]: 1 acre = 0.004047 km^2; [B]: those sources are not listed in the reference list but can be accessed in the SPE database (http://www.spe.org)

V.2 Performance-Based Regulatory Framework

There is a strong impetus in the scientific community to adopt a performance-based regulatory framework (e.g., Tsang et al., 2002; Wilson and Keith, 2003) and it also seems to be the societal trend (e.g., Coglianese et al., 2002). The use of a risk assessment approach should ensure that the stringency of permitting requirements is commensurate with the risks determined from the understanding of the system and from our knowledge obtained from detailed CO_2 pilot sequestration projects. Because leakage is likely to happen, the question should not be construed as either no leakage or leakage, but framed as a probability of having leakage flux above some threshold level or having some measure of USDW loss of quality (e.g., all metals should stay below their MCL). A performance-based process puts the burden of demonstrating the suitability of the site on the applicant, but it also renders the regulator's task more difficult because there are less objective and quantifiable factors to consider. Questions such as "Is the thickness of the primary seal above the main injection formation >30 m (100 ft) at all points?, which are typical of a prescriptive regulation-driven system, are not as relevant in a performance-based system. A performance-based permit allows the permit applicant to adapt the level of information needed/collected to what is required to predict with enough confidence the site behavior. It also allows prioritizing risks (wells, faults). The ultimate criteria for carbon storage is likely to reproduce the long-/short-term dichotomy already encountered several times.

Site assessment must be done at the regional level first before moving into the specifics of one injection site for the reasons detailed above (CO_2 moves updip and could leave the property; pressure effects are likely to be felt far away from the injection site, interferences may occur between multiple injection operations). The large volumes to be injected will necessarily translate into some leakage because it is not sustainable to apply the current level of detailed characterization of pilot sites to all future sites. This does not mean that CO_2 cannot be safely sequestered underground, however. Even in case of leakage, imperfect geologic storage of the CO_2, currently emitted in the atmosphere and partly stored in the ocean, would help in meeting the fundamental goal of carbon sequestration. This observation again suggests that CO_2 injection should be treated at the regional or at least subregional level, allowing leakage in a statistical sense, but whose exact locations and timing may be hard to pinpoint until they occur. Although not all in the public domain, the level of data available is high, owing to oil and gas

exploration, and that effort can be accomplished right away. States, with possible help from Federal agencies (USGS, EPA), would be responsible for developing these models. Individual operators would then apply, on the basis of regional model guidance, for permits that would focus on relatively simpler modeling of specific injection parameters. The state of Texas has already had a successful experience implementing such a system for a sound management of ground-water resources (TWDB, 2006). In this particular example, participation of stakeholders and of other local entities was actively sought and, in most cases, given. It could be used as a starting point to develop a similar management model for CO_2 storage. State and Federal government should be proactive in starting regional studies with stakeholder (general public, local governments, operators, CO_2 generators) input that would rank areas according to criteria agreed upon, possibly with the help of decision-support tools (e.g., Sprague and Carlson, 1982) specifically developed for this purpose. These "risked-based" or "risk-informed" approaches have been used in the administration. Operating in a budget-constrained world, EPA has a long history of ranking sites more or less successfully: DRASTIC (EPA, 1987) and Risk Based Corrective Action (e.g., ASTM, 2002) are two examples. A scoring system was recently used for the ranking of the FutureGen proposals (FutureGen Alliance, 2006). Similar approaches could be used for carbon storage sites. However, there is currently a strong need for standardized integrated screening tools because none exits yet. Formal FEP or a more informal approach but substantially equivalent could be a starting point. It should be noted that a FEP procedure can be understood in very broad sense and tentatively includes all events that could possibly occur at the site. Our understanding of the FEP procedure is more restrictive. It should focus on those events related to subsurface parameters and maybe also include operations.

One of the best ways to deal with risks is the so-called defense in depth (DID), in which several lines of defense are established to prevent or mitigate accidents (**Table 17**). A flaw in, or failure of, one is covered by the other lines of defense that could initially be seen as redundant. Such an approach is used in fields as diverse as nuclear power plant safety, computer network protection, car safety, transportation systems, etc. They can apply to CO_2 storage in the sense that CO_2 will move from the injection zone upward and closer to the ground surface and drinking-water aquifers, similar to the multiple lines of defense of a nuclear power plant (cooling system, containment vessel, siting in sparsely or at least less populated areas). The main attribute of these layered lines of defense is their lack of correlation (problem is known as

"common cause failure" if this happens), such that the probability of a failure of the system (defined by radioactive material reaching population centers or CO_2 impacting people or needed resources) is the product of the probability of the individual components of the system. The first line of defense is to site the storage site deep enough to avoid multiple well penetrations or faults directly communicating with the surface with an appropriate choice for the primary seal; in closed-trap mode, the seal will contain the CO_2 in place whereas in open-trap mode, it will force CO_2 to move along its lower boundary.

Table 17. Defense-in-depth concept

	1st line of defense	2nd line of defense	3rd line of defense
Nuclear plant	Cooling system	Containment vessel	Plant sited away from large population centers
High-level waste	Sturdy containers with low corrosion rates	Favorable geology and climatic conditions both now and in the foreseeable future	Repository located away from large populated centers
CO_2 storage site	Primary seal Away from faults Away from high well density areas	Secondary seals Capillary trapping	Storage site located away from large populated centers

The multiple lines of defense should not be chosen as an afterthought but be truly integrated into the decision process. Lines of defense can also be seen as active (engineered) or passive (siting of the system, favorable geology), although reliance on engineered systems for the life of the storage site should not be expected. A supposedly perfect storage site located close to the surface does not have multiple lines of defense to absorb events that were not predicted. In general, there are barriers in establishing DID systems. The extra cost of redundant systems may not be seen as warranted, and performance of the first line of defense may suffer from additional ones.

V.2.1 Is Performance-Based Approach a Legitimate Approach?

There is limited experience in undertaking risk assessment for compliance (Rechard, 1999), and some researchers doubt the applicability of such an approach to assess impacts on public health and safety (e.g., Ewing et al., 1999). The process differs in spirit from a sophisticated sensitivity analysis to obtain a fine understanding of a geosystem in which compliance is not pertinent. However, we have the successful experience of the WIPP site in New Mexico, where several successive "Performance Assessments" were completed with compliance as a goal. PA analysis of CO_2 storage would differ from that of nuclear waste in several ways: (1) there will be multiple sites; (2) some failure, read *leakage*, is acceptable; (3) the

stored material itself can flow. Some storage sites will undoubtedly be better than others, but in many cases there will be many outcomes to draw experience from during the injection period. This suggests that it would be useful to establish initial studies in a Bayesian framework to take advantage of successive updates. One aspect that makes a risk analysis of CO_2 storage much easier than a similar effort for nuclear or hazardous waste is that only flow is involved. There is no solute flow, per se, to deal with. In addition to the numerical errors typically larger in transport models than in flow models, only one level of uncertainty, that of flow, exists. It is true that models will include dissolution, but the performance criteria of the engineered system will not be designed so that CO_2 aqueous concentration is below some threshold in all points above the base of the USDW. In other words, there is no MCL for CO_2.

Then there is the difficult question of choice of appropriate conceptual model. An incomplete or erroneous conceptual model will add more to the uncertainty of the predictions than an error in some of the parameter values (e.g., Bredehoeft, 2005). It is imperative to involve the regulatory bodies early in the course of the technical studies by the applicant. As in any modeling, the choice of the conceptual model(s) will determine the output.

V.2.2 Problem of Monitoring

A possibly key factor for carbon storage is not addressed in current legislations. Postabandonment monitoring is not required, and the permitting process relies entirely on proving that geology features are sufficient to contain the waste. Unlike a procedural permitting, in which enough conservatism is included in the rules, a performance-based permitting must include means to check that the site is performing as planned and to control gaps in our understanding of the system (that is, areas with the most uncertainty). This approach, thus, requires monitoring potential leaks. In addition, in a market-based carbon-credit trading system, confirmation that most of the alleged injected CO_2 is effectively stored in the subsurface becomes critical. All these tasks are sometimes called monitoring, mitigation and verification (MM&V). An important issue in permit applications is performance monitoring and validation. Validation consists of ensuring that performance predictions are accurate. Monitoring has two purposes: (1) to certify that the CO_2 has been stored in the receiving formation and (2) to demonstrate storage permanence and detect any leakage that may be detrimental to human health and the environment. Point 1 will help in establishing proof of CO_2

injection for receiving carbon credits in a future trading system. Point 2 will initiate corrective action as needed.

Vigorous and original efforts have been made to monitor carbon storage sites. Monitoring goals can be sorted into two groups: operational and leakage. Operational monitoring goals include monitoring the injection well and facilities, verifying that the location of the CO_2 bubble conforms to predictions, including containment within the injection level, and that it follows the plume movement. Monitoring leakage involves quantifying the small amount of CO_2 that may leave the injection level by means described in previous sections. Leakage cannot be determined by subtracting measured downhole volumes from injected volume owing to the large uncertainty in obtaining the former, most likely much larger than the leakage rate. Time-lapse measurements are particularly interesting: Torp and Gale (2004) stated that <1-meter-thick CO_2 accumulations can produce changes in the seismic signal. IPCC (2005, p. 5–50) cited 2,500 to 10,000 tons as CO_2 as the current resolution for a seismic survey. The NETL roadmap (NETL, 2005) suggests that the stored volume can be estimated within 2,500 tons using seismic lapse. Arts et al. (2004) at Sleipner also using time-lapse seismic suggested that accumulation of 4,000 m^3 (2,800 tons) can be detected. Seismic modeling by Hoversten et al. (2006) suggest that a quantity as small as 1,000 tons could be detected through individual seismic surveys.

More generally, numerous techniques and approaches have been proposed to monitor CO_2 storage sites, both in the storage formation and at the ground surface or in the shallow subsurface. Several geophysical techniques can be used for imaging the subsurface. A noncomprehensive list includes high-resolution well-bore and crosswell geophysics, surface reflection seismic, electrical resistance tomography, gravity, and measurement of land surface deformation, either satellite or land-based. Direct CO_2 leakage can be measured, after baselining before injection, by simple geochemical observations (increase in bicarbonate concentration, pH decrease, isotope ratios), vadose or soil gas fluxes (well monitoring, flux chambers) or atmospheric CO_2 measurements (eddy flux towers; remote-sensing lidar technology at larger scale). CO_2 fluxes due to leakage should be independent of seasonal variations. The downside of monitoring point fluxes is the extreme heterogeneity in soil gas concentration rendering any extrapolation from the point measurements difficult. The advantage of geochemical monitoring is that its effects are cumulative, allowing a time- and space- integrated picture of leakage. The

drawback is that the resource has already been impacted. Methods involving tracer injected with CO_2 (noble gas, etc.), as is done with natural gas, is probably impractical, except in some special cases. A "self-tracer," that is, isotopic variations, seems more reliable, cost-efficient, and not susceptible to being doctored (e.g., Cole et al., 2004). It is important to note that no method should be required to adapt to all sites or technological progress developed in response to increasing CO_2 storage operations. Baseline monitoring must be performed before injection (seismic survey and other geophysical methods, ground-water quality, soil gas concentrations, and fluxes).

There are many issues associated with monitoring:

(1) Should it be done at the regional scale under the responsibility of regulatory bodies (most likely state) that would do it under purely technical criteria or at the local scale by the operators on their properties? The most likely answer is a combination of both, in particular because most operators do not have the longevity needed to perform monitoring for decades or longer periods.

(2) Another problem with monitoring CO_2 storage relates to the monitoring location. The footprint of an injection site can be large, and potential leakage monitoring should sensitively be located in expected leakage pathways (abandoned well fields, faults). Doing so, however, would not catch leakage from unexpected pathways.

(3) The most vexing question is monitoring duration. Long-term monitoring will be challenging, and it should be assumed that, if done, it will be no longer than the injection stage (most corporations last less than 100 hundred years, and a state-sponsored monitoring program is not likely to gain overwhelming approval). As suggested by the term "geologic storage," the solution is to rely as much as possible on geological features. Doing so reinforces the need for a performance-based approach able to better constrain geological uncertainty.

V.2.3 Mitigation

One of the legs of the MM&V trilogy, mitigation, has not been given much attention by researchers so far (again, the focus is on the postclosure period). Permitting should include provisions concerning the actions to be taken if leakage is much higher than predicted or if catastrophic leakage occurs (for example, vent the formation by producing from other injectors, pump water, etc.). However, if leaks are detected, it is important to develop contingency plans. They also must be part of any permitting application. Although there is always a possibility for

unexpected events, a performance-based approach helps in allocating resources and train staff in disruptive events, if any, most likely to take place (e.g., unknown abandoned wells). Mitigation or corrective remedial action depends on where the leakage has been identified (injection wells, abandoned wells, formations overlying injection horizon, fault, shallow ground water, surface water, surface depressions, house basements, etc.). An example of mitigation could consist of depressurizing the injection formation by pumping the water out and injecting it in the formation above. Doing so would overpressurize the formation above the seal and reverse the pressure gradient. However, short-term mitigation, as in the Herscher natural gas storage in Illinois, where leaking gas is pumped from shallow wells (Benson et al., 2002), is not viable for long-term geologic storage.

V.2.4 General Permit

An alternative to the full-fledged performance-based approach is to let the regulatory agencies do the general risk assessment and grant general permits for selected areas chosen in a ranking system as described above. Results could be available in an ArcGIS format and posted on the Web, where it could be accessed by all stakeholders. A general permit must be done independently of property and mineral rights ownership; on the other hand, a general risk assessment study should help in untangling and directing these complex issues. Permitting of individual wells in a general permit area is then granted, following a simple administrative review. A similar approach was proposed by Mace et al. (2005) to handle desalination concentrates whose disposal is in a similar regulatory limbo.

V.3 Examples of More Specific Guidelines

In this section, we explore more specific recommendations for developing a permitting protocol.

V.3.1 What Should Be Accomplished by the Regulatory Body?

Given the magnitude of the undertaking, the critical initial step, as described in a previous section, is for the relevant regulatory bodies to develop or have developed sets of paper or virtual (ArcGIS) maps that would depict variations of parameters important for permitting. Investment efforts in time and staff taken by the regulatory agencies need to be commensurate with the scale of the problem. Examples include topographic maps showing depressions where CO_2 can accumulate at the ground surface, given wind and other climatic conditions (e.g., Bogen et al., 2006), or showing depth to the water table, useful for determining

whether dense CO_2 gas could invade basements after outgassing from the water. For example, most soil and gas environmental monitoring for CO_2 leakage so far has been in upland settings with thick unsaturated zones (Hovorka, 2006, personal communication). Accurate maps of the base of fresh water should also be produced (**Figure 50** and **Figure 51**). Previous authors have stated that an average depth to the base of the fresh water is approximately 600 m (2,000 ft) (e.g., Warner et al, 2001, p. 9). However, it may divert considerably from the average when in conductive sand channels, where it could reach a depth of 915 m (3,000 ft). Structural maps in the spirit of the map presented in **Figure 12** could be done at multiple depths. State agencies or their subcontractors could also easily produce maps of elevation/depth of the surface, joining all points at which CO_2 would be in a supercritical state, by collating data from geothermal gradient maps (e.g., Woodruff et al., 1984) and hydrostatic pressure or pressure measurements from wells. For the Texas Gulf Coast, this surface is located in a depth range of 730-1,370 m (2,400–4,500 ft). Pressure-depletion maps would also help because pressure-depleted oil and gas fields could alter the pathway of CO_2 plumes. In case of pressure recovery by strong water drive or other means, the information would also be valuable.

In parallel, research and development in these same agencies or at the Federal level (e.g., DOE) could reduce sources of uncertainty in geologic storage. Some types of uncertainty are easier to resolve—for instance, the equation of state for CO_2 behavior at different temperatures, pressures, salinity, or ionic composition could be resolved by multiple laboratory experiments. By far, the most important field of research is to gain an understanding in the rock-fluid interactions, in particular residual saturation. Detection of unknown abandoned wells is another area where advances could benefit the carbon storage community. Geomagnetic surveys are effective in detecting wells with steel casing, although exploration wells that were never cased or abandoned wells whose casing has been pulled could not be located through this method.

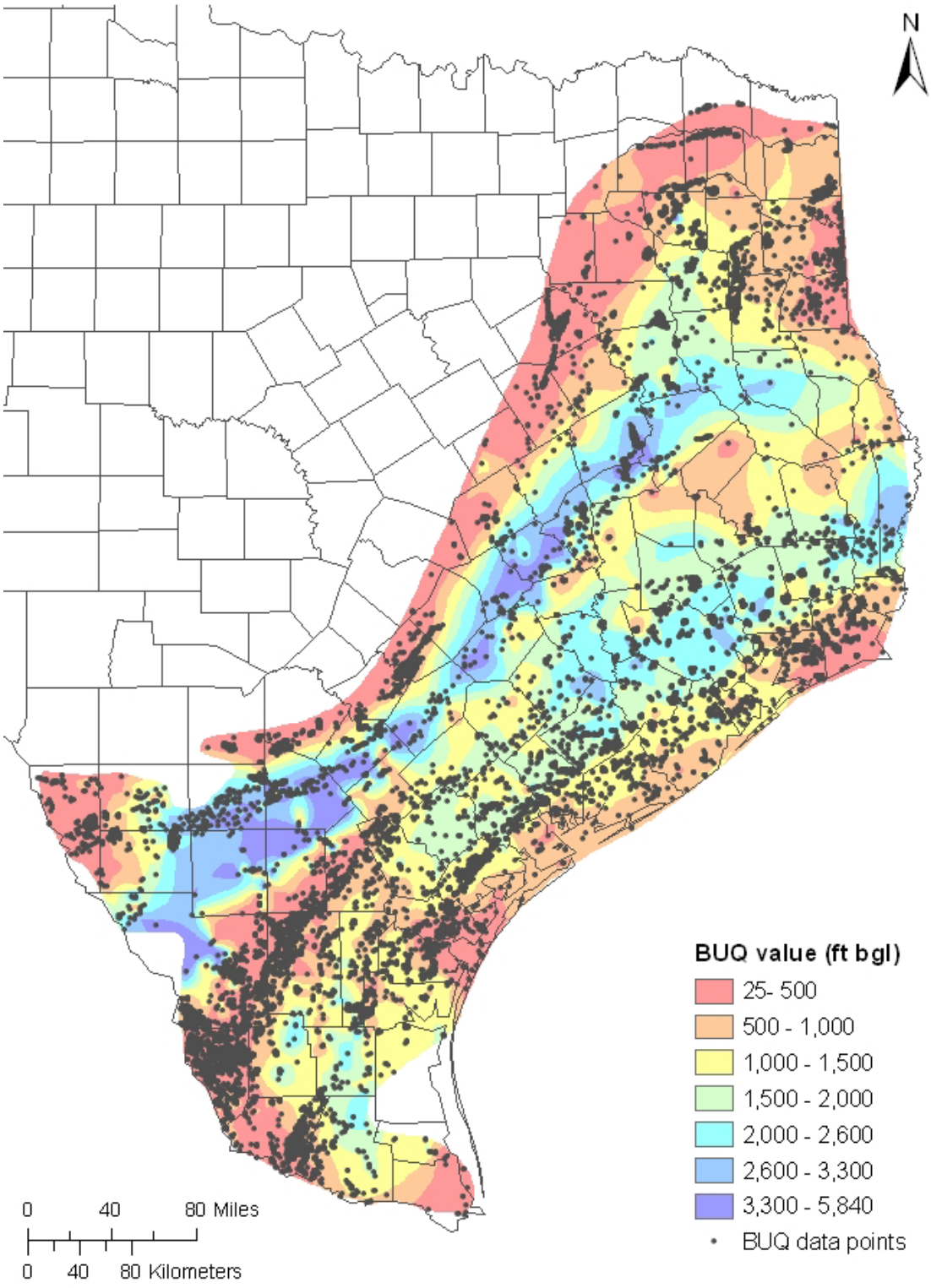

Source: TCEQ data
Figure 50. Base of the usable quality water (<3,000 mg/L) in the Gulf Coast area

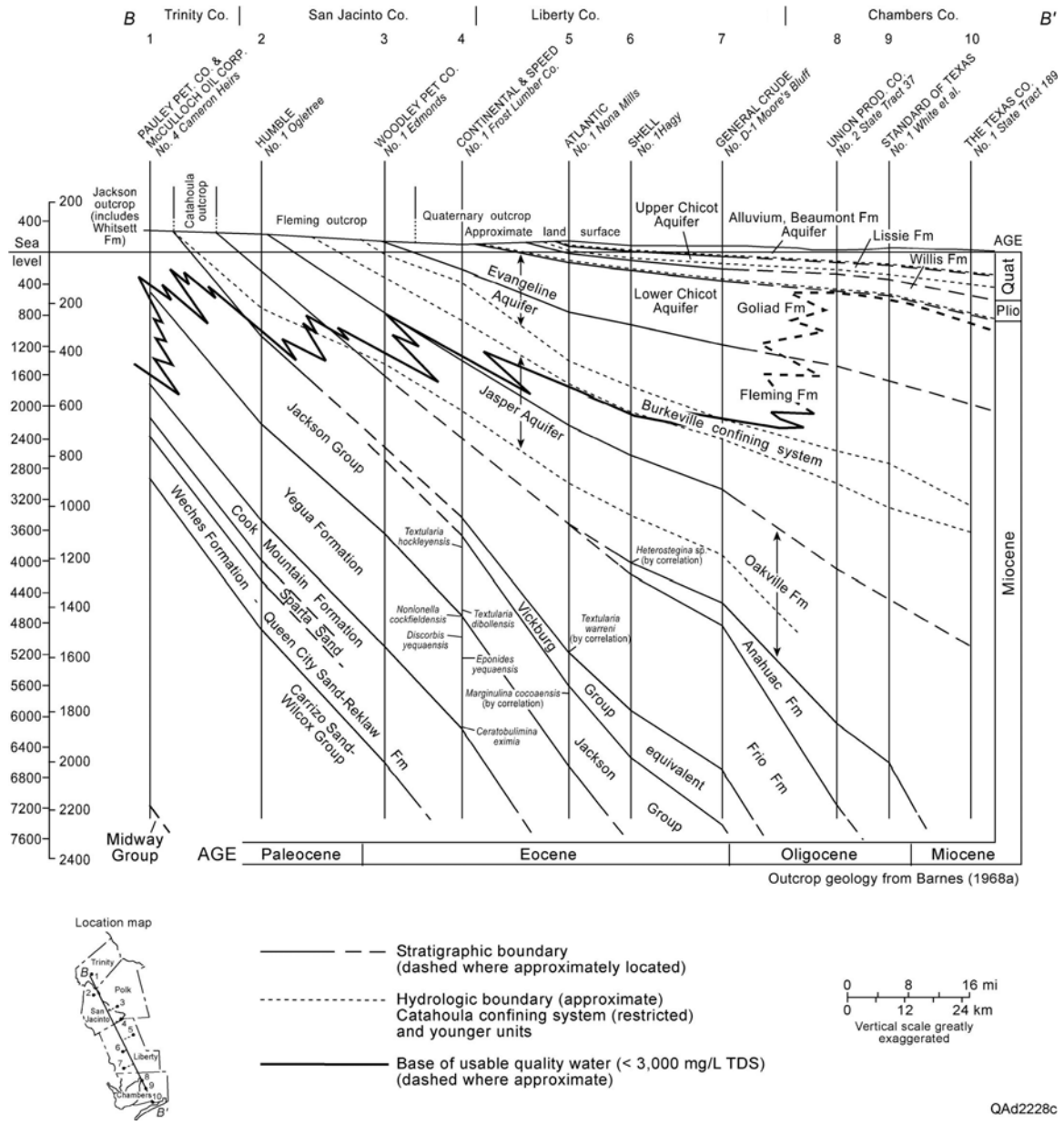

Figure 51. Representative cross section across the northern Texas Gulf Coast showing approximate location of the 3,000 mg/L contour line

V.3.2 What Could Be Included in Permitting?

As in any permitting involving risk, multiple agencies at the Federal and State levels must be involved, i.e., possibly the Army Corps of Engineers or Department of Fish and Wildlife, compliance with the National Environmental Policy Act (NEPA) if the Federal Government is directly involved, or the Endangered Species Act (ESA). The permitting process for experimental injection (~1,600 t of CO_2) at the Frio site essentially included the environmental assessment (EA) of the Federal NEPA process (Knox et al., 2003) and the UIC

permitting performed at the State level by TCEQ (Hovorka et al., 2003). Some aspects, especially related to individual wells (e.g., maximum injection rate) will not change. The permit application should focus on the geology and geological features and strive to show that they will contain CO_2 for long periods of time. It should point out not only the drawbacks of the chosen locations (estimation of leakage rates through space and time), but also positive site attributes (e.g., descending ground-water flow is preferable over regions where ground water is ascending through cross-formational flow to shallow depth). It should include all the processes relevant for the particular site. Processes that may not be important in a decadal timeframe (e.g., diffusion, changes in boundary conditions) become important. Every effort must be make to assess their range of possible values.

The exact nature of injected fluid, including trace gases, can be important because it will impact fluid density (both brine and CO_2-rich phase), capillary properties, and residual saturation. The composition of injected gas must be regulated within an admissible range. Flue gas contains ~10% CO_2 (higher and lower percentage for coal-fired and natural-gas-fired plants, respectively). Compressing costs would translate into an economic incentive to concentrate CO_2 in the injection stream beyond 90%. However, gases in minor amounts (e.g., H_2S, SO_2, NO_x) could add a layer of uncertainty to model prediction. Nonpure CO_2 does not behave as CO_2 and will impact density, viscosity, and chemical reactivity (e.g., Bouchard and Delaytermoz, 2004), although acid gas (CO_2 and H_2S) has been successfully injected in Canada (e.g., Bachu and Gunter, 2004). Modeling studies by Knauss et al. (2005) suggest that H_2S is not an issue but that only minor amounts of SO_2 can be tolerated if it is to be converted in situ into sulfate, as shown in their geochemical modeling of the Frio Formation in the Texas Gulf Coast. NO_x has intermediate results (Knauss, 2004). The maximum authorized injection volume (capacity), as well as the maximum injection rate, should be set for each individual well. However, one can argue against the necessity of constraining the injection rate by the fracture pressure. Geochemical properties should also be characterized because of their impact on mineral trapping, well corrosion, and CO_2 behavior (TDS).

Thorough characterization of all formations above the injection level should be included. It is a necessary step to assess the impact of leakage because the permitting will rely mainly on predictive modeling and appropriate conceptual models. The conceptual model is likely to have more impact on final results than any algorithmic details.

V.3.3 What Should Not Be Included in Permitting?

Operational aspects of the permitting should not be precisely set in the regulations. Siting and monitoring methods should be tailored to each site. One particular method for site characterization (e.g., seismic) or monitoring should not be required, but open to discussion between the operator and the regulatory agency. No particular trapping mode should be favored, as long as the site satisfies the criteria of permanence and limited leakage. Technical aspects, such as horizontal (to maximize capillary and dissolution trapping) vs. vertical, or injection interval (at the formation bottom to take advantage of the vertical baffling due to heterogeneities—e.g., Flett et al., 2004) should be left to the operator. Requiring plugging of abandoned wells with CO_2-resistant cement may also be a disincentive. Adequacy of formation storage capacity with source output should not have to be established. On the other hand, adequacy between demonstrated storage capacity and applied for injected volumes should.

V.4 Impact of CO_2 Storage on Other Industries

The necessarily large magnitude of any sequestration program raised the question of its impact on other subsurface-related activities or, more generally, the protection of the area mineral resources (oil, gas, lignite, uranium, sulfur, salt, geothermal energy, etc.). The effect on ground water has already been discussed. In addition, some ground-water sources deeper than the BUQW could be impacted earlier. These waters are more saline (>10,000 mg/L) but could conceivably be used as feed water for desalination facilities. Impact on future oil and gas activities may be a concern. Operators drill deeper and deeper exploration wells to access ultra-deep viable resources (**Figure 52**), as already seen in **Figure 16** and **Figure 17**. Most future drilling seems to be confined to the offshore area of the State of Texas; however, deep gas exploration and production may take place onshore along the Texas Gulf Coast at 4,570 m (~15,000 ft) or deeper. Oil and gas well construction requirements should include CO_2-resistant cements in the future. Previously uneconomical resources can become attractive because of technological progress. For example, the Barnett shale play in North-Central Texas, southwest of the Dallas–Fort Worth Metroplex, is being actively explored because of developments in horizontal well and induced fracturation technologies. Similar development could take place along the Gulf Coast.

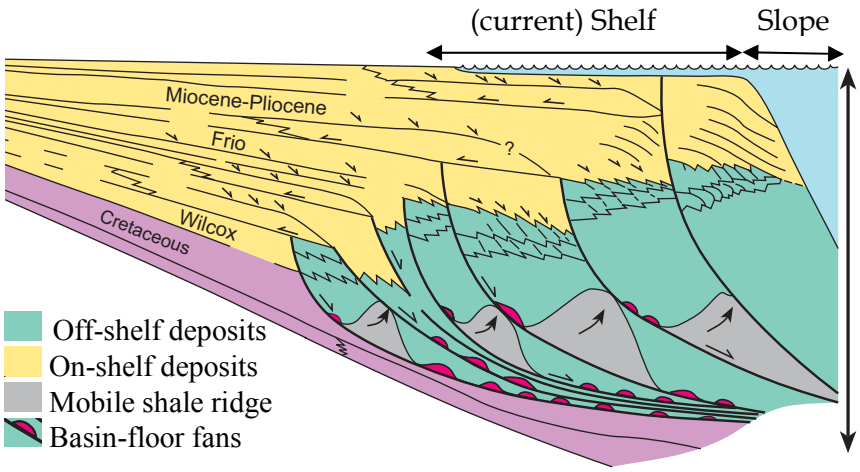

Note: Vertical dimension is 30,000 to 40,000 ft (9 to 12 km)
Figure 52. Conceptual cartoon showing locations of deep gas plays

There are other examples as well. Texas was a major uranium producer in the 1960s and 1970s from deposits hosted by Gulf Coast sediments. It seems, after a 20-year gap, companies are coming back for more in situ leaching. In the 1980s, several studies successfully investigated geothermal opportunities in the Gulf Coast area.

CONCLUSIONS

In this report we have presented an array of issues related to carbon storage in saline aquifers and their implications for permitting. Permitting is important for industrial projects, but no current permitting procedure addresses all aspects of carbon storage. However, the scientific community, as well as involved parties (regulators, operators, the power industry, concerned citizen groups, etc.), realizes that permitting issues are far from being stabilized yet. This report introduces and expands on directions that the permitting process could/should take, given the technical constraints of carbon storage. Challenges brought forward by carbon storage are new in their scale and technical concerns. The volume of CO_2 to be injected into the subsurface is necessarily large to attain the goal of reducing CO_2 atmospheric concentrations. It follows that a governmental agency or some nonprofit group independent of the operators needs to oversee and/or coordinate all injections operations. The CO_2 must stay underground for at least some period of time (still to be defined). The buoyancy of supercritical CO_2 means that, contrary to most other injected fluids, it will tend to flow upward even after the initial pressure pulse has subsided because gravity forces continue acting. Carbon storage thus presents long-term risks not only for the stated goal but also for the health and safety of future

residents in the injection areas. It follows that those long-term risks need to be explicitly quantified, both in terms of hazard description and of their consequences. A performance/risk assessment methodology, rather than a prescriptive approach, is the most practical and recognized approach to achieve this objective. A performance-based approach allows for flexibility and innovation that will benefit the whole carbon storage concept in the long term. There is no consensus on how long postclosure monitoring, if any, should last. The whole concept of geological storage and the uncertainties of the regulatory structure of future societies naturally leads to a necessarily limited monitoring and a strong emphasis on self-reliant sites.

We have proposed a hierarchical approach where, in a first step, the responsible agency/group will perform regional assessment studies and rank injection areas. This assessment can be construed as a general permit that would involve determining, in the regional sense, structural (closed structures), stratigraphic (heterogeneity), and petrophysical (flow parameters) controls on the long-term fate of geologically sequestered CO_2. It will lessen the applicant's burden because the general area of the chosen site will have been ranked more favorably. This first step will be followed by a second step, in which the individual operators will present their own application within the general framework established in the first step. This long-term aspect (100s to 1,000s of years) that must be present in carbon storage permitting is not currently captured in the legislation, even if the U.S. has a relatively well-developed regulatory framework to handle carbon storage, especially in the operational short term. Operational permitting is a minor issue and could be accomplished with little change to the current procedures. Evidently some sites will perform better than others, and it is possible that some leakage will occur somewhere, possibly at a high rate. However, in the societal sense, technical and economic risks of carbon storage should not be examined independently but contrasted to risks of doing nothing, in order to address higher atmospheric CO_2 concentrations. An example, which is not necessarily a good option, could be considering whether society is ready to bear the cost of plugging all abandoned wells with CO_2-resistant cement and possibly retrofitting many wells already plugged with Portland cement to avert a well-known potential leakage source.

CO_2 trapping modes include capillary and structural trappings, in effect, from the beginning of injection to long term, and solubility and mineral trappings that take effect more slowly. Leakage pathways, at least in the Texas Gulf Coast, consist mostly of oil and gas wells,

faults, and subsurface heterogeneity connected in faster pathways (e.g., upward connectivity of transmissive zones through, for example, loss of seal integrity, sand-against-sand fault compartments, or spill points where faults die off). USDWs are the most likely resources to be impacted by unintentional CO_2 leakage. Generally an important factor to consider in the siting of a carbon storage facility should be to avoid well bores that represent the most direct conduit to the USDW and the ground surface. It follows that the injection levels should be as deep as economically feasible. In the Texas Gulf Coast, the best way to achieve this goal is to establish the primary injection level below the total depth of most wells. Similarly, most faults, particularly growth faults, do not reach the surface and do not present a problem. The major and efficient "defense-in-depth" process of capillary trapping (when small, disconnected masses of CO_2 stay behind after the main plume has moved away) could considerably delay and retard any potential leakage. Capillary trapping does not require an obstacle to flow to be efficient. Leakage mechanisms are in essence identical to a "fill-and-spill" operational method, in which multiple individual traps are successively filled. It can thus be argued that no leakage of stored CO_2 as such will occur until the plume has reached the base of the regional seal or even maybe the vicinity of the BUQW. Overall, capillary trapping is likely to be an efficient short-term mechanism to control CO_2 leakage to USDW and beyond to the atmosphere. This capillary process must be well understood and quantified for us to be able to describe accurately enough the fate of any leaked CO_2. It follows that a large effort must be undertaken to understand supercritical CO_2 hysteresis, both in laboratory experiments and in the field. The same comment holds true for the different multiphase flow numerical simulators used by stakeholders that must handle state-of-the art hysteresis formulation. In addition, capillary trapping as a leakage control mechanism will be acceptable only if the contacted volume is large enough to absorb a significant mass of the leaking plume—that is, if the heterogeneity of the sedimentary pile is large enough. It follows that subsurface heterogeneity must also be well understood.

ACKNOWLEDGMENTS

This document was prepared with the support of the U.S. Department of Energy, under award No. DE-FC25-04NT42210, David Hyman (2004-05) and then William O'Dowd (2006), Project Managers. However, any opinions, findings, conclusions, or recommendations expressed herein are those of the authors and do not necessarily reflect the views of the DOE.

Additional funding was provided by the Jackson School of Geosciences, The University of Texas at Austin, and the Gulf Coast Carbon Center, Bureau of Economic Geology, The University of Texas at Austin. This work benefited from discussion with numerous individuals both at the Bureau and PNL but also at multiple external meetings and conferences. We would like to thank Cari Breton and Rebecca Smyth at the Bureau and Randi Ashburn, Khaled Fouad, Edgar Guevara, Paul Knox, and Thet Naing, previously at the Bureau, for their help on this project.

LIST OF FIGURES

LIST OF TABLES

REFERENCES

Abrams, M. A., 1992, Geophysical and geochemical evidence for subsurface hydrocarbon leakage in the Bering Sea, Alaska: Marine and Petroleum Geology, v. 9, no. 2, p. 208-221

Abrams, M. A., 1996a, Distribution of subsurface hydrocarbon seepage in near-surface marine sediments: in Schumacher, D., and Abrams, M. A., editors, Hydrocarbon migration and its near-surface expression: American Association of Petroleum Geologists Memoir 66, p. 1-14.

Abrams, M. A., 1996b, Interpretation of methane carbon isotopes extracted from surficial marine sediments for detection of subsurface hydrocarbons: in D. Schumacher and M. A. Abrams, editors, Hydrocarbon migration and its near-surface expression: American Association of Petroleum Geologists Memoir 66, p. 309-318.

Abrams, M. A., 2005, Significance of hydrocarbon seepage relative to petroleum generation and entrapment: Marine and Petroleum Geology, v. 22, p. 457-477.

Akaku, K., K. Baba, S. Yokoi, and Y. Yamanouchi, 2006, CO2 storage in heterogeneous aquifers without trapping structures: Numerical simulations: Proceedings of 8th International Conference on Greenhouse Gas Control Technologies. IEA Greenhouse Gas Programme.

Akervoll, I., P. Zweigel, and E. Lindeberg, 2006, CO2 storage in open, dipping aquifers: Proceedings of 8th International Conference on Greenhouse Gas Control Technologies. IEA Greenhouse Gas Programme.

Al-Shaieb, Z., J. Cairns, and J. Puckette, 1994, Hydrocarbon-induced diagenetic aureoles: indicators of deeper, leaky reservoirs: Association of Petroleum Explorationists Bulletin, v. 8, p. 24-48.

Al Taaba, A., and D. M. Wood, 1987, Zone measurements of the permeability of Kaolin, Geotechnique, v. 37, p. 499-503.

Ambrose, W. A., S. Lakshminarasimhan, M. H. Holtz, V. Nuñez-Lopez, S. D. Hovorka, and I. Duncan, 2006, Geologic factors controlling CO2 storage capacity and permanence—techniques and case studies based on experience with heterogeneity in oil and gas reservoirs applied to CO2 storage (ext. abs.): Proceedings, CO2SC Symposium, Lawrence Berkeley National Laboratory, Berkeley, California, March 20-22, p. 9-11 + CD-ROM.

Andrade, J. S., Jr., S. V. Buldyrev, N. V. Dokholyan, S. Havlin, P. R. King, Y. Lee, G. Paul, and H. E. Stanley, 2000, Flow between two sites on a percolation cluster: Physical Review E, v. 62, p. 8270-8281.

Ang, A. H.-S., and W. H. Tang, 1990, Probability Concepts in Engineering, Planning and Design, Volume II: Decision, Risk, and Reliability: New York, Wiley, 562 p.

Angevine, C. L., and D. L. Turcotte, 1983, Porosity reduction by pressure solution: a theoretical for quartz arenites: GSA Bulletin, v. 94, p. 1129-1134.

Antonellini, M. A., A. Aydin, and D. D. Pollard, 1994, Microstructures of deformation bands in porous sandstones at Arches National Park, Utah: Journal of Structural Geology, v. 16, p. 941-959.

Anzzolin, A. R., and L. L. Graham, 1984, Abandoned wells—A regulatory perspective, *in* The First National Conference on Abandoned Wells: Problems and Solutions, Environmental and Ground Water Institute: University of Oklahoma, p. 17-35.

Arp, G. K., 1992, Effusive microseepage: a first approximation model for light hydrocarbon movement in the subsurface: Association of Petroleum Explorationists Bulletin, v. 8, p. 1-17.

Arts, R., A. Chadwick, and O. Eiken, 2004, Recent Time-Lapse Seismic Data Show No Indication of Leakage at the Sleipner CO2 Injection Site: Proceedings of 7th International Conference on Greenhouse Gas Control Technologies. Volume 1: Peer-Reviewed Papers and Plenary Presentations, IEA Greenhouse Gas Programme.

ASTM, 2002, Standard Guide for Risk-Based Corrective Action Applied at Petroleum Release Sites, E1739-95, p. 53.

Avci, C. B., 1994, Evaluation of flow leakage through abandoned wells and boreholes: Water Resources Research, v. 30, p. 2565-2578.

Aydin, A., and J. A. M., 1983, Analysis of faulting in porous sandstones: Journal of Structural Geology, v. 5, p. 19-31.

Bachu, S., and J. J. Adams, 2003, Sequestration of CO2 in geological media in response to climate change: capacity of deep saline aquifers to sequester CO2 in solution: Energy Conversion and Management, v. 44, p. 3151-3175.

Bachu, S., and W. D. Gunter, 2004, Acid-gas injection in the Alberta Basin, Canada; a CO2-storage experience, *in* S. J. Baines, and R. H. Worden, eds., Geological Storage of Carbon Dioxide, v. 233: London, U.K., Geological Society Special Publications, Geological Society of London, p. 225-234.

Bachu, S., and T. L. Watson, 2006, Possible Indicators for CO2 leakage along wells, *in* Proceedings of 8th International Conference on Greenhouse Gas Control Technologies. IEA Greenhouse Gas Programme.

Barton, C. A., M. D. Zoback, and D. Moos, 1995, Fluid flow along potentially active faults in crystalline rocks: Geology, v. 23, p. 683-686.

Baumgarte, C., M. Thiercelin, and D. Klaus, 1999, Case studies of expanding cement to prevent microannular formation: Society of Petroleum Engineers paper SPE56535.

Beard, H., 2003, Relative risk assessment of deep well injection and other management options for treated waste water in South Florida, Proceedings of Second International Symposium on Underground Injection Science and Technology, October 22-23, 2003, v. LBNL-53837: Berkeley, CA, Lawrence Berkeley National Laboratory.

Bennion, D. B., F. B. Thomas, T. Ma, and D. Imer, 1995, Detailed protocol for the screening and selection of gas storage reservoirs: Society of Petroleum Engineers paper SPE59738.

Benson, S. M., 2005, Overview of geologic storage of CO2 in carbon dioxide capture for storage in deep geologic formations—Results from the CO2 capture project, Vol. 2: Geologic Storage of Carbon Dioxide with Monitoring and Verification, Elsevier Publishing, UK, p. 665-672.

Benson, S. M., R. Hepple, J. A. Apps, C. F. Tsang, and M. Lippmann, 2002, Lessons Learned from Natural and Industrial Analogs for Storage of Carbon Dioxide in Deep Geological Formations: Berkeley, CA, Lawrence Berkeley National Laboratory, p. 135 + Appendices.

Berger, Z., J. Davies, and R. T. Thompson, 2002, Integrated analysis of high-resolution aeromagnetic (HRAM) and RADARSAT-1 imagery for exploration in mature and frontier basins: in D. Schumacher and L. A. LeSchack, editors, Surface exploration case histories: applications of geochemistry, magnetics, and remote sensing: American Association of Petroleum Geologists Studies in Geology No. 48, p. 345-360.

Bergman, P. D., E. M. Winter, and Z.-Y. Chen, 1997, Disposal of power plant CO2 in depleted oil and gas reservoirs in Texas: Energy Conversion and Management, v. 38, p. S211-S216.

Birkholzer, J., K. Pruess, J. Lewicki, J. Rutqvist, C.-F. Tsang, and A. Karimjee, 2006, Large releases from CO2 storage reservoirs: analogs, scenarios, and modeling needs, *in* Proceedings of 8th International Conference on Greenhouse Gas Control Technologies. IEA Greenhouse Gas Programme.

Bjorkum, P. A., O. Walderhaug, and P. H. Nadeau, 1998, Physical constraints on hydrocarbon leakage and trapping revisited: Petroleum Geoscience, v. 4, no. 3, p. 237-239.

Bliss, K., 2005, IOGCC CO2 Geological Sequestration Task Force: A Regulatory Framework for Carbon Capture and Geological Storage, report prepared for the DOE: The Interstate Oil and Gas Compact Commission P.O. Box 53127 Oklahoma City, OK 53127-3127, 80 p.

Bodner, D. P., and J. M. Sharp, Jr., 1988, Temperature variations in South Texas subsurface: AAPG Bulletin, v. 72, p. 21-32.

Bogen, K. T., S. G. Homann, F. J. Gouveia, and L. A. Neher, 2006, Prototype near-field/GIS model for sequestered-CO2 risk characterization and management, *in* Proceedings, CO2SC Symposium, Lawrence Berkeley National Laboratory, Berkeley, California, March 20-22, p. 237-239 + CD-ROM.

Bonnet, E., O. Bour, N. E. Odling, P. Davy, I. Main, P. Cowie, and B. Berkowitz, 2001, Scaling of fracture systems in geological media: Reviews of Geophysics, v. 39, p. 347-383.

Bossie-Codreanu, D., and Y. Le Gallo, 2004, A simulation method for the rapid screening of potential depleted oil reservoirs for CO2 sequestration: Energy, 6th International Conference on Greenhouse Gas Control Technologies, v. 29, p. 1347-1359.

Bouchard, R., and A. Delaytermoz, 2004, Integrated path towards geological storage: Energy, v. 29, p. 1339-1346.

Bouroullec, R., 2001, Synsedimentary Fault Kinematics and Stratigraphic Response: PhD Thesis, Imperial College, London, 392 p.

Bowden, A. R., and A. Rigg, 2004, Assessing reservoir performance risk in CO2 storage projects, *in* Proceedings of 7th International Conference on Greenhouse Gas Control Technologies. Volume 1: Peer-Reviewed Papers and Plenary Presentations, IEA Greenhouse Gas Programme.

Bredehoeft, J., 2005, The conceptualization model problem—surprise: Hydrogeology Journal, v. 13, p. 37-46.

Brennan, S. T., and R. C. Burruss, 2003, Specific Sequestration Volumes: A Useful Tool for CO2 Storage Capacity Assessment: U.S. Geological Survey Open-File Report 03-452, 12 p.

Bretan, P., G. Yielding, and H. Jones, 2003, Using calibrated shale gouge ratio to estimate hydrocarbon column heights: AAPG Bulletin, v. 87, p. 397-413.

Brooks, J. M., M. C. Kennicutt, R. R. Fay, and T. J. McDonald, 1984, Thermogenic gas hydrates in the Gulf of Mexico: Science, v. 225, p. 409-411.

Brooks, J. M., M. C. Kennicutt, B. D. Carey, 1986, Offshore surface geochemical exploration: Oil and Gas Journal, October 20, p. 66-72.

Brooks, J. M., M. C. Kennicutt, C. R. Fisher, S. A. Macko, K. Cole, J. Childress, R. R. Bidigare, and R. D. Vetter, 1987, Deep-sea hydrocarbon seep communities: evidence for energy and nutritional carbon sources: Science, v. 238, p. 1138-1141.

Bruant, R. G., A. J. Guswa, M. A. Celia, and C. A. Peters, 2002, Safe storage of CO2 in deep saline aquifers: Environmental Science & Technology, v. 36, p. 240A-245A.

Bruce, C. H., 1973, Pressured shale and related sediment deformation: mechanism for development of regional contemporaneous faults: AAPG Bulletin, v. 57, p. 878-886.

Bryant, S. L., S. Lakshminarasimhan, and G. A. Pope, 2006, Buoyancy-dominated multiphase flow and its impact on geological sequestration of CO2: Society of Petroleum Engineers paper SPE99938.

Bundy, J., 2003, Update—World's deepest class V disposal well in its 17th year, *in* Proceedings of Second International Symposium on Underground Injection Science and Technology, October 22-23, 2003, v. LBNL-53837: Berkeley, CA, Lawrence Berkeley National Laboratory.

Burdine, N. T., 1954, Relative permeability calculations from pore-size distribution data, *in* Petroleum Transactions, American Institute of Mining and Metallurgical Engineers: Petroleum Development and Technology, v. 198, p. 71-77.

Caldeira, K., A. K. Jain, and M. I. Hoffert, 2003, Climate sensitivity uncertainty and the need for energy without CO2 emission: Science, v. 299, p. 2052-2054.

Campbell, K. A., 2002, Ancient hydrocarbon seeps from the Mesozoic convergent margin of California; carbonate geochemistry, fluids and palaeoenvironments, *in* J. D. Farmer, and D. Des Marais, eds., Geofluids, United Kingdom, Blackwell Science: Oxford, p. 63-94.

Campbell, J. A., and H. R. Ritzma, 1979, Aeromagnetic detection of diagenetic magnetite over oil fields: discussion: American Association of Petroleum Geologists Bulletin, v. 63, no. 9, p. 1538-1539.

Capuano, R. M., 1993, Influence of fluid flow in microfractures in geopressured shales: AAPG Bulletin, v. 77, p. 1303-1314.

Carle, S. F., and G. E. Fogg, 1996, Transition probability-based Indicator geostatistics: Mathematical Geology, v. 28, p. 453-476.

Carlson, N. R., and K. L. Zonge, 1996, Induced polarization effects associated with hydrocarbon accumulations: minimization and evaluation of cultural influences: in D. Schumacher and M. A. Abrams, editors, Hydrocarbon migration and its near-surface expression: American Association of Petroleum Geologists Memoir 66, p. 127-138.

Cartwright, J. A., R. Bouroullec, D. James, and D. D. Johnson, 1998, Polycyclic motion history of some Gulf Coast growth fault from high resolution displacement analysis: Geology, v. 26, p. 819-822.

Cathles, L. M., 2004, Hydrocarbon generation, migration, and venting in a portion of the offshore Louisiana Gulf of Mexico basin: The Leading Edge, v. 23, p. 760-770.

Celia, M. A., S. Bachu, J. M. Nordbotten, D. Kavetski, and S. E. Gasda, 2006, A risk assessment tool to quantify CO2 leakage potential through wells in mature sedimentary basins, *in* Proceedings of 8th International Conference on Greenhouse Gas Control Technologies. IEA Greenhouse Gas Programme.

Ceron, J. C., and A. Pulido-Bosch, 1996, Groundwater problems resulting from CO2 pollution and overexploitation in Alto Guadalentin aquifer (Murcia, Spain): Environmental Geology, v. 28, p. 223-227.

Chadwick, R. A., P. Zweigel, U. Gregersen, G. A. Kirby, S. Holloway, and P. N. Johannessen, 2004, Geological reservoir characterization of a CO2 storage site: The Utsira Sand, Sleipner, Northern North Sea: Energy, v. 29, p. 1371-1381.

Chester, F. J., and J. M. Logan, 1986, Implication for mechanical properties of brittle faults from observation of the Punchbowl fault zone, California: Pure and Applied Geophysics, v. 124, p. 80-106.

Clark, J. E., D. K. Bonura, P. W. Papadeas, and R. R. McGowen, 2003, Gulf Coast borehole closure test well near Orange, Texas, *in* Proceedings of Second International Symposium on Underground Injection Science and Technology, October 22-23, v. LBNL-53837: Berkeley, CA, Lawrence Berkeley National Laboratory.

Clayton, C. J., and P. R. Dando, 1996, Comparison of seepage and seal leakage rates: in D. Schumacher and M. A. Abrams, editors, Hydrocarbon migration and its near-surface expression: American Association of Petroleum Geologists Memoir 66, p. 169-171.

Cline, J. D., and M. L. Holmes, 1977, Submarine seepages of natural gas in Norton Sound, Alaska: Science, v. 198, p. 1149-1153.

Coglianese, C., J. Nash, and T. Olmstead, 2002, Performance-Based Regulation: Prospects and Limitations in Health, Safety, and Environmental Protection: Regulatory Policy Program Report No. RPP-03, Harvard University, Center for Business and Government, John F. Kennedy School of Government, Cambridge, MA, 25 p.

Cole, D. R., T. J. Phelps, S. Fisher, J. G. Blencoe, J. Horita, B. M. Kennedy, J. C. Parker, A. V. Palumbo, G. R. Moline, and M. C. v. Soest, 2004, Application of natural and introduced tracers for providing process optimization information: The GEO-SEQ Project Results, p. 40-47.

Colling, E. L., R. J. Alexander, and R. L. Phair, 2001, Regional mapping and maturity modeling for the northern deep water Gulf of Mexico, *in* Gulf Coast Section Society of Paleontologists and Mineralogists Foundation, 21st Annual Bob F. Perkins Research Conference, Petroleum Systems of the Deep Water Gulf of Mexico.

Cooper, G. T., C. R. Barnes, J. D. Bourne, and G. J. Channon, 1998, Hydrocarbon leakage on the North West Shelf, Australia; new information from the integration of airborne laser fluorosensor (ALF) and structural data: in Sedimentary Basins of Western Australia: Proceedings of Petroleum Exploration Society of Austrialia Symposium, v. 2, p. 255-272.

Corcoran, D. V., and A. G. Dore, 2002, Top seal assessment in exhumed basin settings—some insights from Atlantic Margin and borderland basins, *in* A. G. Koestler, and R. Hunsdale,

eds., Hydrocarbon Seal Quantification, Papers Presented at the Norwegian Petroleum Society Conference, 16-18 October 2000, Stavanger, Norway, Norwegian Petroleum Society (NPF), Special Publications No. 11, p. 89-107.

Core Laboratories Inc., 1972. A survey of the subsurface saline water of Texas, Vol. 1: Texas Water Development Board, Report 157, 113 p.

Cox, H., J. P. Heederik, L. G. H. Van Der Meer, R. Van Der Straaten, S. Holloway, R. Metcalfe, H. Fabriol, and I. Summerfield, 1996, Safety and stability of underground storage, *in* The Underground Disposal of Carbon Dioxide: Final Report, Joule II project no. CT92-0031, p. 16-162.

Crawford, B. R., 1998, Experimental fault sealing: shear band permeability dependency on cataclastic fault gouge characteristics, *in* M. P Coward, T. S. Daltaban, and H. Johnson, eds., Structural Geology in Reservoir Characterization: London, Geological Society, v. 127, p. 27-47.

Curry, W. H., III, 1984, Evaluation of surface gamma radiation surveys for petroleum exploration in the deep Powder River basin, Wyoming: in M. J. Davidson, editor, Unconventional Methods in Exploration for Petroleum and Natural Gas III: Dallas, Southern Methodist University Press, p. 25-39.

Dando, P. R, and M. Hovland, 1992, Environmental effects of submarine seeping natural gas: Continental Shelf Research, v. 12, no. 10, p. 1197-1207.

Dando, P. R., C. M. O'Hara, L. Schuster, C. J. Taylor, S. Clayton, S. Bayliss, and T. Laier, 1994, Gas seepage from a carbonate-cemented sandstone reef on the Kattegat coast of Denmark: Marine and Petroleum Geology, v. 11, p. 182-189.

Datta Gupta, A., G. A. Pope, and K. Sepehrnoori, 1996, A compositional simulator for modeling surfactant enhanced aquifer remediation, 1 Formulation: Journal of Contaminant Hydrology, v. 23, p. 303-327.

De Boers, R. D., 1977, Pressure solution; Theory and experiments: Tectonophysics, v. 39, p. 287 - 301.

de Figueiredo, M. A., 2005, Property Interests and Liability of Geologic Carbon Dioxide Storage, Special Report to the MIT Carbon Sequestration Initiative: Massachusetts Institute of Technology, 29 p.

de Figueiredo, M. A., D. M. Reiner, and H. J. Herzog, 2005, Framing the long-term in situ liability issue for geologic carbon storage in the United States: Mitigation and Adaptation Strategies for Global Change, v. 10, p. 647-657.

de Marsily, G., 1985, Flow and transport in fractured rocks; connecting and scale, *in* S. P. Neuman and E. S. Simpson, eds., Hydrogeology of Rocks of Low Permeability, v. 17(1), International Association of Hydrogeologists, 17th International Congress, p. 267-277.

DOE, 2003, Finding of No Significant Impact Pilot Experiment for Geological Sequestration of Carbon Dioxide in Saline Aquifer Brine Formations, Frio Formation, Liberty County, Texas: U.S. Department of Energy, 6 p.

DOE, 2005, Compliance Monitoring Implementation Plan for 40 CFR §191.14(b), Assurance Requirement: U.S. Department of Energy, 23 p.

DOE/EIA, 2002, Inventory of Electric Utility Power Plants in the United States 2000: DOE/EIA-00095(2000): Energy Information Administration, March, 339 p.

DOE/EIA, 2003, Inventory of Nonutility Electric Power Plants in the United States 2000: DOE/EIA-00095(2000)/2: Energy Information Administration, January, 258 p.

Donovan, T. J., 1974, Petroleum microseepage at Cement, Oklahoma-evidence and mechanism: American Association of Petroleum Geologists Bulletin, v. 58, p. 429-446.

Donovan, T. J., 1988, Low-level aeromagnetic surveying for petroleum in arctic Alaska: in G. Gryc, editor, Geology and exploration of the National Petroleum Reserve in Alaska, 1974-1982: U.S. Geological Survey Professional Paper 1399, v. 1, p. 623-632.

Donovan, T. J., R. L. Forgey, and A. A. Roberts, 1979, Aeromagnetic detection of diagenetic magnetite over oil fields: American Association of Petroleum Geologists Bulletin, v. 63, p. 245-248.

Dooley, J. J., R. T. Dahowski, C. L. Davidson, M. A. Wise, N. Gupta, S. H. Kim, and E. L. Malone, 2006, Carbon Dioxide Storage and Geologic Storage, a Technology Report from the Second Phase of the Global Energy Technology Strategy Program: Batelle Memorial Institute, 67 p.

Doughty, C., S. M. Benson, and K. Pruess, 2004, Improving the methodology for capacity assessment: The GEO-SEQ Project Results, p. 60-65.

Doughty, C., and K. Pruess, 2005, Modeling supercritical carbon dioxide injection in heterogeneous porous media: Vadose Zone Journal, v. 3, p. 837-847.

Downey, M. W., 1984, Evaluating seals for hydrocarbon accumulations: AAPG Bulletin, v. 68, p. 1752-1763.

Duchscherer, W., Jr., 1984, Geochemical hydrocarbon prospecting, with case histories: Tulsa, PennWell Publishing Co., 196 p.

Durney, D. W., 1972, Solution transfer, and important geological deformation mechanism: Nature, v. 283, p. 315-317.

Dutton, A. R., R. W. Harden, J.-P. Nicot, and D. O'Rourke, 2003, Groundwater Availability Model for the Central Part of the Carrizo-Wilcox Aquifer in Texas: The University of Texas at Austin, Bureau of Economic Geology, final report prepared for Texas Water Development Board, 295 p. + apps.

Eaton, T. T., 2006, Heterogeneity in sedimentary aquifers: Challenges for characterization and flow modeling: Sedimentary Geology, v. 184, p. 183-186.

Eichhubl, P., P. S. D'Onfro, A. Aydin, A. Waters, and D. K. McCarty, 2005, Structure, petrophysics, and diagenesis of shale entrained along a normal fault at Black Diamond Mines, California—Implications for fault seal: AAPG Bulletin, v. 89, p. 1113-1137.

Elfeki, A., and M. Dekking, 2001, A Markov chain model for subsurface characterization: theory and applications: Mathematical Geology, v. 33, p. 569-589.

Ellwood, B. B., and B. Burkart, 1996, Test of hydrocarbon-induced magnetic patterns in soils: the sanitary landfill as laboratory: in D. Schumacher and M. A. Abrams, editors, Hydrocarbon

migration and its near-surface expression: American Association of Petroleum Geologists Memoir 66, p. 91-98.

Engelder, T., 1994, Cataclasis and the generation of fault gouge: GSA Bulletin, v. 85, p. 1515-1522.

Ennis-King, J., and L. Paterson, 2003, Role of convective mixing in the long-term storage of carbon dioxide in deep saline formations: Society of Petroleum Engineers paper SPE84344.

EPA, 1987, DRASTIC: A Standardized System for Evaluating Ground Water Pollution Potential Using Hydrogeologic Settings, EPA 600-2-87-025, 643 p.

EPA, 2002, Technical Program Overview: Underground Injection Control Regulations, EPA 816-R-02-025, 81 p.

Ewing, R. C., M. S. Tierney, L. F. Konikow, and R. P. Rechard, 1999, Performance assessments of nuclear waste repositories: A dialogue on their value and limitations: Risk Analysis, v. 19, p. 933-958.

Farrar, C. D., J. M. Neil, and J. F. Howle, 1999, Magmatic Carbon Dioxide Emissions at Mammoth Mountain, California: Water Resources Investigation Report 98-4217, U.S. Geological Survey.

Farrar, C. D., M. L. Sorey, W. C. Evans, J. F. Howle, B. D. Kerr, B. M. Kennedy, C. Y. King, and J. R. Southon, 1995, Forest-killing diffuse CO2 emission at Mammoth Mountain as a sign of magmatic unrest: Nature, v. 376, p. 675-677.

Faulkner, D. R., and E. H. Rutter, 1998, The gas permeability of clay-bearing fault gouge at 20, *in* G. Jones, Q. J. Fisher, and R. J. Knipe, eds., Fault Sealing and Fluid Flow in Hydrocarbon Reservoirs: Special Publication of Geological Society, London, v. 147, p. 147-156.

Ferer, M., G. S. Bromhal, and D. H. Smith, 2001, Pore-level modelling of carbon dioxide sequestration in brine fields: Journal of Energy and Environmental Research, v. 2, p. 120-132.

Feucht, L. J., and J. M. Logan, 1990, Effects of chemically active solutions on shearing behavior of a sandstone: Tectonophysics, v. 175, p. 159-176.

Fisher, A. T., and G. Zwart, 1996, Relation between permeability and effective stress along a plate-boundary fault, Barbados accretionary complex: Geology, v. 24, p. 307-310.

Fisher, W. L., J. H. McGowen, L. F. J. Brown, and C. G. Groat, 1972, Environmental geologic atlas of the Texas coastal zone—Galveston-Houston area: The University of Texas at Austin, Bureau of Economic Geology, 91 p. + 9 maps.

Flett, M. A., R. M. Gurton, and I. J. Taggart, 2004, Heterogeneous saline formations: Long term benefits for geo-sequestration of greenhouse gases, *in* Proceedings of 7th International Conference on Greenhouse Gas Control Technologies. Volume 1: Peer-Reviewed Papers and Plenary Presentations, IEA Greenhouse Gas Programme.

Fogg, G. E., 1986, Groundwater flow and sand body interconnectedness in a thick, multiple-aquifer system: Water Resources Research, v. 22, p. 679-694.

Fogg, G. E., 1989, Stochastic analysis of aquifer interconnectedness: Wilcox Group, Trawick area, East Texas: The University of Texas at Austin, Bureau of Economic Geology Report of Investigations No 189, 68 p.

Fogg, G. E., S. J. Seni, and C. W. Kreitler, 1983, Three-dimensional ground-water modeling in depositional systems, Wilcox Group, Oakwood Salt Dome area, East Texas: The University of Texas at Austin, Bureau of Economic Geology Report of Investigations No 133, 55 p.

Foote, R. S., 1996, Relationship of near-surface magnetic anomalies to oil- and gas-producing areas: in D. Schumacher and M. A. Abrams, editors, Hydrocarbon migration and its near-surface expression: American Association of Petroleum Geologists Memoir 66, p. 111-126.

Forbes, S. M., 2002, Regulatory Barriers for Carbon Capture, Storage, and Sequestration: U.S. Department of Energy, Office of Fossil Energy, National Energy Technology Laboratory: http://www.netl.doe.gov/publications/carbon_seq/refshelf.html, last accessed 02/26/2006, 7 p.

Frankel, A. D., M. D. Petersen, C. S. Mueller, K. M. Haller, R. L. Wheeler, E. V. Leyendecker, R. L. Wesson, S. C. Harmsen, C. H. Cramer, D. M. Perkins, and R. K.S., 2002, Documentation for the 2002 Update of the National Seismic Hazard Maps: Open-File Report 02-420, U.S. Geological Survey, 33 p. + Maps.

Frazier, M., S. Platt, and P. Osborne, 2004, Does a fixed radius area of review meet the statutory mandate and regulatory requirements of being protective of USDWs under 40 CFR §144.12? UIC National Technical Workgroup, Issue #8, EPA UIC Office Region 6, October 1, 5 p. http://www.epa.gov/r5water/uic/ntwg/aor-zei.pdf , last accessed on May 7, 2006.

Freeze, R. A., and J. A. Cherry, 1979, Groundwater: Prentice-Hall, Englewood Cliffs, N.J., 604 p.

Fuchtbauer, H., 1983, Facies control of sandstone diagenesis, *in* A. Parker and B. W. Sellwood, eds., NATO Advanced Study Institute, v. 115, p. 269-288.

FutureGen Alliance, 2006. Results of site offer or proposal evaluation: Report to the U.S. Department of Energy, July 21, based on work submitted for award DE-FC26-06NT42073, 72 p.

Gale, J., 2004, Geological storage of CO2: What do we know, where are the gaps and what more needs to be done?: Energy, v. 29, p. 1329-1338.

Galloway, W. E., 1982, Epigenic Zonation and Fluid Flow History of Uranium-Bearing Fluvial Aquifer Systems: South Texas Uranium Province: The University of Texas, Bureau of Economic Geology Report of Investigations No 119, 31 p.

Galloway, W. E., T. E. Ewing, G. C. M. Jr., T. N., and D. G. Bebout, 1983, Atlas of Major Texas Oil Reservoirs: The University of Texas at Austin, Bureau of Economic Geology, 139 p.

Galloway, W. E., P. E. Ganey-Curry, X. Li, and R. T. Buffler, 2000, Cenozoic depositional history of the Gulf of Mexico basin: AAPG Bulletin, v. 84, no. 11, p. 1743-1774.

Galloway, W. E., and D. K. Hobday, 1996, Terrigenous Clastic Depositional Systems: Springer-Verlag.

Galloway, W. E., D. K. Hobday, and K. Magara, 1982, Frio Formation of Texas Gulf Coastal-Plain—Depositional systems, structural framework, and hydrocarbon distribution: AAPG Bulletin, v. 66, p. 649-688.

Galloway, W. E., L. A. Jirik, R. A. Morton, and J. R. Dubar, 1986, Lower Miocene (Fleming) Depositional Episode of the Texas Coastal Plain and Continental Shelf: Structural

Framework, Facies, and Hydrocarbon Resources: The University of Texas at Austin, Bureau of Economic Geology Report of Investigations No 150, 50 p. .

GAO (General Accounting Office), 1987, Hazardous Waste, Controls over Injection Well Disposal Operations: Report to the Chairman, Environment, Energy, and Natural Resources Subcommittee, Committee on Government Operations, House of Representatives, GAO/RCED-87-170, 52 p.

Gasda, S. E., S. Bachu, and M. A. Celia, 2004, Spatial characterization of the location of potentially leaky wells penetrating a deep saline aquifer in a mature sedimentary basin: Environmental Geology, v. 46, p. 707-720.

Georgescu, S., E. Lindeberg, and T. Holt, 2006, Co-injection of CO2 and water into non-sealed saline aquifers, *in* Proceedings of 8th International Conference on Greenhouse Gas Control Technologies. IEA Greenhouse Gas Programme.

Gerke, H. H., and M. T. van Genuchten, 1993, Evaluation of a first-order water transfer term for variably saturated dual-porosity flow models: Water Resources Research, v. 29, p. 1225-1238.

Gibson, R. G., 1998, Physical character and fluid flow properties in sandstone derived fault zones, *in* M. P. Coward, T. S. Daltaban, and H. Johnson, eds., Structural Geology in Reservoir Characterization: Geological Society of London, p 83-97.

Gratier, J. P., T. Chen, and R. Hellmann, 1993, Pressure solution as a mechanism for crack sealing around faults: Natural and experimental evidence, *in* S. H. Hickman, R. H. Sibson, and R. L. Bruhn, eds., Proceedings of Workshop LXIII; USGS Red-Book Conference on the Mechanical Involvement of Fluids in Faulting: Open-File Report—U.S. Geological Survey, p. 279-300.

Gratier, J. P., and R. Guiguet, 1986, Experimental pressure solution—deposition on quartz grains: crucial effect of the nature of fluid: Journal of Structural Geology, v. 8, p. 845-856.

Groth, P. K., and L. W. Groth, 1994, Bibliography for surface and near-surface hydrocarbon prospecting methods: Association of Petroleum Geochemical Explorationists, Special Publication, 161 p.

Gunter, W. D., E. H. Perkins, and I. Hutcheon, 2000, Aquifer disposal of acid gases: modelling of water-rock reactions for trapping of acid wastes: Applied Geochemistry, v. 15, p. 1085-1095.

Gupta, N., P. Jagucki, J. Sminchak, D. Meggyesy, F. Spane, T. S. Ramakrishnan, and A. Boyd, 2005, Determining carbon sequestration injection potential at a site-specific location within the Ohio River Valley region, *in* D. W. Keith et al., eds., Proceedings of the 7th International Conference on Greenhouse Gas Control Technologies, 2004, Vancouver, Canada, New York: Elsevier; p. 511-20.

Hanna, S., and J. Chang, 2001, Use of Kit Fox field data to analyze dense gas dispersion modeling issues: Atmospheric Environment, v. 35, p. 2231-2242.

Hardage, B. A., R. A. Levey, V. Pendleton, J. Simmons, and R. Edson, 1994, A 3-D seismic case-history evaluating fluvially deposited thin-bed reservoirs in a gas-producing property: Geophysics, v. 59, p. 1650-1665.

Harding, T. P., and A. C. Tuminas, 1988, Interpretation of footwall (lowside) fault traps sealed by reverse faults and convergent wrench faults: AAPG Bulletin, v. 72, p. 738-757.

Harrison, M. R., and P. F. Ellis, 1995, Risk Assessment of Converting Salt Caverns to Natural Gas Storage: GTI Report: GRI-95/037.

Hartmann, T., P. Paviet-Hartmann, J. B. Rubin, M. R. Fitzsimmons, and K. E. Sickafus, 1999, The effect of supercritical carbon dioxide treatment on the leachability and structure of cemented radioactive waste forms: Waste Management, v. 19, p. 355-361.

Heathman, J., R. Carpenter, K. Marcel, C. Rimer, and A. Badalamenti, 1994, Quality management alliance eliminates plug failures: Society of Petroleum Engineers paper SPE28231.

Hedberg, H., [1981] 1996, Foreword: Utilization of hydrocarbon seep information: in Schumacher, D., and Abrams, M. A., editors, Hydrocarbon migration and its near-surface expression: American Association of Petroleum Geologists Memoir 66, p. iii.

Heinrich, J. J., H. J. Herzog, and D. M. Reiner, 2003, Environmental assessment of geologic storage of CO2, *in* The Second Annual Conference on Carbon Sequestration, p. 11.

Hendriks, C., A. S. van der Waart, C. Byers, D. Phylipsen, M. Voogt, and Y. Hofman, 2002, Building the cost curves for CO2 storage, part 1, sources of CO2: IEA Greenhouse Gas R&D Programme, CD-ROM.

Henry, W. E., 1989, Magnetic detection of hydrocarbon microseepage in a frontier exploration region: Association of Petroleum Geochemical Explorationists Bulletin, v. 5, p. 18-29.

Hepple, R. P., and S. M. Benson, 2005, Geologic storage of carbon dioxide as a climate change mitigation strategy: performance requirements and the implications of surface seepage: Environmental Geology, v. 47, p. 576-585.

Hernandez, G. A., R. O. Bello, D. A. McVay, W. B. Ayers, J. A. Rushing, S. K. Ruhl, M. F. Hoffmann, and R. I. Ramazanova, 2006, Evaluation of the technical and economic feasibility of CO2 sequestration and enhanced coalbed-methane recovery in Texas low-rank coals: Society of Petroleum Engineers paper SPE100584.

Holloway, S., 1997, Safety of the underground disposal of carbon dioxide: Energy Conversion and Management, v. 38, p. S241-S245.

Holtz, M. H., 2002, Residual gas saturation to aquifer influx: A calculation method for 3-D computer reservoir model construction: Society of Petroleum Engineers paper SPE75502.

Holtz, M. H., 2003, Pore-scale influences on saline aquifer CO2 sequestration (abs.): American Association of Petroleum Geologists Annual Convention Official Program, v. 12, p. A79.

Holtz, M. H., 2006, Optimizing Permanent CO2 sequestration in Brine aquifers: Example from the Upper Frio, Gulf of Mexico: West Texas Geological Society Bulletin, v. 44, no. 4, p. 7.

Holtz, M. H., and L. E. McRae, 1995, Identification and Assessment of Remaining Oil Resources in the Frio Fluvial-Deltaic Sandstone Play, South Texas, Austin, TX: The University of Texas at Austin, Bureau of Economic Geology Report of Investigations No. 227, 46 p.

Holtz, M. H., P. Nance, and R. J. Finley, 2001, Reduction of greenhouse gas emissions through CO2 EOR in Texas: Environmental Geosciences, v. 8, p. 187-199.

Holtz, M. H., V. Nuñez-Lopez, and C. L. Breton, 2005, Moving Permian Basin technology to the Gulf Coast: the geologic distribution of CO2 EOR potential in Gulf Coast reservoirs, *in* Peter Lufholm, and Denise Cox, eds., Unconventional reservoirs technology and strategies: alternative perspectives for the Permian Basin: West Texas Geological Society Fall Symposium, October 26-28, Publication #05-115, 10 p.

Hooper, E. C. D., 1991, Fluid migration along growth faults in compacting sediments: Journal of Petroleum Geology, v. 14, p. 161-180.

Hornafius, J. S., D. Quigley, and B. P. Luyendyk, 1999, The world's most spectacular marine hydrocarbon seeps (Coal Oil Point, Santa Barbara Channel, California): quantification of emissions: Journal of Geophysical Research, v. 104, p. 20703-20711.

Horvitz, L., 1939, On geochemical prospecting: Geophysics, v. 4, p. 210-228.

Horvitz, L., 1969, Hydrocarbon prospecting after thirty years: in Heroy, W. B., editor, Unconventional Methods in Exploration for Petroleum and Natural Gas: Dallas, Southern Methodist University Press, p. 205-218.

Horvitz, L., 1985, Geochemical exploration for petroleum: Science, v. 229, p. 821-827.

Hoversten, G. M., E. Gasperikova, and S. M. Benson, 2006, Theoretical limits for seismic detection of small accumulations of carbon dioxide in the subsurface *in* Proceedings of 8th International Conference on Greenhouse Gas Control Technologies: IEA Greenhouse Gas Programme.

Hovland, M., and J. H. Sommerville, 1992, The global production of methane from shallow submarine sources: Continental Shelf Research, v. 12, p. 1231-1238.

Hovland, M., A. G. Judd, and R. A. Burke, 1993, The global flux of methane from shallow submarine sediments: Chemosphere, v. 26, p. 559-578.

Hovorka, S. D., S. M. Benson, C. Doughty, B. M. Freifeld, S. Sakurai, T. M. Daley, Y. K. Kharaka, M. H. Holtz, R. C. Trautz, H. S. Nance, L. R. Meyer, and K. G. Knauss, 2006, Measuring permanence of CO2 storage in saline formations—The Frio experiment: Environmental Geosciences, in press.

Hovorka, S. D., C. Doughty, S. M. Benson, K. Pruess, and P. R. Knox, 2004a, The impact of geological heterogeneity on CO2 storage in brine formations: a case study from the Texas Gulf Coast, *in* S. J. Baines, and R. H. Worden, eds., Geological Storage of Carbon Dioxide, Special Publications, 233: The Geological Society of London, p. 147-163.

Hovorka, S. D., C. Doughty, and M. H. Holtz, 2005, Testing efficiency of storage in the subsurface: Frio Brine Pilot Experiment, *in* M. Wilson, T. Morris, J. Gale, and K. Thambimuthu, eds., Greenhouse Gas Control Technologies, v. II, Elsevier, San Diego, p. 1361-1372.

Hovorka, S. D., C. Doughty, P. R. Knox, and M. H. Holtz, 2004b, Capacity assessment of the Frio Formation, Texas: The GEO-SEQ Project Results, p. 66-70.

Hovorka, S. D., M. H. Holtz, S. Sakurai, P. R. Knox, D. Collins, P. W. Papadeas, and D. Stehli, 2003, Report to the Texas Commission on Environmental Quality to Accompany a Class V Application for an Experimental Technology Pilot Injection Well: Frio Pilot in CO2

Sequestration in Brine-Bearing Sandstones: The University of Texas at Austin, Bureau of Economic Geology, 162 p. + Plates and Appendices.

Hovorka, S. D., M. L. Romero, A. G. Warne, W. A. Ambrose, T. A. Tremblay, and R. H. Trevino, 2000, Tool to facilitate modeling and pilot projects for sequestration of carbon dioxide in saline formations: Abstracts of Papers of the American Chemical Society, v. 220, p. U397-U397.

Ide, S. T., S. J. Friedmann, and H. J. Herzog, 2006, CO2 leakage through existing wells: current technology and regulations, *in* Proceedings of 8th International Conference on Greenhouse Gas Control Technologies: IEA Greenhouse Gas Programme.

IPCC, 2000, Special Report on Emissions Scenarios: Cambridge University Press, Cambridge, UK, 570 p.

IPCC, 2005, Special Report on Carbon Dioxide Capture and Storage: Cambridge University Press, Cambridge, UK, variously paginated.

James, W. R., L. H. Fairchild, G. P. Nakayama, S. J. Hippler, and P. J. Vrolijk, 2004, Fault-seal analysis using a stochastic multifault approach: AAPG Bulletin, v. 88, p. 885-904.

Jimenez, J. A., and R. J. Chalaturnyk, 2003, Are disused hydrocarbon reservoirs safe for the geological storage of CO2?: Proceedings of the 6th International Conference on Greenhouse Gas Control Technologies, Volume I: Elsevier Science Ltd., p. 471-475.

Johnston, O. C., and B. J. Knape, 1986, Pressure Effects of the Static Mud Column in Abandoned Wells: Austin, TX, Texas Water Commission, 99 p.

Jones, E. A., and H. F. Wang, 1981, Ultrasonic velocities in Cretaceous shales from the Williston Basin: Geophysics, v. 46, p. 288-297.

Jones, G., and R. J. Knipe, 1996, Seismic attribute maps: application to structural interpretation and fault seal analysis in the North Sea basin: First Break, v. 14, p. 449-461.

Jones, R. M., and R. R. Hillis, 2003, An integrated, quantitative approach to assessing fault-seal risk: AAPG Bulletin, v. 87, p. 507-524.

Jones, V. T., and R. J. Drozd, 1983, Predictions of oil or gas potential by near-surface geochemistry: American Association of Petroleum Geologists Bulletin, v. 67, no. 6, p. 932-952.

Juanes, R., E. J. Spiteri, F. M. Orr, Jr., and M. J. Blunt, 2005, Impact of relative permeability hysteresis on geological CO2 storage: submitted to Water Resources Research, December 2005.

Kaiser, W. R., W. B. Ayers, Jr., and L. W. LaBrie, 1980, Lignite Resources in Texas: The University of Texas at Austin, Bureau of Economic Geology Report of Investigations No 104, 52 p.

Katz, D. L., and R. L. Lee, 1990, Natural Gas Engineering Production and Storage: McGraw-Hill Publishing Company.

Kelley, V. A., N. E. Deeds, D. G. Fryar, and J.-P. Nicot, 2004, Groundwater Availability Model for the Queen City and Sparta Aquifers: Austin, Texas, INTERA, Inc., final report prepared for the Texas Water Development Board, variously paginated.

Ketzer, J. M., B. Carpentier, Y. Le Gallo, and P. Le Thiez, 2005, Geological sequestration of CO2 in mature hydrocarbon fields: Basin and reservoir numerical modelling of the Forties Field, North Sea: Oil & Gas Science and Technology—Revue IFP, v. 60, p. 259-273.

Kharaka, Y. K., D. R. Cole, J. J. Thordsen, E. Kakouros, and H. S. Nance, 2006, Gas-water-rock interactions in sedimentary basins: CO2 sequestration in the Frio Formation, Texas, USA: Journal of Geochemical Exploration, v. 89, p. 183-186.

King, P. R., S. V. Buldyrev, N. V. Dokholyan, S. Havlin, E. Lopez, G. Paul, and H. E. Stanley, 2002, Using percolation theory to predict oil field performance: Physics A—Statistical Mechanics and its Applications, v. 314, p. 103-108.

Kisslinger, C., 1976, A review of theories of mechanisms of induced seismicity: Engineering Geology, v. 10, p. 85-98.

Klusman, R. W., 1993, Soil gas and related methods for natural resource exploration: New York, John Wiley and Sons, 483 p.

Klusman, R. W., 2003a, Rate measurements and detection of gas microseepage to the atmosphere from an enhanced oil recovery/sequestration project, Rangely, Colorado, USA: Applied Geochemistry, v. 18, p. 1825-1838.

Klusman, R. W., 2003b, A geochemical perspective and assessment of leakage potential for a mature carbon dioxide-enhanced oil recovery project and as a prototype for carbon dioxide sequestration; Rangely field, Colorado: AAPG Bulletin, v. 87, p. 1485-1507.

Klusman, R. W., and M. A. Saeed, 1996, Comparison of light hydrocarbon microseepage mechanisms: in D. Schumacher and M. A. Abrams, editors, Hydrocarbon migration and its near-surface expression: American Association of Petroleum Geologists Memoir 66, p. 157-168.

Knauss, K. G., 2004, Co-Disposal of CO2, H2S, NO2, and SO2: The GEO-SEQ Project Results, p. 12-15.

Knauss, K. G., J. W. Johnson, and C. I. Steefel, 2005, Evaluation of the impact of CO2, co-contaminant gas, aqueous fluid and reservoir rock interactions on the geologic sequestration of CO2: Chemical Geology, v. 217, p. 339-350.

Knipe, R. J., 1992, Fault process and fault seal: Norvegian Petroleum Sociaty NPF Special Publication, v. 1, p. 325-342.

Knott, S. D., 1993, Fault seal analysis in North Sea: AAPG Bulletin, v. 77, p. 778-792.

Knox, P. R., J. G. Paine, and S. D. Hovorka, 2003, Environmental Assessment: Optimal Geological Environments for Carbon Dioxide Disposal in Brine Formations (Saline Aquifers) in the United States-Pilot Experiment in the Frio Formation, Houston Area: The University of Texas at Austin, Bureau of Economic Geology, 54 p.

Koltermann, C. E., and S. M. Gorelick, 1996, Heterogeneity in sedimentary deposits: A review of structure-imitating, process-imitating, and descriptive approaches: Water Resources Research, v. 32, p. 2617-2658.

Konikow, L. F., and R. C. Ewing, 1999, Is a probabilistic performance assessment enough?: Ground Water, v. 37, p. 481-482.

Kosters, E. C., D. G. Bebout, S. J. Seni, C. M. J. Garrett, L. F. J. Brown, H. S. Hamlin, S. P. Dutton, S. C. Ruppel, R. J. Finley, and N. Tyler, 1989, Atlas of Major Texas Gas Reservoirs: The University of Texas at Austin, Bureau of Economic Geology, 161 p.

Kreitler, C. W., 1989, Hydrogeology of sedimentary basins: Journal of Hydrology, v. 106, p. 29-53.

Kreitler, C. W., M. S. Akhter, A. C. A. Donnelly, and W. T. Wood, 1988, Hydrogeology of Formations Used for Deep-Well Injection, Texas Gulf Coast: The University of Texas at Austin, Bureau of Economic Geology, 204 p.

Krooss, B. M., and D. Leythaeuser, 1996, Molecular diffusion of light hydrocarbons in sedimentary rocks and its role in migration and dissipation of natural gas: in D. Schumacher and M. A. Abrams, editors, Hydrocarbon migration and its near-surface expression: American Association of Petroleum Geologists Memoir 66, p. 173-184.

Kumar, A., M. H. Noh, A. Pope, K. Sepehrnoori, B. S., and L. W. Lake, 2004, Reservoir simulation of CO2 storage in deep saline aquifers: Society of Petroleum Engineers paper SPE89343.

Kvenvolden, K. A., 1988, Methane hydrate - a major reservoir of carbon in the shallow geosphere? Chemical Geology, v. 71, p. 41-51.

Land, C. S., 1968, Calculation of imbibition relative permeability for two- and three-phase flow from rock properties: Society of Petroleum Engineers paper SPE1942.

Land, L. S., and G. L. Macpherson, 1992, Origin of saline formation waters, Cenozoic section, Gulf of Mexico sedimentary basin: AAPG Bulletin, v. 76, p. 1344-1362.

LeNeveu, D. M., J. C. Tait, F. B. Walton, K. Haug, and S. Bachu, 2006, The role of the upper geosphere in mitigating CO2 surface releases in wellbore leakage scenarios, *in* Fifth Annual Conference on Carbon Capture and Sequestration, Washington, DC.

Leonenko, Y., D. W. Keith, M. Pooladi-Darvish, and H. Hassanzadeh, 2006, Accelerating the dissolution of CO2 in aquifers, *in* Proceedings of 8th International Conference on Greenhouse Gas Control Technologies: IEA Greenhouse Gas Programme.

LeSchack, L. A., and D. R. Van Alstine, 2002, High-resolution ground-magnetic (HRGM) and radiometric surveys for hydrocarbon exploration: six case histories in western Canada: in D. Schumacher and M. A. Abrams, editors, Surface exploration case histories: applications of geochemistry, magnetics, and remote sensing: American Association of Petroleum Geologists Studies in Geology no. 48, p. 67-156.

Ligtenberg, H., 2004, Fault seal analysis by enhancing fluid flow paths and fault irregularities in seismic data, *in* AAPG Annual Conference Cancun, Mexico.

Lindeberg, E., 1997, Escape of CO2 from aquifers: Energy Conversion and Management, v. 38, p. S235-S240.

Lindsay, N. G., F. C. Murphy, J. J. Walsh, and J. Watterson, 1993, Outcrop studies of shale smears on fault surfaces: Special Publication of the International Association of Sediment, v. 15, p. 113-123.

Loucks, R. G., D. G. Bebout, and W. E. Galloway, 1977, Relationship of porosity formation and preservation to sandstone consolidation history-Gulf Coast lower Tertiary Frio Formation: Gulf Coast Association of Geological Societies Transactions, v. 27, p. 109-120.

Loucks, R. G., M. M. Dodge, and W. E. Galloway, 1984, Regional controls on diagenesis and reservoir quality in lower Tertiary sandstones along the Texas Gulf Coast, *in* D. A. McDonald, and R. C. Surdam, eds., Clastic Diagenesis: AAPG Memoir 37, p. 15-45.

Mace, R. E., J. P. Nicot, A. H. Chowdhury, A. R. Dutton, and S. Kalaswad, 2005, Please pass the salt: using oil fields for the disposal of concentrate from desalination plants: Texas Water Development Board and Texas Bureau of Economic Geology, report prepared for the U.S. Bureau of Reclamation, Desalination and Water Purification Research and Development, 219 p.

Machel, H. G., and E. A. Burton, 1991a, Chemical and microbial processes causing anomalous magnetization in environments affected by hydrocarbon seepage: Geophysics, v. 56, no. 5, p. 598-605.

Machel, H. G., and E. A.Burton, 1991b, Causes and spatial distribution of anomalous magnetization in hydrocarbon seepage environments: American Association of Petroleum Geologists Bulletin, v. 75, no. 12, p. 1864-1876.

Mandl, G., 1988, Mechanics of tectonic faulting; models and basic concepts, *in* Development in Structural Geology, H. J. Zwart, ed. Elsevier Sciences Publishing, 407 p.

Manzocchi, T., J. J. Walsh, P. Nell, and G. Yielding, 1999, Fault transmissibility multipliers for flow simulation models: Petroleum Geoscience, v. 5, p. 53-63.

Mattax, C. C., and R. L. Dalton, 1990, Reservoir Simulation: SPE Monograph Series, v. 13, 173 p.

Matthews, M. D., 1996, Migration - a view from the top: in D. Schumacher and M. A. Abrams, editors, Hydrocarbon migration and its near-surface expression: American Association of Petroleum Geologists Memoir 66, p. 139-155.

Matthews, M. D., V. T. Jones, and D. M. Richers, 1984, Remote sensing and surface hydrocarbon leakage: in Proceedings of the International symposium on remote sensing of environment, Third thematic conference, Remote sensing for exploration geology, v. 3, p. 663-670.

Maury, V., 1997, Effet de la décompression du Champ de Lacq, Point récapitulatif à la fin 1989 sur l'activité sismique et l'affaissement : Bull. Centre. Rech. Elf Exploration Production, v. 21, p. 303-323 (in French).

McDowell, A. N., 1975, What are the problems in estimating the oil potential of a basin? Oil and Gas Journal, v. 73, p. 85-90.

McKenna, S. A., and G. Smith, 2004, Sensitivity of groundwater flow patterns to parameterization of object-based fluvial aquifer models, *in* J. S. Bridge, and D. W. Hyndman, eds., Aquifer Characterization, Special Publication No. 80: Tulsa, SEPM (Society for Sedimentary Geology).

McNeill, D. F., 2000, A Review of Upward Migration of Effluent Related to Subsurface Injection at Miami-Dade Water and Sewer South District Plant: Final report prepared for the Sierra Club—Miami Group, 30 p.

Mijnssen, F. C. J., 1991, Characterization of Deltaic Rocks for Numerical Reservoir Simulation: TNO Anstitute of Applied Science, Delft, The Netherlands, 223 p.

Miller, M. G., 1996, Ductility in fault gouge from a natural fault system, Death Valley, California: A mechanism for fault zone strengthening and relevance to paleoseismicity: Geology, v. 24, p. 603-606.

Milliken, K. L., and L. S. Land, 1994, Influence of fluid flow in microfractures in geopressured shales: Discussion: AAPG Bulletin, v. 78, p. 1637-1640.

Mishra, S., 2002, Assigning probability distributions to input parameters of performance assessment models: Technical Report TR-02-11 prepared by Intera Inc., USA for SKB, Stockholm, Sweden, 49 p.

Mohan, M., T. S. Panwar, and M. P. Singh, 1995, Development of dense gas dispersion model for emergency preparedness: Atmospheric Environment, v. 29, p. 2075-2087.

Montgomery, P. C., and D. K. Smith, 1959, Oil Well Cementing Practices and Materials: Petroleum Engineering 270, The University of Texas at Austin, Halliburton Oil Well Cementing Company, 32 p.

Mörner, N.-A., and G. Etiope, 2002, Carbon degassing from the lithosphere: Global and Planetary Change, v. 33, p. 185-203.

Morris, A., D. A. Ferril, and D. B. Henderson, 1996, Slip-tendency analysis and fault reactivation: Geology, v. 24, p. 275-278.

Morrow, C. A., L. Q. Shi, and J. D. Byerlee, 1981, Permeability and strength of San Andreas fault gouge under high pressure: Geophysical Research Letters, v. 8, p. 325-328.

Morton, R. A., T. E. Ewing, and N. Tyler, 1983, Continuity and Internal Properties of Gulf Coast Sandstones and their Implications for Geopressured Fluid Production: The University of Texas at Austin, Bureau of Economic Geology Report of Investigations No. 132, 70 p.

Morton, R. A., and L. S. Land, 1987, Regional variations in formation water chemistry, Frio Formation (Oligocene), Texas Gulf Coast: AAPG Bulletin, v. 71, p. 191-206.

Moshier, S. O., and D. W. Waples, 1985, Quantitative evaluation of Lower Cretaceous Mannville Group as source rock for Alberta's oil sands: American Association of Petroleum Geologists Bulletin, v. 69, p. 161-172.

National Research Council (NRC), 2006. Surface temperature reconstructions for the last 2,000 years: The National Academies Press, Washington D.C., 141p.

NETL, 2005, Carbon Sequestration: Technology Roadmap and Program Plan 2005: Developing the Technology Base and Infrastructure to Enable Sequestration as a Greenhouse Gas Mitigation Option: U.S. Department of Energy, Office of Fossil Energy, National Energy Technology Laboratory, 27 p.

Nichol, J. R., and S. N. Kariyawasam, 2000, Risk assessment of temporarily abandoned or shut-in wells: Department of the Interior, Minerals Management Service, 27 p.

Nicot, J.-P., A. H. Chowdhury, and A. R. Dutton, 2005, Please Pass the Salt: Using Oil Fields for the Disposal of Concentrate from Desalination Plants: The University of Texas at Austin,

Bureau of Economic Geology, final report prepared for Texas Water Development Board, 241 p.

Noh, M. H., 2003, Reactive Transport Modeling in Fractures and Two-Phase Flow: Ph.D. thesis, The University of Texas at Austin, Austin, TX, 181 p.

Nordbotten, J. M., M. A. Celia, and S. Bachu, 2004, Analytical solutions for leakage rates through abandoned wells: Water Resources Research, v. 40.

Nordbotten, J. M., M. A. Celia, S. Bachu, and H. K. Dahle, 2005, Semianalytical solution for CO2 leakage through an abandoned well: Environmental Science & Technology, v. 39, p. 602-611.

Nuñez-López, V., and M. H. Holtz, 2006, GCCC EOR Database: The University of Texas at Austin, Bureau of Economic Geology, Gulf Coast Carbon Center.

Oda, M., 1985, Permeability tensor for discontinuous rock masses: Geotechnique, v. 35, p. 483-495.

Oldenburg, C. M., and A. J. A. Unger, 2003, On leakage and seepage from geologic carbon sequestration sites: unsaturated zone attenuation: Vadose Zone Journal, v. 2, p. 287-296.

Oldenburg, C. M., A. J. A. Unger, R. P. Hepple, and P. D. Jordan, 2002, On Leakage and Seepage from Geologic Carbon Sequestration Sites: Berkeley, CA, Lawrence Berkeley National Laboratory, 31 p. + Appendices.

Oreskes, N., K. Shrader-Frechette, and K. Belitz, 1994, Verification, validation, and confirmation of numerical models in the earth sciences: Science, v. 293, p. 641-646.

Paine, J. G., A. R. Dutton, and M. U. Blum, 1999, Using airborne geophysics to identify salinization in West Texas: The University of Texas at Austin, Bureau of Economic Geology Report of Investigations No. 257, 69 p.

Palmer, C. D., and J. A. Cherry, 1984, Geochemical reactions associated with low-temperature thermal energy storage in aquifers: Canadian Geotechnical Journal, p. 475-488.

Parry, W. T., P. N. Wilson, and R. L. Bruhn, 1988, Pore fluid chemistry and mechanical reactions on the Wasatch normal fault, Utah: Geochemica and Cosmochemica Acta, v. 52, p. 2053-2063.

Patankar, S. V., 1980, Numerical Heat Transfer and Fluid Flow: Hemisphere Publishing Corporation, Washington D.C., 197 p.

Pate-Cornell, M. E., 1996, Uncertainties in risk analysis: Six levels of treatment: Reliability Engineering and System Safety, v. 54, p. 95-111.

Pawar, R., J. Carey, S. Chipera, J. Fessenden, J. Kaszuba, G. Keating, P. Lichtner, S. Seth Olsen, P. P. Stauffer, H. Viswanathan, H. Ziock, and G. Guthrie, 2006, Development of a framework for long-term performance assessment of geologic CO2 sequestration sites, *in* Proceedings of 8th International Conference on Greenhouse Gas Control Technologies: IEA Greenhouse Gas Programme.

Peckmann, J., 1999, Cold seep deposits of Beauvoisin (Oxfordian; southeastern France) and Marmorito (Miocene; northern Italy); microbially induced authigenic carbonates, *in* V. Thiel, W. Michaelis, P. Clari, C. Gaillard, L. Martire, and J. Reitner, eds., International Journal of

Earth Sciences, Federal Republic of Germany, Springer International: Berlin, Federal Republic of Germany, p. 60-75.

Peirce, J. W., S. A. Goussev, R. A. Charters, H. J. Abercrombie, and DePaoli, G. R., 1998, Intrasedimentary magnetization by vertical fluid flow and exotic geochemistry: The Leading Edge, v. 17, p. 89-92.

Pittman, E. D., 1981, Effects of fault-related granulation on porosity and permeability of quartz sandstone, Simpson Group (Ordovician), Oklahoma, AAPG Bulletin, v. 65, p. 2381-2387.

Platt, S., 1998, An underground injection control summary of regional and state implementation of the area of review: UIC National Technical Workgroup, Issue #2, EPA UIC Office Region 3, March 17, 7 p. http://www.epa.gov/r5water/uic/ntwg/aorsum.pdf, last accessed on June 13, 2006.

Potter, P. E., J. B. Maynard, and W. A. Pryor, 1980, Sedimentology of Shale—Study Guide and Reference Source: New-York, Springer-Verlag, 306 p.

Pruess, K., and J. Garcia, 2002, Multiphase flow dynamics during CO2 disposal into saline aquifers: Environmental Geology, v. 42, p. 282-295.

Pruess, K., J. Garcia, T. Kovscek, C. Oldenburg, J. Rutqvist, C. Steefel, and T. Xu, 2004, Code intercomparison builds confidence in numerical simulation models for geologic disposal of CO2: Energy, in Proceedings of 6th International Conference on Greenhouse Gas Control Technologies, v. 29, p. 1431-1444.

Pruess, K., T. F. Xu, J. A. Apps, and J. Garcia, 2001, Numerical modeling of aquifer disposal of CO2: Society of Petroleum Engineers paper SPE66537.

Purnell, P., N. R. Short, and C. L. Page, 2001, Super-critical carbonation of glass-fibre reinforced cement. Part 1. Mechanical testing and chemical analysis: Composites Part A, v. 32, p. 1777-1787.

Rechard, R. P., 1999, Historical relationship between performance assessment for radioactive waste disposal and other types of risk assessment: Risk Analysis, v. 19, p. 763-807.

Reeves, M., and R. M. Cranwell, 1981, User's manual for the Sandia Waste-Isolation Flow and Transport Model (SWIFT), release 4.81, Report SAND81-2516, 145 p.

Reiner, D. M., and H. J. Herzog, 2004, Developing a set of regulatory analogs for carbon sequestration: Energy, v. 29, p. 1561-1570.

Richers, D. M., and L. E. Maxwell, 1991, Application and theory of soil gas geochemistry in petroleum exploration: in R. K. Merrill, editor, Source and Migration Processes and Techniques: American Association of Petroleum Geologists Treatise of Petroleum Geology, Handbook of Petroleum Geology, p. 141-158.

Rish, W. R., 2003, A probabilistic risk assessment of Class I hazardous waste injection wells, *in* Proceedings of Second International Symposium on Underground Injection Science and Technology, October 22-23, v. LBNL-53837: Berkeley, CA, Lawrence Berkeley National Laboratory.

Roberts, H. H., R. Sassen, and P. Aharon, 1989, Petroleum-derived authigenic carbonates of the Louisiana continental slope: Proceedings of the Oceans '88 Conference, Baltimore, Maryland, p. 101-105.

Rock, B. N., 1984, Remote detection of geobotanical anomalies associated with hydrocarbon microseepage using Thematic Mapper Simulation (TMS) and Airborne Imaging Spectrometer (AIS) data: international Union of Geological Sciences and UNESCO, BRGM document no. 82, p. 299-309.

Ross, R. M., W. F. Krise, L. A. Redell, and R. M. Bennett, 2000, Effects of dissolved carbon dioxide on the physiology and behavior of fish in artificial streams: Environmental Toxicology, v. 16, p. 84-95.

RRC, 2000, Well Plugging Primer, Railroad Commission of Texas.

Rubin, J. B., J. Carey, and C. M. V. Taylor, 1997, Enhancement of Cemented Waste Forms by Supercritical CO2 Carbonation of Standard Portland Cements: Los Alamos National Laboratory Report LA-UR 97-1859, 8 p.

Rutherford, J. C., 1994, River Mixing: John Wiley & Sons, New York.

Rutqvist, J., and C. F. Tsang, 2002, A study of caprock hydromechanical changes associated with CO2-injection into a brine formation: Environmental Geology, v. 42, p. 296-305.

Rutter, E. H., S. H. Hall, and S. H. White, 1986, Comparative microstructure of natural and experimentally produced clay-bearing fault gouges: Pure and Applied Geophysics, v. 124, p. 149-164.

Saripalli, K. P., N. M. Mahasenan, and E. M. Cook, 2002, Risk and hazard assessment for projects involving the geological sequestration of CO2, *in* Sixth International Conference on Greenhouse Gas Control Technologies, October 1-4.

Saripalli, P., and P. McGrail, 2002, Semi-analytical approaches to modeling deep well injection of CO2 for geological sequestration: Energy Conversion and Management, v. 43, p. 185-198.

Schiemer, E. J., G. Stober, and E. Faber, 1985, Surface geochemical exploration for hydrocarbons in offshore areas - principles, methods, and results: in Petroleum Geochemistry in Exploration of the Norwegian Shelf: London, Graham and Trotman, p. 223-238.

Schumacher, D., 1996, Hydrocarbon-induced alteration of soils and sediments: in D. Schumacher and M. A. Abrams, editors, Hydrocarbon migration and its near-surface expression: American Association of Petroleum Geologists Memoir 66, p. 71-89.

Schumacher, D., 1999, Surface geochemical exploration for petroleum: in E. A. Beaumont and N. H. Foster, editors, Exploring for Oil and Gas Traps: Handbook of Petroleum Geology: Treatise of Petroleum Geology: Tulsa, American Association of Petroleum Geologists, p. 18-1 to 18-27.

Schwartz, D. P., and K. J. Coppersmith, 1984, Fault behavior and characteristic earthquakes: examples from the Wasatch and San Andreas fault zones: Journal of Geophysical Research, v. 89.

Sibson, R. H., 1987, Earthquake rupturing as a hydrothermal mineralizing agent: Geology, v. 15, p. 701-704.

Sibson, R. H., 1989, Earthquake faulting as a structural process: Journal of Structural Geology, v. 11, p. 1-14.

Sibson, R. H., 1990, Condition of fault-valve behaviour, *in* R. J. Knipe and E.H Rutter eds., Deformation Mechanisms, Rheology and Tectonics: Geological Society Special Publication, v. 54, p. 15-28.

Simunek, J., and D. Suarez, 1993, Modeling of carbon dioxide transport and production in soil, I. Model development: Water Resources Research, v. 29, p. 487-497.

Sloan, E. D., 1998a, Gas hydrates: review of physical/chemical properties: Energy & Fuels, v. 12, p. 191-196.

Sloan, E. D., 1998b, Physical/chemical properties of gas hydrates and application to world margin stability and climatic change: in J. P. Henriet and J. Mienert, editors, Gas hydrates; relevance to world margin stability and climate change: Geological Society Special Publications, v. 137, p. 31-50.

Sminchak, J. R., D. F. Dominic, and R. W. Ritzi, Jr., 1996, Indicator geostatistical analysis of sand interconnections within a till: Ground Water, v. 34, p. 1125-1131.

Sminchak, J., and G. Neeraj, 2002, Issues related to seismic activity induced by the injection of CO2 in deep saline aquifers: Journal of Energy and Environmental Research, v. 2, p. 32-46.

Smith, D. A., 1966, Theoretical considerations of sealing and non-sealing faults: AAPG Bulletin, v. 50, p. 363-374.

Smith, D. A., 1980, Sealing and non-sealing faults in Louisiana Gulf Coast salt basin: AAPG Bulletin, v. 64, p. 145-172.

Smith, D. K., 1976, Cementing: Society of Petroleum Engineers of AIME Monograph Volume 4, 184 p.

Smith, D. K., 1993, Handbook on Well Plugging and abandonment: Pennwell Publishing Company, Tulsa, 399 p.

South, D. L., and J. J. K. Daemen, 1986, Permeameter Studies of Water Flow through Cement and Clay Borehole Seals in Granite, Basalt, and Tuff.: Washington, DC, U.S. Nuclear Regulatory Commission, 213 p.

Sperrevik, S., P. A. Gillespie, Q. J. Fisher, T. Halvorsen, and R. J. Knipe, 2002, Empirical estimation of fault rock properties, *in* A. G. Koestler, and R. Hunsdale, eds., Hydrocarbon Seal Quantification, Papers Presented at the Norwegian Petroleum Society Conference, 16-18 October 2000, Stavanger, Norway, Norwegian Petroleum Society (NPF), Special Publications No. 11, p. 109-125.

Sposito, G., 1989, The Chemistry of Soils: Oxford University Press, New York, 277 p.

Sprague, R. H., Jr., and E. D. Carlson, 1982, Building Effective Decision Support Systems: Prentice-Hall, Inc., Englewood Cliffs, N.J.

Sternberg, B. K., 1991, A review of some experience with the induced-polarization/resistivity method for hydrocarbon surveys: success and limitations: Geophysics, v. 56, p. 1522-1532.

Stevens, S. H., J. M. Pearce, and A. A. J. Rigg, 2001, Natural analogs for geologic storage of CO2 ; an integrated global research program, *in* First Conference on Carbon Sequestration, Washington, DC.

Streit, J. E., and S. F. Cox, 2000, Asperity interactions during creep of simulated faults at hydrothermal conditions: Geology, v. 28, p. 231-234.

Striz, E. A., and M. L. Wiggins, 1998, A coupled model to predict interformation flow through an abandoned well: Society of Petroleum Engineers paper SPE49151.

Strutt, M. H., S. E. Beaubien, J. C. Beaubron, M. Brach, C. Cardellini, R. Granieri, D. G. Jones, S. Lombardi, L. Penner, F. Quattrocchi, and N. Voltatorni, 2002, Soil gas as a monitoring tool of deep geological sequestration of carbon dioxide: preliminary results from the Encana EOR project in Weyburn, Saskatchewan (Canada), *in* Sixth International Conference on Greenhouse Gas Control Technologies, October 1-4.

Torp, T. A., and J. Gale, 2004, Demonstrating storage of CO2 in geological reservoirs: The Sleipner and SACS projects, *in* Energy, 6th International Conference on Greenhouse Gas Control Technologies, v. 29, p. 1361-1369.

Tsang, C. F., S. M. Benson, B. Kobelski, and R. E. Smith, 2002, Scientific considerations related to regulation development for CO2 sequestration in brine formations: Environmental Geology, v. 42, p. 275-281.

TWDB, 2006, GAM program. http://www.twdb.state.tx.us/GwRD/pages/gwrdindex.html, last accessed on May 14, 2006.

Tyler, N., and W. A. Ambrose, 1985, Facies architecture and production characteristics of strandplain reservoirs in the Frio Formation, Texas: The University of Texas at Austin, Bureau of Economic Geology Report of Investigations No 146, 42 p.

Tyler, N., W. E. Galloway, C. M. J. Garrett, and T. E. Ewing, 1984, Oil accumulation, production characteristics, and targets for additional recovery in major oil reservoirs of Texas: The University of Texas at Austin, Bureau of Economic Geology, Geological Circular No 84-2, 31 p.

van Genuchten, M. T., 1980, A closed form equation for predicting the hydraulic conductivity of unsaturated soils: Soil Science Society of America Journal, v. 44, p. 892-898.

Vasseur, G., I. Djeran-Maigre, D. Grunberger, G. Rousset, D. Tessier, and B. Velde, 1995, Evolution of structural and physical parameters of clays during experimental compaction: Marine and Petroleum Geology, v. 12, p. 941-954.

Walton, F. B., J. C. Tait, D. LeNeveu, and M. I. Sheppard, 2004, Geological storage of CO2: A statistical approach to assessing performance and risk, *in* Proceedings of 7th International Conference on Greenhouse Gas Control Technologies. Volume 1: Peer-Reviewed Papers and Plenary Presentations, IEA Greenhouse Gas Programme.

Warner, D. L., 1997, On "Subsurface fault detection using seismic data for hazardous-waste-injection well permitting: An example from St. John the Baptist Parish, Louisiana'" by E. V. Zinni (March-April 1995 Geophysics, 60, p. 468-475): Geophysics, v. 62, p. 381-383.

Warner, D. L., 2001, Technical and Economic Evaluation of the Protection of Saline Ground Water under the Safe Drinking Water Act and the UIC Regulations: Report to the Ground Water Protection Research Foundation, 44 p.

Warner, D. L., L. Koederitz, S. Dunn-Norman, and R. C. Laudon, 1996, Application of an AOR Variance Methodology to the Permian Basin, Texas: prepared for The American Petroleum Institute, 288 p.

Warner, D. L., L. Koederitz, and R. C. Laudon, 1997, Application of an Area-of-Review (AOR) Concept to the East Texas Field and Other Selected Texas Oilfields: University of Missouri-Rolla, Final Report for U.S. Department of Energy Grant No DE-FG22-94MT-94002, 402 p.

Watts, N. L., 1987, Theoretical aspects of cap-rock and fault seals for single-phase and 2-phase hydrocarbon columns: Marine and Petroleum Geology, v. 4, p. 274-307.

Weber, K. J., G. Mandl, W. F. Pilaar, F. Lehner, and P. G. Precious, 1978, The role of faults in hydrocarbon migration and draping in Nigerian growth fault structures, *in* 10th Annual Offshore Technology Conference, p. 2643-2653.

Weber, K. J., and L. C. van Gueuns, 1990, Framework for constructing clastic reservoir simulation models: Journal of Petroleum Technology, v. 34, p. 439-453.

Welte, D. H., B. Horsfield, and D. R. Baker, 1997, Petroleum and Basin Evolution: Insights from Petroleum Geochemistry, Geology, and Basin Modeling: New York, Springer, 535 p.

Westphalen, O., m. Peterson, and d. Heins, 1995, Vertical Induction Profiling for Hydrocarbon Plumes: SAGEEP, p. 757-773.

Weyl, P. K., 1959, Pressure solution creep and force of crystallization, a phenomenological theory: Journal of Geophysical Research, v. 64, p. 2001-2025.

Whelan, J., L. Eglinton, L. M. Cathles, S. Losh, and H. Roberts, 2005, Surface and subsurface manifestations of gas movement through a N-S transect of the Gulf of Mexico: Marine and Petroleum Geology, v. 22, p. 479-497.

White, M. D., and M. Oostrom, 2004, STOMP Subsurface Transport over Multiple Phases, Version 3.1, user's guide: Richland, Washington, Pacific Northwest National Laboratory, 317 p.

Williams, A., A. Kloster, R. Duckworth, and N. Piggott, 1995. The role of the Airborne Laser Fluorosensor (ALF) and other seepage detection methods in exploring frontier basins: in S. Hansjien, editor, Petroleum Exploration and Exploitation in Norway: NPF Special Publication 4, p. 421-431.

Wilson, E. J., 2003, Subsurface property rights: Implications for geologic CO2 storage, *in* Proceedings of Second International Symposium on Underground Injection Science and Technology, October 22-23, v. LBNL-53837: Berkeley, CA, Lawrence Berkeley National Laboratory.

Wilson, E. J., 2004, Managing the Risks of Geologic Carbon Sequestration: A Regulatory and Legal Analysis: Ph.D. thesis, Carnegie Mellon University, Pittsburgh, PA, 160 p.

Wilson, E. J., and D. W. Keith, 2003, Geologic carbon storage: understanding the rules of the underground, *in* Proceedings of the 6th Greenhouse Gas Control Conference, Kyoto Japan, p. 229-234.

Wilson, M., and M. Monea, eds., 2004, IEA GHG Weyburn CO2 Monitoring & Storage Project Summary Report 2000-2004, from the Proceedings of the 7th International Conference on

Greenhouse Gas Control Technologies, September 5-9, Vancouver, Canada, PTRC (Petroleum Technology Research Center), Regina, Saskatchewan, Canada, 273 p.

Wilson, R., and E. A. C. Crouch, 2001, Risk-Benefit Analysis: Center for Risk Analysis, Harvard University, 370 p.

Wiprut, D., and M. D. Zoback, 2000, Fault reactivation and fluid flow along a previously dormant normal fault in the northern North Sea: Geology, v. 28, p. 592-598.

Wolery, T. J., and S. A. Daveler, 1992, EQ6, A Computer Program for Reaction Path Modeling of Aqueous Geochemical Systems: Theoretical Manual, User's Guide, and Related Documentation (Version 7.0). UCRL-MA-110662 PT IV: Livermore, California: Lawrence Livermore National Laboratory.

Woodruff, C. M., C. Gever, and W. D, 1984, Geothermal Gradient Map of Texas: The University of Texas at Austin, Bureau of Economic Geology, scale 1:1,000,000.

Woodyard, A. H., 1982, Risk analysis of well completion systems: Society of Petroleum Engineers paper SPE09414.

World Oil, 1992. U.S. drilling heads down: World Oil, v. 213, no 2, p. 51-56.

Wu, F. T., 1978, Mineralogy and physical nature of clay gouge: Paleogeography v. 116, p. 655-689.

Xu, T. F., J. A. Apps, and K. Pruess, 2003, Reactive geochemical transport simulation to study mineral trapping for CO2 disposal in deep arenaceous formations: Journal of Geophysical Research-Solid Earth, v. 108.

Xu, T. F., E. Sonnenthal, N. Spycher, and K. Pruess, 2006, TOUGHREACT—A simulation program for non-isothermal multiphase reactive geochemical transport in variably saturated geologic media: Applications to geothermal injectivity and CO2 geological sequestration: Computers & Geosciences, v. 32, p. 145-165.

Yielding, G., 2002, Shale gouge ratio—calibration by geohistory, *in* A. G. Koestler, and R. Hunsdale, eds., Hydrocarbon Seal Quantification: Papers Presented at the Norwegian Petroleum Society Conference, 16-18 October 2000, Stavanger, Norway, Norwegian Petroleum Society (NPF), Special Publications No. 11, p. 1-15.

Yielding, G., B. Freeman, and D. T. Needham, 1997, Quantitative fault seal prediction: AAPG Bulletin, v. 81, p. 897-917.

Yielding, G., T. Needham, and H. Jones, 1996, Sampling of fault populations using sub-surface data: A review: Journal of Structural Geology, v. 18, p. 135-146.

Zhang, S., T. E. Tullis, and V. Scruggs, 1999, Permeability anisotropy and pressure dependency of permeability in experimentally sheared gouge materials: Journal of Structural Geology, v. 21, p. 795-806.

Zhang, Y. X., 1996, Dynamics of CO2-driven lake eruptions: Nature, v. 379, p. 57-59.

Zhou, W., M. Stenhouse, S. Whittaker, D. H.-S. Law, R. Chalaturnyk, and W. Jazrawi, 2004, The IEA Weyburn CO2 Monitoring and Storage Project—Modeling of the long-term migration of CO2 from Weyburn, *in* Proceedings of 7th International Conference on Greenhouse Gas

Control Technologies. Volume 1: Peer-Reviewed Papers and Plenary Presentations, IEA Greenhouse Gas Programme.

Zieglar, D. L., 1992, Hydrocarbon columns, buoyancy pressures, and seal efficiency—Comparisons of oil and gas accumulations in California and the Rocky-Mountain Area: AAPG Bulletin, v. 76, p. 501-508.

Zinni, E. V., 1995, Subsurface fault-detection using seismic data for hazardous-waste-injection well permitting—an example from St. John the Baptist Parish, Louisiana: Geophysics, v. 60, p. 468-475.

LIST OF ACRONYMS AND ABBREVIATIONS

AOR	Area of review
API	American Petroleum Institute
ASTM	American Society for Testing and Materials
BEG	Bureau of Economic Geology
bgs	Below ground surface
BUQW	Base of usable quality water
CDF	Cumulative distribution function
CSP	Clay shear potential
DOE	Department of Energy
DID	Defense in depth
EOR	Enhanced oil recovery
EPA	Environmental Protection Agency
FEP	Features, events, and processes
gpm	Gallon per minute
Gt	Gigatons (10^9 tons)
H&S	Health and safety
IFT	Interfacial tension
IOGCC	Interstate Oil and Gas Compact Commission
IPCC	Intergovernmental Panel on Climate Change
MCL	Maximum contaminant level
MIT	Mechanical integrity testing
MM&V	Monitoring, mitigation and verification
MMbbl	Millions of barrels (N.B: many industries use M for millions, but common use in the oil and gas industry is M for thousands and MM for millions)
ms	Milliseconds
Mt	Millions of tons, Megatons (10^6 tons)
MTTF	Mean time to failure
NGCAS	Next Generation Capture and Storage, project funded by European Union
NRC	National Research Council
NRC	Nuclear Regulatory Commission
NWPA	Nuclear Waste Policy Act (1982)
OOIP	Original oil in place
PA	Performance assessment

PDF	Probability density function
RA	Risk analysis
RCRA	Resource Conservation and Recovery Act
RFP	Request for proposal
RRC	Railroad Commission of Texas
SDWA	Safe Drinking Water Act
SGR	Shale gouge ratio
SPE	Society of Petroleum Engineers
TAC	Texas Administrative Code
TCEQ	Texas Commission on Environmental Quality
TDS	Total dissolved solids
TGC	Texas Gulf Coast
TWDB	Texas Water Development Board
UIC	Underground injection control
USDW	Underground source of drinking water
USGS	U.S. Geological Survey
WIPP	Waste isolation pilot plant
ZEI	Zone of endangering influence

APPENDIX A: Geology of Gulf Coast Basin

The state of Texas can be divided into several geologically significant areas, mostly along boundaries of sedimentary basins. Two basins stand out by their size and their economic significance: the Gulf Coast Basin and the Permian Basin (**Figure 53**). Beginning in Triassic time (250 million years ago), Texas was subject to extension and volcanism, leading to Jurassic rifting of the continental margin and creation of the Gulf of Mexico and Atlantic Ocean. The small rift basins that initially formed were buried under abundant salt accumulation (Louann Salt). As the weight of sediments increased, the salt became unstable and started locally to move upward in diapirs, a phenomenon still active today. During the Cretaceous, sediments deposited from shallow inland seas formed broad continental shelves that covered most of Texas. In the Tertiary (starting 65 million years ago), as the Rocky Mountains to the west started rising, large river systems flowed toward the Gulf of Mexico, carrying an abundant sediment load, in the fashion of today's Mississippi River. Sediments also contained local sources, including erosional detritus from the multiple Tertiary volcanic centers in West Texas and Mexico.

Stratigraphy:

Six major progradation events (Galloway et al., 2000), in which the sedimentation built out into the Gulf Coast Basin, including the Frio deltaic and strandplain sedimentation, most likely targeting the Gulf Coast area, have been described (**Figure 3** and **Figure 54** for a more accurate cross section). Each progradation event is also paired with a major sea-level rise that typically deposited regionally extensive marine clays that could act as regional seals to limit upward migration of CO_2. Volumetrically important progradation wedges include the Wilcox and the Vicksburg/Frio. The Wilcox wedge is directly overlain by the Reklaw shale. Basinward, the Reklaw shale merges with marine clays associated with the smaller progradation wedges of the Queen-City, Sparta, Yegua, and Jackson Formations. Their updip equivalents include the Weches and Cook Mountain Formations. The Frio wedge is the target of choice in the analysis area (**Figure 54**). It is covered by another marine clay, the Anahuac shale (**Figure 55**). The next wedge, the Oakville/Fleming Formation, could also be an attractive target. It is overlain by the *Amphistegina* B shale. The last major progradation wedge of Plio-Pleistocene age is still active and is too shallow to be of prime interest for CO_2 storage.

The set of depositional systems is the same throughout the Tertiary period: fluvial, deltaic, barrier bar/strandplain, and slope/basin depositional systems (**Figure 56**). Little

variation occurred in the location of the main depocenters, resulting in individualized subbasins. The Tertiary Gulf Coast formations can be subdivided into three regions (**Figure 57**): the Houston Embayment, with a thick sediment accumulation (also true for salt accumulation, hence the diapirism); the San Marcos Arch, with a less abundant sediment influx; and the Rio Grande Embayment in South Texas. The nature of the depositional system has important consequences on our understanding of fluid flow in general and carbon storage in particular. Vertical continuity of sand in main depocenters is impacted by the wavering of channels. Channel sand bodies will vertically stack in a rapidly subsiding basin, as in the Gulf Coast, whereas in a more stable tectonic environment, distributary channels may wander more, resulting in vertically offset sand bodies. Lateral continuity can also be understood in terms of depositional system. Wave-dominated deltaic and strandplain systems present a high lateral continuity and could be thick, whereas fluvial and fluvial deltaic systems can present abrupt lateral facies changes. Wave-dominated deltaic and strandplain systems are also well sorted. In general, sand permeability is correlated with body thickness—that is, transmissivity increases more than linearly with thickness.

Geographic extent of seals should be understood within the local history of the depositional systems, for example—in the context of second- (e.g., Anahuac shale), third-, fourth-, and fifth- (e.g., very local shale layer of limited extend in a fluvial channel) order flooding-event shales.

Faulting:

Growth faults, resulting from sediment loading on unstable substrates, periodically develop. Intermittent movement along these growth faults has accommodated accumulation of enormous masses of sediments. Growth faults are mostly syndepositional faults. Zones of growth faulting mark the basinward movement of the shelf edge. Fault-bounded reservoir compartments create many structural traps in the Tertiary stratigraphic section of the southern Gulf Coast Basin.

Hydrocarbon Resources:

Outlines of the oil and gas fields present are shown in **Figure 4**. **Figure 58** provides a visual aid to the stratigraphic source of oil resources in the Gulf Coast. The Frio Formation is a major hydrocarbon source in the Gulf Coast.

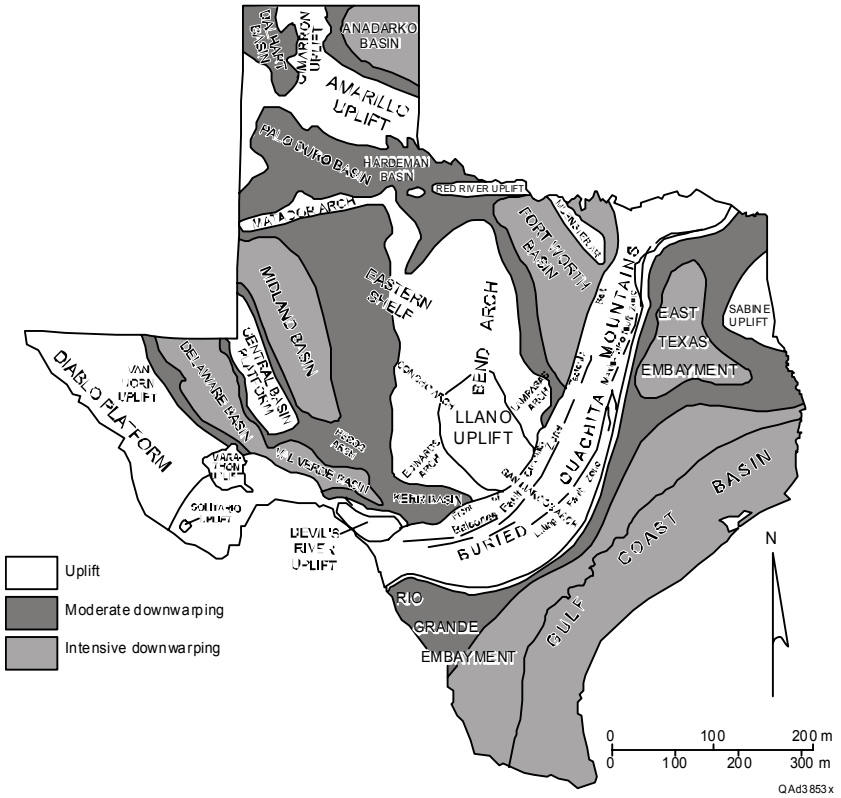

Source: Modified from Kreitler, 1989
Figure 53. Generalized tectonic map of Texas showing location of sedimentary basins

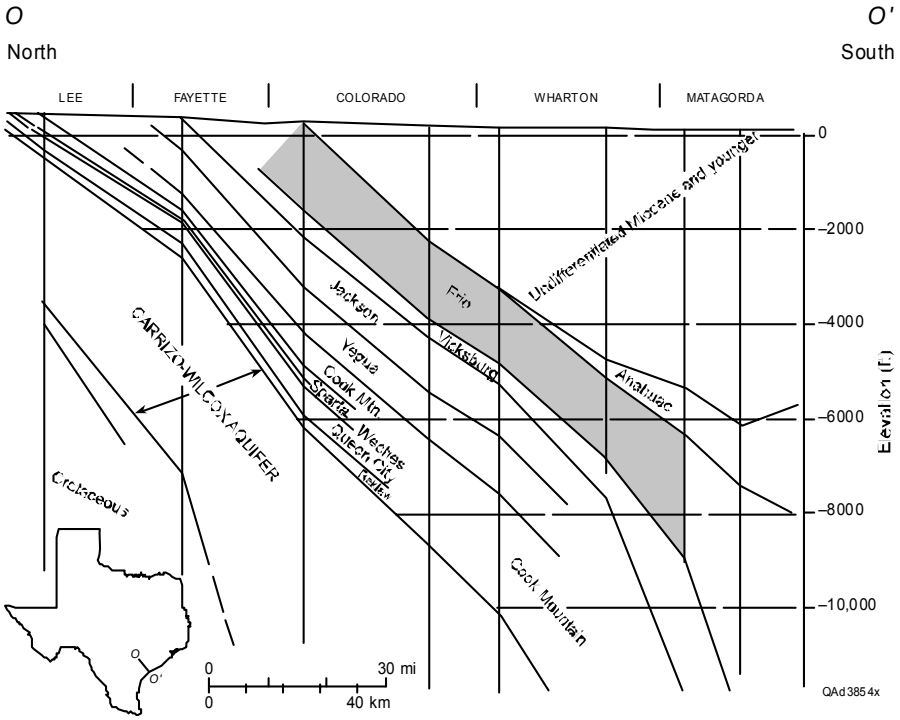

Source: Modified from Core Laboratories Inc., 1972
Note: Frio Formation is solid gray
Figure 54. Simplified cross section of the Gulf Coast

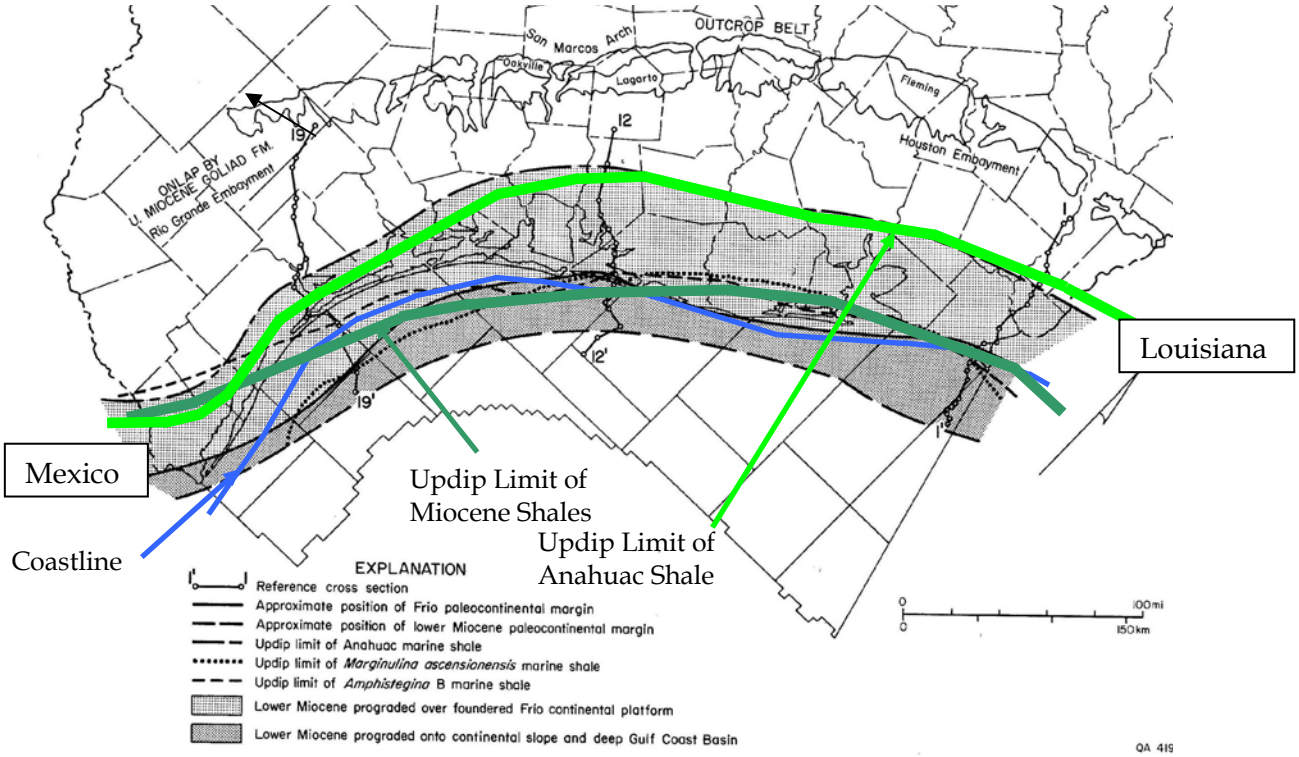

Source: Galloway et al., 1986, Fig. 3

Figure 55. Maximum inland extent of two extensive marine clays: the Anahuac shale and the *Amphistegina* B shale

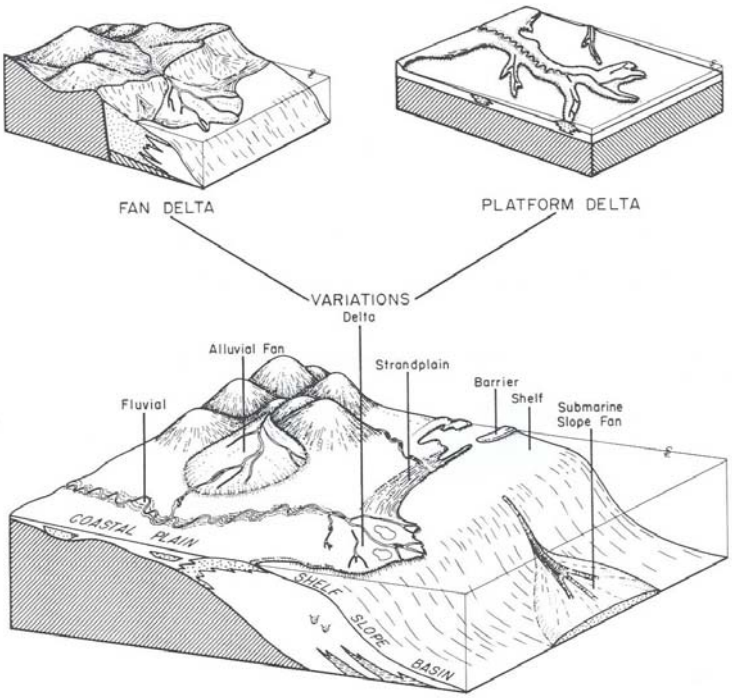

Source: Galloway et al. (1983)

Figure 56. Cartoon of typical Gulf Coast depositional systems (except alluvial fan)

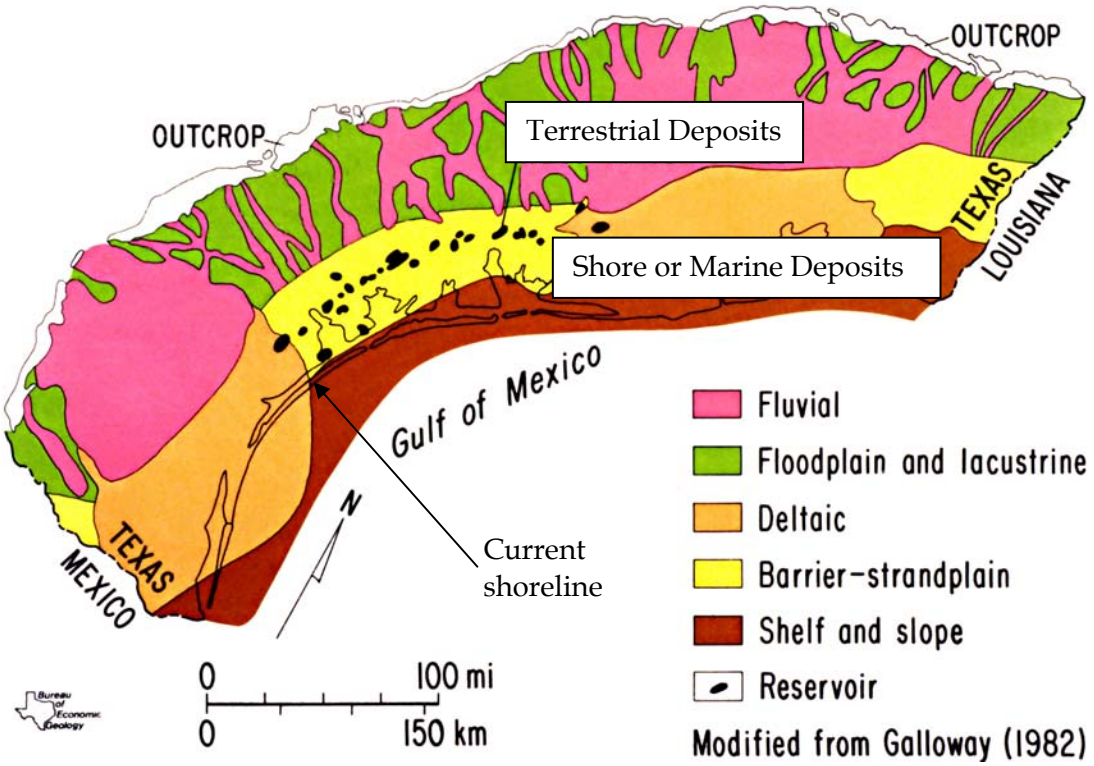

Figure 57. Frio barrier-strandplain and deltaic systems showing oil and gas reservoirs of the Frio barrier and strandplain trend

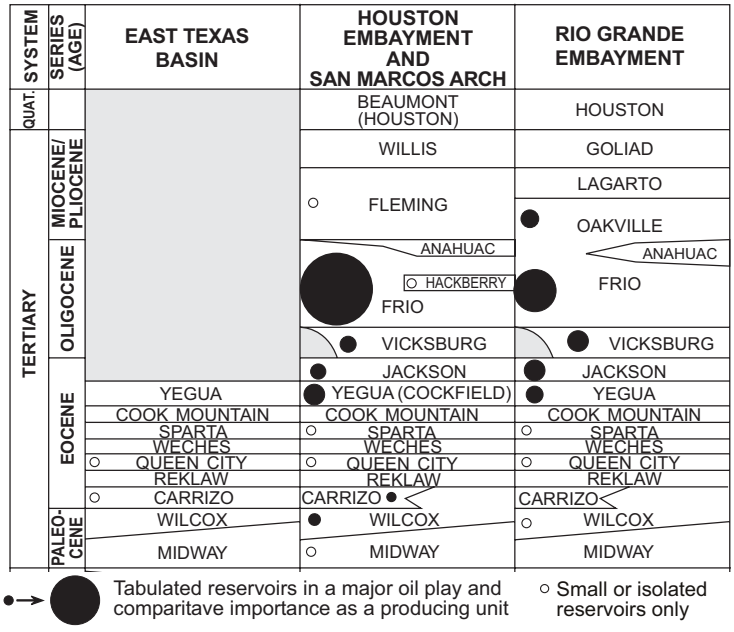

Source: Modified from Galloway et al., 1983

Figure 58. Stratigraphic column and relative oil production for the Gulf Coast and East Texas Basins

APPENDIX B: The Hydrocarbon Proxy for Potential Carbon Dioxide Leakage from Subsurface Reservoirs

Carbon (primarily in the form of methane and carbon dioxide) is added to the atmosphere from many natural and anthropogenic sources. Primary natural sources include volcanism, mantle degassing, liberation from carbonate crustal rocks, and leakage from hydrocarbon reservoirs (Mörner and Etiope, 2002). Methane leakage from hydrocarbon reservoirs, in particular, is estimated at 8 to 65 Mt per year (Hovland et al., 1993; Hornafius et al., 1999) in marine environments and perhaps an equal amount in subaerial environments (Mörner and Etiope, 2002). Leakage of light hydrocarbons (chiefly methane through pentane) is an appealing analog for examining potential leakage of CO_2 from subsurface sequestration sites owing to the similarities in molecular size and mass among CO_2 and the light hydrocarbons. CO_2 molecules have a mass of 44 atomic mass units (amu) and a diameter of 0.35 nm, whereas light hydrocarbons range from 16 to 72 amu in mass and are 0.4 nm and larger in diameter. We can thus gain insight into the possible migration mechanisms and flux rates of CO_2 sequestered in geologic reservoirs by examining hydrocarbon migration in similar geologic settings.

Evidence of Vertical Hydrocarbon Migration

Direct and indirect geologic, geophysical, biological, and chemical evidence of hydrocarbon migration from reservoirs to the surface has been widely reported. Direct evidence includes the presence of macroseeps at the ground surface and on the sea floor, manifested as direct gas discharge of lighter hydrocarbons, accumulations of heavier hydrocarbons at or near the land surface or seabed, and the widespread occurence of marine gas hydrates (e.g. Abrams, 1992, 1996a; Brooks et al., 1984, 1987; Cline and Holmes, 1977; Dando and Hovland, 1992; Dando et al., 1994; Hedberg, 1981; Kvenvolden, 1988; Roberts et al., 1989; Sloan, 1998a and b). Most instances of macroseepage are thought to occur along structural features such as faults and fractures.

Indirect evidence includes diagenetic effects on near-surface materials and unique microbiological and botanical communities associated with near-surface "chimneys" above hydrocarbon reservoirs. Near-surface diagenetic changes can include precipitation of magnetic and nonmagnetic iron sulfides and oxides, carbonates and carbonate cements, and paraffin dirt (e.g. Schumacher, 1996, 1999; Ellwood and Burkart, 1996; Machel and Burton, 1991a and b; Al-

Shaieb et al., 1994; Donovan, 1974). Many of these effects require more diffuse vertical migration of hydrocarbons than typically occurs along structural features.

Leakage Mechanisms, Rates, and Volumes

Many of the direct indicators of hydrocarbon migration, such as gas discharges and heavier hydrocarbon accumulations at the land surface and seabed, have been attributed to preferential volume flow along structural features such as faults and fractures (Schumacher, 1999; Horvitz, 1939, 1985; Jones and Drozd, 1983). More widespread presence of light hydrocarbons near the land surface as well as indirect indicators such as diagenetic alteration and biological responses are attributed to "microseepage," with the assumption that geologic traps are not perfect seals (Matthews, 1996; Schumacher, 1999). Further evidence for microseepage includes (1) increased concentration of light hydrocarbons and hydrocarbon-oxidizing microbes above reservoirs, (2) increased light hydrocarbon ratios in soil gas over oil and gas reservoirs, (3) sharp lateral changes in concentrations and ratios at the edges of subsurface projections of reservoirs, (4) similarity of stable carbon isotopic ratios for methane and other light hydrocarbons in soil gases similar to those in underlying reservoirs, and (5) ephemeral appearance of soil gas and microbial anomalies in response to reservoir depletion and repressuring (Schumacher, 1999).

Proposed vertical migration mechanisms include volume (Darcy) flow, molecular diffusion, separate-phase flow, dissolution in water and subsequent migration, and transport along kerogen pathways (Matthews, 1996; Krooss and Leythaeuser, 1996). Many of the proposed mechanisms for hydrocarbon migration are valid, but most are of secondary importance and are only recognizable in special situations (Matthews, 1996). The dominant vertical microseepage mechanism is interpreted to be buoyancy-driven gas flow within reservoir rocks and capillary imbibition from sources and seals in carrier rocks (Schumacher, 1999; Matthews, 1996; Clayton et al., 1999; Clayton and Dando, 1996; Bjorkum et al., 1998). Migration pathways are strongly influenced by three-dimensional heterogeneity at all scales from individual pore systems to facies relationships (Matthews, 1996).

Buoyancy forces, small molecular sizes, and imperfect seals can produce relatively rapid rates of vertical ascent for light hydrocarbons. Krooss and Leythaeuser (1996) interpret very low methane transport rates by molecular diffusion through seals, ranging from 0.16 to 89 $m^3/km^3/yr$. Compressible volume flow through shale 50 to 450 m thick with a permeability of 1

nanodarcy is much higher, ranging from 100 to 1000 $m^3/km^3/yr$ (Krooss and Leythaeuser, 1996). Light hydrocarbons have been reported to move through thousands of meters of strata without observable faults or fractures in time periods of weeks to years (Schumacher, 1999); other reported ascent rates range from less than 1 m/day to 10s of m/day (Arp, 1992; Klusman and Saeed, 1996; Matthews, 1996).

Larger scale leakage studies that combine macro- and microseepage volumes suggest that vertical hydrocarbon fluxes can be very large, even in producing fields. Cathles (2004) estimates that 131 billion tons of hydrocarbon have been vented from a 24,000 km^2 area near South Marsh Island in offshore Louisiana, and 15 billion tons are currently migrating in that system. Over a salt diapir in the Ekofisk Field in the North Sea, gas seepage through 120 seeps at the seabed have a total flow rate of about 3000 $m^3/day/km^2$ (Hovland and Sommerville, 1992). On Denmark's Kattegat Coast, fault-line leakage of methane from geologically recent sources has a mean flow rate of 1400 $m^3/day/km^2$ (Dando et al., 1994).

Detection Methods

The concept of vertical migration of hydrocarbons from subsurface reservoirs to the ground surface or seabed forms the basis of several types of near-surface hydrocarbon exploration methods. These methods either directly detect hydrocarbons through chemical analysis (most atmospheric, soil, and shallow sediment approaches) or detect the alterations geophysically in the chimney above the reservoir that may be caused by the migration (Groth and Groth, 1994). Macroseeps and soil and botanical characteristics associated with the presence of hydrocarbons can be examined using remote-sensing methods (e.g. Berger et al., 2002; Matthews et al., 1984; Copper et al., 1998; Williams et al., 1995; Rock, 1984). Geochemical analyses of gases from soil and shallow sediments are commonly the most reliable indicator of vertical hydrocarbon migration. These include carbon isotopic composition, relative concentrations of light hydrocarbons, and identification of trace elements associated with hydrocarbon generation and migration (e.g. Abrams, 1996b; Brooks et al., 1986; Duchscherer, 1984; Horvitz, 1939, 1969, 1985; Klusman, 1993; Richers and Maxwell, 1991; Schiemer et al., 1985; Schumacher, 1999).

Several geophysical methods might also be applied to identifying indirect evidence of past hydrocarbon seepage and leakage potential of overlying CO_2 sequestration reservoirs. These include ground and airborne electrical methods that explore for enhanced conductivity

associated with reducing environments within the hydrocarbon chimney, induced polarization (IP) anomalies associated with sulfide precipitation, and shallow resistive horizons related to precipitation of carbonates in the oxidizing zone (e.g. Carlson and Zonge, 1996; Sternberg, 1991; Westphalen et al., 1995). Airborne radiometric surveys are intended to identify gamma lows over oil and gas fields caused by conversion of potassium-bearing clays to other potassium-deficient clays during the hydrocarbon-induced, near-surface diagenetic process (Curry, 1984; Schumacher, 1996). Perhaps most common are high-resolution aeromagnetic surveys intended to identify near-surface changes in magnetic susceptibility associated with diagenetic processes within the hydrocarbon alteration chimney (e.g. Campbell and Ritzma, 1979; Donovan et al., 1979; Donovan, 1988; Foote, 1996; Henry, 1989; LeSchack and van Alstine, 2002; Peirce et al., 1998).

Conclusion

The prospects for CO_2 storage of in geologic reservoirs can be enhanced by recognizing that light hydrocarbons can serve as a proxy for long-term migration behavior of CO_2. Methods developed to explore for the near-surface manifestation of deeper hydrocarbon accumulations can be used to determine whether there is evidence for hydrocarbon leakage through proposed sequestering strata that overlie hydrocarbon reservoirs. Permitting procedures in these settings might include a typical suite of relatively low cost near-surface hydrocarbon exploration methods (geochemical and geophysical) to help assess long-term seal integrity above proposed sequestration reservoirs.

APPENDIX C: Fault Data Matrix

Results of systematic fault length and density analysis are presented in Excel files and matrix form for each horizon before being processed for statistical study. **Table 18** shows an example of how fault length measurements were organized. Length values accompanied with the symbol greater than (">") denote faults whose lengths were bigger than those of the coverage of the 3D volume. An example of the horizontal distribution of faults along horizon4 in Gillock 3-D volumes is illustrated in **Table 19**

Table 18. Fault length for horizon 4 in Gillock 3-D volume

Fault Name	Length (ft)
F5	>7693
F7	4327
F8	4698
F9	6799
F10	5079
F11	2283
F12	>5939
F13	5807
F14	4487
F15	>4248

Note: 1 ft = 0.3048 m

Table 19. Measurements (ft) between faults for horizon 4 in Gillock 3-D volume

Trace	F8	F9	F10	F13
F5	2762			
F8		1164		
F9			1461	
F10				2243

Note: 1 ft = 0.3048 m

APPENDIX D: Scaling Analysis of the Spread of CO_2 through a Leak in a Homogeneous Geological Formation: (1) Theoretical Developments

1 Introduction

This study presents scaling estimates of extents of spread of CO_2, which result from a leak through a point source. The estimates, which are in the form of analytical expressions, are obtained from the governing equations for two-phase flow in porous media. This work also identifies dimensionless numbers that significantly influence the flow of CO_2 in geological formations and quantifies their influence on the extents of spread. The effect of domain inclination on the estimates is also investigated. Scaling analysis is performed for both two-dimensional (2D) and three-dimensional (3D) flows. Fluid flows that demonstrate negligible variations in the cross-flow direction can be approximated as 2D flows. Two-phase flows in geological formations with narrow width are likely to result in 2D flows. In addition, flow through a long fault or fissure that spans the width of the formation would be predominantly 2D.

This work ignores the effect of capillary pressure on the spread of CO_2. In addition, viscous and buoyancy-driven fingering phenomena, which can significantly influence the flow of CO_2, are not considered here. This article is organized as follows. The following section presents the governing equations for the two-phase flow of CO_2 and water in porous media. The next two sections present scaling analyses for 2D flows without and with inclinations. The following three sections present scaling analyses for 3D flows with no inclination, inclination in the flow direction only, and inclinations in both flow and cross-flow directions.

2 Two-Phase Fractional Flow Model

The two-phase flow of CO_2 in water is described by saturations S_g and S_w, and the velocities $v_g \equiv (v_x^g, v_y^g, v_z^g)$ and $v_w \equiv (v_x^w, v_y^w, v_z^w)$. The application of mass conservation for the two phases provides the following equations:

$$\phi \frac{\partial s_g}{\partial t} + \frac{\partial v_x^g}{\partial x} + \frac{\partial v_y^g}{\partial y} + \frac{\partial v_z^g}{\partial z} = 0 \tag{1}$$

$$\phi \frac{\partial s_w}{\partial t} + \frac{\partial v_x^w}{\partial x} + \frac{\partial v_y^w}{\partial y} + \frac{\partial v_z^w}{\partial z} = 0 \tag{2}$$

Here, φ represents the porosity of the medium. The saturations of the two phases are such that $S_g + S_w = 1$. The velocities of the two phases are given by Darcy's law:

$$V_g = -\frac{k_{rg}}{\mu_g} K \cdot \left(\nabla P_g + \rho_g g e_z\right) \tag{3}$$

$$V_w = -\frac{k_{rw}}{\mu_w} K \cdot \left(\nabla P_w + \rho_w g e_z\right) \tag{4}$$

The permeability K is a diagonal tensor, given by

$$K = \begin{pmatrix} K_x & 0 & 0 \\ 0 & K_y & 0 \\ 0 & 0 & K_z \end{pmatrix} \tag{5}$$

In the above equations, μ_g and μ_w are the viscosities of the two phases; K_x, K_y and K_z are the permeability of the medium in x, y and z directions, respectively; $k_{rg} \equiv k_{rg}\left(s_g\right)$ and $k_{rw} \equiv k_{rw}\left(s_w\right)$ are the relative permeabilities; and P_g and P_w are the pressures in the two phases. The difference in pressure between the two phases is defined as the capillary pressure:

$$P_c \equiv P_c\left(S_g\right) \equiv P_g - P_w \tag{6}$$

Water phase velocity v_w can be eliminated by introducing total velocity $v = v_g + v_w$. Gas phase velocity v_g can be expressed in terms of total velocity and gas saturation. For 3D flows through a domain whose inclination along x direction is θ_x and along y direction is θ_y, the components of gas phase velocity v_g are given by

$$v_x^g = \frac{1}{1 + \frac{\mu_g}{\mu_w}\frac{k_{rw}}{k_{rg}}}\left[v_x + K_x k_{rw}\frac{\left(\rho_w - \rho_g\right)g}{\mu_w}\sin\theta_x - K_x\frac{k_{rw}}{\mu_w}\frac{\partial P_c}{\partial x}\right] \tag{7}$$

$$v_y^g = \frac{1}{1 + \frac{\mu_g}{\mu_w}\frac{k_{rw}}{k_{rg}}}\left[v_y + K_y k_{rw}\frac{\left(\rho_w - \rho_g\right)g}{\mu_w}\sin\theta_y - K_y\frac{k_{rw}}{\mu_w}\frac{\partial P_c}{\partial y}\right] \tag{8}$$

$$v_z^g = \frac{1}{1 + \frac{\mu_g}{\mu_w}\frac{k_{rw}}{k_{rg}}}\left[v_z + K_z k_{rw}\frac{\left(\rho_w - \rho_g\right)g}{\mu_w}\left(1 + \tan^2\theta_x + \tan^2\theta_y\right)^{-1/2} - K_z\frac{k_{rw}}{\mu_w}\frac{\partial P_c}{\partial z}\right] \tag{9}$$

Relative permeabilities k_{rg} and k_{rw}, and capillary pressure P_c are known functions of gas saturation s_g.

3 Dimensionless Numbers

This section lists the dimensionless numbers that significantly influence the spread of CO_2 in a homogeneous porous media. The gravity number N_G is defined as the ratio of velocity of rise of CO_2 due to buoyancy effects to the velocity of spread due to convection, i.e.

$$N_G \equiv \frac{\text{Velocity of rise due to buoyancy}}{\text{Velocity of spread due to convection}}$$

$$N_G = k_{rw} \frac{(\rho_w - \rho_g)g}{\mu_w} K_z \frac{1}{u_0^c} \tag{10}$$

The scaling relationship for convection velocity u_0^c is derived for 2D and 3D flows in the following sections. Permeability ratios K_r^z and K_r^y are defined as follows:

$$K_r^y \equiv \frac{K_y}{K_x} \qquad K_r^z \equiv \frac{K_z}{K_x} \tag{11}$$

The viscosity ratio μ_r is defined as

$$\mu_r = \frac{\mu_g}{\mu_w} \tag{12}$$

4 Scaling analysis: 2D flows

Let the rate of flow of CO_2 from the leak be Q (m^3/s) and duration of leak be $t_l(s)$. Let the width of the geological formation (and that of flow) be B (m). If the two-phase flow of CO_2 in brine is dominated by convection, the gas-phase region would resemble a circle whose radius scales as

$$r_0^c \sim \left(\frac{Qt_l}{B}\right)^{1/2} \tag{13}$$

The convection velocity of CO_2 phase is then given by

$$u_0^c \sim \frac{r_0^c}{t_l} \sim \left(\frac{Q}{Bt_l}\right)^{1/2} \tag{14}$$

Let x_0 and z_0 denote the extent of spread of CO_2 in x and z directions, respectively. The conservation of volume of CO_2 requires that

$$\phi x_0 B z_0 \sim Q t_l \tag{15}$$

The gas-phase mass conservation equation (1) relates the scale factors for extents, velocity components, and time, i.e.:

$$\frac{\phi}{t_0} \sim \frac{v^g_{x,0}}{x_o} \sim \frac{v^g_{z,0}}{z_0} \tag{16}$$

Here, t_0 represents the estimate of time taken for the two-phase flow system to reach a steady state.

4.1 Domain without Inclination

Gas-phase velocity vg can be obtained from equations 7 through 9 by setting $\theta_x = \theta_y = 0$. These equations provide the scale factors for gas-phase velocity components. They are given by

$$v^g_{x,0} \sim \frac{1}{1+\mu_r \dfrac{k_{rw}}{k_{rg}}} \left(\frac{Q}{Bt_l} \right)^{1/2} \tag{17}$$

$$v^g_{z,0} \sim \frac{1}{1+\mu_r \dfrac{k_{rw}}{k_{rg}}} k_{rw} \frac{(\rho_w - \rho_g)g}{\mu_w} K_z \tag{18}$$

In deriving the scale factor $v^g_{x,0}$, the scale factor for total velocity is $v_x \sim u^c_0$. The set of equations 15 through 18 constitute five equations in five unknowns, x_0, y_0, t_0, $v^g_{x,0}$ and $v^g_{z,0}$. The estimates for the extent of spread of CO_2 are given by

$$x_0 \sim N_G^{-1/2} \phi^{-1/2} r_c \tag{19}$$

$$z_0 \sim N_G^{1/2} \phi^{-1/2} r_c \tag{20}$$

The aspect ratio of the spread of CO_2 is given by

$$a \equiv \frac{z_0}{x_0} \sim N_G \tag{21}$$

The estimate of time needed to reach steady state is

$$t_0 \sim \frac{1}{1+\mu_r \dfrac{k_{rw}}{k_{rg}}} N_G^{-1/2} \phi^{1/2} t_l \tag{22}$$

4.2 Domain with Inclination

The domain is inclined along flow direction at an angle θ_x to the horizontal. The scale factors for velocity for this case are given by

$$v_{x,0}^{g} \sim \frac{1}{1+\mu_r \dfrac{k_{rw}}{k_{rg}}} k_{rw} \frac{(\rho_w - \rho_g)g}{\mu_w} \sin\theta_x K_x \tag{23}$$

$$v_{z,0}^{g} \sim \frac{1}{1+\mu_r \dfrac{k_{rw}}{k_{rg}}} k_{rw} \frac{(\rho_w - \rho_g)g}{\mu_w} \sin\theta_x K_z \tag{24}$$

Estimates for the extent of spread of CO_2 can be obtained by solving the above equations in conjunction with equations 15 and 16. They are given by

$$x_0 \sim \left(K_r^z\right)^{-1/2} \phi^{-1/2} \left(\tan\theta_x\right)^{1/2} r_0^c \tag{25}$$

$$z_0 \sim \left(K_r^z\right)^{1/2} \phi^{-1/2} \left(\tan\theta_x\right)^{-1/2} r_c \tag{26}$$

The aspect ratio is given by

$$a \sim K_r^z \left(\tan\theta_x\right)^{-1} \tag{27}$$

The estimate for time is given by

$$t_0 \sim \frac{1}{1+\mu_r \dfrac{k_{rw}}{k_{rg}}} N_G^{-1} \left(K_r^z\right)^{1/2} \phi^{1/2} \left(\sin\theta_x \cos\theta_x\right)^{-1/2} t_l \tag{28}$$

5 Scaling Analysis: 3D Flows

Let x_0, y_0 and z_0 represent the estimates of the extent of spread of CO_2 through a leak in the three directions. Let $v_{x,0}^{g}, v_{y,0}^{g}, v_{z,0}^{g}$ represent the velocity estimates. The convection length and velocity scales are given by

$$r_0^c \sim \left(Q t_l\right)^{1/3}, \qquad u_0^c \sim \frac{r_0^c}{t_l} \sim \left(\frac{Q}{t_l^2}\right)^{1/3} \tag{29}$$

The conservation of volume of spread of CO_2 requires that

$$\phi x_0 y_0 z_0 \sim Q t_l \tag{30}$$

The mass conservation equation (1) relates the estimates of extents, velocity and time, i.e.

$$\frac{\phi}{t_0} \sim \frac{v_{x,0}^{g}}{x_0} \sim \frac{v_{y,0}^{g}}{y_0} \sim \frac{v_{z,0}^{g}}{z_0} \tag{31}$$

5.1 Domain without Inclination

Owing to the symmetry of flow in x and y directions,

$$x_0 \sim y_0, \qquad v_{x,0}^g \sim v_{y,0}^g \tag{32}$$

Estimates for gas-phase velocity can be obtained from equations 7 through 9. They are

$$v_{x,0}^g \sim v_{y,0}^g \sim \frac{1}{1+\mu_r \frac{k_{rw}}{k_{rg}}} \left(\frac{Q}{t_l^2}\right)^{1/3} \tag{33}$$

$$v_{z,0}^g \sim \frac{1}{1+\mu_r \frac{k_{rw}}{k_{rg}}} k_{rw} \frac{(\rho_w - \rho_g)}{\mu_w} K_z \tag{34}$$

The above equations in conjunction with equations 30 and 31 can be solved for the extents of spread of CO_2 and time:

$$x_0 \sim y_0 \sim N_G^{-1/3} \phi^{-1/3} r_0^c \tag{35}$$

$$z_0 \sim N_G^{2/3} \phi^{-1/3} r_0^c \tag{36}$$

The aspect ratio of spread of CO_2 scales as z_0

$$a = \frac{z_0}{x_0} \sim N_G \tag{37}$$

The estimate for the time needed for the system to reach steady state is given by

$$t_0 \sim \left(1+\mu_r \frac{k_{rw}}{k_{rg}}\right) N_G^{-1/3} \phi^{2/3} t_l \tag{38}$$

It should be noted that the two following derivations do not converge to this section's results when the inclination approaches zero because of the assumption that the inclination is the most relevant parameter.

5.2 Domain with Inclination along *x*-Direction Only

The domain is inclined along flow direction at an angle θ_x to the horizontal. The scale factors for velocity for this case are given by

$$v_{x,0}^g \sim \frac{1}{1+\mu_r \frac{k_{rw}}{k_{rg}}} k_{rw} \frac{(\rho_w - \rho_g)g}{\mu_w} \sin\theta_x K_x \tag{39}$$

$$v_{y,0}^g \sim \frac{1}{1+\mu_r \frac{k_{rw}}{k_{rg}}} \left(\frac{Q}{t_l^2}\right)^{1/3} \tag{40}$$

$$v_{z,0}^{g} \sim \frac{1}{1+\mu_r \dfrac{k_{rw}}{k_{rg}}} k_{rw} \frac{(\rho_w - \rho_g)g}{\mu_w} \cos\theta_x K_x \tag{41}$$

The above equations in conjunction with equations 30 and 31 can be solved for the extents of spread of CO_2 and time:

$$x_0 \sim N_G^{1/3} \left(K_r^z\right)^{-2/3} \phi^{-1/3} \left(\sin\theta_x \tan\theta_x\right)^{1/3} r_0^c \tag{42}$$

$$y_0 \sim N_G^{-2/3} \left(K_r^z\right)^{1/3} \phi^{-1/3} \left(\sin\theta_x \cos\theta_x\right)^{-1/3} r_0^c \tag{43}$$

$$z_0 \sim N_G^{1/3} \left(K_r^z\right)^{1/3} \phi^{-1/3} \left(\cos\theta_x \cot\theta_x\right)^{1/3} r_0^c \tag{44}$$

The aspect ratio of spread of CO_2 scales as

$$a_{xz} = \frac{z_0}{x_0} \sim K_r^z \cot\theta_x, \qquad a_{yz} = \frac{z_0}{y_0} \sim N_G \cos\theta_x \tag{45}$$

The estimate for the time needed for the system to reach steady state is given by

$$t_0 \sim \left(1+\mu_r \frac{k_{rw}}{k_{rg}}\right) N_G^{-2/3} \left(K_r^z\right)^{1/3} \phi^{2/3} \left(\sin\theta_x \cos\theta_x\right)^{-1/3} t_l \tag{46}$$

5.3 Domain with Inclinations in *x*- and *y*-Directions

The domain is inclined along *x*-direction at an angle of θ_x and along *y*-direction at an angle of θ_y to the horizontal. The scale factors for gas-phase velocity are

$$v_{x,0}^{g} \sim \frac{1}{1+\mu_r \dfrac{k_{rw}}{k_{rg}}} k_{rw} \frac{(\rho_w - \rho_g)g}{\mu_w} \sin\theta_x K_x \tag{47}$$

$$v_{y,0}^{g} \sim \frac{1}{1+\mu_r \dfrac{k_{rw}}{k_{rg}}} k_{rw} \frac{(\rho_w - \rho_g)g}{\mu_w} \sin\theta_y K_y \tag{48}$$

$$v_{z,0}^{g} \sim \frac{1}{1+\mu_r \dfrac{k_{rw}}{k_{rg}}} k_{rw} \frac{(\rho_w - \rho_g)g}{\mu_w} \left(1+\tan^2\theta_x + \tan^2\theta_y\right)^{-1/2} K_z \tag{49}$$

The above equations in conjunction with equations 30 and 31 can be solved for the extents of spread of CO_2 and time:

$$x_0 \sim \left(K_r^y\right)^{-1/3}\left(K_r^z\right)^{-1/3}\phi^{-1/3}\left(\frac{\sin^2\theta_x(1+\tan^2\theta_x+\tan^2\theta_y)^{1/2}}{\sin\theta_y}\right)^{1/3} r_0^c \tag{50}$$

$$y_0 \sim \left(K_r^y\right)^{2/3}\left(K_r^z\right)^{-1/3}\phi^{-1/3}\left(\frac{\sin^2\theta_y(1+\tan^2\theta_x+\tan^2\theta_y)^{1/2}}{\sin\theta_x}\right)^{1/3} r_0^c \tag{51}$$

$$z_0 \sim \left(K_r^y\right)^{-1/3}\left(K_r^z\right)^{2/3}\phi^{-1/3}\left(\frac{1}{\sin\theta_x\sin\theta_y(1+\tan^2\theta_x+\tan^2\theta_y)}\right)^{1/3} r_0^c \tag{52}$$

The aspect ratio of spread of CO_2 scales as

$$a_{xz} = \frac{z_0}{x_0} \sim K_r^z \frac{1}{\sin\theta_x(1+\tan^2\theta_x+\tan^2\theta_y)^{1/2}} \tag{53}$$

$$a_{yz} = \frac{z_0}{y_0} \sim \left(K_r^y\right)^{-1} K_r^z \frac{1}{\sin\theta_y(1+\tan^2\theta_x+\tan^2\theta_y)^{1/2}} \tag{54}$$

The estimate for the time needed for the system to reach steady state is given by

$$t_0 \sim \left(1+\mu_r\frac{k_{rw}}{k_{rg}}\right) N_G^{-1}\left(K_r^y\right)^{2/3}\left(K_r^z\right)^{-1/3}\phi^{2/3}\left(\frac{\left(1+\tan^2\theta_x+\tan^2\theta_y\right)^{1/2}}{\sin\theta_x\sin\theta_y}\right)^{1/3} t_l \tag{55}$$

6 Conclusions

In the absence of domain inclination, the aspect ratio of the spread of CO_2 scales as N_G in both 2D (Equation 21) and 3D (Equation 37) flows. Thus, in the absence of inclination, the aspect ratio is significantly influenced only by the ratio of buoyancy to convection velocity scales and not by any other factor such as average porosity or permeability of the geological formation. The extents of spread, however, are influenced by porosity φ.

In the case of domain with inclination in 2D flows (Section 4.2 of Appendix) and domain with inclinations in both x- and y-directions (Section 5.3 of Appemdix) in 3D flows, the aspect ratios are influenced by permeability ratios and not by gravity number. In the case of 3D flows with inclination in x-direction only (Section 5.2 of Appendix), the aspect ratio is influenced by the gravity number and permeability ratio. In all cases, the extent of spread of CO_2 is influenced by the average porosity of the domain. However, it has no impact on the aspect ratio in any case. The time scale needed for the two-phase flow system to reach steady state is influenced by N_G, φ and μ_r in all cases. It is influenced by permeability ratios in cases where the domain is

inclined. The viscosity ratio μ_r has an influence only on the time scale and not on extents of spread of CO_2 in all cases.

APPENDIX E: Scaling Analysis of the Spread of CO_2 through a Leak in a Homogeneous Geological Formation: (2) Applications

Some useful dimensionless numbers were developed in Appendix D. In Appendix E, the scaling parameters are estimated and calibrated by running multiple simulations. They were run on GEM (by CMG, http://www.cmgroup.com) with the standard CO_2 properties. Other parameters are given in **Table 20**: Side boundary conditions are producer wells that allow water and/or CO_2 to leave the system. The injection time of 100 days was chosen as representative of steady-state conditions. Aspect ratio and spread change very little for longer times.

Table 20. Input parameters for the base case of the scaling runs

Parameter	**Value**
# of grid cells	100
Size of each cell	0.6 m (2 ft)
Size of domain	81 m (200 ft)
Inclination	0
Depth of top of domain	2,250 m (5300 ft)
Permeability	100 md
Porosity	0.25
Solubility of CO_2 in brine	0
Capillary pressure	0
Maximum residual gas saturation	0
Injection rate	1,000 scf/day
Injection time	100 days
Simulation time	30 years
Max residual gas saturation	0.286

The bulk of the work was done assuming no capillary effect. As an example, we present here the results from a set of 2D simulations. The relevant dimensionless numbers identified in Appendix D are

- Gravity number N_G
- Permeability ratio $K_r = K_y/K_x$
- Viscosity ratio $\mu_r = \mu_g/\mu_w$. Viscosity is a function of temperature and pressure. Hence, μ_r cannot be varied in the numerical simulations.

The dimensionless gravity number, NG, is defined by Equation 10 in Appendix D as follows: $N_G = \left[k_{rw} \frac{(\rho_w - \rho_g)g}{\mu_w} \right] K_z \frac{1}{u_0^c}$.

The term in square brackets does not change significantly in the simulations, nor in real situations. Hence, in the calculations of the coefficients of scaling expressions for x_0, y_0 and z_0, N_G is calculated using the revised formula

$$N_G = K_z \frac{1}{u_0^c}$$

where K_z is in mD and u_0^c is in ft/day. Clearly the revised form of N_G is not dimensionless, but this approach is adopted in the literature. One advantage is that this approach yields $O(1)$ values for all coefficients. With the original definition, values would go to very small values or to very large values. Another advantage is that it is now simpler for a user to calculate N_G and obtain x_0, y_0 and z_0. Because u_0^c is in ft/day in the calculation of N_G, all lengths must be in feet, time in days, volume flow rate in ft^3/day and permeability in mD. In the simulations, the gravity number N_G is varied by varying flow rate, horizontal permeability, and cumulative volume.

Simulations 1, 2 and 3 (**Table 21** and **Figure 59**) show the effect of increasing flow rate or decreasing N_G (with everything else held constant). Decrease in N_G results in a decrease in the vertical rise of CO_2 and an increase in the horizontal spread of CO_2. Simulations 1, 4, and 5 show the effect of decreasing horizontal permeability or decreasing N_G. Decrease in N_G once again shows the same tendency to limit the vertical rise and increase the horizontal spread of CO_2. Simulations 2 and 4 have the same value for N_G. The saturation profiles obtained from these two simulations are comparable, especially the spread in the two cases. Similar observations can be found from simulations 3 and 5, which also have the same N_G value. Simulations 1, 6, and 7 show the effect of decreasing cumulative flow or decreasing N_G. Decrease in cumulative flow results in a decrease in both the vertical rise as well as the horizontal spread of CO_2. However, the decrease in the vertical rise is much more pronounced than that in the horizontal spread. In other words, the ratio of maximum horizontal spread to maximum vertical rise of CO_2 increases with decrease in N_G. This observation is consistent with

the earlier observations. Simulations 8, 9, and 10 show the effect of decreasing the permeability ratio (vertical permeability/horizontal permeability). As we would expect, decrease in permeability ratio decreases vertical rise and increases horizontal spread of CO_2. Scaling coefficients are given in **Table 22**.

Comparison of simulations 1 and 11 shows the limited impact of capillary pressure on the aspect ratio and spread of the CO_2 bubble. It should be noted that, if the source stops leaking, the ultimate saturation distribution is very different in the cases with or without capillary pressure.

Table 21. Input parameters for selected 2D simulations

Run#	Hor. K (mD)	Inj. Time (days)	Flow Rate (Mm^3/yr)	Cum. Flow (m^3)	N_G	Perm. Ratio Y/X	Total Time (yr)	Comments
Change flow rate with cumulative volume constant								
1	100	100	0.03	8,495	2.60E-05	1	30	
2	100	50	0.06	8,495	4.10E-04	1	30	
3	100	25	0.12	8,495	2.05E-04	1	30	
Change of permeability with flow rate and cumulative volume constant								
4	50	100	0.03	8,495	4.10E-04	1	30	Same N_G value as run #2
5	25	100	0.03	8,495	2.05E-04	1	30	Same N_G value as run #3
Change of cumulative volume alone								
6	100	50	0.03	4,248	5.17E-04	1	30	
7	100	25	0.03	2,124	3.25E-04	1	30	
Change of permeability ratio								
8	100	100	0.03	8,495	8.20E-04	0.5	60	
9	100	100	0.03	8,495	8.20E-04	0.25	120	
10	100	100	0.03	8,495	8.20E-04	0.1	300	
Addition of capillary pressure								
11	100	100	0.03	8,495	8.20E-04	1	30	Nonzero cap press, otherwise same as run #1

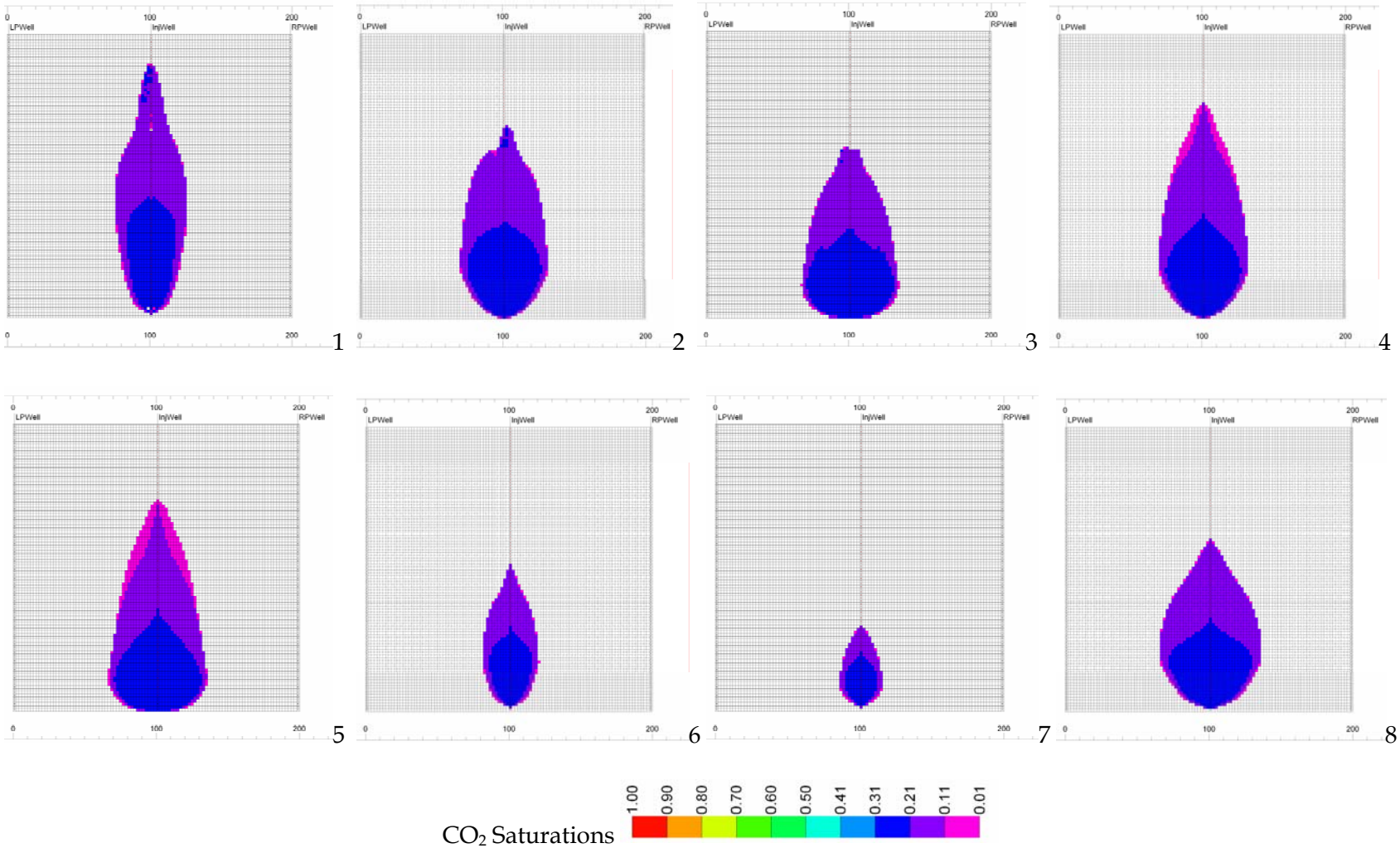
LPWell
InjWell
RPWell
0
100
200
1
2
3
4
5
6
7
8
CO_2 Saturations
1.00
0.90
0.80
0.70
0.60
0.50
0.41
0.31
0.21
0.11
0.01

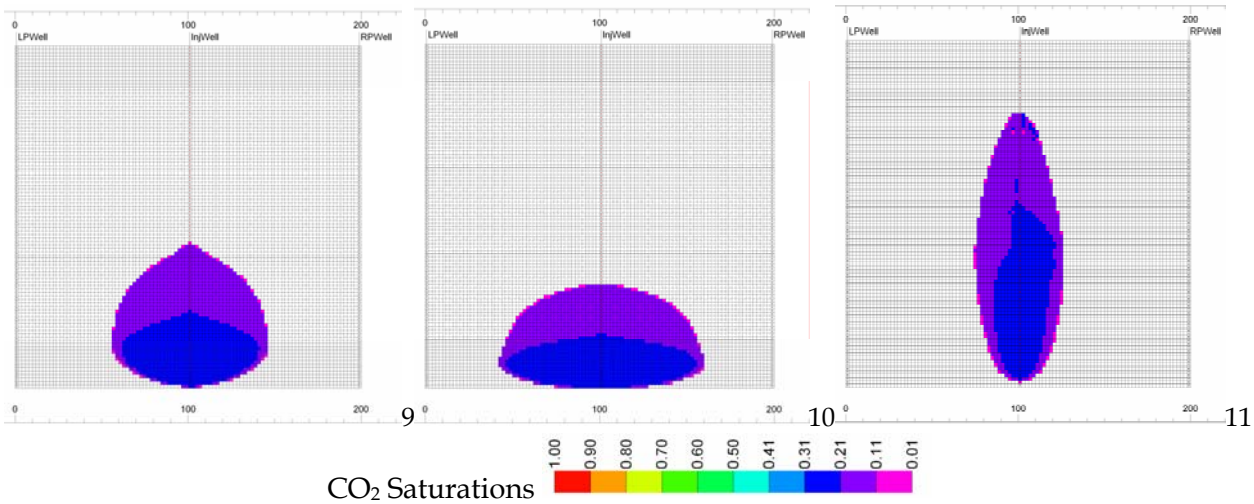

Note: Numbers correspond to the run # given in **Table 21**

Figure 59. Steady-state saturation distribution for selected 2D simulations

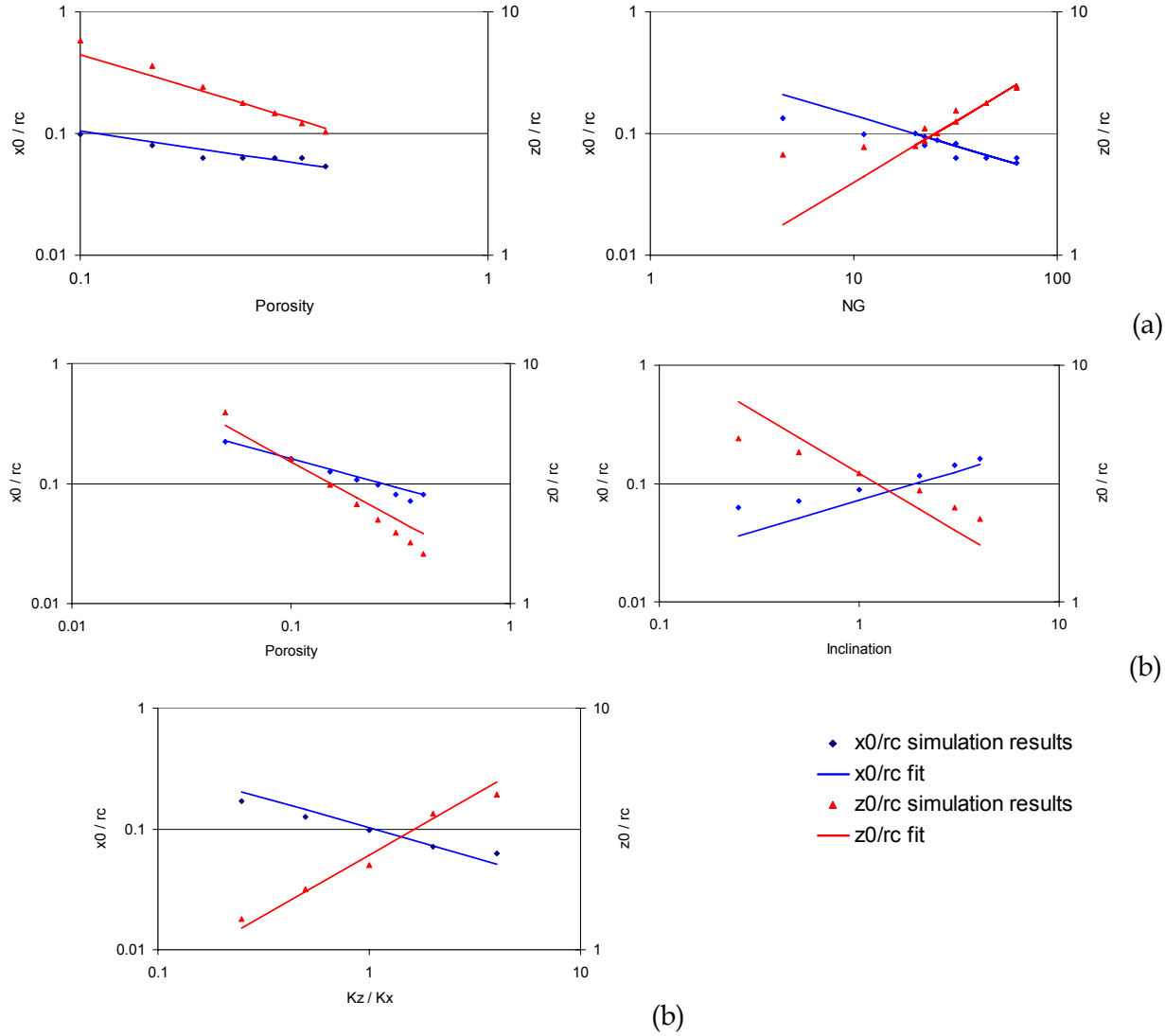

Figure 60. 2D simulation results with (a) no inclination and (b) inclination

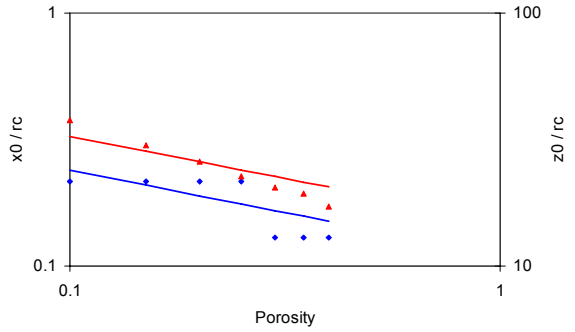
x0 / rc
z0 / rc
Porosity
1
0.1
100
10

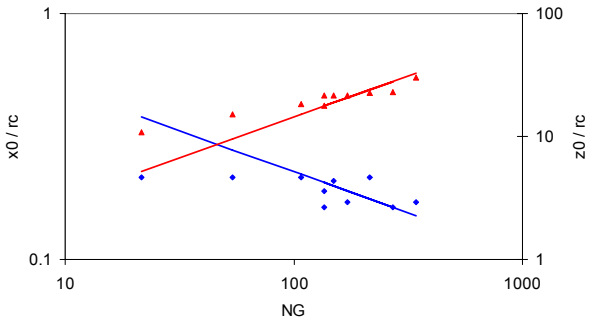
x0 / rc
z0 / rc
NG
10
100
1000

(a)

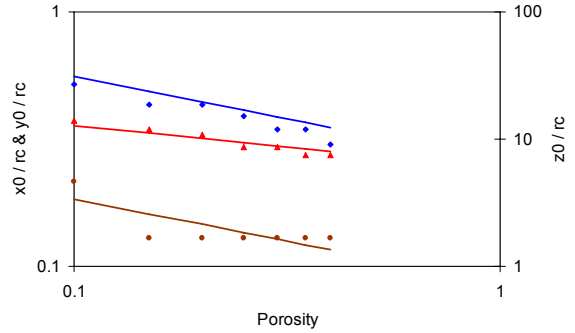
x0 / rc & y0 / rc
z0 / rc
Porosity

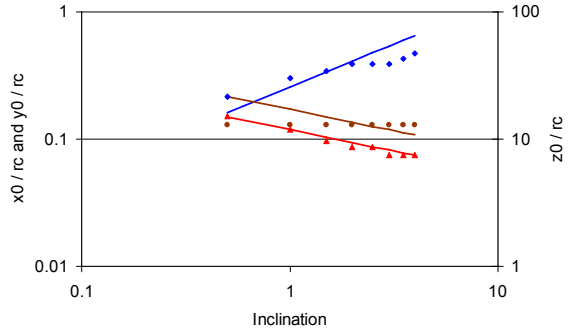
x0 / rc and y0 / rc
z0 / rc
Inclination

(b)

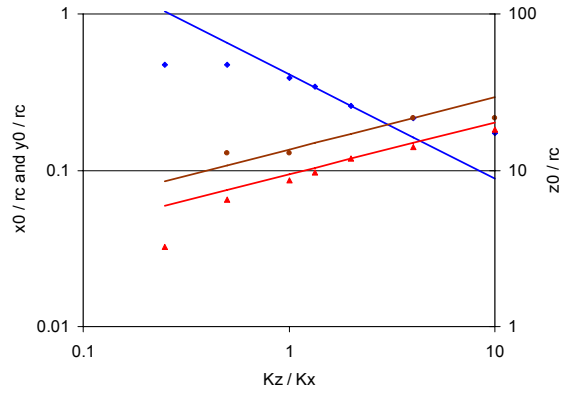
x0 / rc and y0 / rc
z0 / rc
Kz / Kx

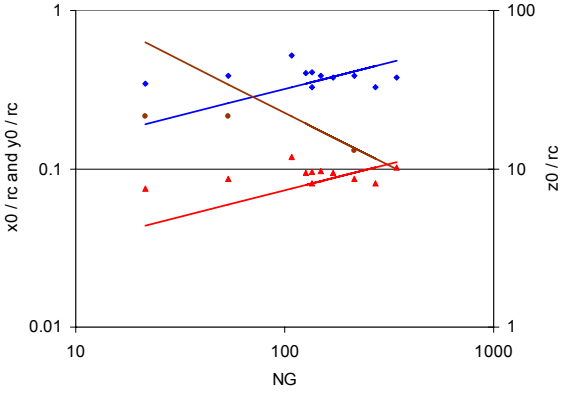
x0 / rc and y0 / rc
z0 / rc
NG

(b)

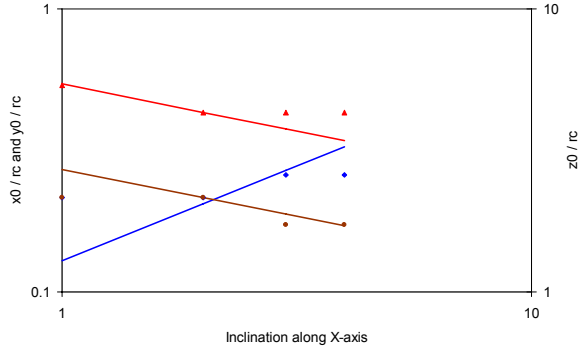
x0 / rc and y0 / rc
z0 / rc
Inclination along X-axis

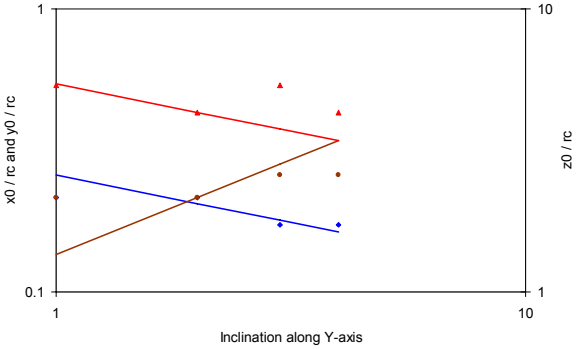
x0 / rc and y0 / rc
z0 / rc
Inclination along Y-axis

(c)

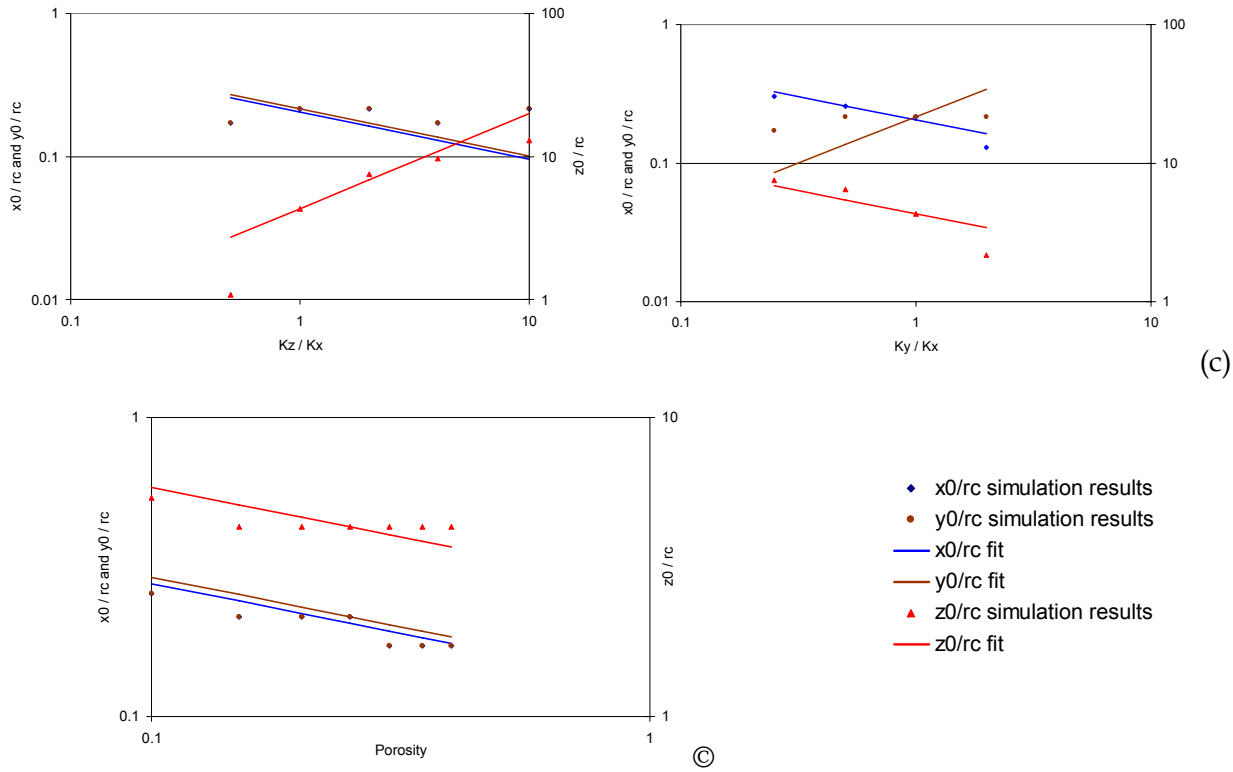

Figure 61. 3-D simulation results with (a) no inclination, (b) inclination along one axis, and (c) inclination along two axes

Table 22. Scaling coefficients

Equation Number	Variable Name	Value of Coefficient
2D Flow: No Inclination		
19	x_0	0.2220
20	z_0	0.3149
2D Flow: With Inclination		
25	x_0	0.2724
26	z_0	0.2304
3D Flow: No Inclination		
35	x_0 & y_0	0.6643
36	z_0	0.4209
3D Flow: Inclination along x-direction only		
42	x_0	0.4037
43	y_0	1.0039
44	z_0	0.3230
3D Flow: Inclinations along x- and y-directions		
50	x_0	0.3954
51	y_0	0.4151
52	z_0	0.2901

APPENDIX F: Integrated Numerical Models and STOMP-CO_2

An integrated numerical fate and transport model, using PNNL's STOMP-CO_2 code (White and Oostrom, 2004) as the basis, has been developed and used for modeling key issues related to a field-scale carbon sequestration project, which includes injectivity, seepage and leakage of CO_2, and risk and consequence assessment. Results from this work applied to monitoring sensor network design and permitting guidance are planned to be reported elsewhere. The hypothetical site used for this purpose was modeled after the typical injection field on the Mountaineer site, used as a test source of potential CO_2 leakage, and leaking CO_2 concentrations and fluxes were used as the key measures of risk and consequence to humans, animals, biota, property, agriculture, and water resources. Methods presented earlier for quantifying the leakage rates via different pathways into various media and the resulting CO_2 concentrations, consequences, and risks were used in this study. To enable the STOMP-CO_2 code to simulate the necessary scenarios, new computational modules were developed for simulating the fate and transport of leaking CO_2 through the vadose zone, abandoned and leaking wells, faults, and other higher permeability zones. Similarly atmospheric dispersion and aqueous dispersion modules for the CO_2 and risk and consequence assessment modules were added.

As explained earlier, modeling the flow and transport of CO_2 through fractured caprocks is an important part of the integrated modeling in support of permitting. To address the issue of leakage via modeling fractured caprocks and host zones containing faults, we have developed a fractured medium flow and transport modeling capability associated with the STOMP numerical model. We will present the algorithms and code implementation in STOMP to enable its use as a fractured media flow and transport model with triply porous, fractured medium properties. We first present the development of a fractured media flow and transport model, using a dual continuum modeling approach implemented in an existing porous media model, i.e. the STOMP reservoir model developed at PNNL. The governing equations for fluid and mass transport through the matrix and fractures will be derived according to the dual-continuum model of Gerke and van Genuchten. (1993). The equations are coupled by a transfer function that describes mass transfer between matrix blocks and the fracture. For the dual-continuum approach to be valid, the fractures should behave as a continuum of fracture networks. In other words, adequate connectivity of fractures for flow is assumed. The

connectivity of fractures in rock can be simulated using percolation theory (e.g., de Marsily 1985). Described below is the numerical formulation of the equivalent continuum and dual permeability models, which addresses the appropriateness of the fracture models through a series of simulations ranging from simple to complex.

Dual Continuum Governing Equations

The STOMP simulator has been designed to solve coupled conservations for component mass and energy that describe subsurface flow over multiple phases through variably saturated geologic media. The resulting flow fields are used to sequentially solve conservation equations for solute transport through the subsurface media. The STOMP simulator has capabilities of modeling subsurface flow and transport over three distinct phases: aqueous, gas, and NAPL. Each coupled flow equation combination, which does not comprise all of the possible governing equations, is referred to as an operational mode of STOMP (White and Oostrom, 2004). For example, a water-energy operational mode solves water mass and energy conservation equations. The present work focuses on aqueous flow and transport only, but it was developed on operational mode STOMP-WACS, a combination of water, air, CO_2, and NaCl, to easily extend to two-phase flow in the future.

The dual-porosity model implemented in STOMP follows Gerke and Van Genuchten (1993). Following STOMP's notation (White and Oostrom, 2004) and using water as an example, the governing equations for flow in the fracture continuum and matrix continuum can be written as equations 1 and 2, respectively. The governing equations for solute transport in the fracture continuum and matrix continuum can be written as equations 3 and 4, respectively. Symbols in the equations are explained in the STOMP User Guide.

Water Mass Conservation Equation in Matrix and Fractures:

$$\frac{\partial}{\partial t}\left[\sum_{\gamma=l,g} n_{Dm}\omega^w_{\gamma m}\rho_{\gamma m}s_{\gamma m}\right] = -\sum_{\gamma=l,g}\left(\nabla F^w_{\gamma m}+\nabla J^w_{\gamma m}\right)+\dot{m}^w_m+\frac{\Gamma^w_s}{1-w_f} \qquad (1)$$

$$\frac{\partial}{\partial t}\left[\sum_{\gamma=l,g} n_{Df}\omega^w_{\gamma f}\rho_{\gamma f}s_{\gamma f}\right] = -\sum_{\gamma=l,g}\left(\nabla F^w_{\gamma f}+\nabla J^w_{\gamma f}\right)+\dot{m}^w_f-\frac{\Gamma^w_s}{w_f} \qquad (2)$$

where $\Gamma^w_s = \sum_{\gamma=l,g}(1-d)\Gamma_\gamma n_{Df}\omega^w_{\gamma f}\rho_{\gamma f}s_{\gamma f}+d\Gamma_\gamma n_{Dm}\omega^w_{\gamma m}\rho_{\gamma m}s_{\gamma m}$

in which $\Gamma_\gamma = \alpha_\gamma\left(h_{\gamma f}-h_{\gamma m}\right)$ and $d = 0.5\left(1-\frac{\Gamma_\gamma}{|\Gamma_\gamma|}\right)$, *if* $\Gamma_\gamma \neq 0$

Mass conservation equations for air and its components are nearly identical in form to water, and they are not repeated here.

Solute Transport Equation in Matrix and Fractures

$$\frac{\partial C_m}{\partial t} = -\sum_{\gamma=l,g}\left(\nabla\left[C_{\gamma m}\mathbf{V}_{\gamma m}\right]\right) + \dot{m}_m^C - \dot{R}_m^C C_m + \sum_{\gamma=l,g}\left(\nabla\left[\left(\tau_{\gamma m} s_{\gamma m} n_{Dm} D_\gamma^C + s_{\gamma m} n_{Dm}\mathbf{D}_{h\gamma m}\right)\nabla C_{\gamma m}\right]\right) + \sum_{\gamma=l,g}\frac{\Gamma_s^{C_\gamma}}{n_{Dm} s_{\gamma m}\left(1-w_f\right)} \tag{3}$$

$$\frac{\partial C_f}{\partial t} = -\sum_{\gamma=l,g}\left(\nabla\left[C_{\gamma f}\mathbf{V}_{\gamma f}\right]\right) + \dot{m}_f^C - \dot{R}_f^C C_f + \sum_{\gamma=l,g}\left(\nabla\left[\left(\tau_{\gamma f} s_{\gamma f} n_{Df} D_\gamma^C + s_{\gamma f} n_{Df}\mathbf{D}_{h\gamma f}\right)\nabla C_{\gamma f}\right]\right) + \sum_{\gamma=l,g}\frac{\Gamma_s^{C_\gamma}}{n_{Df} s_{\gamma f}\left(1-w_f\right)} \tag{4}$$

where

$$\Gamma_s^{C\gamma} = \sum_{\gamma=l,g}(1-d)\Gamma_\gamma \phi_f C_{\gamma f} s_{\gamma f} + d\Gamma_\gamma \phi_m C_{\gamma m} s_{\gamma m} + \alpha_s\left(1-w_f\right) n_{Dm}\left(C_{\gamma f} s_{\gamma f} - C_{\gamma m} s_{\gamma m}\right)$$

$$\phi_f = w_f \frac{n_{Df}}{w_f n_{Df} s_{\gamma f} + \left(1-w_f\right) n_{Dm} s_{\gamma m}};\ \phi_m = \left(1-w_f\right)\frac{n_{Dm}}{w_f n_{Df} s_{\gamma f} + \left(1-w_f\right) n_{Dm} s_{\gamma m}}$$

Governing conservation equations are discretized to algebraic form following the integrated-finite-difference method in STOMP (White and Oostrom, 2004). Each computational cell is subdivided into an overlapped fracture and matrix block portion. The fracture portion can communicate with all other fracture volumes in the numerical grid. Likewise, the matrix portion can communicate with all other matrix volumes in the numerical grid. In addition, the matrix portion is allowed to communicate only with the fracture portion in the same computational cell. The system's nonlinear algebraic equations are nonlinear resulting from the constitutive functions. The Newton-Raphson technique is used to solve the coupled nonlinear system. We also developed separate algorithms to model effective properties of porous media containing discrete, multiple fractures in random orientations following Oda's approach (Oda, 1985). As a result, we can now take actual field fracture distribution data and simulate water flow through such fractured media in STOMP.

Solute mass conservation is discretized by assuming a piecewise profile for the solute concentration between node points and integrating over the node volume. The transport terms of the solute mass conservation equation are resolved with either the power-law scheme of Patankar (1980) or with the third-order scheme using Total Variation Diminishing (TVD)

criteria (Datta Gupta et al., 1996). For accuracy, transport equations for fractures and matrix are solved together.

The model was verified by assuming a zero mass transfer coefficient between the fractures and matrix blocks. Both regions gave the same result, given identical material properties and initial and boundary conditions. This capability needs to be extensively tested and validated using actual field data sets.

APPENDIX G: Leakage and Distribution Modeling

The methodology presented here consists of an assessment of (1) normal ranges of CO_2 concentrations in the environmental media of interest, (2) consequences of exceeding these normal CO_2 concentrations, (3) possible perturbations in CO_2 concentrations in each of the environmental media due to the occurrence of any of the hazards considered, and (4) risks, using the data from tasks 1 through 3 as a basis, in concert with the probability or frequency of occurrence of a given hazard.

G1 Integrated Fate and Transport Modeling, Risk and Consequence Assessment

G1.1 Normal ranges of CO_2 concentrations

The receptor media of interest are ground water, air, surface water (lakes, streams, and rivers), buildings, biota, and soils. Because CO_2 is colorless, odorless, relatively inactive, and nonflammable, it is difficult for humans or animals to sense its presence by sight, smell, or taste. The natural ranges of CO_2 concentrations in various media, reported in the hydrologic, atmospheric, agricultural, and limnologic literature, were collected and used as a basis to define the norm or background, in the absence of any hazard. In **Table 13** are the ranges of CO_2 concentrations in different environmental media, under normal environmental conditions.

G1.2 Abnormal events involving the leakage of CO_2

The Lake Nyos disaster in West-Central Africa and the Mammoth Mountain forest kills in California are two representative examples of the highly unusual, above-normal events of CO_2 release to soil-atmospheric and soil-water interfaces, respectively. Additional examples can be found in Benson (2005). The catastrophic release of CO_2 gas from Lake Nyos in 1986 was attributed to the continuous CO_2 efflux at the bottom of the lake, which caused deaths of more than 1,700 people and many animals in the area. The release was localized in the form of a fountain 120 m high, which formed a ground-hugging cloud that flowed down valleys and traveled as far as 25 km from the lake, at velocities fast enough to flatten vegetation, including a few trees (Farrar et al., 1995). Lake water pH was documented to vary from 7.6 at the surface to 5.6 at a depth of 90 m, where the CO_2 saturation was found to be maximum (150 mmol/L water). A potential danger of gas explosion is still high at the lake, and artificial degassing of the lakes is being performed to remedy the hazard.

Mammoth Mountain, a dormant volcano in the eastern Sierra Nevada, California, has been passively degassing large quantities (45 to 133 t/day) of cold magmatic CO_2 since 1990,

following a 6-month-long earthquake swarm. Maximum efflux of CO_2 was as high as 10,000 g/m^2·day, whereas the background biogenic soil CO_2 efflux ranged from 0 to 15 g/m^2·day (Farrar et al., 1995). Tree mortality observed at several locations on Mammoth Mountain was linked to the exposure of roots to toxic concentrations of CO_2 gas, which was controlled by faults and/or fractures that serve as conduits of enhanced permeability for gas escaping from a magmatic CO_2 reservoir at a depth of 2 to 4 km, depths comparable to a geological sequestration reservoir. CO_2 concentrations lethal to animals (15–90% by volume) were found to be common in the shallow soil and snow pack within the tree-kill areas. Dead rodents and birds were found in such areas, and in May 1998 a cross-country skier at HSL died after falling into a depression in the snow containing 70% CO_2, due to CO_2 toxicity. The Mammoth Mountain CO_2 efflux serves as an important example of the potential pathways, magnitude, duration, and consequences of leakage from a geological reservoir serving as a CO_2 storage sink.

Both the Lake Nyos and Mammoth Mountain events reveal that the leakage of CO_2 is a potentially significant contributor to a variety of hazards, which could compromise safety, environmental quality, and the objectives of sequestration (reduction of atmospheric CO_2 concentration). A severe, albeit unlikely, cause of major leakage is a sudden, acute release of stored CO_2 due to well-cap failure. Modeling studies (Lindeberg, 1997; Saripalli and McGrail, 2002) indicate that the ability of CO_2 to leak is a strong function of the hydrogeologic characteristics of the caprock and the ultimate distribution of the free-phase CO_2 bubble in the formation.

G2 Leakage and Distribution Modeling

Important pathways for leakage of CO_2 include (1) vertical migration through fractures in the caprock, (2) buoyancy-driven flow through permeable zones of caprock, (3) leakage of CO_2 through the well bore (blowout), (4) escape through the well casing to thief zones in the overburden and subsequent bubbling to the surface, and (5) diffusion as a dissolved phase through water saturated caprock. Physical processes that influence leakage, such as phase change, buoyant floating, advection, and dispersion, are strongly dependent upon CO_2 phase pressure. Chemical processes that influence leakage, such as diffusion, dissolution, exsolution, and precipitation, are strong functions of CO_2 concentration. Because these processes usually operate together, it is necessary to model their performance in a coupled manner. Analytical

methods model the physico-chemical behavior subject to simplifying assumptions, such as uniform host domain characteristics and uniform or uniformly varying pressure and concentration fields, etc., many of which are not strictly valid in geological formations because of their heterogeneous structure. However, analytical solutions have been found to provide excellent fundamental insights into system behavior, which often adequately model the measured behavior. Stochastic numerical models are capable of more accurately the heterogeneous flow and concentration fields and variability in the various processes of interest.

In the following sections, semianalytical approaches (Saripalli and McGrail, 2002) are used to model the leakage of CO_2 from a typical host formation and its distribution in the various environmental media surrounding the sequestration field. The objective of such modeling is to identify and preliminarily assess key phenomena that mediate the leakage of CO_2 and the CO_2 fluxes and concentrations in each of the environmental media, which serve as necessary inputs to consequence and risk assessment calculations. Accordingly, a fully screened, perforated injection well in a sequestration field injecting CO_2 into a 160-m-thick sandstone formation bounded by impermeable layers at the top and bottom is considered to be the base case for this analysis, following our earlier work. The injection and formation parameters for the base case, represent a typical gas injection operation similar to the base case simulation of Lindeberg (1997). **Figure 62** shows the distribution of injected CO_2 saturation at 10,000 days after the commencement of injection, representing the initial condition for the following analysis.

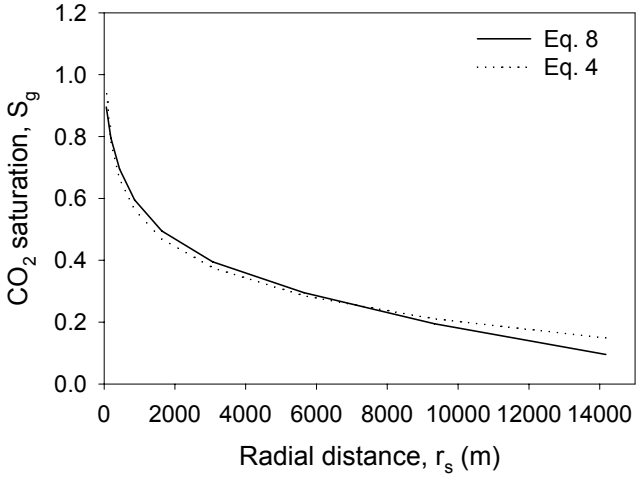

Figure 62. CO_2 saturation distribution after 10,000 days of injection as predicted by Buckley-Leverett theory (Eq. 4) and an empirical model fit (Eq. 8), using m = -0.148 and n = 1.5634 (R^2 = 0.983)

G2.1 Dissipation of Free-phase CO_2 bubble

The CO_2 bubble growing during injection simultaneously dissolves in the formation waters and floats toward the top confining layers owing to buoyancy. In **Figure 63** are results from a set of simulations in which CO_2 was injected for a period of 10,000 days and then allowed to dissolve and float. The curves represent the immiscible CO_2–water contact in formations of different porosities, after buoyant floating and equilibrium dissolution. The region above this contact is rich in free-phase CO_2 and could serve as a source of leakage. It has a large area of contact with the flowing ground-water phase and is likely to progressively dissolve in ground water. Under moderate ground-water velocities (10 m/day), assuming that the dissolution of CO_2 in water is rapid without significant rate limitations, the following analysis can be used to estimate the time taken to completely dissolve and dissipate the free-phase CO_2 bubble. To simplify the analysis, the free-phase bubble can be reasonably approximated to be an inverted cone of radius equal to the maximum radius of review of the bubble R_b, and height equal to $h_{b,max}$, at the injection well. Instantaneous dissolution at a solubility (C_w) of 6% by volume in water within a cylindrical ground-water column of radius R_b and height $h_{b,max}$, which contains the free-phase CO_2 bubble is assumed. Ground water in this volume will dissolve a fraction of the free-phase CO_2 and carry it away when its water volume 'turns over' in one residence time (T_r), which is given by $2R_b/v$, where v is flowing ground-water velocity. Volume of water (V_s) in contact with the cone surface in an imaginary cylindrical volume of radius R_b and height $h_{b,max}$ is given as:

$$V_s = \frac{2}{3}\pi R_b^2 h_{b,\max} \qquad (1)$$

Volume of free-phase CO_2 dissolved and carried away in time T_r is given as $C_w V_s$. Time required to completely dissolve away the free-phase bubble (T_d) is then equal to

$$T_d = \frac{\pi R_b^2 h_{b,\max}}{3C_w V_s} T_r \qquad (2)$$

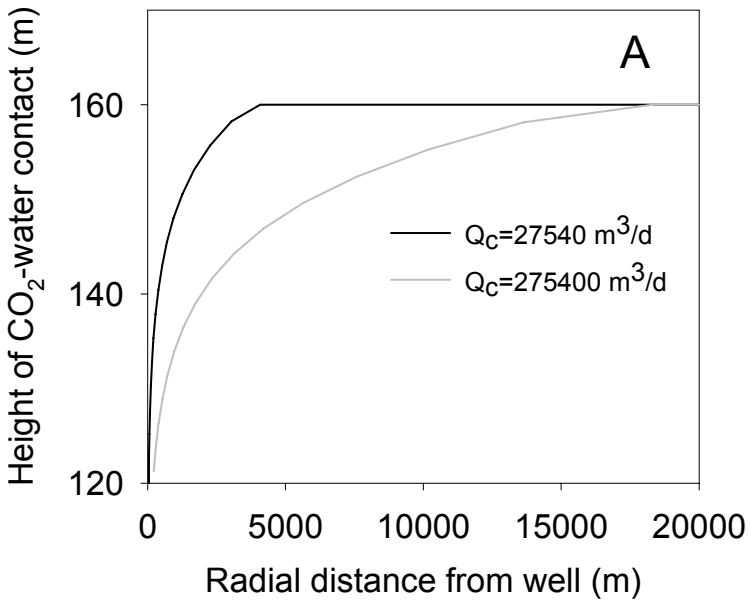

Figure 63. Distribution of free-phase CO_2 bubble after 10,000 days of injection at two different injection rates

For the example case, assuming a conical bubble of maximum bubble height of 40 m near the injection well, and maximum bubble radius of 17,000 m in contact with a ground water of velocity 10 m/day, residence time of the cylindrical water element (T_r) is 3,400 days. Thus, at a rate of dissolution of 4.27×10^5 m^3 of CO_2 in 9.3 years, it will require about 78 years to completely dissolve and dissipate the originally present free-phase CO_2 bubble. It should be noted that bubble volume and height are not constant during this long period of dissolution, as assumed in this analysis, but progressively decrease owing to dissolution itself. A more accurate estimation of T_d requires that we take into account such time-dependent changes in the bubble dimensions. However, the above analysis serves to emphasize the point that the free-phase volume and pressure, which critically govern the leakage rates and the resulting risks, dissipate with time, thus causing a corresponding lowering of leakage and risk.

G2.2 Migration through Fractures in the Caprock

Migration of CO_2 through fractured caprocks and through leaky, abandoned wells represents the two significant sources of risk at sequestration sites. Recent research (e.g., Celia et al, 2006) that focused on leaky abandoned wells demonstrates methods to model the latter source. As a part of the present project, we also have developed a numerical modeling module for simulating the transport of CO_2 through leaky caprocks, which is presented in later sections of this report. For free-phase CO_2 to enter a pore or fracture of size $2d$, the capillary pressure (P_c)

needs to be $\geq 2\sigma/d$, where σ is the CO_2-brine interfacial tension. The vertical buoyant pressure exerted on the top confining layer by the CO_2 bubble floating at the top is

$$P_b = \Delta\rho g h_b \tag{3}$$

where $\Delta\rho$ is the density difference between the brine and CO_2 and h_b is the thickness of the CO_2 bubble floating near the top confined layer. For CO_2 to enter the caprock through the fracture, P_b must exceed P_c, thus satisfying the following condition:

$$h_b \geq \frac{2\sigma}{\Delta\rho g d} \tag{4}$$

Rate of flow of free-phase CO_2 through a vertical fracture of aperture $2d$, length l_f and width w is given as

$$q_f = \frac{\Delta\rho g w d^3}{12\mu}\left(\frac{dH_c}{dz}\right) \tag{5}$$

where H_c is the CO_2 head causing flow along the vertical direction (z). In the case of a continuous fracture connecting the confined formation to the ground surface, the gradient term in Eq. 5 is equal to $h_c/(h_c+l_f)$.

Assuming a density difference of 400 kg/m^3 between brine and supercritical CO_2 and a bubble thickness h_b m, the buoyant pressure exerted on the caprock will be $3924h_b$ Pa. Assuming a CO_2-brine interfacial tension of 35 mN/m, an entry pressure of $0.07/d$ Pa is required for the CO_2 to break into the water-saturated caprock. Thus, for CO_2 to enter the caprock through a fracture of aperture size of 2 microns, minimum floating-bubble thickness (h_b) should be 17.8 m. Because the floating bubble thickness is 20 m or larger near the injection well for the base case simulation, if fractures or crevices of width of at least 2 microns are available in the caprock's structure, a CO_2 bubble thickness of 17.8 m would be sufficient to cause leakage. The leakage rates (m^3 per year), expressed as a percentage of the total volume of CO_2 injected during the 10,000-day injection of the base case, are calculated using Eq. 5 for a fracture 10 m wide and half-aperture ranging from 1 to 3,000 microns. The fracture is assumed to be in contact with the free-phase CO_2 bubble, 20 m thick on one end and passing through an overburden 300 m thick to the atmosphere. In this case, it is estimated that a continuous fracture with an aperture size of 2000 microns is sufficient to cause leakage on the order of 0.1% of the total volume stored per year.

G2.3 Buoyant Flow through a Permeable Caprock

In the case of a caprock with zones of significant permeability, the free phase CO_2 in contact with the permeable zone will migrate upward owing to buoyant floating. Such migration is governed by Darcy's law, and the resulting CO_2 flux (q_b) is given as

$$q_b = -\frac{k\Delta\rho g}{\mu}\left(\frac{dH_c}{dZ}\right) \tag{6}$$

with notation similar to that used in Eq. 5. Assuming that a strong, positively buoyant gradient for upward migration of CO_2 is present within a radial distance of 100 m around the injection well, where such gradient is the strongest, leakage rates (m^3 CO_2 leaked per year) were calculated as a function of the permeability of the radial leaking zone, ranging from 1 md to 6 D. Results indicate that significant leakage rates are possible when the permeability of the overburden is greater than 1 D, which corresponds to fine sands. In such rare cases, about 0.05% of the total volume of CO_2 stored can be lost via leakage through a permeable caprock.

G2.4 Leakage through the Well Bore and Casing

Failure of the well cap could lead to an acute release of a large volume of CO_2 gas into the atmosphere, depending on the flowing pressure gradient in the well, which in turn depends on the CO_2 phase pressure distribution in the reservoir that is in contact with the well casing. Katz and Lee (1990) derived the following equation for modeling the rate of flow out of gas wells:

$$P_s^2 - e^s P_w^2 = 6.67x10^{-4}\,\frac{(QT_aZ_a)^2(e^s-1)f}{d^5}$$
$$s = \frac{0.0375Gh}{T_aZ_a} \tag{7}$$

where P_s (psia) is the flowing CO_2-phae pressure in contact with the well face, P_w (psia) is the flowing wellhead pressure, Q (Mcf/day) is the leakage flow rate of CO_2, d (in.) the inside diameter of the well bore, T_a (^{o}R) is the average reservoir temperature, f is the Moody friction factor, Z_a is the average compressibility factor at mean temperature and pressure, G is gas gravity, and h (ft) is the depth of the well. Escape of CO_2 owing to a minor well leak can also be modeled using Eq. 7, approximating the leak to be of a small, circular cross section. The Moody friction factor f is given for small and large leaks as

$$f = \frac{m}{d^n} \tag{8}$$

where m =0.0175 and n = 0.224 for small leaks (d < 4.277 in), and m = 0.01603 and n = 0.164 for large leaks (d > 4.277 in).

Using the CO_2 phase pressure data corresponding to the example case, we estimate that a complete blowout of a 12-inch-diameter well in the first few years after completion of injection will cause a leakage of 8.36×10^6 m^3 of CO_2/day to the atmosphere. In case of a partial leak of 1-inch diameter, the leakage rate will be ~16,760 m^3 of CO_2/day. Because the leakage rate increases exponentially with leak size, it is important to contain the size of the leak in the case of an acute release, to minimize impacts.

G2.5 Atmospheric Dispersion Modeling

CO_2 leaking into the atmosphere is likely to spread and disperse into the atmosphere. If the release of CO_2 is close to the ground, the released CO_2 is known to form a ground-hugging cloud and settle near the ground surface and, hence, should be modeled as a dense gas dispersion phenomenon. Recent findings (Mohan et al., 1995; Hanna and Chang, 2001) reveal that released dense gas initially tends to settle near the point of release toward the ground surface owing to gravity effects. However, after a critical time T_c, which depends on the prevailing wind velocity and the density difference between the gas and air phases, the released dense gas may be sufficiently disperse to obey Gaussian dispersion models. Mohan et al. (1995) provided the following criteria for transition of a negatively buoyant dense gas plume to become passive, assuming that the initial gas plume is approximately cylindrical in shape. These are, respectively, conditions on the growth of the radius of the plume, height of the plume, and the density difference between gases. In the case of gas-plume radius (R), the velocity due to mechanical turbulence U_* has to be equal to or greater than the rate of radial spread of the plume dR/dt, as below:

$$\overline{C}\overline{U} = \left[\frac{\Delta\rho g h}{\rho_a}\right]^{1/2} \tag{9}$$

where $\overline{C}$ is a surface drag constant that depends on the weather category, $\overline{U}$ is the average wind speed, U_* is equal to $\overline{C}\overline{U}$, h is the initial height of the cylindrical gas plume, ρ_a is air density, and $\Delta\rho$ is the density difference between the released CO_2 and air. The condition for dispersal is that air entrainment velocity U_e should be equal to longitudinal turbulence velocity U_l, taken as $3U_*$. Air entrainment velocity is

$$U_* = \alpha' U_l R_i^{-1} \tag{10}$$

where α' is an entrainment constant, l_s is the turbulence length scale ($l_s = 5.88h^{0.48}$), and the Richardson number R_i is given by

$$R_i = \frac{g l_s \Delta\rho}{\rho_a U_l^2} \tag{11}$$

Both of the above conditions should be satisfied before the released CO_2 plume will transition from being negatively buoyant to passive.

Inspection of Eq. 9 reveals that cylindrical plume height h is a critical parameter in determining whether a given volume of CO_2 will transition from initial 'ground-hugging' status to a passive state, more amenable to turbulent dispersion. For typical stack gases, plume height or rise is given by Holland's formula:

$$h = \frac{v_s d}{\bar{U}}\left[1.5 + \frac{0.0268 P d (T_s - T_a)}{T_s}\right] \tag{12}$$

where v_s is the stack velocity (m/s), d is the stack diameter (m), P is atmospheric pressure, and T_s and T_a refer to the temperature of the stack and air phases, respectively. A significant difference between sequestered CO_2 leaking out of a well and typical stack gases is that the well temperature (T_s) for CO_2 is considerably lower than T_a. As such, initial height of the CO_2 plume (h) is likely to be small because the temperature gradient (Eq. 12) necessary for the development of a tall CO_2 plume is absent. Further, CO_2 being a dense gas, the negative buoyancy also will act to cause the CO_2 cloud to settle closer to the ground, in a ground-hugging fashion. Experiments and observations involving the release of CO_2 near ground surface corroborate this view.

The Kit Fox field experiment (Hanna and Chang, 2001) offers valuable insights into how a ground-level release of CO_2 is likely to spread in the air environment. The field data set consists of 52 trials in which short-duration CO_2 gas releases (44 to 176×10^3 m^3/day) were made at ground level over a rough surface during neutral to stable conditions, comparable to an accidental release volume from geological sequestration operations. On the basis of downwind CO_2 concentration data, plume height was found to range between 3 and 6.5 m, in a distance of 100 m around the source, and larger at higher wind speeds.

Eq. 9 through 12 can be used to estimate the average wind speed necessary to cause the transition of a CO_2 cloud of given height from the negatively buoyant state to a passive state. For example, an average cloud height of 3 m requires a wind velocity of 80 miles/hour before such transition can occur. Such high wind speeds are unlikely at typical sequestration sites. In

summary, it appears that, if large volumes of CO_2 are released closer to the ground surface in an accidental release during sequestration, the dense CO_2 plume will be only a few meters tall and will spread laterally around the release source. Such a cloud will remain negatively buoyant (ground-hugging) for a long time before it can transition to a passive state and disperse in the atmosphere owing to turbulent air entrainment. In the case of a complete well blowout and CO_2 release over a day under the test case scenario, where the CO_2 leakage rate out of the well is estimated to be about 8.36×10^6 m^3/day, the released volume is likely to spread over a land area of 2.8 square kilometers (assuming a cloud height of 3 m). The consequences in this area will be lethal because the concentration of CO_2 in air will be much larger than the lethal level of 20%. Assuming a subsequent dispersion of the CO_2 cloud, an aerial extent five times larger (11.6 km^2) will be similarly affected before the consequences will transition to sublethal levels. In summary, leakage of even moderate amounts of CO_2 is likely to have dire consequences and should be monitored and avoided.

G2.6 Aqueous Dispersion Modeling

Dissolution of CO_2 in ground-water results in the formation of aqueous species H_2CO_3, HCO_3^- and CO_3^{2-} and can cause changes in the acidity of ground water. PCO_2 measurements in soils were shown to be up to 500 times larger than the atmospheric level of $10^{-3.5}$ bar. Consequences of increasing PCO_2 in natural waters can be assessed using pH as the master variable. Such increases in PCO_2 cause a corresponding reduction in pH of the ground water, by 0.7 pH units for every log unit of PCO_2 increase (Palmer and Cherry, 1984). Sposito (1989) provided the following equation for the estimation of changes in pH of water as a function of PCO_2 and the bicarbonate ion concentration [HCO_3^-].

$$pH = 7.8 + \log[HCO_3^-] - \log[PCO_2] \qquad (13)$$

An accurate calculation of the changes in pH requires calculation of changes in the bicarbonate ion concentration, which depends on the type of minerals in contact with ground water and the geochemical reactions influencing the system, such as mineral precipitation and dissolution. The leaking CO_2 into the overlying aquifers is likely to cause an increase in the PCO_2 of the ground water and in the unsaturated soil-air phase. In case of pure CO_2 replacing the soil-air phase of an initial PCO_2 of 10^{-2} bar, the resulting PCO_2 would be 1 bar. Depending on the [HCO_3^-] concentration, this increase in PCO_2 could cause a reduction in pH by several logarithmic units. Assuming a typical concentration of 0.003 mol/L for the aquifer media, the

effect of increasing PCO_2 due to the leakage of CO_2 on the pH of aqueous phase is plotted in **Figure 64**. It can be seen that the leakage of CO_2 can lead to a significant reduction in pH value. At a given site of sequestration, the actual geochemical response of the aquifer can be modeled using geochemical equilibrium codes (e.g., EQ3/6) and reactive transport codes.

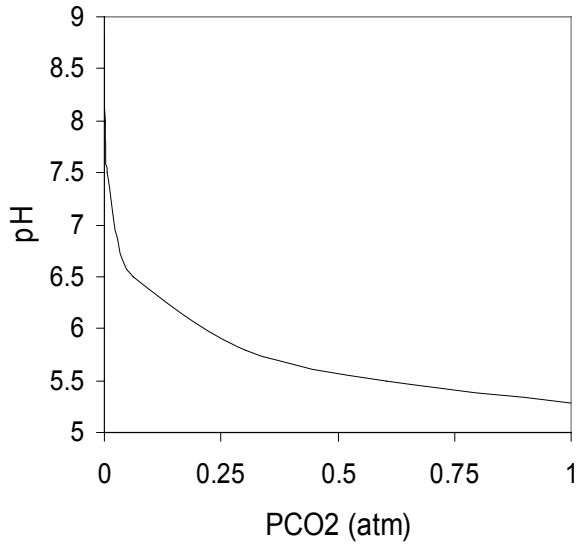

Figure 64. Variation in aqueous pH as a function of CO_2 partial pressure

G2.7 Mixing in Rivers and Lakes

The leaking CO_2 may find its way to surface water bodies, such as lakes, streams, and rivers, if the volume of the leak is sufficient to rise through the subsurface overburden, after a part of it is lost to dissolution in ground water. Alternatively, significant influx of CO_2 to the surface waters is also possible through normal ground-water inflow channels, when such inflows are saturated with CO_2 owing to prior contact in the aquifer (Freeze and Cherry, 1979). The Lake Nyos disaster discussed earlier is an example of such influx. Two important consequences of such mixing of CO_2 from a subsurface source into the surface waters are: (1) a buoyant expulsion and release of CO_2 gas to the atmosphere and (2) a mixing and transport of the CO_2 in the surface waters by dissolution, advection, and dispersion. Advection dominates the transport of dissolved CO_2 in streams and rivers under turbulent flow conditions, whereas dispersion and diffusion are predominant in lakes. The mixing equation (Rutherford, 1994) used to describe the mixing and transport processes in surface waters is

$$\frac{\partial C}{\partial t} + u_x \frac{\partial C}{\partial x} + u_y \frac{\partial C}{\partial y} + u_z \frac{\partial C}{\partial z} = \frac{\partial}{\partial x}\left(e_x \frac{\partial C}{\partial x}\right) + \frac{\partial}{\partial y}\left(e_y \frac{\partial C}{\partial y}\right) + \frac{\partial}{\partial z}\left(e_z \frac{\partial C}{\partial z}\right) \qquad (14)$$

where C is the concentration of dissolved phase CO_2 in water; x, ,y and z are, respectively, the river flow axis and vertical and transverse axes of its cross section, u_i; e_i represents, respectively, velocity of flow and eddy diffusivity along i direction; and t is time. Considering the dissolved fraction of the CO_2 coming in contact with the surface water to be a steady point source, and assuming that the river has an unbounded, rectangular channel section, with flow primarily along x direction ($u_y = u_z = 0$), in the case of constant diffusivities, Eq. 14 simplifies to

$$u_x \frac{\partial C}{\partial x} = e_y \frac{\partial^2 C}{\partial y^2} + e_z \frac{\partial^2 C}{\partial z^2} \tag{15}$$

with the following solution:

$$C(x,y,z) = m \frac{\exp\left(-\frac{u_x (y-y_o)^2}{4e_y x}\right)}{\sqrt{4\pi e_y x}} \frac{\exp\left(-\frac{u_x (z-z_o)^2}{4e_z x}\right)}{\sqrt{4\pi e_z x}}$$

Aqueous concentration contours can be developed as a function of CO_2 leakage rate using Eq. 16 to assess the consequences to water quality and biota. **Figure 65** shows CO_2 concentration profiles in a river around a steady point source of dissolved CO_2.

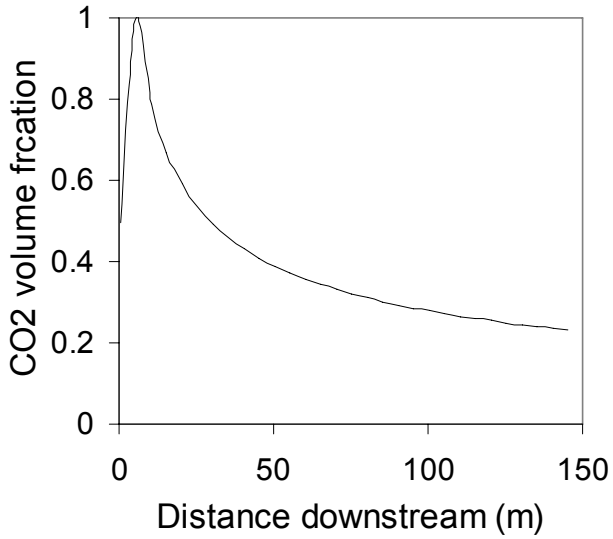

Figure 65. Distribution of CO_2 released into a river

If the volumetric flow rate of the gaseous leak into a lake is q_r, the total volume of CO_2 influx into the lake or river, V_r, in a given time, t, is equal to tq_r. Out of this, a volume V_d is dissolved into a cylindrical zone of water around the point source, which is equal to $2C_w\pi r^2 d$, where d is the depth of the lake and r is the radius of the zone of dissolution, which can be estimated using Eq. 16 above. The volume released to the atmosphere can then be calculated as

the difference $V_r - V_d$. However, low volumetric rates of a typical leak may not be sufficient to saturate the capacity of large volumes of water in lakes and rivers for CO_2 dissolution and lead to a direct atmospheric effusion. In stead, the CO_2 leaking from the subsurface into water bodies may be more likely to accumulate first as a dissolved phase, as the Lake Nyos experience suggests. It should also be noted here that the leaking CO_2 will first partition significantly into the ground water and soil-air phases of the overburden (formation), which lie between surface water bodies receiving the leakage and host formation layers used for sequestration. Such partitioning of CO_2 into the overburden is discussed below.

G2.8 Distribution in Soil and Overburden

Even under normal conditions, soil CO_2 concentrations are much larger in the soil gas than in the atmosphere. PCO_2 measurements in soils were shown to be up to 500 times larger than the atmospheric level of $10^{-3.5}$ bar. A fraction of the CO_2 leaking through the caprock will partition into the ground water and soil within the saturated (aquifer) and unsaturated zones of the overburden. Further, the soil-air volume available in the unsaturated zone of the overburden has to be saturated with the gaseous CO_2, before the excess CO_2 finds its way to the soil surface. If the leakage flux is larger than the volume of CO_2 required to saturate these sinks, the remaining CO_2 volume will be emitted to the atmosphere as a gaseous efflux. The geochemical conditions necessary for a significant loss of dissolved CO_2 to mineral trapping by precipitation are not typically prevalent in the overburden formations. As such, in this model, loss of dissolved CO_2 to mineral trapping is not considered. The water volume available in the overburden (saturated and vadose zones) above a leaking caprock atop a unit planar area of leak is taken as

$$V_{w,OB} = H_s + \theta_w H_u \tag{16}$$

where H_s and H_u are, respectively, thickness of the saturated and unsaturated zones. Similarly, the total air volume available in the unsaturated zones above the leaking caprock, corresponding to a unit planar area of leak is taken as

$$V_{g,OB} = (1-\theta_w) H_u \tag{17}$$

The residual gaseous CO_2 flux through the soil surface, q_r, accounting for dissolution in the overburden and replacement of vadose zone air with CO_2 is

$$q_r = q_l - u_w C_w V_{w,OB} - u_g V_{g,OB} \tag{18}$$

where u_w and u_g are the horizontal components of the ground-water velocity and soil-air velocity, respectively. If the leaking CO_2 flux is not sufficient to saturate the entire air phase volume of the unsaturated overburden, then the soil-air CO_2 concentration, C_a, at a time t after the initiation of the leak, can be calculated as below:

$$C_a = \frac{q_r t}{V_{g,DB}} \tag{19}$$

The soil-air CO_2 concentration will steadily increase with a continuous leak of CO_2 until a critical time t^*, at which time the soil air will be completely replaced by CO_2.

G3 Consequence Assessment

Consequences of leakage of CO_2 into various receptor media are considered in this section and summarized in a tabular form that relates the CO_2 concentration to the corresponding consequence. Density of air at atmospheric pressure and sea level is 1.275 kg/m^3, whereas the density of CO_2 gas under similar conditions is 1.96. As such, if large volumes of CO_2 are released closer to the ground surface, in the absence of significant wind velocities, the released CO_2 is likely to form a ground-hugging cloud closer to the source location. CO_2 gas at high concentrations is acrid owing to the formation of carbonic acid in the nasal passage. Air containing over 10% by volume CO_2 is toxic.

G3.1 Risks Caused by CO_2 in Water

Two major consequences of CO_2 pollution in water are (1) corrosion of equipment and wells in contact with the water and (2) changes in the hydrologic properties of the aquifer media. Changing pH due to high concentrations of CO_2 in ground water was shown to cause pollution of the aquifer and abandonment of numerous wells due to water corrosiveness, which attacks pumping equipment, casing of wells, and pipes. Rapid corrosion of metal parts, precipitation of carbonates, loss of pumping volume (reduced yield), and breakage of pressure pipes from cavitation caused by excess gas pressure were reported to be the predominant consequences of CO_2 pollution in aquifers (Ceron and Pulido-Bosch, 1995). The Frio experiment, performed by Susan Hovorka (BEG) in the Houston vicinity near a salt dome (formation water with a salinity of 100 g/L TDS), provides some insight. It was observed, after CO_2 injection, that pH dropped from 6.5 to 5.7; alkalinity increased from 100 to 3,000 mg/L; Fe was mobilized (30 to 1,200 mg/L), as well as Mn, and Ca concentration increased (Kharaka et al., 2006). This observation suggested not only pH buffering by calcite dissolution, but also Fe increase by dissolution of iron oxides and a parallel increase in metal concentration (Zn, Pb, Mo) desorbed

from iron oxides (Kharaka et al., 2006). In addition, when large quantities of CO_2 are dissolved in water, some wells and pumps are seriously damaged by gas lift. The content of the dissolved gas increases with pressure and, as a consequence, during the rise of the water with CO_2 from deep zones, part of the dissolved gas can be liberated in a liquid phase, transforming it into an emulsion of liquid and gas with a very low density that favors ascent of the water. Because the aqueous carbonate reactions are reversible, pumping of carbonated waters can be significantly affected by this phenomenon, producing a precipitation of carbonates near the surface. CO_2 pollution in the Alto Guadalentin detrital aquifer (Ceron and Pulido-Bosch, 1995), which contained HCO_3^- of between 1,000 and 1990 mg/L, and PCO_2 of between 0.041 and 1.497 bars, caused the abandonment of numerous wells owing to water corrosiveness, which attacks pumping equipment. Using CO_2-laden waters for irrigation shows no adverse effects on some crops, although others are quite sensitive. A deposit of iron carbonate develops in the soils, impeding aeration in the root zone, and salts precipitated in the soil give rise to compounds such as sodium bicarbonate that are toxic to plants. In Spain, heavy economic costs were attributed to CO_2 pollution of the aquifer, which caused yield reduction (frequently 30%), equipment breakdowns (generally every 3 months and resulting in the abandonment of many wells), and increased pumping costs (volumes extracted contain a minimum of 30% gas).

G3.2 Effects on Biota

Physiological effects on fish may be considered to be representative of the biological consequences of releasing large quantities of CO_2 into water bodies. High CO_2 levels may cause some inhibition of respiration in fish, but direct symptoms of suffocation are unlikely. Acidosis, both environmental, owing to a low pH in water, and respiratory, owing to an accumulation of CO_2 in fish, can be considered a direct effect of high CO_2 in the water. Furthermore, CO_2 accumulation above water can cause asphyxiation by preventing atmospheric oxygen from entering the water. Ross et al. (2000) investigated fish health risks associated with episodes of high carbon dioxide levels in treated waters, by subjecting three species of fish to-24 hour exposures to elevated dissolved CO_2 at three levels, ranging from 1.0 % (low) to 6.3 % (high), under laboratory conditions. Blood physiological variables, as well as behavior, including feeding responses, were measured before, during, and after exposure. Many of the 11 observed behavioral variables, related to swimming, feeding, social, and illness factors were found to be affected by elevations of dissolved CO_2, although physiological responses differed by species.

Ross et al (2000) concluded that elevated levels of CO_2 can cause significant stress in at least some species of fish. It should be noted that the high dissolved concentration of CO_2 in their study (6.3%) is the same as the maximum aqueous solubility of CO_2 in fresh water. On the basis of Ross et al. (2000) and similar earlier reports, it is reasonable to specify a CO_2 concentration range of 1 to 6.3% in water to be progressively stress inducing to biota.

G3.3 Effects on Soil and Agriculture

Effects of elevated CO_2 concentrations due to global climate change, under increasing scrutiny in recent years, indicate that there may be some beneficial effects to crops, such as an increase in crop yield for at least some crops, owing to an increase in CO_2 concentration. Such investigations focus on the effects of moderate elevations in CO_2 concentrations on plant physiology. In contrast, elevation of CO_2 concentrations in the soil-gas phase and the unsaturated zone owing to a direct leakage of CO_2 from below is likely to have different consequences. The presence of CO_2 in large concentrations in soil air and soil water has a significant influence on soil geochemical and biological processes. Lowering of soil pH because of the generation of carbonic acid has a dominant effect on the chemistry of nutrients and redox-sensitive elements, such as Fe, Mn, As, and Se, and an indirect effect on trace metals, such as Cu, Zn and Pb, as well as an adverse effect on plant growth (Simunek and Suarez, 1993). Reduction of soil pH by even one pH unit has a significant influence on the crop yield. On the basis of extensive soil-gas measurements over a 30-hectare tree kill at Mammoth Mountain, trees were found dead irrespective of age or species in zones where soil CO_2 concentration was higher than 30% (Farrar et al., 1995).

Soil scientists typically use a nominal CO_2 concentration of 1% in the soil-gas phase, which is several times larger than atmospheric CO_2 concentration. On the basis of a predictive simulation model for modeling the transport and production of CO_2 in soil (SOILCO2) and measurements of soil gas from agricultural fields at several locations in the USA, the % CO_2 concentration in soil gas phase was reported (Simunek and Suarez, 1993) to be in the range of 1 to 8%, varying as a function of the Julian day, owing to differences in temperature and soil conditions. When soil CO_2 concentration exceeds this range, deposit of iron carbonate develops in soils, impeding aeration in the root zone, and salts precipitated in the soil give rise to compounds, such as sodium bicarbonate, which are toxic to plants On the basis of these observations, it is reasonable to conclude that elevation of soil-gaseous CO_2 concentrations

above 5% is likely to have moderate deleterious effects on plant health and yield, whereas such consequences will be severe in the 5 to 30% range and lethal above 30%. On the basis of the foregoing analysis, consequence tables have been prepared in the form of a numerical index (0, 0.5, and 1, for low, moderate, and high consequences, respectively) in order to summarize consequences of increasing CO_2 concentrations in various environmental media.

APPENDIX H: List of Papers and Presentations Stemming from This Research

Nicot, J. -P., P. Saripalli, S. D. Hovorka, and S. Lakshminarasimhan, 2006, Leakage pathways from potential CO2 storage sites in the Texas Gulf coast and implications for permitting (abs.), *in* Fifth Annual Conference on Carbon Capture & Sequestration: Taking Steps toward Deployment Utilizing the Accumulated Knowledge Base, May 8–11, Alexandria, Virginia, unpaginated.

Nicot, J. -P., P. Saripalli, and Y. Fang, 2006, Carbon storage: what are the potential impacts on groundwater in the Texas Gulf Coast (abs.), *in* Abstract Book of the 2006 Ground Water Summit: National Ground Water Association, p. 173.

Nicot, J. -P., S. D. Hovorka, P. R. Knox, and T. Naing, 2006, Area of review: how large is large enough for carbon storage? (abs.) *in* Proceedings of the 2006 UIC Conference of the Groundwater Protection Council, Abstract 17.

Nicot, J. -P., S. Lakshminarasimhan, and S. D. Hovorka, 2006, Capillary trapping in the overburden as a defense-in-depth mechanism against leakage from CO2 storage sites: the case of the Tertiary Texas Gulf Coast (ext. abs.), *in* Proceedings, CO2SC Symposium, Lawrence Berkeley National Laboratory, Berkeley, California, March 20-22, p. 173-175 + CD-ROM.

Nicot, J. -P., S. D. Hovorka, and S. Lakshminarasimhan, 2006. Leakage Pathways from Potential CO_2 Storage Sites and Importance of Open Traps: Case of the Texas Gulf Coast. In preparation for AAPG special publication on CO_2 sequestration in geological media.

Nicot, J.-P. and I. J. Duncan. Science-Based Permitting for Geological Sequestration of CO_2 in Brine Reservoirs in the U.S. In preparation.

Nicot, J.-P. Oil and Gas Wells and Geological Sequestration of CO_2 in the Texas Gulf Coast, USA. In preparation.

Papers and presentations, as well as this report, are posted on the Gulf Coast Carbon Center (Bureau of Economic Geology, The University of Texas at Austin, Austin, TX) web site at:

http://www.beg.utexas.edu/environqlty/co201.htm